Retina Atlas

Series Editors: Sandeep Saxena · Richard F. Spaide · Eric H. Souied · Timothy Y.Y. Lai

Duangnate Rojanaporn
Editor

Ocular Oncology

Springer

Retina Atlas

Series Editors

Sandeep Saxena, MS, FRCSEd, FRCS, FRCOphth
Department of Ophthalmology,
King George's Medical University,
Lucknow, Uttar Pradesh, India

Richard F. Spaide, MD
Vitreous Retina Macula Consultants of New York,
New York, NY, USA

Eric H. Souied, MD
Department of Ophthalmology,
University Paris-Est Créteil,
Créteil Cedex, France

Timothy Y.Y. Lai, MD, FRCS, FRCOphth
Department of Ophthalmology and Visual Sciences,
Chinese University of Hong Kong,
Hong Kong, Hong Kong

The 9-volume atlas covers validated and comprehensive information on retinal imaging, retinal vascular disorders, macular disorders, vitreoretinal surgical diseases, infectious and inflammatory disorders, retinal degenerations and dystrophies, pediatric retinal diseases, oncology, and trauma. This atlas with over 100 chapters is well supported with hundreds of high-quality images and text notes providing in-depth details and information in a well-organized manner.

The editors Sandeep Saxena (India), Richard F. Spaide (USA), Eric H. Souied (France) and Timothy Y.Y. Lai (Hong Kong), volume editors and contributing authors are reputed eye physicians in their field with vast clinical experience. This series has a full dedicated volume on imaging and includes various imaging technologies like optical coherence tomography, fluorescein angiography, etc. It provides global perspective of vitreoretinal diseases extensively covering medical and surgical aspects of the disease. Uncommon retinal findings in diseases such as Dengue hemorrhagic fever, malaria etc. are also covered well.

Retina Atlas is a useful go-to series meant for ophthalmology residents, retina fellows, and retina specialists as well as general ophthalmologists.

'Retina Atlas' series includes the following 9 Volumes:

1. Retinal Imaging
2. Retinal Vascular Disorders
3. Macular Disorders
4. Surgical Retina
5. Inflammatory and Infectious Ocular Disorders
6. Hereditary Chorioretinal Disorders
7. Pediatric Retinal Diseases
8. Ocular Oncology
9. Trauma and Miscellaneous Disorders in Retina

More information about this series at http://www.springer.com/series/16451

Duangnate Rojanaporn
Editor

Ocular Oncology

Springer

Editor
Duangnate Rojanaporn
Department of Ophthalmology
Faculty of Medicine
Ramathibodi Hospital
Mahidol University
Bangkok
Thailand

ISSN 2662-5741 ISSN 2662-575X (electronic)
Retina Atlas
ISBN 978-981-13-2335-5 ISBN 978-981-13-2336-2 (eBook)
https://doi.org/10.1007/978-981-13-2336-2

This Springer imprint is published by the registered company Springer Nature Singapore Pte Ltd.
The registered company address is: 152 Beach Road, #21-01/04 Gateway East, Singapore 189721, Singapore

Contents

About The Editor

Duangnate Rojanaporn, MD, FICO graduated from Mahidol University, Bangkok, Thailand, before completing an International Council of Ophthalmology (ICO) fellowship in medical and surgical retina at New York Eye and Ear Infirmary and a fellowship in ocular oncology at Wills Eye Hospital, USA. She is the Director of the Ocular Oncology Service, and course instructor for the Retina Service at the Department of Ophthalmology, Ramathibodi Hospital. Dr. Rojanaporn is a pioneer of plaque brachytherapy, and intra-arterial chemotherapy for retinoblastoma in the South East Asia region. She coordinates the ocular oncology program for several international conferences and has been invited to deliver presentations at numerous local, regional, and international meetings. Dr. Rojanaporn received an ICO fellowship grant in 2008, a Professor Yasuo Tano travel grant for the Asia-Pacific Academy of Ophthalmology (APAO) meeting in 2013, and an Asia-Pacific Academy of Ophthalmology Achievement Award in 2018.

The original version of this book was revised. An erratum to this book can be found at https://doi.org/10.1007/978-981-13-2336-2_18

Choroidal Nevus

1

Carol L. Shields and Jerry A. Shields

1.1 Introduction

Choroidal nevus is the most common benign intraocular tumor, found predominantly in Caucasian patients (Chien et al. 2017; Shields and Shields 2015; Kaliki and Shields 2015). This tumor is generally asymptomatic but can carry risk for visual acuity loss, especially if located near the fovea, and risk for transformation into malignant melanoma. Several features allow clinical identification of choroidal nevus and differentiation from melanoma.

1.2 Prevalence

There have been a few population-based studies reporting on the prevalence of choroidal nevus including the Blue Mountains Eye Study (6.5%), Beijing Eye Study (BES) (2.9%), Singapore Malay Eye Study (SiMES) (1.4%), Multi-Ethnic Study of Atherosclerosis (MESA) (2.1%), Central India Eye and Medical Study (CIEMS) (0.3%), and National Health and Nutrition Examination Survey (NHANES) (4.7%) (Sumich et al. 1998; Jonas et al. 2008; Ng et al. 2009; Greenstein et al. 2011; Nangia et al. 2012; Qiu and Shields 2015). Most of the population-based studies have focused on specific ethnic groups such as Australian (Sumich et al. 1998), Chinese (Jonas et al. 2008), or Asian Indian (Ng et al. 2009) population. The NHANES study reviewed all ethnic groups in the United States (US) and found overall prevalence of choroidal nevus in US adult population≥40 years old was 4.7%, and this lesion was most commonly detected in Whites at 5.6% (Ng et al. 2009) (Table 1.1).

Population-based studies often limit inclusion criteria to study a certain age group, generally adults without inclusion of younger age group, or study a prominent ethnic group, or study only a limited portion of the fundus. The NHANES study included all ethnicities but was deficient in that it studied only individuals >40 years old and was limited to two 45-degree photographs of the macula and optic disc (Qiu and Shields 2015). This study potentially underrepresented the true prevalence of choroidal nevus in US adults as one might speculate that if the entire fundus was included, the prevalence of choroidal nevus could reach as high as 20–25% (Qiu and Shields 2015).

1.3 Clinical Features

Choroidal nevus is a flat or minimally elevated mass with brown pigmentation (melanotic; pigmented) or without (amelanotic; nonpigmented) (Chien et al. 2017; Sumich et al. 1998; Jonas et al. 2008; Ng et al. 2009; Greenstein et al. 2011; Nangia et al. 2012; Qiu and Shields 2015; Shields et al. 2008a; Shields et al. 2010; Shields and Shields 2015; Kaliki and Shields 2015). This tumor is classically in the post-equatorial fundus (91%) or pre-equatorial fundus (9%), and most nevi are pigmented (77%) (Shields et al. 2008a) (Table 1.2). The distribution of choroidal nevus is equivalent in all quadrants (Shields et al. 2008a). Most choroidal nevi are extrafoveolar (94%) compared to subfoveolar (6%). Tumor size varies depending on the study, but one tertiary ocular oncology clinic-based center found mean basal tumor diameter was 5 mm and thickness was 1.5 mm, compared to a population-based study where choroidal nevus was found to have mean basal diameter of 1.25 mm (Sumich et al. 1998; Shields et al. 2008a).

C. L. Shields (✉) · J. A. Shields (✉)
Ocular Oncology Service, Wills Eye Hospital, Philadelphia, PA, USA

Department of Ophthalmology, Thomas Jefferson Unversity, Philadelphia, PA, USA

D. Rojanaporn (ed.), *Ocular Oncology*, https://doi.org/10.1007/978-981-13-2336-2_1

Table 1.1 Prevalence of choroidal nevus from a population-based study (National Health and Nutrition Examination Survey 2005–2008) in the United States: grouped by age, sex, and race[a]

		Sex			Race					
	Number of patients	Male (n = 2785)	Female (n = 2790)	P value[b]	White (n = 3012)	Black (n = 1133)	Hispanic (n = 1249)	Other (n = 181)	P value[b]	Total
Age, yrs										
40–50	1483	5.0%	4.4%	0.7	5.8%	0.7%	1.3%	4.4%	**0.005**	4.7%
50–60	1322	3.3%	2.9%	0.7	3.7%	0.3%	2.9%	0.0%	**0.04**	3.1%
60–70	1384	6.5%	4.4%	0.2	6.3%	0.9%	4.1%	0.8%	**0.002**	5.4%
70–80	915	6.8%	6.5%	0.9	7.3%	0.0%	5.6%	1.6%	0.2	6.6%
≥80	471	7.5%	7.5%	0.9	7.7%	0.1%	8.5%	11.6%	0.6	7.5%
P value[b]		0.07	0.1	n/a	0.08	0.6	0.07	0.08	n/a	n/a
Race										
White	3012	6.2%	5.2%	0.4	n/a	n/a	n/a	n/a	n/a	5.6%
Black	1133	1.0%	0.2%	0.07	n/a	n/a	n/a	n/a	n/a	0.6%
Hispanic	1249	2.8%	2.5%	0.8	n/a	n/a	n/a	n/a	n/a	2.7%
Other	181	0.5%	3.5%	**0.02**	n/a	n/a	n/a	n/a	n/a	2.1%
P value[b]		**<0.0001**	**0.0001**	n/a	n/a	n/a	n/a	n/a	n/a	n/a
Total	5575	5.0%	4.4%	n/a	5.6%	0.6	2.7%	2.1%	n/a	4.7%

n/a = not available, Other—East Asians, Asian Indians, and non-Hispanic multiracial individuals
Information adapted from a population-based study, [9]Qui M, Shields CL. Choroidal Nevus in the United States Adult Population: Racial Disparities and Associated Factors in the National Health and Nutrition Examination Survey. Ophthalmology 2015;122:2071–83
[a]Proportions are weighted estimates of US population characteristics, taking into account the sampling design of NHANES
[b]P values are unadjusted and calculated using the Rao-Scott Pearson chi-square test

Table 1.2 Choroidal nevus in 3422 eyes from an ocular oncology clinic-based study: tumor features based on patient age at initial examination

Nevus feature	Young patients (≤ 20 years old) (n = 63) [n (%)]	Mid-adults (21–50 years old) (n = 795) [n (%)]	Older adults (>50 years old) (n = 2564) [n (%)]
Anteroposterior location			
Macula	22 (35)	186 (23)	504 (20)
Macula-equator	40 (63)	548 (69)	1821 (71)
Equator-ora serrata	1 (2)	61 (8)	239 (9)
Quadrantic location			
Macula	22 (35)	186 (23)	504 (20)
Inferior	7 (11)	140 (18)	460 (18)
Temporal	11 (17)	162 (20)	631 (25)
Superior	8 (13)	116 (15)	410 (16)
Nasal	15 (23)	191 (24)	559 (22)
Location relative to foveolar			
Subfoveolar	9 (14)	53 (7)	143 (6)
Extrafoveolar	54 (86)	742 (93)	2421 (94)
Basal diameter (mm) [median (mean, range)]	5.0 (5.6, 0.75–24)	4.5 (4.7, 0.5–14)	5 (5.2, 0.4–20)
Thickness (mm) [median (mean, range)]	1 (1.2, 0.6–22)	1.5 (1.5, 0.7–3.7)	1.5 (1.6, 0.7–4.5)
Color			
Melanotic	56 (89)	591 (74)	1981 (77)
Amelanotic	4 (6)	83 (10)	269 (10)
Mixed	3 (5)	121 (15)	313 (12)

Information adapted from an ocular oncology clinic-based case series, [10]Shields CL, et al. Clinical spectrum of choroidal nevi based on age at presentation in 3422 consecutive eyes. Ophthalmology 2008;115:546–52

1.3.1 Low-Risk Choroidal Nevus

Choroidal nevus can be categorized into low or high risk for transformation into melanoma. Low-risk nevus is one that carries low likelihood for transformation into melanoma. Features include thickness ≤2 mm and absence of subretinal fluid, orange pigment, and symptoms. These lesions classically appear echodense on ultrasonography and demonstrate overlying retinal pigment epithelium (RPE) alterations such as drusen, RPE atrophy, and dependent RPE trough from previous subretinal fluid, RPE hyperplasia, RPE detachment, RPE fibrous metaplasia, and RPE osseous metaplasia (Shields et al. 2008a; Kaliki and Shields 2015) (Figs. 1.1, 1.2, 1.3, 1.4 and 1.5). Rarely, choroid nevus can produce chronic RPE damage that leads to development of choroidal neovascular membrane (Shields et al. 2008a) (Fig. 1.6).

1.3.2 High-Risk Choroidal Nevus

High-risk nevus is one that carries high likelihood for transformation into melanoma. Features include thickness >2 mm, presence of subretinal fluid, orange pigment and/or symptoms, acoustic hollowness on ultrasonography, and absence of chronic features such as drusen or surrounding halo (Shields et al. 2009) (Table 1.3) (Figs. 1.7 and 1.8). Location can be a factor as nevi within 3 mm of the optic disc are more likely to evolve into melanoma. High-risk nevus classically appears with little to no overlying RPE alterations such as drusen.

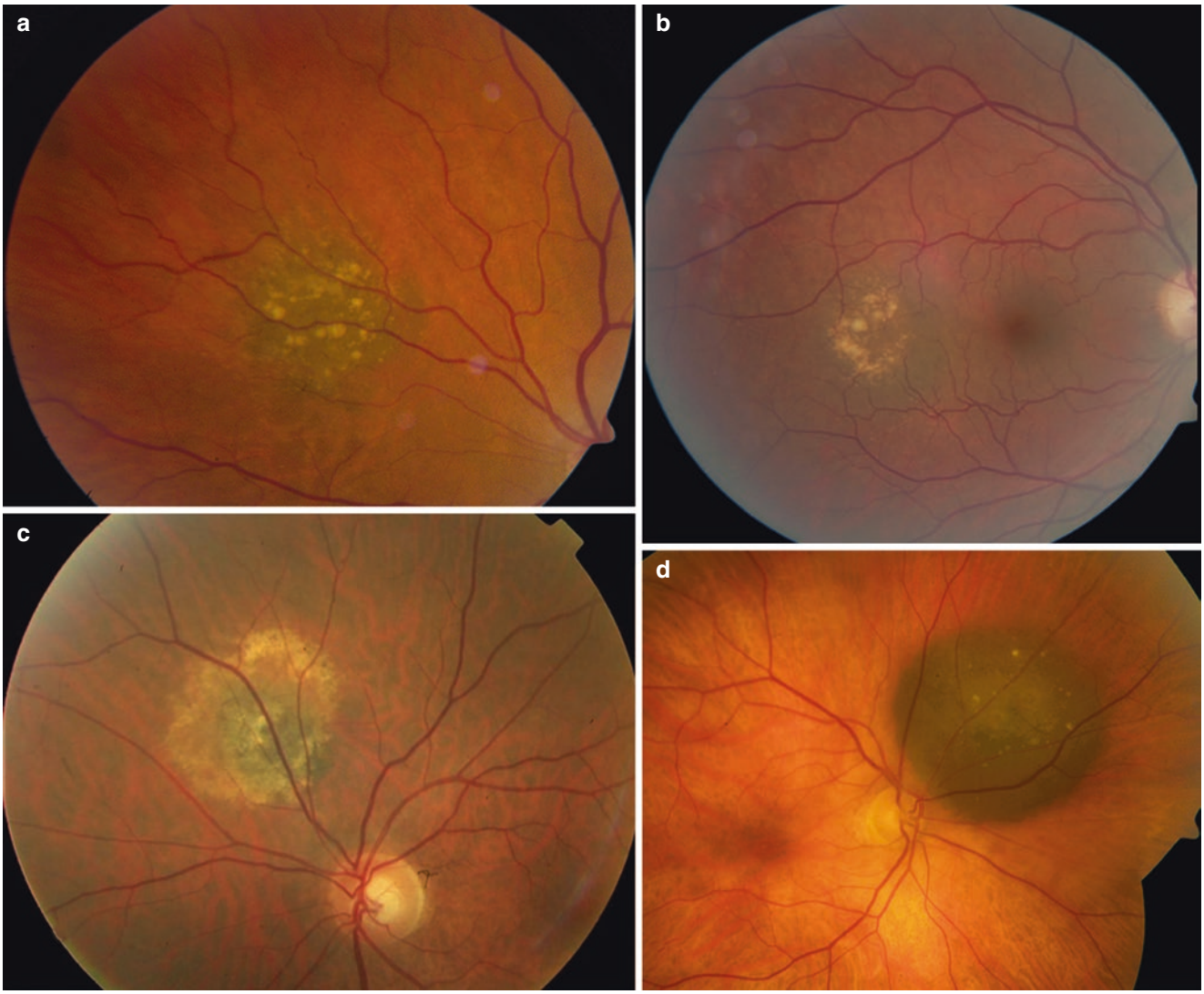

Fig. 1.1 Choroidal nevus with overlying drusen. (**a**) Drusen covering the entire aspect of the nevus. (**b**) Drusen covering the central apex of the nevus. (**c**) Drusen extending beyond the nevus margins. (**d**) Larger choroidal nevus with central retinal pigment epithelial atrophy and drusen

1.3.3 Halo Nevus

Halo nevus is an unusual form of cutaneous nevus, displaying a central pigmented portion with surrounding depigmented halo, most often found in young patients and believed to represent an immune response. Halo choroidal nevus is characterized by a pigmented nevus surrounded by a nonpigmented nevus halo, representing 5% of all choroidal nevi (Shields et al. 2010) (Fig. 1.9). Choroidal halo nevus has been found most often to signify a "low-risk" nevus (Shields et al. 2009). In one analysis of 150 patients with halo choroidal nevus, Shields et al. found relationship to previous history of skin melanoma ($p < 0.001$) and no association with autoimmune dysfunction or vitiligo (Shields et al. 2010). They speculated that cytotoxic lymphocytes acting toward the skin melanoma could target similar antigens present on choroidal nevus cells resulting in halo formation. An unusual variant of halo nevus is "reverse halo" where the center is amelanotic and the surround is melanotic. Dolz-Marco et al. has documented a relationship of posterior scleral bowing on EDI-OCT with halo choroidal nevus (Dolz-Marco et al. 2015).

1.3.4 Giant Nevus

Giant choroidal nevus is defined as a nevus with basal diameter ≥10 mm and represents 8% of all choroidal nevi seen in an ocular oncology referral practice (Li et al. 2010) (Fig. 1.10). Due to its large basal dimension and

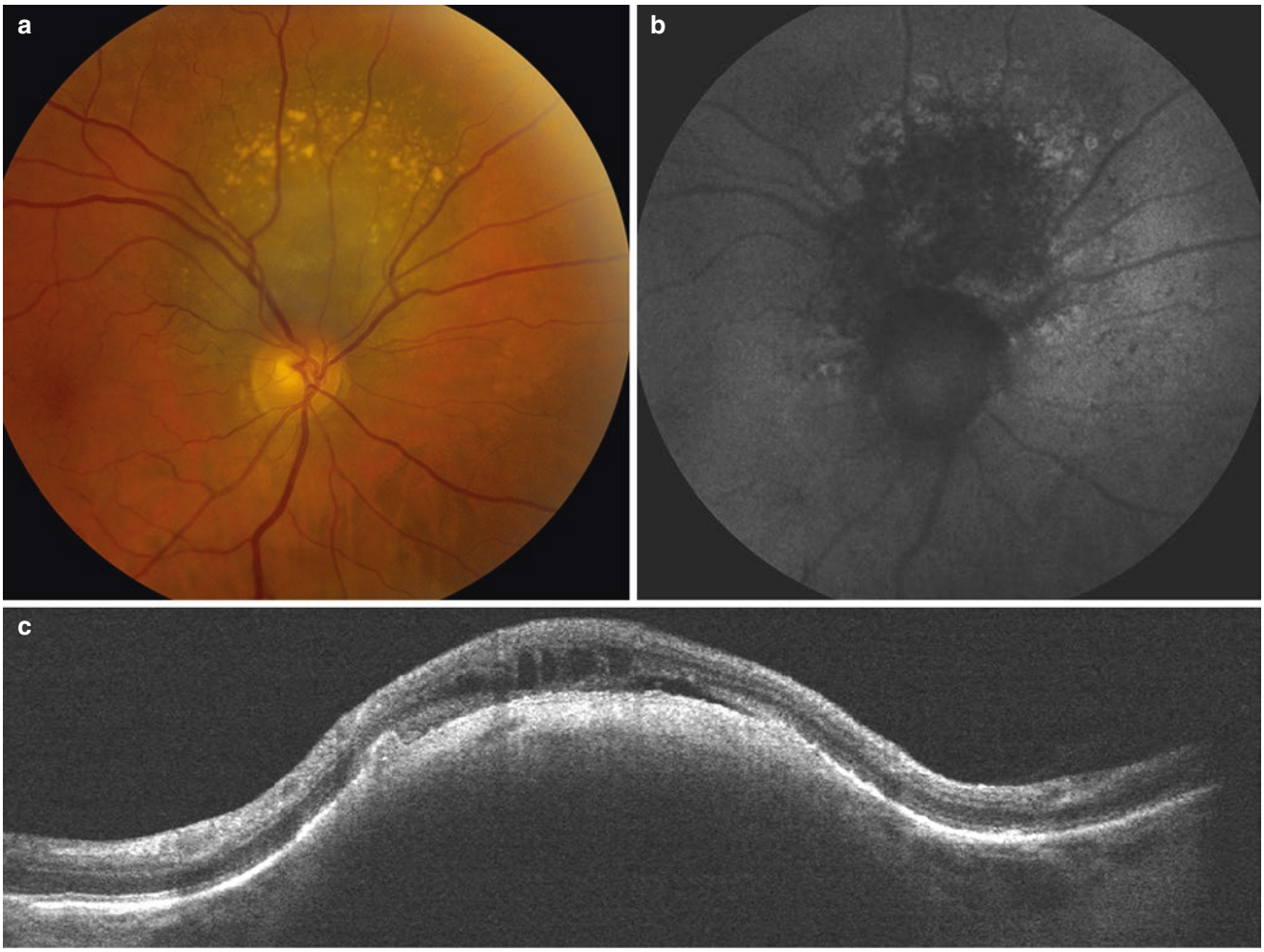

Fig. 1.2 Chronic choroidal nevus with overlying drusen. (**a**) Choroidal nevus with overlying retinal pigment epithelial (RPE) atrophy and drusen. (**b**) Autofluorescence documents the dark RPE loss as well as the ring-shaped hyperautofluorescence of soft drusen, representing tiny RPE detachments. (**c**) Optical coherence tomography documents overlying retinal edema, outer retinal disorganization and retraction, small RPE detachment, and choroidal mass with compression of the choriocapillaris

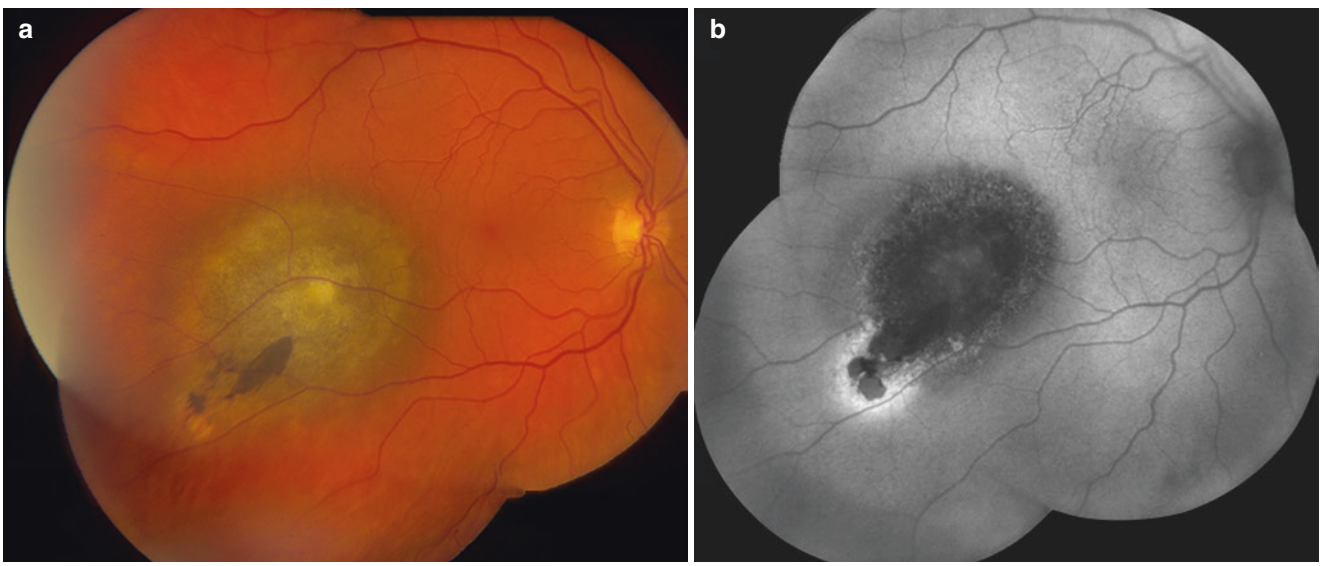

Fig. 1.3 Choroidal nevus with overlying retinal pigment epithelial (RPE) alterations. (**a**) Choroidal nevus with surface demonstrating white RPE fibrous metaplasia, RPE atrophy, and dark RPE hyperplasia. (**b**) Autofluorescence documents the dark appearance of RPE atrophy and hyperplasia. The bright signal at the anterior margin likely represents partially damaged RPE

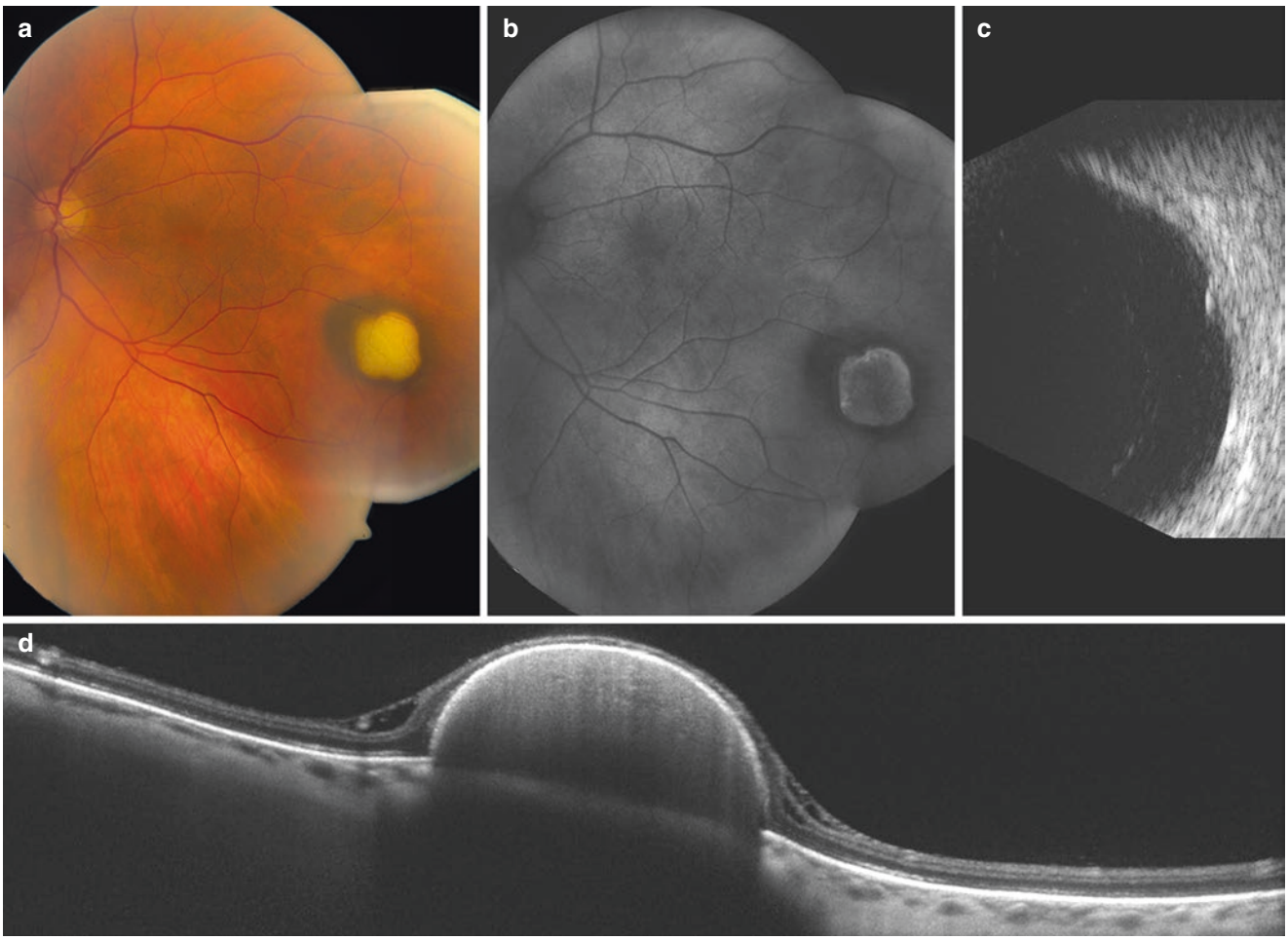

Fig. 1.4 Choroidal nevus with overlying retinal pigment epithelial (RPE) detachment. (**a**) Choroidal nevus with overlying yellow RPE detachment. (**b**) Autofluorescence documents the bright signal of the RPE detachment and the dark signal of the nevus. (**c**) Ultrasonography shows the minimal elevation and acoustic hollowness of the RPE detachment. (**d**) Optical coherence tomography demonstrates the abruptly elevated RPE detachment with draped overlying retina and deep shadowing

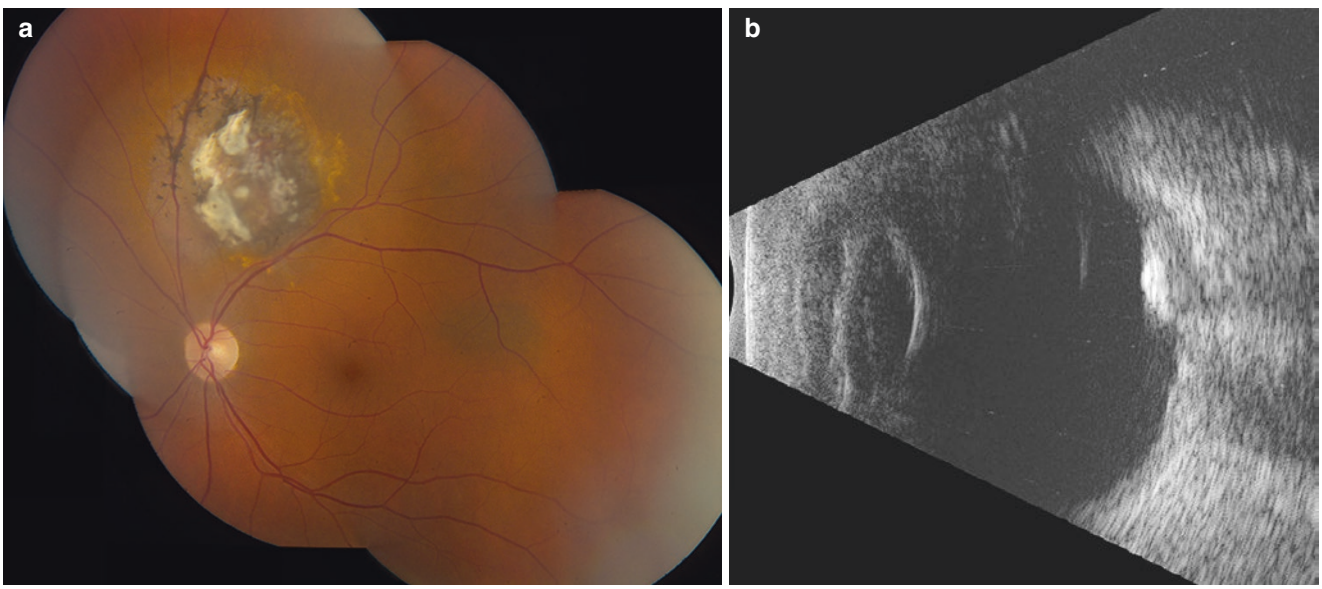

Fig. 1.5 Choroidal nevus with overlying retinal pigment epithelial (RPE) osseous metaplasia. (**a**) Chronic choroidal nevus with overlying white osseous changes in the RPE as well as RPE hyperplasia and atrophy. Note the second nevus in the temporal macular region. (**b**) Ultrasonography confirms the dense, echogenic calcific plaque overlying the nevus

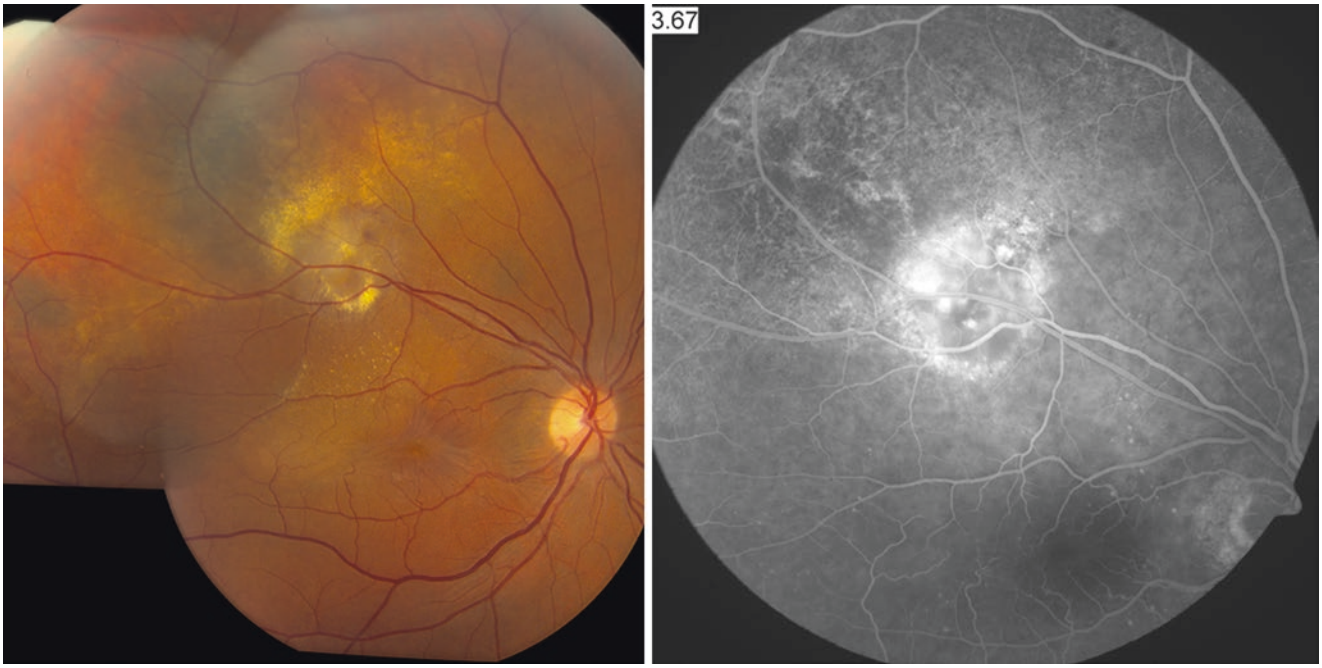

Fig. 1.6 Choroidal nevus with overlying choroidal neovascularization. (**a**) Ill-defined choroidal nevus with overlying shallow subretinal fluid with exudation and precipitation, extending into the fovea. (**b**) Fluorescein angiography documents hypofluorescence of the choroidal nevus and hyperfluorescence of the choroidal neovascularization with leakage

Table 1.3 Clinical factors at initial examination predictive of choroidal nevus transformation into melanoma

Mnemonic	Initial	Variable	Hazard ratio (compared to nevus without feature)	*P* value
To	**T**	**T**hickness > 2 mm (vs. ≤2 mm[a,b])	2	<0.001
Find	**F**	Subretinal **f**luid present (vs. absent [a])	3	0.002
Small	**S**	**S**ymptoms		
		Decreased vision (vs. none [a])	2	0.02
		Flashes/floater (vs. none [a])	2	0.002
Ocular	**O**	**O**range pigment present (vs. absent [a])	3	<0.001
Melanoma	**M**	**M**argin distance to optic nerve ≤3 mm (vs. >3 mm [a])	2	0.001
Using helpful	**UH**	**U**ltrasonographic acoustic **h**ollowness (vs. solid [a])	3	<0.001
Hints	**H**	**H**alo absent (vs. present [a])	6	0.009
Daily	**D**	**D**rusen absent (vs. present)	na	na

Analysis of 2514 patients from an ocular oncology clinic-based population
Information adapted from a retrospective medical record review study, [10]Shields CL, Furuta M, Berman EL, et al. Choroidal nevus transformation into melanoma: analysis of 2514 consecutive cases. Arch Ophthalmol 2009;127:981–987
[a]Reference variable. Na-not significant in this study but was found significant in other studies
[b]When assessing tumor thickness as a continuous variable, significance was found in the multivariate model (hazard ratio, 2.75, per 1-mm increase; $P < 0.001$). When assessing distance to the optic nerve as a continuous variable, significance was found in the multivariate model (hazard ratio, 0.90, per 1-mm increase; $P < 0.001$)

thickness, it can be mistaken for choroidal melanoma. In an analysis of 322 consecutive cases, Li et al. found giant nevus transformed into melanoma in 18% at 10 years (Li et al. 2010). The features significantly predictive of transformation included close proximity to the foveola ($p = 0.02$) and ultrasonographic evidence of acoustic hollowness ($p = 0.05$) (Li et al. 2010).

1.4 Imaging

Choroidal nevus is currently evaluated with fundus photography, ultrasonography, fluorescein angiography (FA), indocyanine green angiography (ICGA), optical coherence tomography (OCT), fundus autofluorescence (FAF), and OCT angiography (OCTA).

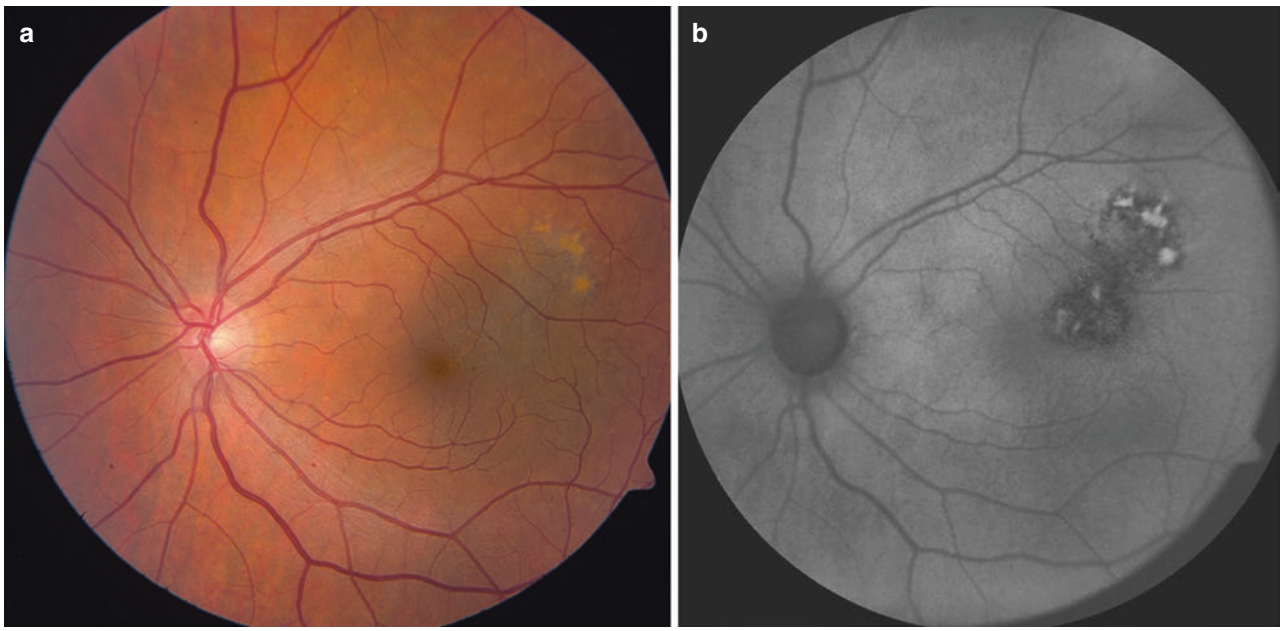

Fig. 1.7 Choroidal nevus with overlying mild orange pigment. (**a**) Submacular choroidal nevus with overlying orange pigment. (**b**) Autofluorescence documents the hyperautofluorescence of the orange pigment representing lipofuscin within macrophages

Fig. 1.8 Choroidal melanocytic tumor with overlying marked orange pigment. (**a**) Choroidal melanocytic tumor with prominent overlying orange pigment, strongly suggestive of small melanoma rather than nevus. (**b**) Autofluorescence documents the orange pigment (lipofuscin) hyperautofluorescence, suggestive of activity. (**c**) Optical coherence tomography demonstrates shallow subretinal fluid with photoreceptor loss and underlying choroidal mass

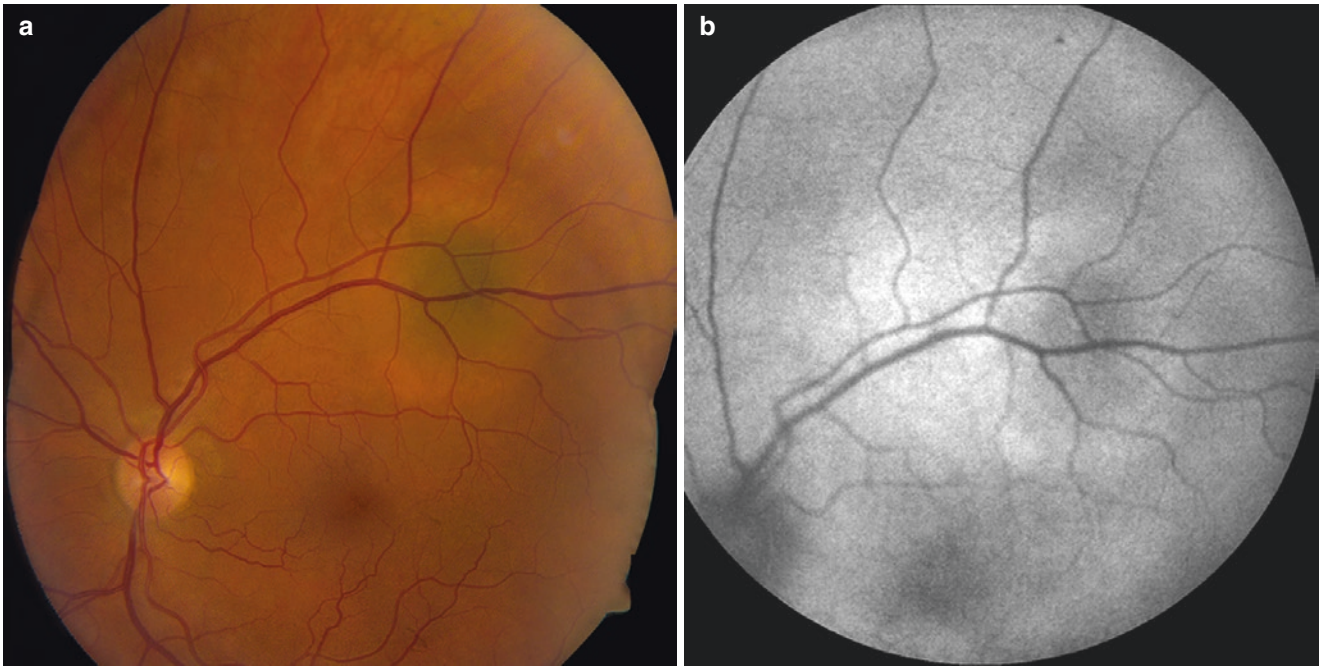

Fig. 1.9 Choroidal halo nevus. (**a**) The choroidal nevus is surrounded by a subtle yellow halo. (**b**) Autofluorescence documents the central nevus as dark and the surrounding halo as brighter, believed to represent unmasking of scleral autofluorescence

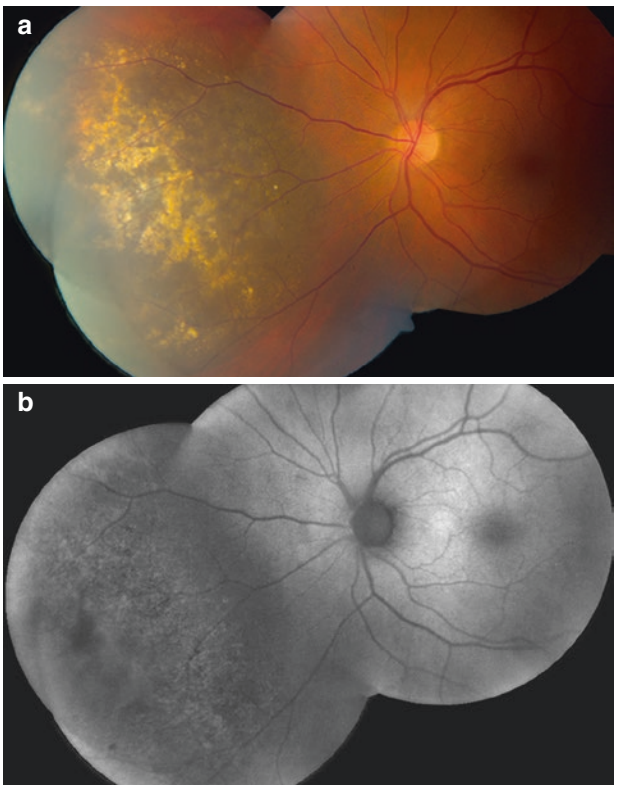

Fig. 1.10 Giant choroidal nevus. (**a**) Large choroidal nevus measuring >10 mm diameter (giant) and with confluent overlying drusen. (**b**) Autofluorescence documents the dark nevus and slight hyperautofluorescence of the drusen

1.4.1 Ultrasonography

Ultrasonography is employed for tumor-thickness measurement as well as intrinsic tumor echogenicity. Many choroidal nevi are nearly flat and are detected as only a single echo. Ultrasonography can provide baseline tumor thickness for future comparison. Nevus tends to demonstrate high internal reflectivity on A scan and echodensity on B scan (Chien et al. 2017; Shields and Shields 2015; Kaliki and Shields 2015). In contrast, melanoma demonstrates by low to medium internal reflectivity on A scan and echolucency on B scan.

1.4.2 Fluorescein Angiography

In the past, FA was more often employed in the evaluation of choroidal nevus, but currently, FA is reserved for nevus with subretinal fluid, hemorrhage, or exudation to identify pinpoint RPE leaks or choroidal neovascular membrane (CNVM). In some instances, FA can be useful in the differentiation of choroidal nevus from small choroidal melanoma as nevus remains typically hypofluorescent, whereas melanoma can demonstrate intrinsic vascularity (double circulation) or overlying pinpoint RPE leaks (Chien et al. 2017; Shields and Shields 2015; Kaliki and Shields 2015).

1.4.3 Indocyanine Green Angiography

The role of ICGA in the management of choroidal nevus is yet to be defined. Studies on ICGA for intraocular tumors reveal that this technology could be useful for differentiating choroidal hemangioma and metastasis from melanoma and nevus (Shields et al. 1995a). Thin melanoma and nevus tend to be hypocyanescence. ICGA might be useful in delineating overlying CNVM related to nevus.

1.4.4 Optical Coherence Tomography

Enhanced depth imaging OCT (EDI-OCT) is a highly valuable tool for evaluation of choroidal nevus, particularly the status of the overlying retina and RPE. EDI-OCT can image choroidal nevus, even those that are flat and undetectable by ultrasonography (Torres et al. 2011; Shah et al. 2012). We reported characteristic features of choroidal nevus on EDI-OCT, including choriocapillaris thinning over the nevus apex (94%) and partial (59%) or complete (35%) choroidal shadowing deep to the nevus, depending on nevus pigmentation, RPE atrophy (43%), and photoreceptor loss (43%) (Shah et al. 2012). It was found that relatively low-resolution ultrasonography overestimated nevus thickness measurements compared to high-resolution EDI-OCT by approximately 126% (Shah et al. 2012). Subretinal fluid was noted overlying nevus (16%), and the chronicity of fluid could be important in the nevus status as thinned outer retina with photoreceptor retraction ("stalactite" appearance) or absence ("cleft") typically signifies chronic retinal degeneration from long-standing fluid. This feature was more often found with nevus rather than melanoma (Shields et al. 2012; Shields et al. 2014). By EDI-OCT, small choroidal melanoma shows partial (73%) or complete (27%) choroidal shadowing deep to the melanoma, similar to nevus. However, the major differences are in the subretinal fluid (92% with melanoma), showing typical "shaggy" photoreceptors and subretinal lipofuscin deposition (95%), both suggestive of tumor activity (Shields et al. 2012). By comparison, EDI-OCT of small melanoma versus nevus showed melanoma with greater irregularity of inner plexiform layer ($p = 0.04$), loss of the ellipsoid zone ($p = 0.02$), shaggy photoreceptors ($p < 0.001$), loss of photoreceptors ($p = 0.05$), loss of external limiting membrane ($p = 0.008$), and intraretinal edema ($P = 0.003$) (Shields et al. 2012). "Shaggy" photoreceptors are speculated to represent subretinal macrophages aligning on the posterior retinal surface or swollen photoreceptors. Shields et al. documented "shaggy" photoreceptors in 49% of small melanoma and in 0% eyes with nevus (Shields et al. 2012).

Choroidal halo nevus shows an interesting finding on EDI-OCT in many cases, with posterior bowing of the sclera at the site of the nevus base (Dolz-Marco et al. 2015).

1.4.5 Fundus Autofluorescence

Fundus autofluorescence (FAF) can be a reliable marker of nevus as nevus tends to be hypoFAF, whereas small melanoma tends to be hyperFAF (Shields et al. 2008b; Almeida et al. 2013). Shields et al. evaluated 64 eyes with choroidal nevus and found features of overlying RPE isoFAF or hypoFAF in most cases, from RPE atrophy or fibrous metaplasia (Shields et al. 2008b). In contrast, small choroidal melanoma demonstrates overlying RPE hyperFAF, correlating one-to-one with lipofuscin. Recently, Albertus et al. developed a novel quantification method for FAF of lipofuscin and proposed that this method could be useful to clinically differentiate between nevus and melanoma (Albertus et al. 2013).

1.4.6 Optical Coherence Tomography Angiography

OCTA is a fairly new noninvasive microvascular imaging technique for the retina, permitting imaging of three capillary plexuses including the radial peripapillary, superficial capillary, and deep capillary plexuses. OCTA enables segmental quantification of each plexus, not possible on conventional FA (Spaide et al. 2015). A recent analysis on OCTA of nevus versus small melanoma by Valverde-Megias et al. showed eyes with nevus had similar central macular thickness, foveal avascular zone area, and capillary vascular density in the affected eye compared to the unaffected eye (Valverde-Megias et al. 2017). By comparison, eyes with small melanoma showed increased central macular thickness, enlarged foveal avascular zone, and reduction of capillary vascular density in the eye with melanoma compared to normal opposite eye (Valverde-Megias et al. 2017).

1.5 Risk Factors

1.5.1 Risk for Vision Loss

Vision loss with choroidal nevus strongly depends on the proximity of the nevus to the foveola. Shields et al. analyzed 3422 eyes with choroidal nevus for visual outcomes and found eye with subfoveolar nevus was significantly more likely to develop reduced visual acuity (26%) compared to those with extrafoveolar nevus (2%) by 15 years (Shields et al. 2007). Factors predictive of visual acuity loss of three or

more logMAR lines included eyes with initial visual acuity of 20/50 or worse (relative risk [RR] 15.40), juxtapapillary nevus location (RR 4.52), subfoveolar nevus location (RR 15.52), nevus thickness greater than 2 mm (RR 3.89), overlying RPE detachment (RR 22.16), and foveal edema (RR 9.02) (Shields et al. 2007). Factors predictive of ultimate poor visual acuity of 20/200 vision or worse included subfoveolar nevus location (RR 11.32), overlying orange pigment (RR 3.68), RPE detachment overlying nevus (RR 12.80), and foveal edema (RR 18.72) (Shields et al. 2007). Thus, vision loss overtime should be anticipated in patients with subfoveal nevi.

1.5.2 Risk for Growth into Melanoma

Choroidal nevus should be routinely monitored for potential for malignant transformation into melanoma (Shields et al. 1995b; Singh et al. 2005; Kivela and Eskelin 2006; Mashayekhi et al. 2011; Shields et al. 2017a, b) (Fig. 1.11). Some nevi demonstrate slow and minimal growth of approximately 0.06 mm/year over long period of time (10 years) and that is not equivalent with transformation (Mashayekhi et al. 2011). Transformation is suspected with growth and occurs over a relatively short period of time, like 1–2 years or less (Shields et al. 1995b; Shields et al. 2009). Early identification of transformation is important for prompt treatment at a time when the melanoma is small and systemic prognosis is favorable.

In 1995, Shields et al. identified several risk factors predictive of small nevus growth into melanoma, and these risk factors are remembered by the mnemonic "To find small ocular melanoma" representing thickness >2 mm (T)(RR 5.2), subretinal fluid (F)(RR 1.4), symptoms (S) of flashes/floaters (RR 1.8) and blurred vision (RR 1.6), orange pigment (O) (RR 1.5), and margin less than or equal to 3 mm from optic disc (M)(RR 1.4) (Shields et al. 1995b). Later analysis of 2514 cases by Shields et al. confirmed previous risk factors and identified additional two risk factors of ultrasonographic hollowness (UH)(RR, 2.9) and absence of halo (H)(RR, 6.5) (Shields et al. 2009). Tumors with three or more risk factors likely represent small melanoma and demonstrate malignant transformation in >50% of cases at 5 years (Shields et al. 2009), and treatment should be considered early. Tumors with combination of thickness greater than 2 mm, symptoms positive, and tumor margin near the disc showed greatest risk (69%) for malignant transformation (Shields et al. 2009). Median hazard ratio (HR) for nevus transformation to melanoma for those with 1 or 2, 3 or 4, 5 or 6, and for all 7 risk factors were 3, 5, 9, and 21, respectively (Shields et al. 2009).

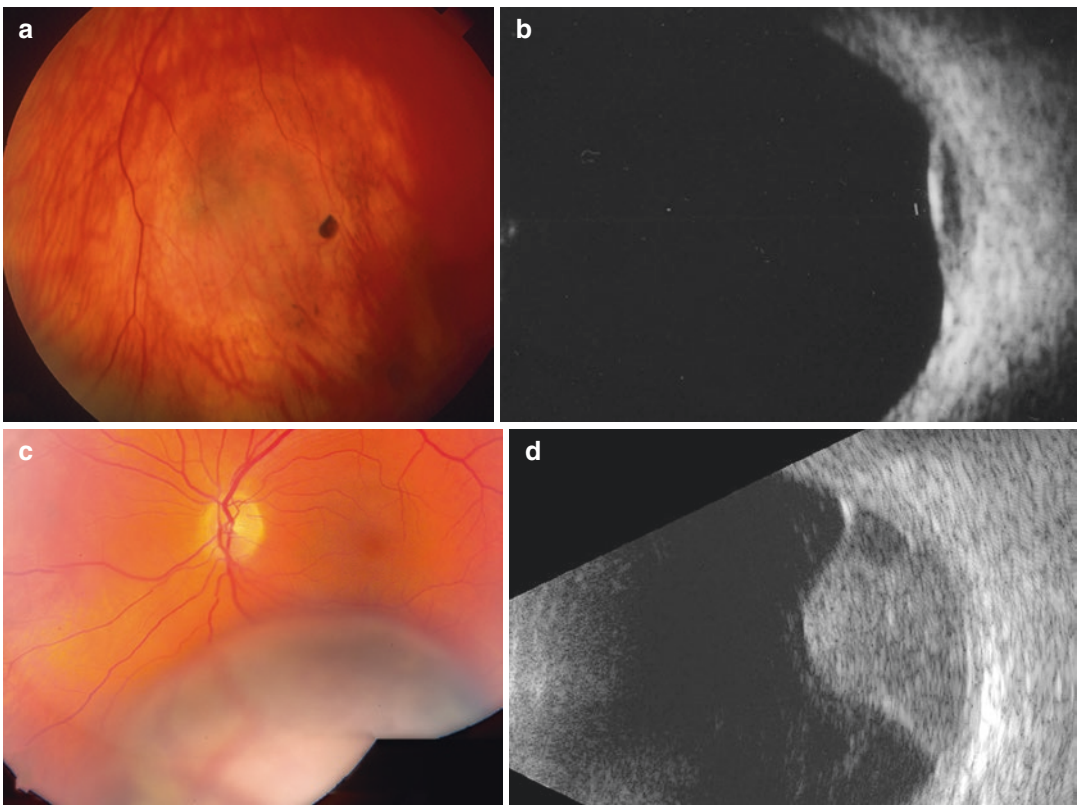

Fig. 1.11 Choroidal nevus growth into melanoma. (**a**) Small amelanotic choroidal nevus with clump of overlying retinal pigment epithelial hyperplasia. (**b**) Ultrasonography demonstrates thin, acoustically hollow mass. (**c**) Several years later, the mass has enlarged into elevated melanoma. (**d**) At that time, the mass had assumed a mushroom shape and subretinal fluid

Assuming that all choroidal melanoma arise from preexisting nevus, Singh et al. reported the estimated annual rate of malignant transformation of nevus into melanoma was 1 in 8845 Caucasian Americans based on the data calculated from the Surveillance, Epidemiology, and End Results (SEER) cancer database (Singh et al. 2005). The annual rate of malignant transformation increases with age from 1 out of 269,565 for a young age group (15–19 years) to 1 out of 3664 for an older age group (80–84 years) (Singh et al. 2005). This study did not determine the true risk of malignant change of nevus, because the frequency of melanoma developing de novo was not known (Singh et al. 2005). Later, Kivela and Eskelin calculated an adjusted lifetime risk estimate of 0.2% for malignant transformation of choroidal nevus under the assumption that at least 1 in 5 uveal melanomas develop from choroidal nevus (Kivela and Eskelin 2006). This suggests that the lifetime risk of malignant transformation of nevus may be more significant than previously proposed (Kivela and Eskelin 2006).

1.6 Management

1.6.1 Observation

Most choroidal nevi are managed with periodic observation. Fundus photography, ultrasonography, and potentially EDI-OCT are useful imaging modalities at each visit.

1.6.2 Management of Subretinal Fluid

Choroidal nevus demonstrates related overlying subretinal fluid in approximately 10% of patients (Shields et al. 2008a). Imaging with EDI-OCT to confirm the fluid is important, and FA to determine the source of fluid can be helpful. If the fluid is extrafoveal, most clinicians would cautiously observe, whereas if the fluid is subfoveal and symptomatic, then intervention with intravitreal anti-vascular endothelial growth factor (anti-VEGF), photodynamic therapy (PDT), or oral or topical acetazolamide is considered. In a case series of 15 eyes with choroidal nevus treated with PDT for subretinal fluid, resolution of subfoveal fluid was achieved in 87% of eyes, and visual acuity improved in 53% of eyes (Pointdujour-Lim et al. 2017). In most cases one PDT session achieves fluid control and improvement in visual acuity (Pointdujour-Lim et al. 2017).

1.6.3 Management of Choroidal Neovascularization

Choroidal nevus demonstrates related overlying CNVM in approximately 1% of patients (Shields et al. 2008a) (Fig. 1.6). Management of CNVM secondary to nevus typically involves monthly anti-VEGF therapy with functional and anatomical improvements in 66% of treated eyes (Shields et al. 2008a).

1.6.4 Management of Growth into Melanoma

Choroidal nevus growth into melanoma is confirmed by imaging modalities, and treatment is instituted with plaque radiotherapy, proton beam radiotherapy, transpupillary thermotherapy, Aura-011 nanoparticle therapy, transscleral resection, or enucleation. Please refer to the chapter on choroidal melanoma.

References

Albertus DL, Schachar IH, Zahid S, et al. Autofluorescence quantification of benign and malignant choroidal nevomelanocytic tumors. JAMA Ophthalmol. 2013;131:1004–8.

Almeida A, Kaliki S, Shields CL. Autofluorescence of intraocular tumours. Curr Opin Ophthalmol. 2013;24:222–32.

Chien JL, Sioufi K, Surakiatchanukul T, et al. Choroidal nevus: a review of prevalence, features, genetics, risks, and outcomes. Curr Opin Ophthalmol. 2017;28:228–37.

Dolz-Marco R, Hasanreisoglu M, Shields JA, et al. Posterior scleral bowing with choroidal nevus on enhanced-depth imaging optical coherence tomography. JAMA Ophthalmol. 2015;133:1165–70.

Greenstein MB, Myers CE, Meuer SM, et al. Prevalence and characteristics of choroidal nevi: the multi-ethnic study of atherosclerosis. Ophthalmology. 2011;118:2468–73.

Jonas JB, You QS, Xu L, et al. Choroidal nevi in adult chinese. Ophthalmology. 2008;115:1102.

Kaliki S, Shields CL. Choroidal nevus. In: Moorthy RS, Gombos DS, Browning DJ, editors. Focal points: clinical modules for ophthalmologists, vol. 33. San Francisco: Number 1; 2015.

Kivela T, Eskelin S. Transformation of nevus to melanoma. Ophthalmology. 2006;113:887–8.

Li HK, Shields CL, Mashayekhi A, et al. Giant choroidal nevus clinical features and natural course in 322 cases. Ophthalmology. 2010;117:324–33.

Mashayekhi A, Siu S, Shields CL, et al. Slow enlargement of choroidal nevi: a long-term follow-up study. Ophthalmology. 2011;118:382–8.

Nangia V, Jonas JB, Agarwal S, et al. Choroidal nevi in adult Indians: The Central India eye and medical study. Br J Ophthalmol. 2012;96:1443–4.

Ng CH, Wang JJ, Mitchell P, et al. Prevalence and characteristics of choroidal nevi in an Asian vs white population. Arch Ophthalmol. 2009;127:314–9.

Pointdujour-Lim R, Mashayekhi A, Shields JA, et al. Photodynamic therapy for choroidal nevus with subfoveal fluid. Retina. 2017;37:718–23.

Qiu M, Shields CL. Choroidal nevus in the United States adult population: racial disparities and associated factors in the national health and nutrition examination survey. Ophthalmology. 2015;122:2071–83.

Shah SU, Kaliki S, Shields CL, et al. Enhanced depth imaging optical coherence tomography of choroidal nevus in 104 cases. Ophthalmology. 2012;119:1066–72.

Shields JA, Shields CL. Intraocular tumors: an atlas and textbook. 3rd ed. Philadelphia: Wolters Kluwer; 2015.

Shields CL, Shields JA, De Potter P. Patterns of indocyanine green videoangiography of choroidal tumours. Br J Ophthalmol. 1995a;79:237–45.

Shields CL, Shields JA, Kiratli H, et al. Risk factors for growth and metastasis of small choroidal melanocytic lesions. Ophthalmology. 1995b;102:1351–61.

Shields CL, Furuta M, Mashayekhi A, et al. Visual acuity in 3422 consecutive eyes with choroidal nevus. Arch Ophthalmol. 2007;125:1501–7.

Shields CL, Furuta M, Mashayekhi A, et al. Clinical spectrum of choroidal nevi based on age at presentation in 3422 consecutive eyes. Ophthalmology. 2008a;115:546–52.

Shields CL, Pirondini C, Bianciotto C, et al. Autofluorescence of choroidal nevus in 64 cases. Retina. 2008b;28:1035–43.

Shields CL, Furuta M, Berman EL, et al. Choroidal nevus transformation into melanoma: analysis of 2514 consecutive cases. Arch Ophthalmol. 2009;127:981–7.

Shields CL, Maktabi AM, Jahnle E, et al. Halo nevus of the choroid in 150 patients: the 2010 Henry van Dyke Lecture. Arch Ophthalmol. 2010;128:859–64.

Shields CL, Kaliki S, Rojanaporn D, et al. Enhanced depth imaging optical coherence tomography of small choroidal melanoma: comparison with choroidal nevus. Arch Ophthalmol. 2012;130:850–6.

Shields CL, Pellegrini M, Ferenczy SR, et al. Enhanced depth imaging optical coherence tomography of intraocular tumors: from placid to seasick to rock and rolling topography--the 2013 Francesco Orzalesi Lecture. Retina. 2014;34:1495–512.

Shields CL, Say EAT, Hasanreisoglu M, et al. Personalized prognosis of uveal melanoma based on cytogenetic profile in 1059 patients over an 8-year period: the 2017 Harry S. Gradle Lecture. Ophthalmology. 2017a;124:1523–31.

Shields CL, Say EAT, Hasanreisoglu M, et al. Cytogenetic abnormalities in uveal melanoma based on tumor features and size in 1059 patients: the 2016 W. Richard Green Lecture. Ophthalmology. 2017b;124:609–18.

Singh AD, Kalyani P, Topham A. Estimating the risk of malignant transformation of a choroidal nevus. Ophthalmology. 2005;112:1784–9.

Spaide RF, Klancnik JM Jr, Cooney MJ. Retinal vascular layers imaged by fluorescein angiography and optical coherence tomography angiography. JAMA Ophthalmol. 2015;133:45–50.

Sumich P, Mitchell P, Wang JJ. Choroidal nevi in a white population: the Blue Mountains Eye Study. Arch Ophthalmol. 1998;116:645–50.

Torres VL, Brugnoni N, Kaiser PK, et al. Optical coherence tomography enhanced depth imaging of choroidal tumors. Am J Ophthalmol. 2011;151:586–93.

Valverde-Megias A, Say EA, Ferenczy SR, et al. Differential macular features on optical coherence tomography angiography in eyes with choroidal nevus and melanoma. Retina. 2017;37:731–40.

Choroidal Melanoma

2

Carol L. Shields and Jerry A. Shields

2.1 Introduction

Melanoma is a dangerous malignancy that can involve the skin, the uvea, and the mucous membranes (Shields et al. 2015b; Shields et al. 2014; Shields and Shields 2015a; Kaliki and Shields 2017; Shields and Shields 2015b; Chang et al. 1998). In a review of 84,836 cases from the National Cancer Data Base, including cases diagnosed between 1985 and 1994, the percentages of melanomas arising from the skin, eye and adnexa, mucosa, and unknown primaries were 91, 5, 1, and 2%, respectively (Chang et al. 1998). In North America, it is estimated that approximately 2500 persons develop uveal melanoma annually (Kivela 2009). Worldwide, it is estimated that there are 7095 new cases of uveal melanoma annually with 4747 in White non-Hispanic, 738 in Hispanic, 1286 in Asian, and 316 in African patients (Kivela 2009). The incidence of uveal melanoma has been relatively stable over past decades.

2.2 Demographics

Choroidal melanoma is the most common primary intraocular malignant tumor among White patients (Shields and Shields 2015a). In North America, estimates find that approximately 2500 persons develop uveal melanoma annually (Kivela 2009). Worldwide uveal melanoma affects approximately 7095 persons per year with 4747 in Whites, 738 in Hispanics, 1286 in Asians, and 316 in Africans (Kivela 2009).

The mean age-adjusted incidence of uveal melanoma is 4.3 per million (Singh and Topham 2003). This figure has remained relatively stable over the past five decades. In an analysis of 2493 cases of uveal melanoma from the National Cancer Institute's Surveillance, Epidemiology, and End Results (SEER) database, uveal melanoma at all ages was more common in men (4.9 per million) compared with women (3.7 per million) (Singh and Topham 2003). The mean age at presentation was 60 years, and the age-specific incidence per million population (male/female) is listed in Table 2.1.

Table 2.1 Age-specific incidence of uveal melanoma per million in the United States

Age (years)	Males	Females
0–4	0	0
10–14	0.2	0
20–24	0.4	0.6
30–34	1.7	1.7
40–44	3.9	2.4
50–54	10.5	6.5
60–64	14.9	11.7
70–74	24.5	17.8
80–84	23.2	16.1

Table data adapted from Singh AD, Topham A. Incidence of uveal melanoma in the United States: 1973–1997. Ophthalmology 2003;110(5):956–61

In an analysis of 8033 patients with uveal melanoma from a single tertiary referral center over a four-decade period, Shields and coworkers reported melanoma primarily involving the choroid (90%), ciliary body (6%), or iris (4%) (Shields et al. 2012a). The tumor affected males and females equivalently and primarily occurred in Caucasians (98%). In this clinic-based study, the mean patient age at detection was 58 years and specifically occurred in children <20 years (1%), mid-adults 21–60 years (53%), and older adults >60 years (45%) (Shields et al. 2012a).

2.3 Symptoms

Choroidal melanoma usually manifests with symptoms of photopsia (flashes), floaters, visual field loss or visual acuity loss, or no symptoms (Shields et al. 2012a). If the tumor involves the ciliary body, sentinel vessels can be noted. Rarely melanoma

C. L. Shields (✉) · J. A. Shields (✉)
Ocular Oncology Service, Wills Eye Hospital, Philadelphia, PA, USA

Department of Ophthalmology, Thomas Jefferson Unversity, Philadelphia, PA, USA

D. Rojanaporn (ed.), *Ocular Oncology*, https://doi.org/10.1007/978-981-13-2336-2_2

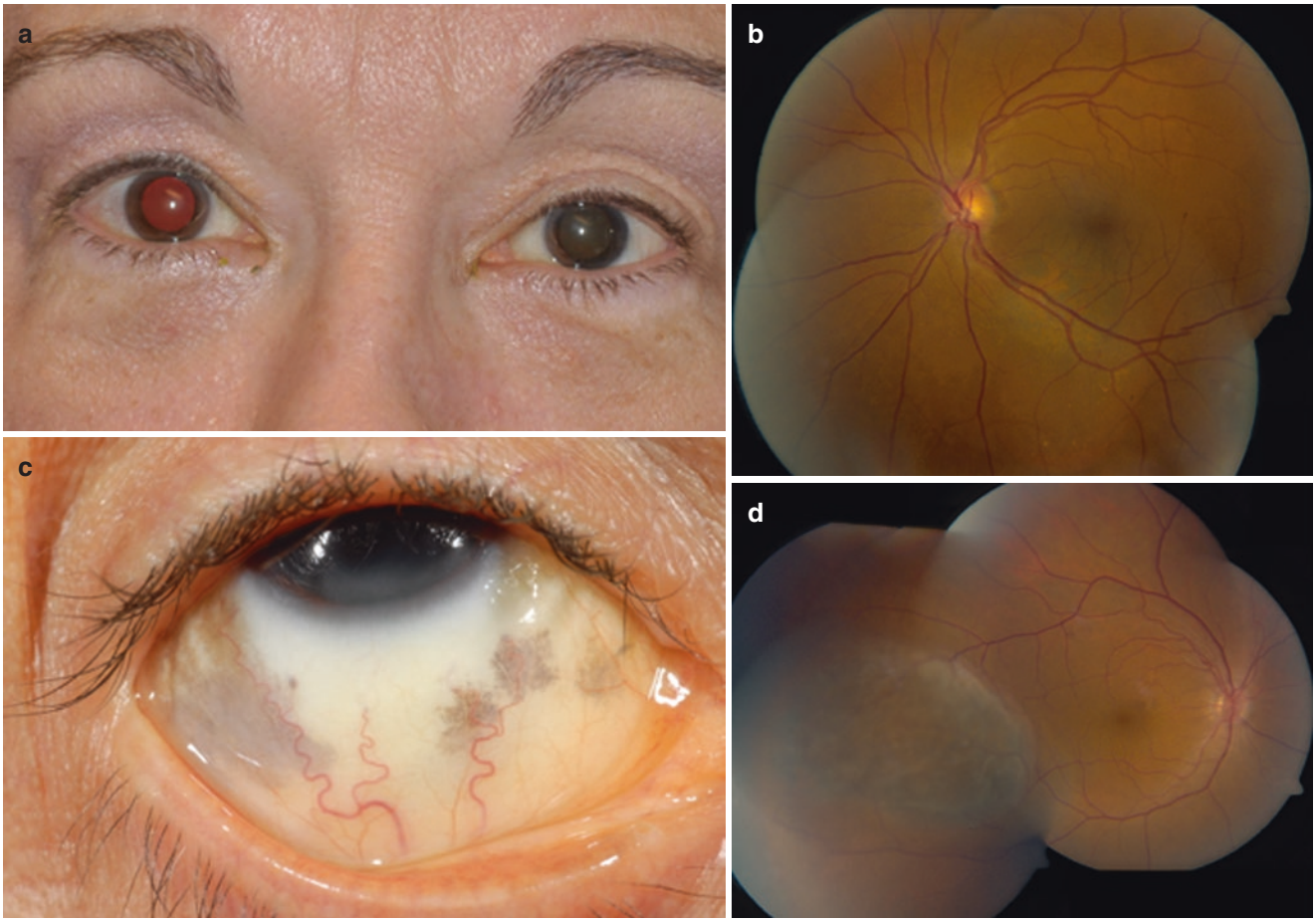

Fig. 2.1 Predisposing factors to choroidal melanoma. (**a**) Ocular melanocytosis of the left eye with melanocoria (brown pupil) and (**b**) with small choroidal melanoma with overlying orange pigment in the inferior macula. (**c**) Ocular melanocytosis of the right eye with scleral melanocytosis and (**d**) with choroidal melanoma with overlying orange pigment in the temporal macula

can cause pain from secondary glaucoma or tumor-related inflammation or necrosis (Rishi et al. 2013). The importance of annual eye examination is emphasized for earliest detection.

2.4 Predisposing Factors

Factors related to the development of uveal melanoma involve host, environmental, and genetic factors. Weis and coworkers provided a meta-analysis of all published reports on host factors for uveal melanoma and found that light eye color, fair skin color, and inability to tan were risk factors for development of uveal melanoma (Weis et al. 2006). Shah and coworkers investigated environmental factors and found that intermittent ultraviolet exposure to arc welding was a significant risk factor (Shah et al. 2005). Chronic ultraviolet exposure and occupational sunlight exposure were borderline factors. Factors such as geographic birth latitude and outdoor leisure sunlight exposure were not related to the development of uveal melanoma.

Two important host factors for development of uveal melanoma are the presence of a pre-existing choroidal nevus and the presence of congenital ocular (dermal) melanocytosis, also termed "nevus of Ota" (Fig. 2.1). Ocular (dermal) melanocytosis manifests as a gray episcleral and cutaneous pigmentation, often with related uveal hyperpigmentation. This condition carries a 1 in 400 lifetime risk for uveal melanoma in Caucasians (Singh et al. 1998). Melanoma that arises from melanocytosis carries double the risk for metastatic disease (Shields et al. 2013c). The other factor, choroidal nevus, is generally detected in preteenage or teenage patients as a pigmented choroidal mass that gradually acquires chronic overlying drusen and retinal pigment epithelial (RPE) changes. Qiu and Shields found prevalence of choroidal nevus was 4.7% overall and increased with age (4.7, 3.1, 5.4, 6.6, and 7.5% in subjects aged 40–49, 50–59, 60–69, 70–79, and > 80 years, respectively) (Qiu and Shields 2015). Singh and associates estimated transformation in 1 in 8845 in the White population (Singh et al. 2005). Shields and coworkers further investigated the clinical risk factors for transforma-

tion of choroidal nevus into melanoma (Shields et al. 1995; Shields et al. 2000a; Shields et al. 2009a) (Table 2.2).

There is a newly recognized genetic trait for the development of uveal melanoma, and that is the BRCA1-associated protein-1 (BAP1) cancer predisposition syndrome. This germline mutation predisposes to mesothelioma, renal cell carcinoma, cutaneous melanoma, and uveal melanoma (Rai et al. 2016). There is a benign cutaneous marker in some cases, termed melanocytic BAP1-mutated intradermal tumors (MBAITs). Patients with germline BAP1-related uveal melanoma often demonstrate larger tumors, second cancers, worse prognosis, and multiple family members affected with cancer (Gupta et al. 2015).

Table 2.2 Risk factors for growth of choroidal nevus into melanoma

Initial	Mnemonic	Feature	Hazard ratio
T	To	Thickness > 2 mm	2
F	Find	Fluid	3
S	Small	Symptoms	2
O	Ocular	Orange pigment	3
M	Melanoma	Margin ≤3 mm to disc	2
UH	Using helpful	Ultrasonographic hollowness	3
H	Hints	Halo absence	6
D	Daily	Drusen absence	<1

Adapted from Shields CL, Furuta M, Berman EL, et al. Choroidal nevus transformation into melanoma: analysis of 2514 consecutive cases. Arch Ophthalmol 2009;127:981–7 and Collaborative Ocular Melanoma Study Group. Factors predictive of growth and treatment of small choroidal melanoma: COMS report No. 5. Arch Ophthalmol 1997;115:1537–1544

2.5 Clinical Features

Choroidal melanoma is pigmented in 55%, nonpigmented in 15%, and mixed pigmented/nonpigmented in 30% (Shields et al. 2014; Shields et al. 2012a). Choroidal melanoma is classified as small (0–3 mm), medium (3–8 mm), or large (>8 mm), based on thickness (Figs. 2.2, 2.3 and 2.4). The mean basal dimension is 11.3 mm, and mean thickness is 5.5 mm (Shields et al. 2012a; Shields et al. 2009b). Choroidal

Fig. 2.2 Small choroidal melanoma. (**a**) Small darkly-pigmented melanoma with orange pigment. (**b**) Small amelanotic melanoma with brown lipofuscin pigment. (**c**) Small juxtapapillary melanoma with subretinal fluid, visible on the (**d**) horizontal and (**e**) vertical orientation of optical coherence tomography

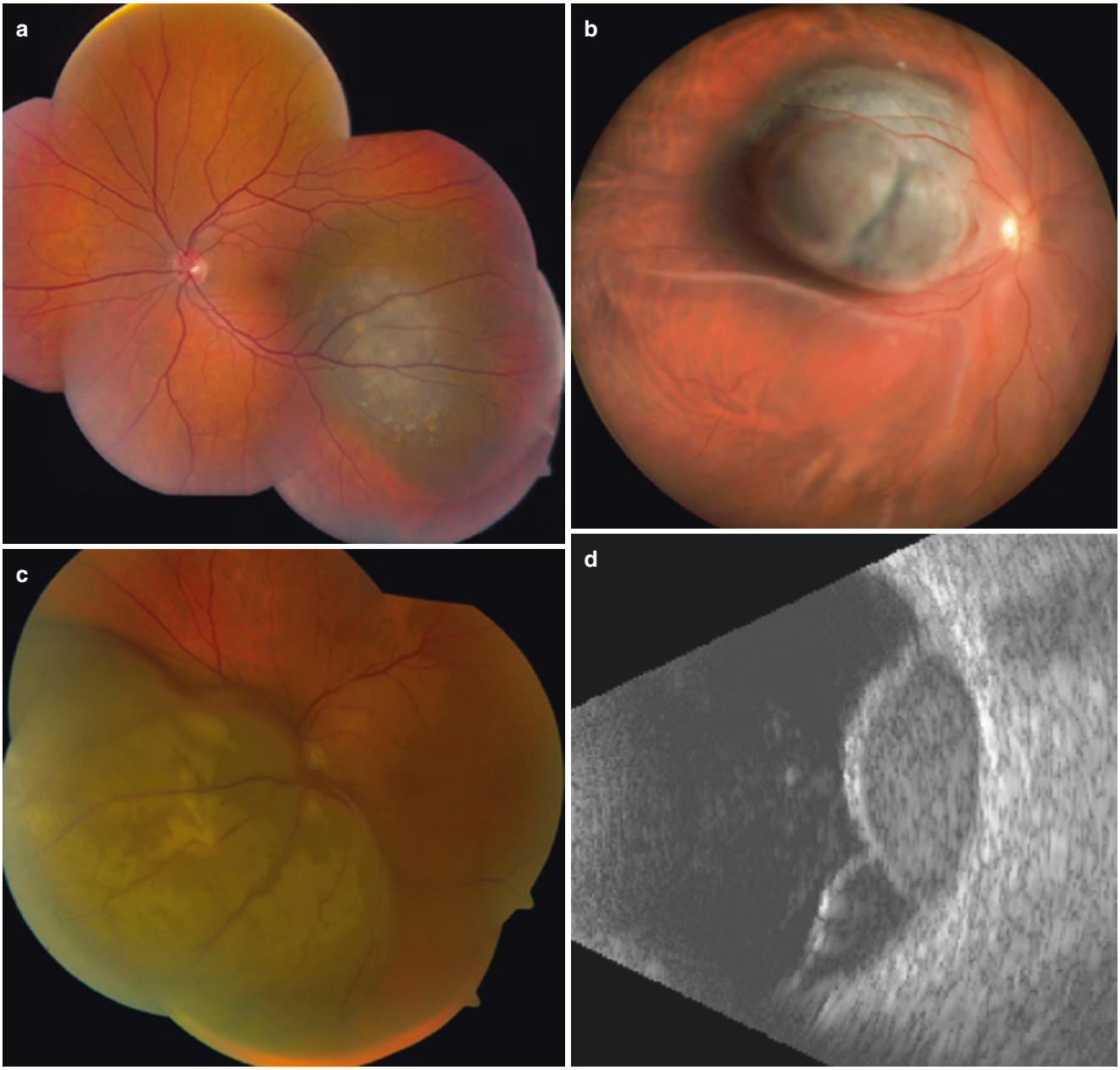

Fig. 2.3 Medium choroidal melanoma. (**a**) Medium choroidal melanoma with overlying orange pigment. (**b**) Medium choroidal melanoma with dependent subretinal fluid. (**c**) Medium juxtapapillary choroidal melanoma, visible on (**d**) ultrasonography and with dependent subretinal fluid

melanoma appears in one of three configurations including dome (75%), mushroom (20%), or diffuse (5%) (Figs. 2.5, 2.6, 2.7 and 2.8). Mushroom-shaped choroidal melanoma develops when the tumor breaks through Bruch's membrane and herniates into the subretinal space, giving a bilobed appearance to the tumor. Diffuse melanoma is flat and is often mistaken for a choroidal nevus (Shields et al. 2013b).

Choroidal melanoma appears as a mass deep to the retina, without retinal feeder vessels, and often producing retinal detachment. Occasionally subretinal hemorrhage is present from rupture in Bruch's membrane, and occasionally vitreous hemorrhage is present from retinal invasion. Both can obscure a view of the tumor. In these cases, the tumor can be visible on ocular ultrasonography or magnetic resonance imaging. Rarely, secondary glaucoma can develop. A melanoma or other neoplasm should be suspected in any eye that has unexplained hazy or opaque ocular media.

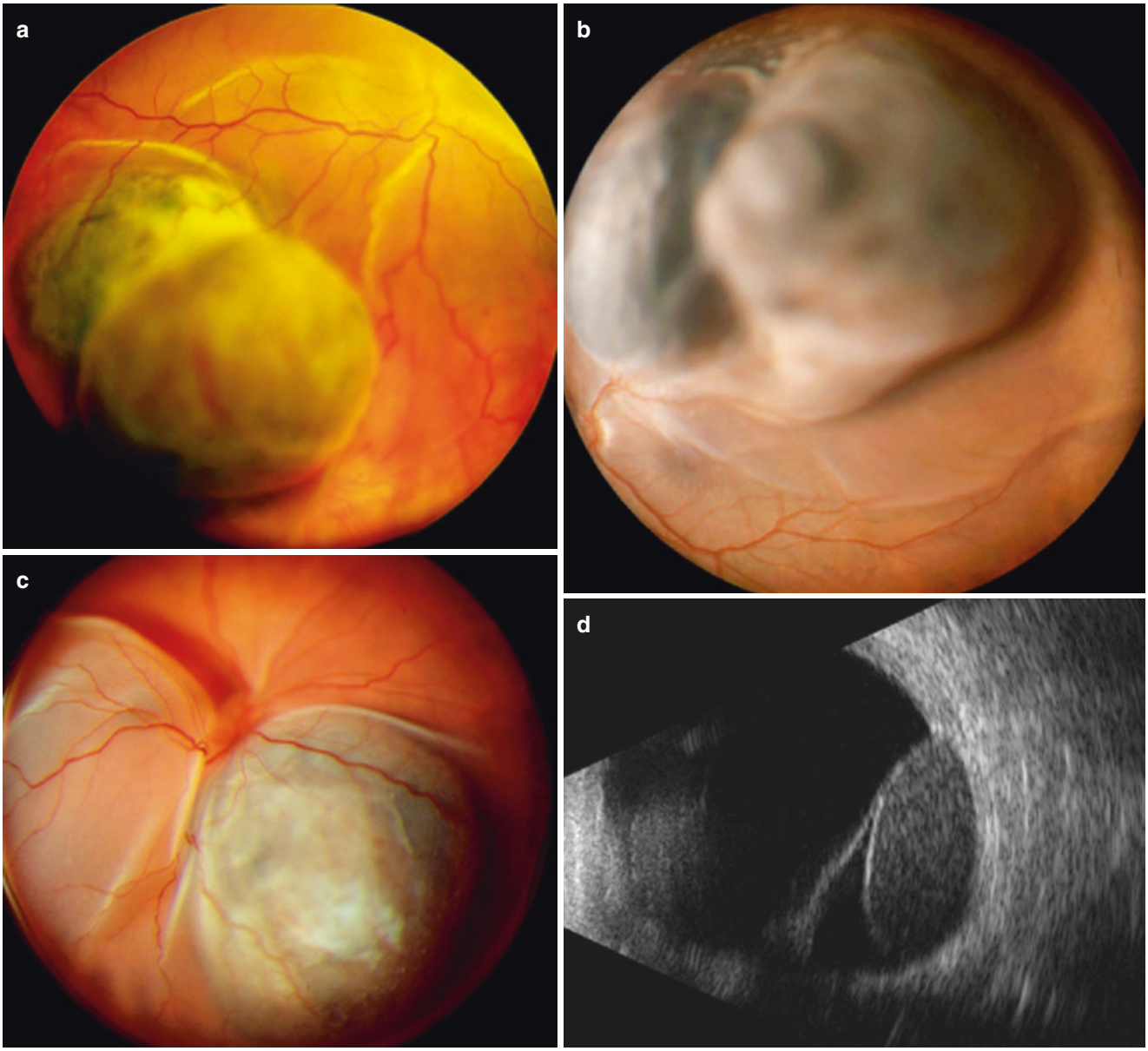

Fig. 2.4 Large choroidal melanoma. (**a**) Large choroidal melanoma with subretinal fluid. (**b**) Large choroidal melanoma with surface break in Bruch's membrane. (**c**) Large choroidal melanoma with subretinal fluid and pigment, visible on (**d**) ultrasonography

Choroidal melanoma is clinically grouped into three sizes based on tumor thickness including small (0–3.0 mm), medium (3.1–8.0 mm), and large (8.1 mm or greater). In the 1970s, the average melanoma thickness at diagnosis was 5.5 mm. This decreased to approximately 4.5 mm in the 1990s and is currently approximately 4.0 mm (Shields et al. 2009b). There is hope that efforts at early detection using the mnemonic "To Find Small Ocular Melanoma—Using Helpful Hints Daily" will assist in earlier recognition of melanoma and differentiation from nevus (Shields et al. 1995; Shields et al. 2000a; Shields et al. 2009a) (Table 2.2).

2.6 Classification

The American Joint Committee on Cancer (AJCC) staging manual, eighth edition, provides a detailed classification for posterior (ciliary body (CB) and choroid) uveal melanoma for prognostication. This classification categorizes melanoma based on tumor basal diameter and thickness, labeled as T1, T2, T3, and T4 24 (Table 2.3). Further classification regarding CB involvement and extraocular extension (EOE) is considered. Analysis of posterior uveal melanoma using the AJCC seventh edition classification confirmed the

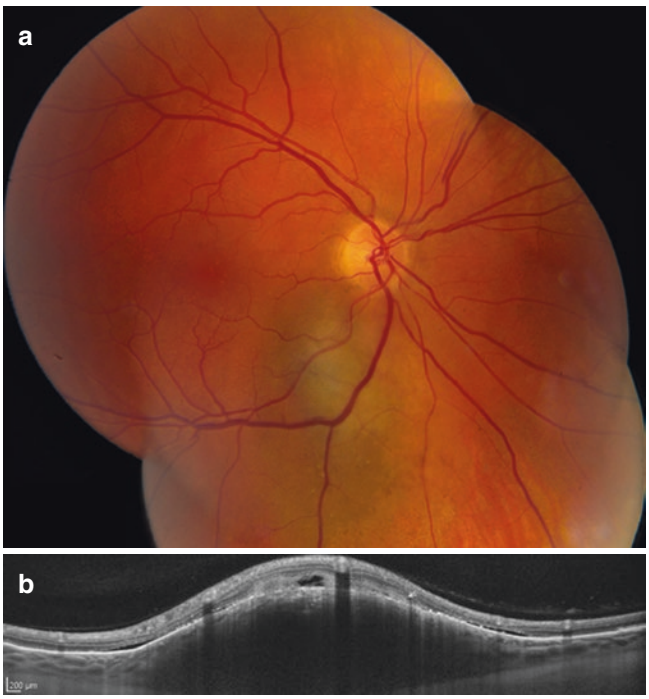

Fig. 2.5 Dome-shaped choroidal melanoma. (**a**) Small juxtapapillary choroidal melanoma with (**b**) shallow subretinal fluid and smooth dome-shape configuration on optical coherence tomography

predictive power (Shields et al. 2013a, 2015a; Kujala et al. 2013). Kaplan Meier estimates of metastasis at 10 years were 15% for T1, 25% for T2, 49% for T3, and 63% for T4 (Shields et al. 2013a). Compared with uveal melanoma classified as T1, the rate of metastasis and death was two times greater for T2, four times greater for T3, and eight times greater for T4 (Shields et al. 2013a).

2.7 Diagnostic Testing

The diagnosis of choroidal melanoma is generally based on a spectrum of findings during clinical examination. Ancillary testing using transillumination, fluorescein angiography, indocyanine green angiography, ultrasonography, enhanced depth imaging optical coherence tomography, autofluorescence, and fine-needle aspiration biopsy can also be helpful (Shields and Shields 2015a; Almeida et al. 2013; Shields et al. 2012b).

Transillumination is used to document the shadow caused by uveal melanoma and to rule out simulating conditions such as uveal effusion. The size of the shadow is helpful in determining the type and extent of treatment. Fluorescein angiography documents intrinsic tumor vascularity with early mottled hyperfluorescence and progressive increasing hyperfluorescence into the recirculation phase. Some larger melanomas, especially those with Bruch's membrane rupture, demonstrate "double circulation" showing intrinsic dilated tumor vessels and overlying normal retinal vessels. Flat, pigmented melanoma can be completely hypofluorescent. Indocyanine green angiography can better delineate the intratumoral blood vessels that may not be evident with ophthalmoscopy or standard fluorescein angiography.

B-scan ultrasonography demonstrates a dome-shaped, mushroom-shaped, or plateau-shaped choroidal mass with acoustic hollowness, choroidal excavation, and sometimes orbital shadowing. A-scan ultrasonography shows relatively low internal reflectivity within the tumor. With thicker tumors, spontaneous vascular pulsations can be visualized with dynamic standardized A-scan or B-scan ultrasonography. OCT depicts small melanoma within the choroid as dome shaped and often with overlying subretinal fluid that shows shaggy photoreceptors (Shields et al. 2012b) (Fig. 2.9). Larger tumors are not well imaged with OCT, but shallow subretinal fluid can be seen. Small to medium melanoma tends to show hyperautofluorescence from overlying orange pigment, representing lipofuscin (Almeida et al. 2013). In the occasional case that is atypical and defies diagnosis with less invasive measures, fine-needle aspiration biopsy (FNAB) can be employed to establish the diagnosis (Shields et al. 1993).

2.8 Cytogenetics

Cytogenetic analysis of melanoma using DNA or RNA methods can add to the prognostication of uveal melanoma. Regarding DNA evaluation, the original work from Prescher et al. demonstrated that uveal melanoma with chromosome 3 monosomy imparted poor prognosis with metastatic disease in 50% by 3 years (Prescher et al. 1996). Shields et al. reported on 1059 eyes with melanoma sampled by fine-needle aspiration biopsy for cytogenetics and noted increasing tumor thickness demonstrated greater cytogenetic alterations, suggesting that prompt management of small melanoma could reduce chromosomal instability and improve overall patient survival (Shields et al. 2017) (Table 2.4).

Regarding RNA evaluation, gene expression profiling (GEP) has been employed. Tschentscher et al. identified two groups of melanoma that correlated with monosomy 3 and disomy 3 tumors (Tschentscher et al. 2003). Walter et al. found Class 2 uveal melanomas (poor prognosis) had better prognosis when the tumor diameter was less than 12 mm at the time of treatment (Walter et al. 2016).

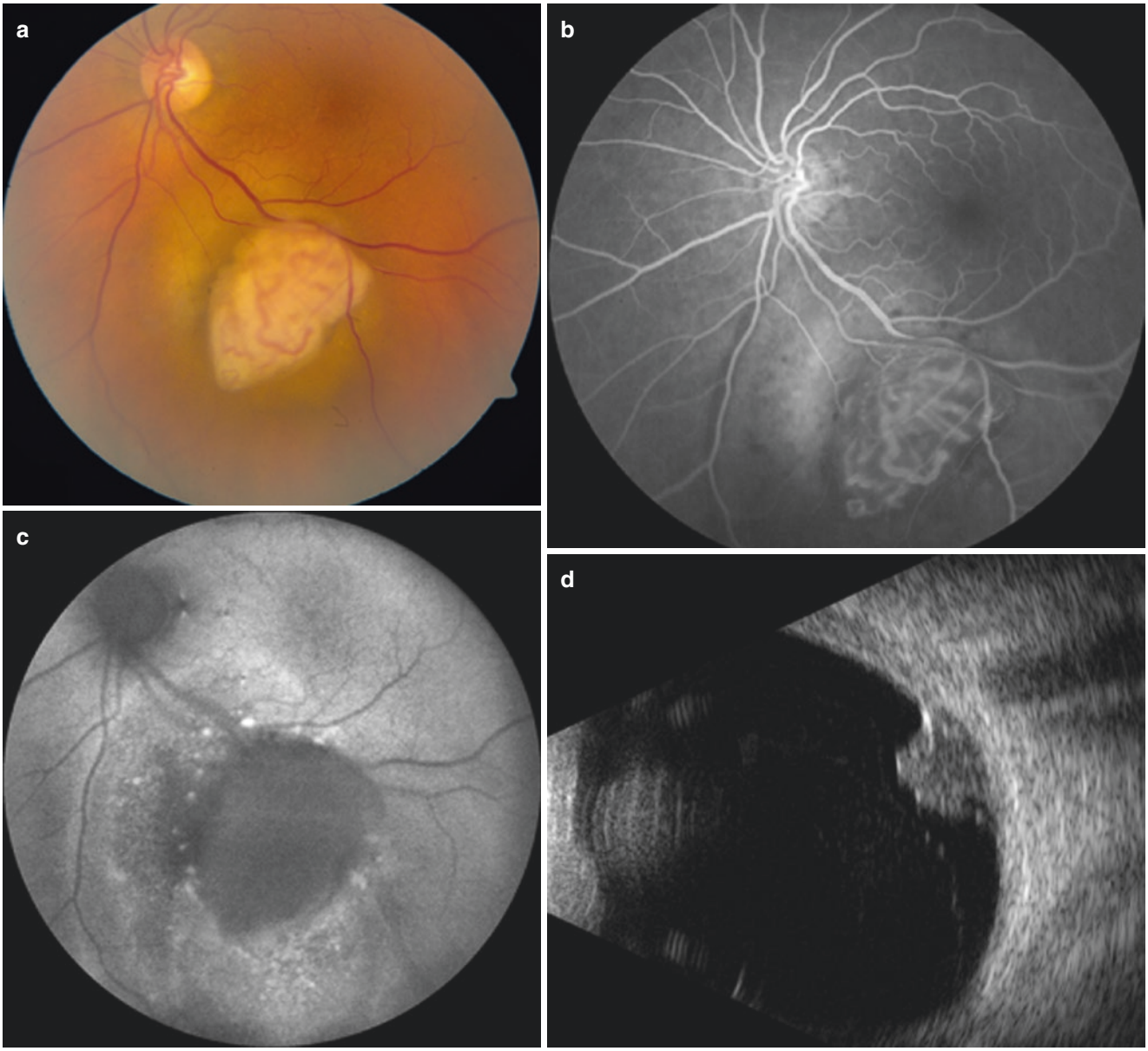

Fig. 2.6 Mushroom-shaped medium choroidal melanoma. (**a**) Mushroom-shaped medium choroidal melanoma with (**b**) "double circulation" on fluorescein angiography, (**c**) hyperautofluorescence from lipofuscin, and (**d**) small mushroom-shape on ultrasonography

2.9 Management

The management of posterior uveal melanoma depends on tumor size, location, associated features, status of the opposite eye, patient systemic status, and patient desire. Management choices for choroidal melanoma include transpupillary thermotherapy, plaque radiotherapy, charged particle irradiation, local resection, enucleation, orbital exenteration, and a new investigational nanoparticle therapy (AU-011) (Shields and Shields 2015a; Kaliki and Shields 2017; Shields and Shields 2015b). The two most frequently employed treatments for choroidal melanoma include enucleation or focal radiotherapy, using plaque radiotherapy or proton beam radiotherapy. The goal of treatment is to eradicate or inactivate the tumor before metastasis occurs. Systemic monitoring for metastatic disease is important using physical examination, blood studies for liver enzymes, chest X-ray, and magnetic resonance imaging (MRI) of the liver. Most patients have initial negative

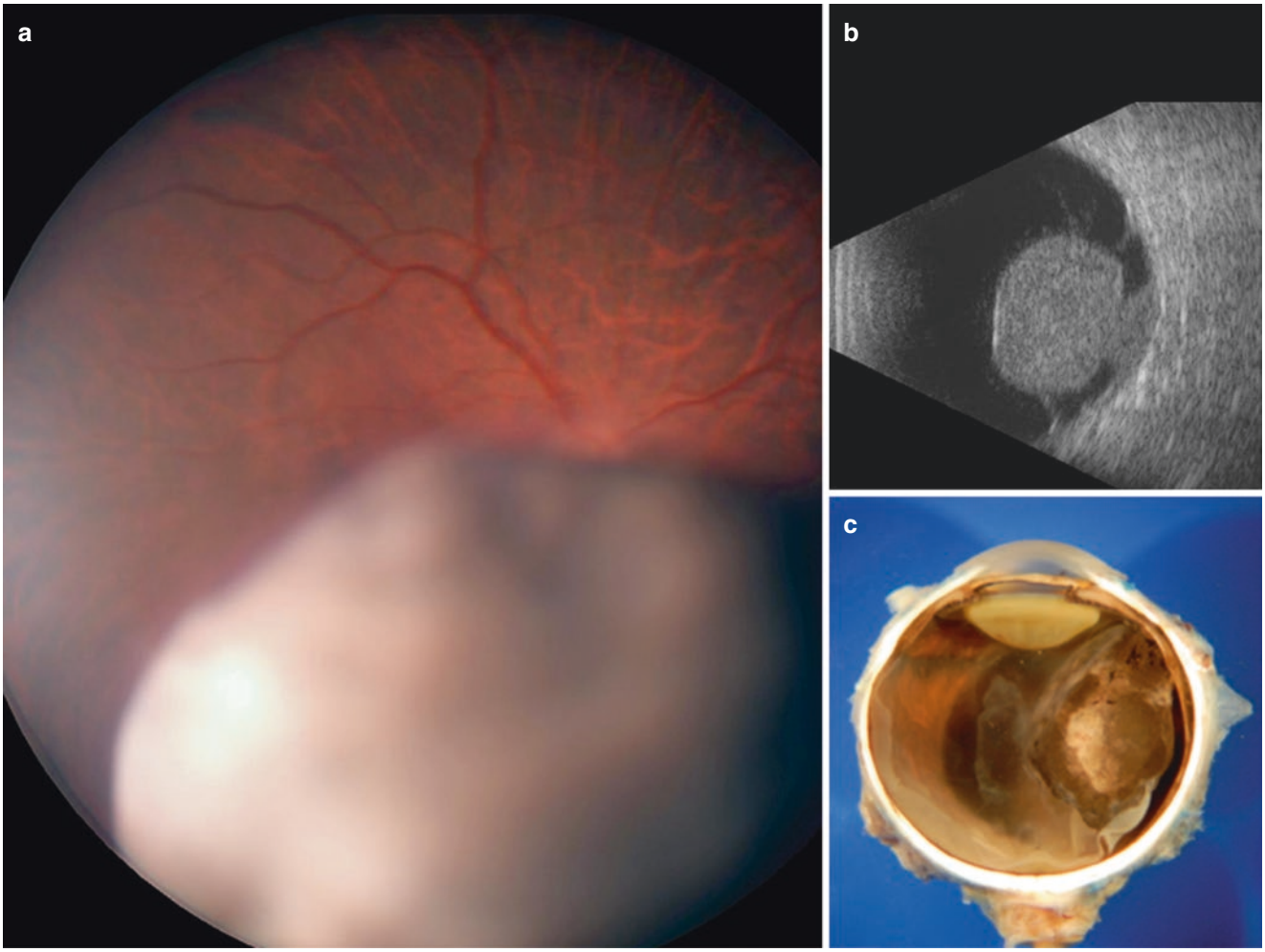

Fig. 2.7 Mushroom-shaped large choroidal melanoma. (**a**) Mushroom-shaped large choroidal melanoma overhanging the optic disc with (**b**) classic mushroom-shape on ultrasonography, (**c**) confirmed following enucleation

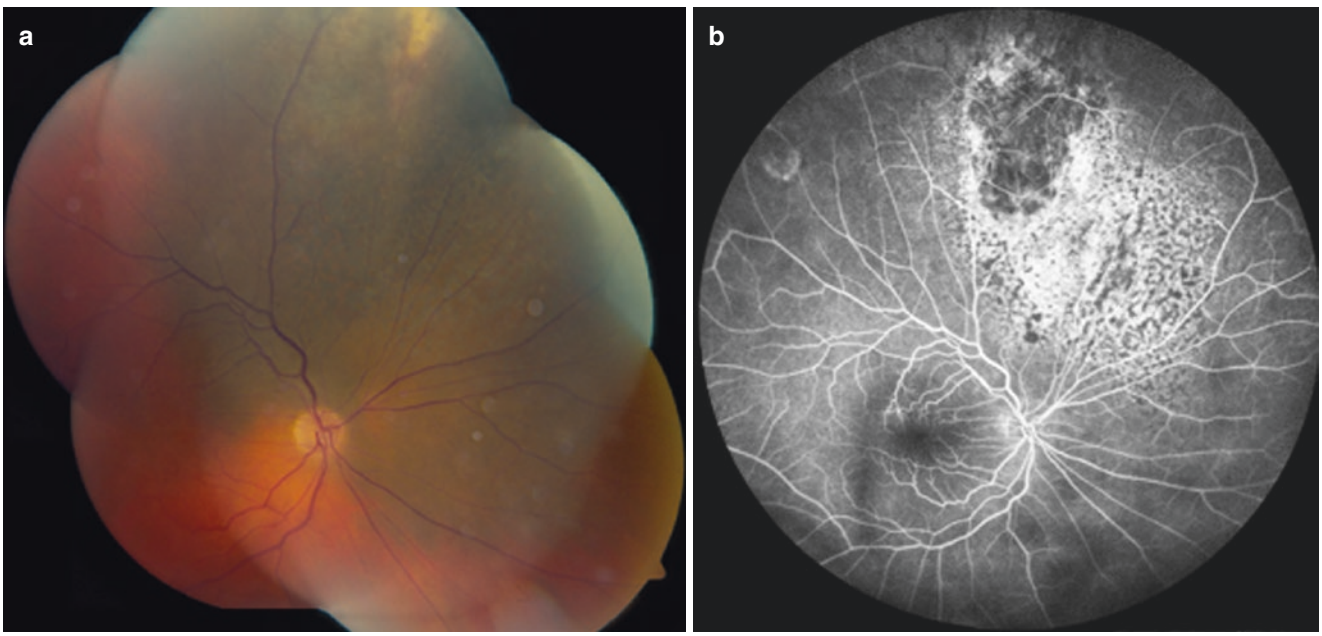

Fig. 2.8 Diffuse choroidal melanoma. (**a**) Extensive flat, diffuse choroidal melanoma, (**b**) showing diffuse hyperfluorescence on angiography, (**c**) mottled bright fluorescence on red-free image, and (**d**) plateau configuration on ultrasonography

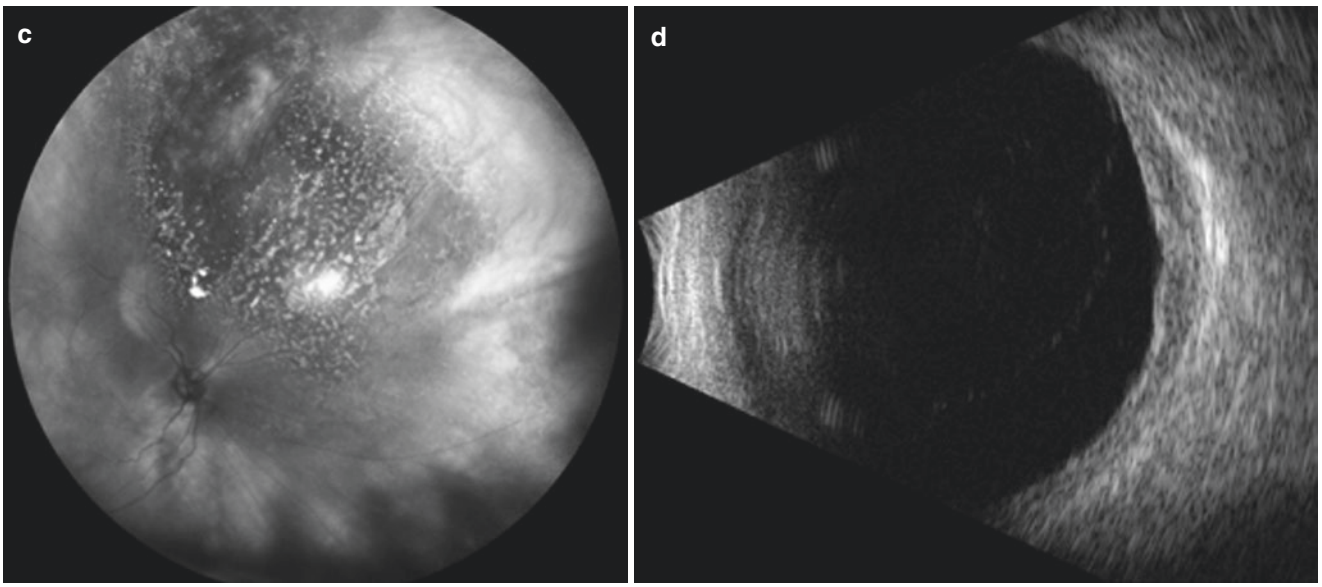

Fig. 2.8 (continued)

systemic evaluation, and metastatic disease is usually detected approximately 3–10 years later (Shields et al. 2009b).

Transpupillary thermotherapy (TTT) is a method of treatment for small, pigmented choroidal melanoma that is pigmented, 3 mm or less in thickness, outside the macular and juxtapapillary region, and with minimal related subretinal fluid or other risk factors (Mashayekhi et al. 2015). Focused heat is delivered to the tumor with an infrared diode laser. A large spot size of 3.0 mm and long exposure of 1 min per spot provide deep slow burns to the choroid, leading to focal choroidal atrophy. TTT is also used as consolidation therapy following plaque radiotherapy to minimize tumor recurrence.

Photodynamic therapy with verteporfin dye is occasionally used as a primary or secondary treatment for amelanotic melanoma, but large cohort analysis for outcomes has not yet been published.

Radiotherapy is effective for treatment of melanoma using a radioactive plaque (brachytherapy) or charged particles (proton beam or helium ion). The most commonly used radioactive isotopes for plaque include iodine 125 and ruthenium 106 (Shields et al. 2000b; Hawkins 2004; Collaborative Ocular Melanoma Study Group 2006; Sagoo et al. 2007, 2008, 2011). The Collaborative Ocular Melanoma Study (COMS) demonstrated that plaque radiotherapy provided equivalent life prognosis compared to enucleation for medium-sized melanoma (Hawkins 2004). For melanoma near the optic nerve, special notched radioactive plaques are used (Sagoo et al. 2007, 2008, 2011).

Local resection is a surgical method to excise melanoma and salvage the eye, particularly for those tumors located in the ciliary body or peripheral choroid. This technique, termed partial lamellar sclerouvectomy, allows removal of the tumor with a thin scleral base, leaving intact the outer sclera and the retina. It is a difficult surgical procedure and is best performed by ophthalmic oncologists who are experienced with such surgery.

Enucleation is employed for large melanoma or those where no useful vision can be expected with conservative methods. A replacement implant, such as hydroxyapatite, is used. When a melanoma demonstrates transscleral extension with massive orbital involvement, then eyelid-sparing orbital exenteration is warranted.

A new investigational laser-activated nanoparticle therapy (AU-011) is currently under trials for safety and efficacy. This medication could prove beneficial for small and medium melanoma (Kaliki and Shields 2017).

2.10 Prognosis

Patients with uveal melanoma are at risk for metastatic disease to the liver, lung, and skin. Systemic monitoring with physical examination and liver function tests twice yearly and chest radiograph and liver imaging using magnetic resonance imaging or ultrasonography annually are advised.

Shields et al. reviewed 8033 affected patients and found that each millimeter of increase thickness was related to 5%

Table 2.3 American Joint Committee on Cancer (AJCC 8th edition) classification of posterior uveal melanoma into tumor category and then tumor stage

Melanoma thickness (mm)	Tumor category (T1–T4)						
>15.0					4	4	4
12.1–15.0				3	3	4	4
9.1–12.0		3	3	3	3	3	4
6.1–9.0	2	2	2	2	3	3	4
3.1–6.0	1	1	1	2	2	3	4
≤ 3.0	1	1	1	1	2	2	4
	≤3.0	3.1–6 0.0	6.1–9.0	9.1–12.0	12.1–15.0	15.1–18.0	>18.0
	Melanoma basal diameter (mm)						

Tumor subcategory		
Primary tumor (T)	Ciliary body involvement	Extraocular extension
T1		
T1a	No	No
T1b	Yes	No
T1c	No	Yes ≤5 mm diameter
T1d	Yes	Yes ≤5 mm diameter
T2		
T2a	No	No
T2b	Yes	No
T2c	No	Yes ≤5 mm diameter
T2d	Yes	Yes ≤5 mm diameter
T3	Yes or no	Yes or no
T3a	No	No
T3b	Yes	No
T3c	No	Yes ≤5 mm diameter
T3d	Yes	Yes ≤5 mm diameter
T4		
T4a	No	No
T4b	Yes	No
T4c	No	Yes ≤5 mm diameter
T4d	Yes	Yes ≤5 mm diameter
T4e	Any tumor size with extraocular extension >5 mm diameter	

Tumor stage			
Tumor category (T)	Node (N)	Metastasis (M)	Stage
T1a	N0	MO	I
T1b–d	N0	MO	IIA
T2a	N0	MO	IIA
T2b	N0	MO	IIB
T3a	N0	MO	IIB
T2c–d	N0	MO	IIIA
T3b–c	N0	MO	IIIA
T4a	N0	MO	IIIA
T3d	N0	MO	IIIB
T4b–c	N0	MO	IIIB
T4d–e	N0	MO	IIIC
Any T	N1	MO	IV
Any T	Any N	M1	IV

Adapted from Kivela T, Simpson ER, Grossniklaus HE, et al. Uveal melanoma. In Amin MB, Edge SB, Greene FL, et al.,, eds. In: AJCC Cancer Staging Manual. 8th ed. New York, NY: Springer; 2017:805–15

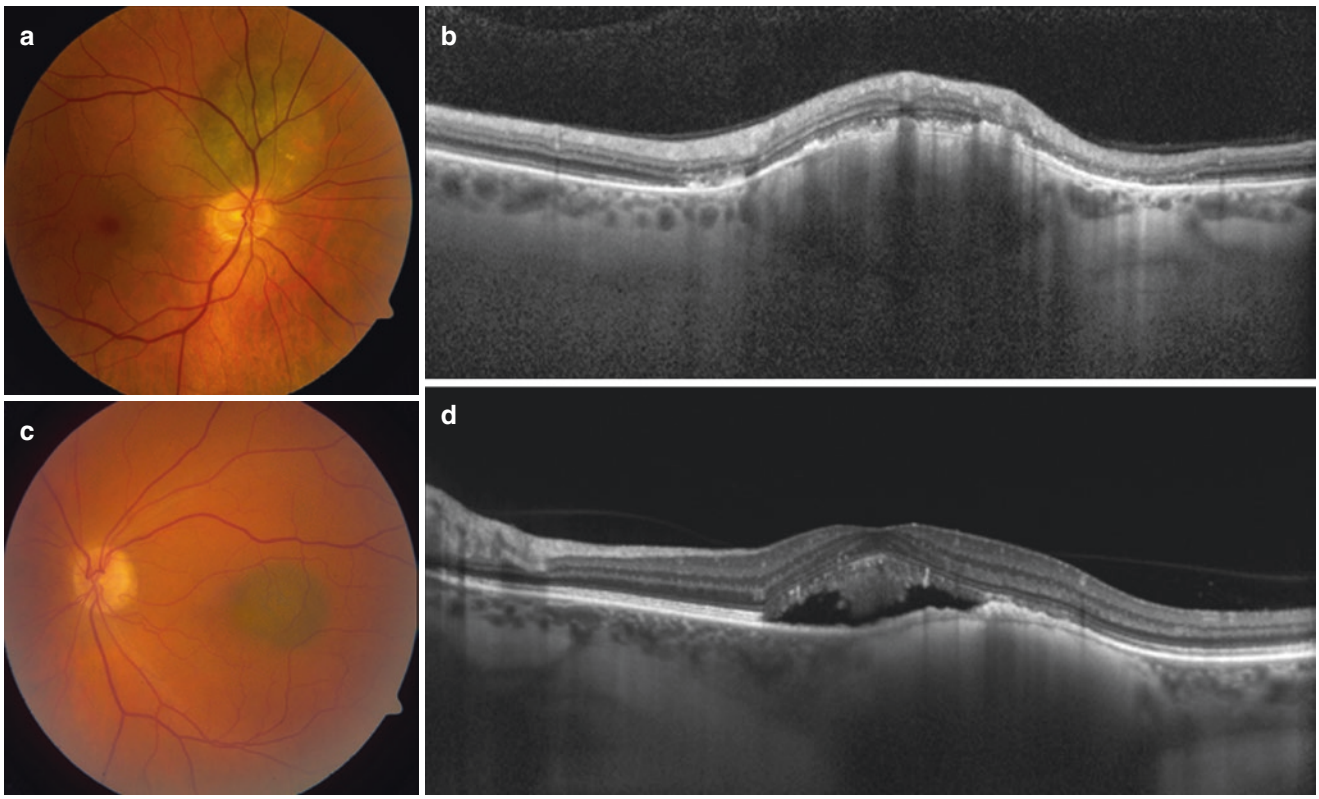

Fig. 2.9 Optical coherence tomography (OCT) of small choroidal melanoma. (**a**) Small, juxtapapillary choroidal melanoma with (**b**) OCT features of dome-configuration and overlying trace subretinal fluid with other retinal hyper-reflectivity. (**c**) Small, submacular choroidal melanoma with (**d**) OCT features of dome configuration and overlying moderate subretinal fluid with shaggy photoreceptors and thickening of the retinal pigment epithelial layer which could represent lipofuscin (orange pigment)

Table 2.4 Uveal melanoma prognosis based on high-risk cytogenetics based on chromosomes 3, 6, and 8 alterations

Chr 3	Chr 6q loss/gain	Chr 6p loss/gain	Chr 8q gain	Chr 8p loss/gain	# Cases (%)	# Metastasis (%)	KM estimate to metastasis†			p-value	Hazard ratio§
							1-year	3-year	5-year		
0	0	0	0	0	189 (35)	2 (1)	0.78	0.78	3.7		1.00
0	0	Gain	0	0	38 (7)	2 (5)	2.8 [0–8.1]	2.8 [0–8.1]	14.9 [0–38]	0.131	4.54
0	Loss	0	Gain	Gain	1 (<1)	1 (100)	0	100	100	<0.001	197
0	Loss	Gain	Gain	0	18 (3)	1 (6)	0	0	33.3 [0–87]	0.155	5.74
Loss	0	0	0	0	47 (9)	1 (2)	0	7.7 [0–22]	7.7 [0–22]	0.449	2.53
Loss	0	0	Gain	0	51 (10)	12 (24)	7.7 [0–16]	27.4 [12–43]	38.7 [19–58]	<0.001	19.5
Loss	0	0	Gain	Loss	34 (6)	4 (12)	3.3 [0–10]	28.4 [3–53]	NE	<0.001	31.6
Loss	0	0	Gain	Gain	17 (3)	2 (12)	14.3 [0–40]	14.3 [0–40]	NE	0.019	18.3
Loss	0	Gain	Gain	0	13 (2)	2 (15)	0	28.6 [0–62]	28.6 [0–62]	0.018	10.6
Loss	0	Gain	Gain	Gain	2 (<1)	0 (0)	0	NE	NE	–	–
Loss	Loss	0	0	0	3 (<1)	0 (0)	0	0	0	–	–
Loss	Loss	0	Gain	0	2 (<1)	1 (50)	0	100	100	0.001	60.9
Loss	Loss	0	Gain	Loss	5 (1)	3 (60)	20 [0–55]	60 [17–100]	NE	<0.001	123

(continued)

Table 2.4 (continued)

Chr 3	Chr 6q loss/gain	Chr 6p loss/gain	Chr 8q gain	Chr 8p loss/gain	# Cases (%)	# Metastasis (%)	KM estimate to metastasis†			p-value	Hazard ratio§
							1-year	3-year	5-year		
Loss	Loss	0	Gain	Gain	2 (<1)	0 (0)	0	0	NE	–	–
Loss	Loss	Loss	Gain	0	1 (<1)	1 (100)	0	0	100	0.002	49.3
Loss	Loss	Gain	0	0	2 (<1)	0 (0)	0	NE	NE	–	–
Loss	Loss	Gain	Gain	0	5 (1)	2 (40)	50 [1–99]	50 [1–99]	NE	<0.001	77.2
Loss	Loss	Gain	Gain	Loss	6 (1)	1 (17)	25 [0–67]	NE	NE	<0.001	113.1
Partial loss	0	0	Gain	Loss	2 (<1)	1 (50)	50 [0–100]	NE	NE	<0.001	141
Partial loss	0	Gain	Gain	0	1 (<1)	1 (100)	0	0	100	0.006	29.4

Adapted from Shields CL, Say EAT, Hasanreisoglu M, et al. Personalized uveal melanoma prognosis based on cytogenetic profile in 1059 cases over an 8-year period. The 2017 Harry S. Gradle Lecture. Ophthalmology 2017;124:1523–1531

Table 2.5 Choroidal pseudomelanomas in 1739 cases. Most common diagnoses

Rank	Diagnosis	Number	%
1	Choroidal nevus	851	49
2	Peripheral exudative hemorrhagic chorioretinopathy	139	8
3	Congenital hypertrophy of retinal pigment epithelium	108	6
4	Idiopathic hemorrhagic detachment retina or pigment epithelium	86	5
5	Circumscribed choroidal hemangioma	79	5
6	Age-related macular degeneration	76	4
7	Hyperplasia or RPE	42	2
8	Optic disc melanocytoma	37	2
9	Choroidal metastasis	34	2
10	Hemorrhagic choroidal detachment	29	2
11	Vasoproliferative tumor	20	1
12	Rhegmatogenous retinal detachment	18	1
13	Choroidal detachment	17	1
14	Uveal effusion syndrome	17	1
15	Choroidal or disc granuloma	14	1
16	Adenoma RPE or CPE	13	<1
17	Sclerochoroidal calcification	12	1
18	Staphyloma	12	1
19	Cataract	10	1
20	Retinal capillary hemangioma (capillary or cavernous)	10	1
21	Adenoma of nonpigmented ciliary body epithelium	10	<1
22	Leiomyoma, ciliary body	10	<1
23	Degenerative retinoschisis	8	<1
24	Retinal cavernous hemangioma	7	<1
25	Chorioretinal scar	7	<1
26	Vortex vein varix	7	<1
27	Vitreous hemorrhage	7	<1
28	Choroidal osteoma	5	<1
29	Preretinal macular gliosis	5	<1
30	Scleritis	5	<1

Adapted from Shields JA, Mashayekhi A, Ra S, Shields CL. Pseudomelanomas of the posterior uveal tract. The 2006 Taylor Smith Lecture. Retina 2005;25:767–71

increased rate of metastasis (Shields et al. 2009b). In addition, ocular melanocytosis imparts a 1.9–2.6 times higher risk for metastasis (Collaborative Ocular Melanoma Study Group 2006).

The Collaborative Ocular Melanoma Study (COMS) included three trials regarding large, medium, and small choroidal melanoma. The large tumor trial showed no difference in patient survival when comparing enucleation versus pre-enucleation radiation groups (Hawkins 2004). The medium tumor trial showed no difference in patient survival when comparing enucleation versus plaque radiotherapy (Collaborative Ocular Melanoma Study Group 2006). The cumulative all-cause mortality at 12 years was 43% for patients in the plaque radiotherapy group versus 41% for those in the enucleation group. The small tumor trial showed that small choroidal melanomas managed by observation showed tumor growth in 21% by 2 years and 31% by 5 years (The Collaborative Ocular Melanoma Study Group 1997).

2.11 Pseudomelanoma

There are conditions that can clinically simulate melanoma, leading to diagnostic difficulty. In an analysis of 12,000 patients referred for possible uveal melanoma over a 25-year period, 1739 were found to have pseudomelanoma (Shields et al. 2014; Shields et al. 2005). The most frequent included choroidal nevus (49%), peripheral exudative hemorrhagic chorioretinopathy (PEHCR) (8%), congenital hypertrophy of the retinal pigment epithelium (CHRPE) (6%), hemorrhagic detachment of the retina or retinal pigment epithelium (5%), circumscribed choroidal hemangioma (5%), and age-related macular degeneration (4%) (Fig. 2.10) (Table 2.5).

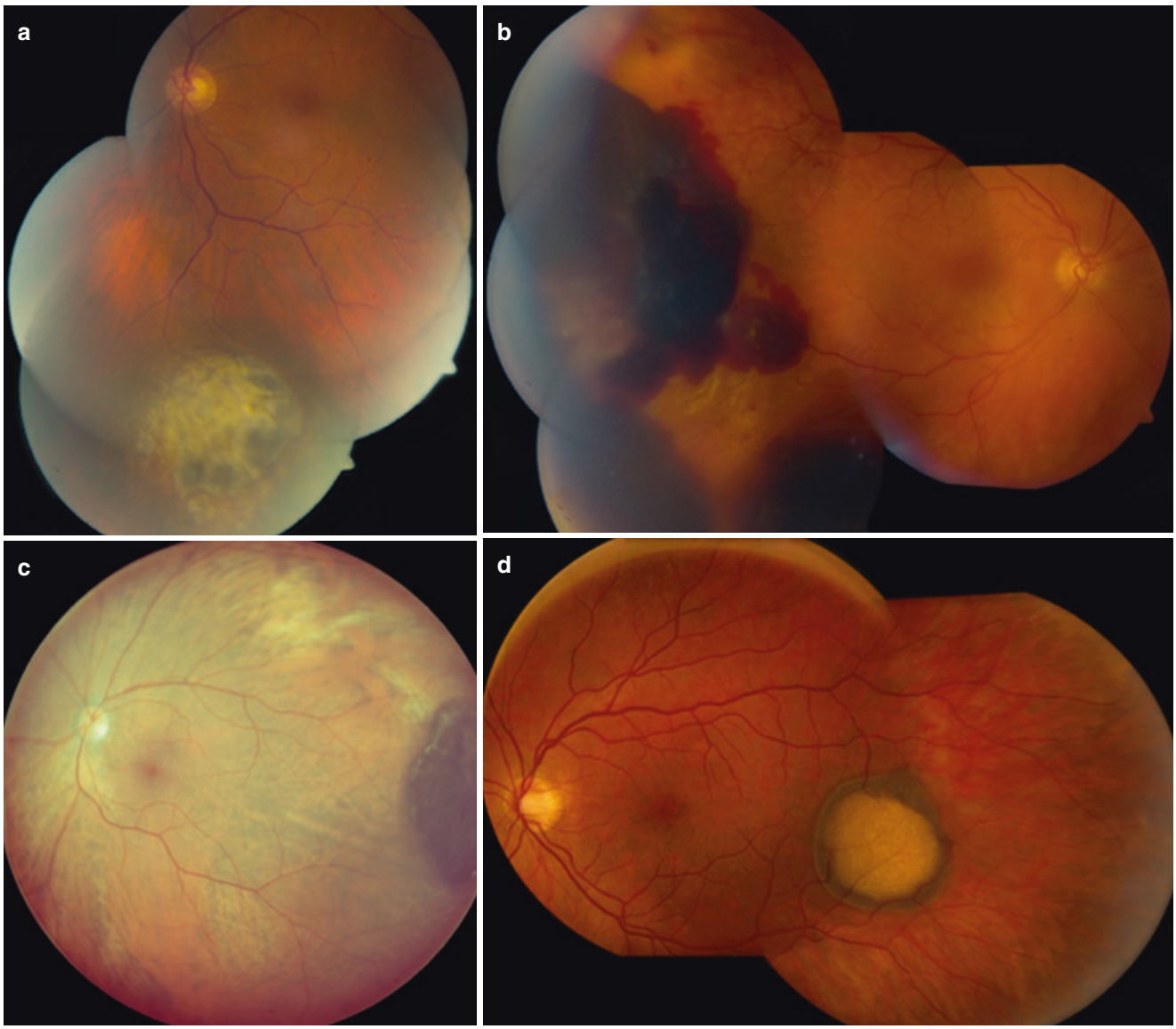

Fig. 2.10 Choroidal pseudomelanoma. (**a**) Choroidal nevus with overlying drusen. (**b**) Peripheral exudative chorioretinopathy with hemorrhagic pigment epithelial detachment and subretinal hemorrhage. (**c**) Congenital hypertrophy of the retinal pigment epithelium. (**d**) Choroidal nevus with giant overlying pigment epithelial detachment

2.12 Summary

Choroidal melanoma is a malignant tumor with moderate risk for metastasis and death. Patients with choroidal nevus should be evaluated for possible risk factors suggestive of transformation into melanoma. Early detection of melanoma is important, particularly when the tumor is small, to minimize risk for metastasis. Patients with suspected choroidal melanoma should have prompt ocular treatment.

References

Almeida A, Kaliki S, Shields CL. Autofluorescence of intraocular tumours. Curr Opin Ophthalmol. 2013;24:222–32.

Chang AE, Karnell LH, Menck HR. The National Cancer Data Base report on cutaneous and noncutaneous melanoma: a summary of 84,836 cases from the past decade. The American College of Surgeons Commission on Cancer and the American Cancer Society. Cancer. 1998;83:1664–78.

Collaborative Ocular Melanoma Study Group. The COMS randomized trial of iodine 125 brachytherapy for choroidal melanoma: V. twelve-year mortality rates and prognostic factors: COMS report No. 28. Arch Ophthalmol. 2006;124:1684–93.

Gupta MP, Lane AM, DeAngelis MM, et al. Clinical characteristics of uveal melanoma in patients with germline BAP1 mutations. JAMA Ophthalmol. 2015;133:881–7.

Hawkins BS. The Collaborative Ocular Melanoma Study (COMS) randomized trial of pre-enucleation radiation of large choroidal melanoma: IV. Ten-year mortality findings and prognostic factors. COMS report number 24. Am J Ophthalmol. 2004;138:936–51.

Kaliki S, Shields CL. Uveal melanoma: relatively rare but deadly cancer. Eye (Lond). 2017;31:241–57.

Kivela T. The epidemiological challenge of the most frequent eye cancer: retinoblastoma, an issue of birth and death. Br J Ophthalmol. 2009;93:1129–31.

Kujala E, Damato B, Coupland SE, et al. Staging of ciliary body and choroidal melanomas based on anatomic extent. J Clin Oncol. 2013;31:2825–31.

Mashayekhi A, Shields CL, Rishi P, Shields JA, et al. Primary transpupillary thermotherapy for choroidal melanoma in 391 cases: importance of risk factors in tumor control. Ophthalmology. 2015;122:600–9.

Prescher G, Bornfeld N, Hirche H, et al. Prognostic implications of monosomy 3 in uveal melanoma. Lancet. 1996;347:1222–5.

Qiu M, Shields CL. Choroidal nevus in the United States adult population: racial disparities and associated factors in the national health and nutrition examination survey. Ophthalmology. 2015;122:2071–83.

Rai K, Pilarski R, Cebulla CM, et al. Comprehensive review of BAP1 tumor predisposition syndrome with report of two new cases. Clin Genet. 2016;89:285–94.

Rishi P, Shields CL, Khan MA, et al. Headache or eye pain as the presenting feature of uveal melanoma. Ophthalmology. 2013;120:1946–7.

Sagoo MS, Shields CL, Mashayekhi A, et al. Plaque radiotherapy for choroidal melanoma encircling the optic disc (circumpapillary choroidal melanoma). Arch Ophthalmol. 2007;125:1202–9.

Sagoo MS, Shields CL, Mashayekhi A, et al. Plaque radiotherapy for juxtapapillary choroidal melanoma overhanging the optic disc in 141 consecutive patients. Arch Ophthalmol. 2008;126:1515–22.

Sagoo MS, Shields CL, Mashayekhi A, et al. Plaque radiotherapy for juxtapapillary choroidal melanoma: tumor control in 650 consecutive cases. Ophthalmology. 2011;118:402–7.

Shah CP, Weis E, Lajous M, et al. Intermittent and chronic ultraviolet light exposure and uveal melanoma: a meta-analysis. Ophthalmology. 2005;112:1599–607.

Shields JA, Shields CL. Intraocular tumors: an atlas and textbook. 3rd ed. Philadelphia: Wolters Kluwer; 2015a.

Shields JA, Shields CL. Management of posterior uveal melanoma: past, present, and future: the 2014 Charles L. Schepens lecture. Ophthalmology. 2015b;122:414–28.

Shields JA, Shields CL, Ehya H, et al. Fine-needle aspiration biopsy of suspected intraocular tumors. The 1992 Urwick lecture. Ophthalmology. 1993;100:1677–84.

Shields CL, Shields JA, Kiratli H, et al. Risk factors for growth and metastasis of small choroidal melanocytic lesions. Trans Am Ophthalmol Soc. 1995;93:259–75.

Shields CL, Cater J, Shields JA, et al. Combination of clinical factors predictive of growth of small choroidal melanocytic tumors. Arch Ophthalmol. 2000a;118:360–4.

Shields CL, Shields JA, Cater J, et al. Plaque radiotherapy for uveal melanoma: long-term visual outcome in 1106 consecutive patients. Arch Ophthalmol. 2000b;118:1219–28.

Shields JA, Mashayekhi A, Ra S, et al. Pseudomelanomas of the posterior uveal tract: the 2006 Taylor R. smith lecture. Retina. 2005;25:767–71.

Shields CL, Furuta M, Berman EL, et al. Choroidal nevus transformation into melanoma: analysis of 2514 consecutive cases. Arch Ophthalmol. 2009a;127:981–7.

Shields CL, Furuta M, Thangappan A, et al. Metastasis of uveal melanoma millimeter-by-millimeter in 8033 consecutive eyes. Arch Ophthalmol. 2009b;127:989–98.

Shields CL, Kaliki S, Furuta M, et al. Clinical spectrum and prognosis of uveal melanoma based on age at presentation in 8,033 cases. Retina. 2012a;32:1363–72.

Shields CL, Kaliki S, Rojanaporn D, et al. Enhanced depth imaging optical coherence tomography of small choroidal melanoma: comparison with choroidal nevus. Arch Ophthalmol. 2012b;130:850–6.

Shields CL, Kaliki S, Furuta M, et al. American joint committee on cancer classification of posterior uveal melanoma (tumor size category) predicts prognosis in 7731 patients. Ophthalmology. 2013a;120:2066–71.

Shields CL, Kaliki S, Furuta M, et al. Diffuse versus nondiffuse small (</= 3 MM thickness) choroidal melanoma: comparative analysis in 1,751 cases. The 2012 F. Phinizy Calhoun lecture. Retina. 2013b;33:1763–76.

Shields CL, Kaliki S, Livesey M, et al. Association of ocular and oculodermal melanocytosis with the rate of uveal melanoma metastasis: analysis of 7872 consecutive eyes. JAMA Ophthalmol. 2013c;131:993–1003.

Shields CL, Manalac J, Das C, et al. Choroidal melanoma: clinical features, classification, and top 10 pseudomelanomas. Curr Opin Ophthalmol. 2014;25:177–85.

Shields CL, Kaliki S, Furuta M, et al. American joint committee on cancer classification of uveal melanoma (anatomic stage) predicts prognosis in 7,731 patients: the 2013 Zimmerman lecture. Ophthalmology. 2015a;122:1180–6.

Shields CL, Kels JG, Shields JA. Melanoma of the eye: revealing hidden secrets, one at a time. Clin Dermatol. 2015b;33:183–96.

Shields CL, Say EAT, Hasanreisoglu M, Saktanasate J, Lawson BM, Landy JE, Badami AU, Sivalingam MD, Mashayekhi A, Shields JA, Ganguly A. Cytogenetic abnormalities in uveal melanoma based on tumor features and size in 1059 patients: the 2016 W. Richard green lecture. Ophthalmology. 2017;124:609–18.

Singh AD, Topham A. Incidence of uveal melanoma in the United States: 1973-1997. Ophthalmology. 2003;110:956–61.

Singh AD, De Potter P, Fijal BA, et al. Lifetime prevalence of uveal melanoma in white patients with oculo(dermal) melanocytosis. Ophthalmology. 1998;105:195–8.

Singh AD, Kalyani P, Topham A. Estimating the risk of malignant transformation of a choroidal nevus. Ophthalmology. 2005;112:1784–9.

The Collaborative Ocular Melanoma Study Group. Factors predictive of growth and treatment of small choroidal melanoma: COMS report no. 5. Arch Ophthalmol. 1997;115:1537–44.

Tschentscher F, Husing J, Holter T, et al. Tumor classification based on gene expression profiling shows that uveal melanomas with and without monosomy 3 represent two distinct entities. Cancer Res. 2003;63:2578–84.

Walter SD, Chao DL, Feuer W, et al. Prognostic implications of tumor diameter in association with gene expression profile for uveal melanoma. JAMA Ophthalmol. 2016;134:734–40.

Weis E, Shah CP, Lajous M, et al. The association between host susceptibility factors and uveal melanoma: a meta-analysis. Arch Ophthalmol. 2006;124:54–60.

Choroidal Metastasis

3

Greg Bever, Armin Afshar, and Bertil Damato

3.1 Introduction

Uveal metastasis is the most common intraocular malignancy and can often be the presenting finding for the primary tumor (Konstantinidis et al. 2014; Shields et al. 1997a, b). Within the uveal tract, metastatic lesions most commonly locate to the choroid (88% of cases) and less frequently to the iris (9% of cases) and the ciliary body (2% of cases) (Shields et al. 1997a, b). Histologic studies have suggested that, of patients that have died with metastatic carcinoma, an estimated 5% may have ocular involvement (Eliassi-Rad et al. 1996).

A diagnosis of ocular metastasis can be incredibly distressing to a patient. For patients without a known malignancy, such a finding triggers an extensive systemic workup and is often associated with advanced systemic malignancy. For patients who already have known advanced and/or metastatic disease, a lesion found in the eye can lead to rightful worry about impending vision loss and subsequent decrease in the quality of life. Additionally, uveal metastasis can be mistaken for inflammatory lesions and delay appropriate treatment. It is important to keep these considerations in mind when counseling patients and their family.

3.2 Epidemiology

The most common sources of choroidal metastasis are breast cancer followed by lung cancer (Shields et al. 1997a, b). Other primary malignancies that have, less commonly, been found to metastasize to the choroid (in descending order of frequency) include gastrointestinal, prostate, kidney, and skin cancers (Shields et al. 1997a, b). Rarely, choroidal metastases can arise from primary cancers of the uterus, thyroid, bone, adrenal gland, ovary, and testicle (Shields et al. 1997a, b).

Nearly all patients with intraocular metastasis from breast cancer report known disease at the time of discovery of the intraocular involvement (Damato et al. 2017). Intraocular metastasis from breast cancer presents at a mean age of 57 years and at a median of 2 years after the diagnosis of the primary tumor, with ocular presentation being sooner in more advanced primary disease (Damato et al. 2017). Only about 50% of patients with uveal metastasis from lung cancer have a known history of the primary tumor at time of ocular diagnosis; the mean age is 63 years (Damato et al. 2017). Compared to breast cancer, patients with metastatic lung cancer have a much shorter interval between diagnosis of the primary tumor and presentation of ocular metastasis (Damato et al. 2017). By the time a primary malignancy has metastasized to the choroid, it has usually spread to other organs. Nonocular metastases (usually involving the lung, bone, liver, or brain) are evident or later develop in about 75% of patients with ocular metastases (Damato et al. 2017).

3.3 Clinical Features

The most common symptom of intraocular metastasis is blurred vision, which is usually caused by macular involvement of macular edema, retinal detachment, or the tumor itself (Konstantinidis et al. 2014). One large study of 109 eyes found that symptoms at presentation included blurred vision or loss of vision in 55% of cases, metamorphopsia in 12%, ocular pain in 12%, floaters in 12%, photopsia in 14%, and visual field defects in 16%, while 14% of cases remained asymptomatic (Konstantinidis et al. 2014). Pain is caused by conditions such as neovascular glaucoma or uveitis, but unexplained pain has also been reported (Konstantinidis et al. 2014; Shah et al. 2014). Ocular pain without any apparent cause can help differentiate choroidal

G. Bever · A. Afshar
Department of Ophthalmology, University of California, San Francisco, CA, USA

B. Damato (✉)
Department of Ophthalmology, University of California, San Francisco, CA, USA

Nuffield Department of Clinical Neurosciences, West Wing, John Radcliffe Hospital, University of Oxford, Oxford, UK

D. Rojanaporn (ed.), *Ocular Oncology*, https://doi.org/10.1007/978-981-13-2336-2_3

metastasis from lesions such as uveal melanoma, which is not painful in the absence of glaucoma or uveitis.

On ophthalmoscopy, choroidal metastases usually appear as a creamy white or pale yellow mass and are often associated with overlying subretinal fluid or complete retinal detachment (Fig. 3.1). Rarely, lesions can have an orange/red color which may indicate thyroid, renal, or carcinoid origin (Konstantinidis and Damato 2017). Metastases from cutaneous melanomas can appear amelanotic, brown, gray, or tan. Though not typical, there have been descriptions of pigmented choroidal tumors in cases of breast or lung cancer metastasis. Clusters of dark pigment and/or orange lipofuscin may be present on the tumor surface giving a "leopard skin" appearance (Konstantinidis and Damato 2017). Unlike uveal melanoma, choroidal metastases usually do not have visible intratumoral blood vessels on ophthalmoscopy and tend to be flat or plateau shaped. Mushroom-shaped metastases are very rare.

Most choroidal metastases are postequatorial with up to 40% being located in the macula (Freedman and Folk 1987). There can be optic nerve involvement via spread from adjacent choroid or direct invasion of the optic nerve itself. Such involvement causes yellow-white thickening of the nerve and/or optic disc swelling. Large studies report the mean number of metastatic lesions per eye to be between 1.4 and 1.6 (Konstantinidis et al. 2014; Shields et al. 1997a, b). About a third of patients have more than one metastatic lesion in the same eye, while a third of patients have bilateral metastases; these multiple and bilateral lesions are more common with breast cancer (Damato et al. 2017).

As this chapter is dedicated specifically to choroidal metastasis, we will not discuss ciliary body, iris, or retinal metastases. They are much less common than choroidal metastases.

Fig. 3.1 Fundus photograph showing a choroidal metastatic lesion in the macula of the left eye of a 58-year-old man with lung cancer

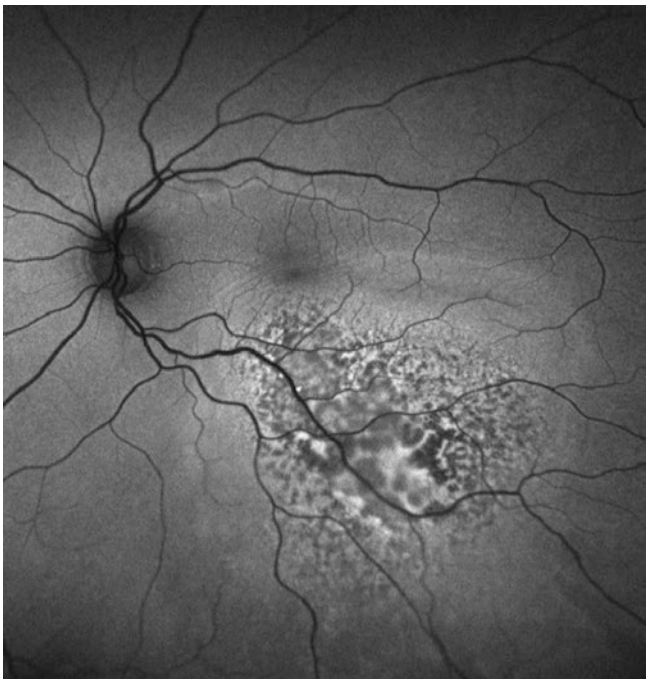

Fig. 3.2 Fundus autofluorescence imaging showing hyperfluorescent lipofuscin and hypofluorescent stippling in a choroidal metastatic lesion from lung cancer

3.4 Diagnostic Evaluation

3.4.1 Color Photography

Photography is useful for documenting tumor number, size, and extent (Fig. 3.1) which can help facilitate care over many years and between different providers. Care must be taken when making a diagnosis on the basis of color photography because some cameras such as the Optos (Optos, Dunfermline, Scotland) may distort the true tumor color and falsely suggest pigmentation of the lesion. It is, therefore, preferably to reply on ophthalmoscopy when making a diagnosis.

3.4.2 Fundus Autofluorescence

On autofluorescence, choroidal metastasis shows hyper- and hypofluorescent stippling in areas where the retinal pigment epithelium is disturbed (Fig. 3.2). Autofluorescence imaging may also highlight clumps of hyperfluorescent lipofuscin that are difficult to appreciate on ophthalmoscopy.

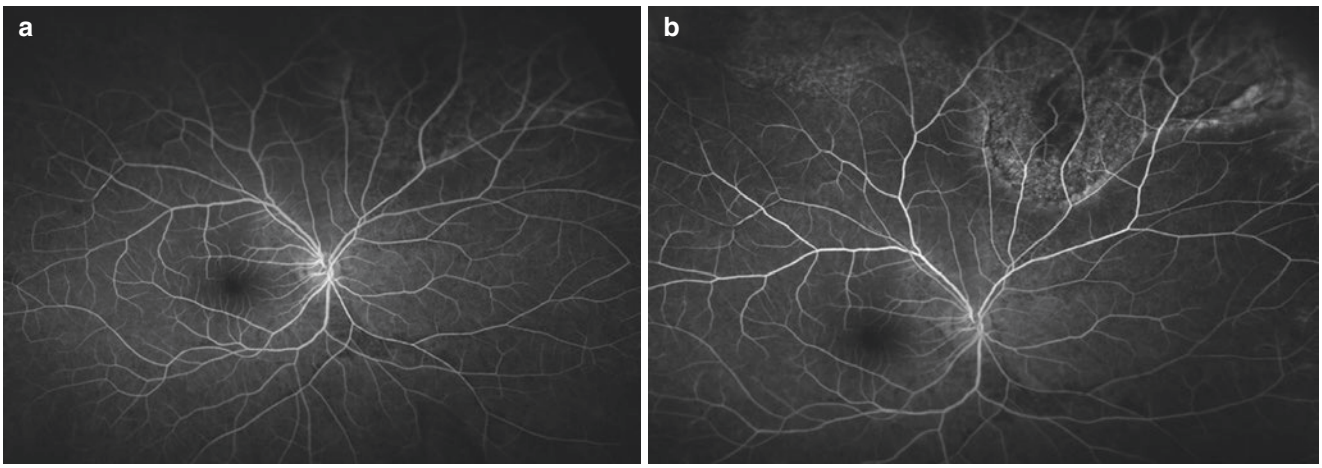

Fig. 3.3 Fluorescein angiography of superior choroidal metastasis of right eye from breast carcinoma in a 53-year-old female. (**a**) Early phase showing hypofluorescence of the lesion superiorly. (**b**) Late phase showing pinpoint hyperfluorescence of the superior lesion. Note the lack of visible tumor vessels

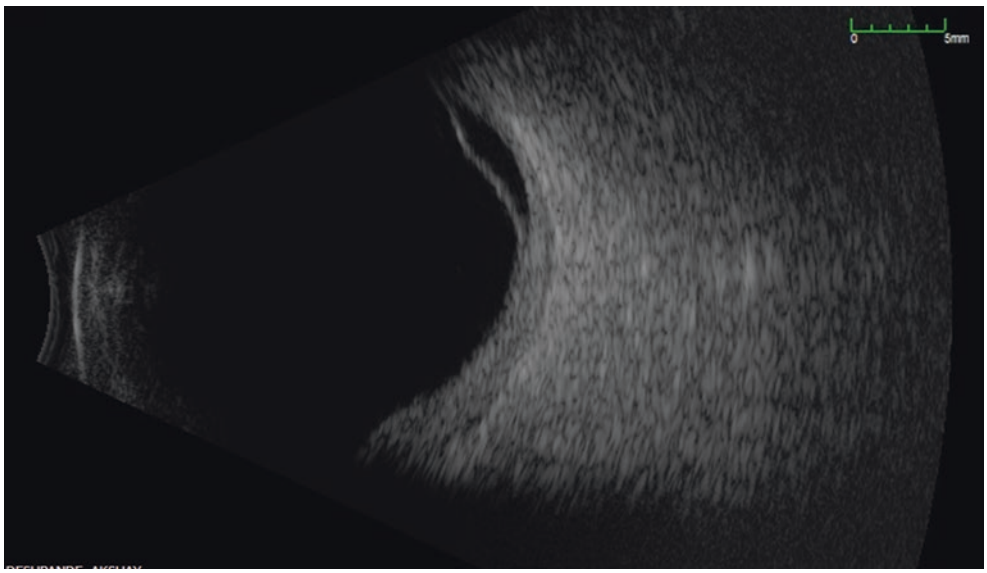

Fig. 3.4 B-scan ultrasonography of choroidal metastasis from the lung (same patient as Fig. 3.1) showing thickened choroidal lesion at bottom of image and small retinal detachment at top of image

3.4.3 Fluorescein Angiography

Choroidal metastatic lesions usually show early hypofluorescence (Fig. 3.3a) followed by hyperfluorescence and possible multifocal pinpoint hyperfluorescence (Fig. 3.3b) in the late phase. There is an absence of "double circulation."

3.4.4 Ultrasonography

Ultrasonography is useful for measuring tumor dimensions, particularly tumor thickness (Fig. 3.4). The internal acoustic reflectivity of choroidal metastases is moderate to high (Fig. 3.5). This is higher than most uveal melanomas and lower than most choroidal hemangiomas. Rarely when a metastatic lesion is mushroom shaped, its internal reflectivity will be equally high throughout the tumor, whereas a mushroom-shaped uveal melanoma would show high reflectivity only in the prolapsed, intraretinal head of the tumor (Damato et al. 2017). Ultrasonography can be useful for detecting extraocular extensions of choroidal metastases (Jakobiec et al. 2016).

3.4.5 Optical Coherence Tomography

Optical coherence tomography (OCT) can show subretinal fluid containing bright dots/speckles, outer retinal degeneration with shaggy photoreceptors, compression of the choriocapillaris overlying the tumor, posterior shadowing, and an irregular "lumpy bumpy" anterior choroidal surface

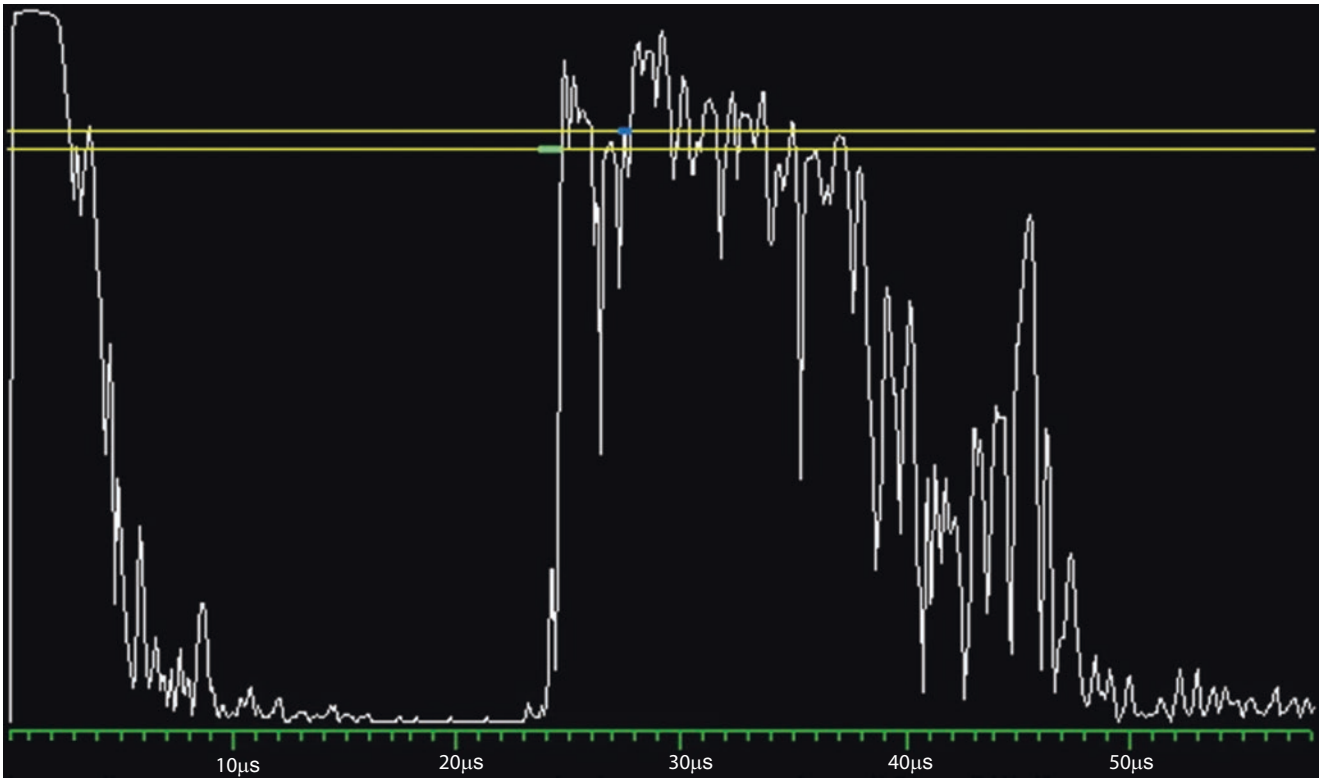

Fig. 3.5 A-scan ultrasonography of the same choroidal metastases from the lung shown in Fig. 3.5. Medium to high internal reflectivity can be appreciated at the location of the thickened choroidal mass

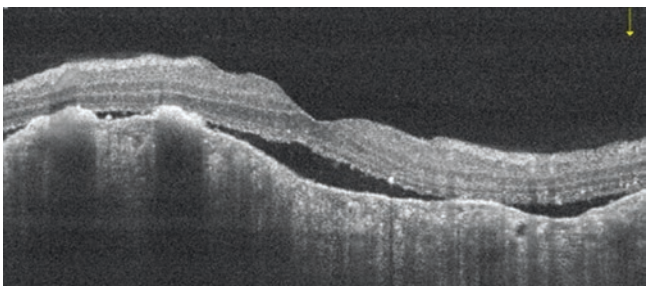

Fig. 3.6 Optical coherence tomography of lung cancer that had metastasized to the choroid (same patient as Fig. 3.1). It shows a "lumpy bumpy" appearance of anterior choroid surface, compression of the choriocapillaris, shaggy photoreceptors, and subretinal fluid

(Fig. 3.6). Additionally, enhanced depth imaging OCT is more reliable than ultrasonography in revealing subclinical metastases when the tumor is very thin (Al-Dahmash et al. 2014; Arevalo et al. 2005; Demirci et al. 2014).

3.4.6 Magnetic Resonance Imaging and Computed Tomography

Magnetic resonance imaging (MRI) usually shows a well-delineated choroidal lesion that is iso-intense relative to the vitreous on T1 imaging and hypo-intense relative to the vitreous on T2 imaging (Konstantinidis and Damato 2017; Peyster et al. 1988). There can, however, be exceptions to this rule. Computed tomography (CT) poorly defines choroidal metastases and is rarely useful. Similarly, positron emission tomography (PET) is not useful in this setting.

3.4.7 Ocular Tumor Biopsy

Generally, biopsy is most useful when there is a high suspicion for choroidal metastases without evidence of primary malignancy following systemic workup (Eide and Walaas 2009). Some institutions perform biopsy before systemic investigation to enable more targeted systemic imaging based on histopathologic findings from the choroidal biopsy. The biopsy is generally performed transretinally through the pars plana with a fine needle or vitreous cutter when the metastatic lesion is postequatorial. In these instances, vitrectomy, retinopexy, and tamponade are not needed. The biopsy can also be done transsclerally if the lesion is very anterior. Ideally, a cytologist should be present in the operating room to ensure an adequate specimen for analysis. If there is any possibility of retinoblastoma, biopsy is contraindicated because of the high risk of seeding (Shen et al. 2015). Uveal melanoma, on the other hand, has a very low risk of seeding with small gauge needles and

vitreous cutters (e.g., 25 or 27 gauge) and therefore would be an acceptable lesion to have on the differential when performing a biopsy.

If tissue biopsy is not possible at other sites in the body, a choroidal biopsy can guide therapy. For example, it can determine if a breast cancer is HER2/*neu*, estrogen receptor, or progesterone receptor positive, thereby enabling targeted therapy. Similarly, testing tissue for epidermal growth factor receptor (EGFR) alterations guides systemic treatment in some types of lung cancer.

3.4.8 Systemic Assessment

Diligent history taking is important when working up a choroidal lesion that is suspected to be metastatic. A personal or family history of cancer, recent symptoms of systemic illness, or a history of smoking can direct investigations to locate the primary malignancy. The possibility of dual pathology should always be considered; patients with systemic malignancy can also develop uveal melanoma or other primary intraocular tumors.

Systemic evaluation should always be performed in conjunction with a medical oncologist. Commonly, their workup for an unknown primary malignancy will include serum studies for relevant cancer biomarkers and mammography as well as CT, MRI, and/or PET imaging of the chest, abdomen, and pelvis (Konstantinidis and Damato 2017). It is particularly important to detect any brain involvement so that radiotherapy to any such lesions can be administered simultaneously with any necessary ocular irradiation. If, following ocular radiotherapy, it subsequently becomes necessary to irradiate brain lesions, the radiation fields from the two treatments may overlap, and parts of the brain may receive a high total dose of radiation, which can lead to dementia.

3.5 Differential Diagnosis

The differential diagnosis of choroidal metastasis includes choroidal osteoma, choroidal melanoma, choroidal neovascularization, choroidal hemangioma, and posterior scleritis. Choroidal osteomas tend to be flatter with wavy, discrete margins and very high internal reflectivity (Kadrmas and Weiter 1997). Choroidal melanomas are normally pigmented and mushroom shaped with visible tumor vasculature; these features are unusual with choroidal metastases. Choroidal hemangiomas are pink with high internal reflectivity and large choroidal vessels below a smooth surface on OCT (Mashayekhi and Shields 2003). Posterior scleritis presents with pain, boggy pink swelling, and a T-sign on ultrasonography.

3.6 Management

Treatment generally starts with systemic management for the primary malignancy but depends on the patient's systemic status as well as the location, number, and laterality of the ocular lesions. Observation can be considered for small peripheral choroidal lesions in patients with poor systemic status. Enucleation may be necessary for blind painful eyes.

3.6.1 Systemic Treatment

Ocular metastasis can respond dramatically, even completely, to the systemic chemotherapy regimen used to treat the primary malignancy (Kosmas et al. 2000; Shome et al. 2007; Yang et al. 2014). Close monitoring is essential, however, because tumor persistence or recurrence can cause irreversible vision loss.

3.6.2 Ocular Radiotherapy

External beam radiation therapy (EBRT) is the most widely used local treatment modality (Chan and Young 2005). It induces tumor regression in 80–100% of patients (Chan and Young 2005). EBRT is most often given as a total dose of 30–40 Gy in 10–20 fractions over 2–4 weeks. This high degree of fractionation diminishes radiation-induced complications; however, in seriously ill patients, a short, hypofractionated course can be given (25 Gy delivered in five fractions).

Brachytherapy can be particularly useful in cases where choroidal metastasis has recurred after EBRT. It delivers a high dose of radiation to a small volume, thus avoiding collateral damage to the macula and optic nerve. Radioactive plaques using radioisotopes such as iodine-125, ruthenium-106, and palladium-103 are used to deliver an apex dose of 45–70 Gy over 3–4 days. It is thought that ruthenium plaques (emitting shorter-range beta radiation) may cause less collateral damage than iodine plaques (emitting longer-range gamma radiation) due to the difference in radiation emission range (Damato et al. 2017). A major advantage of plaque brachytherapy is the short treatment course of only 3–4 days; however, it requires two surgical procedures for the plaque insertion and removal. A 94% regression rate has been reported in 36 patients treated with plaque brachytherapy (Shields et al. 1997a, b).

Proton bream radiotherapy (PBRT) has the advantage of highly localized radiation requiring minimal fractionation. It can be given in only two fractions of 14 cobalt gray equivalents, and, unlike with PBRT for uveal melanomas, no tantalum marker placement is necessary prior to radiation. Tumor regression in 84% of choroidal metastases has been reported (Tsina et al. 2005).

Stereotactic radiosurgery (SRS) uses many precisely focused radiation beams to deliver high doses in a small number of fractions. It has great utility when a tumor is too large or too close to the optic nerve for plaque brachytherapy. There are many different SRS methods. One example involves using a linear accelerator to deliver 30 Gy in ten fractions over 2 weeks.

3.6.3 Photodynamic Therapy

Photodynamic therapy (PDT) has been used more recently for treatment of small choroidal metastatic lesions. Though its use is relatively new for this indication, a recent study showed tumor regression in 81% of cases (Ghodasra and Demirci 2016). Moving forward, PDT may prove to be an effective strategy for treating these lesions.

3.6.4 Transpupillary Thermotherapy

With transpupillary thermotherapy (TTT) an 810 nm diode laser is used to raise the tumor temperature by a few degrees for about 1 min to disrupt metabolic activity in the tumor and induce cell death. Reports have shown that TTT alone is capable of inducing metastatic tumor regression (Vianna et al. 2004). While TTT may be effective for small tumors, it can cause a scotoma from damage to the retina overlying the tumor.

3.6.5 Intravitreal Antiangiogenic Therapy

Some reports have suggested intravitreal bevacizumab may induce regression of choroidal metastasis, but many of these cases had also received systemic chemotherapy or radiation. This modality may be useful as adjuvant treatment in cases of radiation-induced retinopathy causing cystoid macular edema or neovascularization but is likely not an effective primary strategy for choroidal metastases.

3.6.6 Surgical Resection

Local resection has rarely been performed when other methods are not possible or have failed. Generally radiotherapy or another treatment modality should be attempted first. The literature reports a case of successful eyewall resection of a radio-resistant choroidal metastasis from a pulmonary leiomyosarcoma (Anderson et al. 2011). Vitrectomy may, occasionally, serve a palliative role to improve vision in patients with vitreous metastasis (Shankar et al. 2002).

3.7 Prognosis

Generally, life expectancy is poor in patients with choroidal metastases. In a recent series of deceased patients, the median survival time between diagnosis of choroidal metastasis and death was only 6 months (Konstantinidis et al. 2014). Survival time is lower in patients with lung cancer compared to patients with breast cancer. Life expectancy is especially poor when nonocular metastases are also present.

3.8 Conclusions

Patients with choroidal metastases need to be managed on a case-by-case basis. Management depends on many factors including the patient's general medical status. Recent advances in systemic chemotherapy as well as ocular diagnostic and therapeutic modalities have greatly improved outcomes for patients with this condition.

References

Al-Dahmash SA, Shields CL, Kaliki S, et al. Enhanced depth imaging optical coherence tomography of choroidal metastasis in 14 eyes. Retina. 2014;34:1588–93.

Anderson MF, Coupland SE, Bissett D, et al. Choroidal metastasis form primary pulmonary leiomyosarcoma. Clin Exp Ophthalmol. 2011;39:705–7.

Arevalo JF, Fernandez CF, Garcia RA. Optical coherence tomography characteristics of choroidal metastasis. Ophthalmology. 2005;112:1612–9.

Chan PRV, Young LH. Treatment options for metastatic tumors to the choroid. Semin Ophthalmol. 2005;20:207–16.

Damato BE, Stewart JM, Afshar AR. Intraocular metastases. In: Rao PK, Moorthy RS, editors. Focal points: clinical practice perspectives. 1st ed. San Francisco: American Academy of Ophthalmology; 2017.

Demirci H, Cullen A, Sundstrom JM. Enhanced depth imaging optical coherence tomography of choroidal metastasis. Retina. 2014;34:1354–9.

Eide N, Walaas L. Fine-needle aspiration biopsy and other biopsies in suspected intraocular malignant disease: a review. Acta Ophthalmol. 2009;87:588–601.

Eliassi-Rad B, Albert DM, Green WR. Frequency of ocular metastasis in patients dying of cancer in eye bank populations. Br J Ophthalmol. 1996;80:125–8.

Freedman MI, Folk JC. Metastatic tumors to the eye and orbit: patient survival and clinical characteristics. Arch Ophthalmol. 1987;105:1215–9.

Ghodasra DH, Demirci H. Photodynamic therapy for choroidal metastasis. Am J Ophthalmol. 2016;161:104–9.

Jakobiec FA, Ramsey DJ, Stagner AM, et al. Pulmonary adenocarcinoma metastatic to the choroid diagnosed by biopsy of an extrascleral nodule. Ocul Oncol Pathol. 2016;2:24–8.

Kadrmas EF, Weiter JJ. Choroidal osteoma. Int Ophthalmol Clin. 1997;37:171–82.

Konstantinidis L, Damato BE. Intraocular metastases – a review. Asia Pac J Ophthalmol. 2017;6:208–14.

Konstantinidis L, Rospond-Kubiak I, Zeolite I, et al. Management of patients with uveal metastases at the Liverpool Ocular Oncology Centre. Br J Ophthalmol. 2014;98:92–8.

Kosmas C, Malamos NA, Antonopoulos M. Complete regression of choroidal metastases from breast cancer after docetaxel-based systemic chemotherapy. Med Pediatr Oncol. 2000;34:229–30.

Mashayekhi A, Shields CL. Circumscribed choroidal hemangioma. Curr Opin Ophthalmol. 2003;14:142–9.

Peyster RG, Augsburger JJ, Shields JA, et al. Intraocular tumors: evaluation with MR imaging. Radiology. 1988;168:773–9.

Shah SU, Mashayekhi A, Shields CL, et al. Uveal metastasis from lung cancer: clinical features, treatment, and outcome in 194 patients. Ophthalmology. 2014;121:352–7.

Shankar J, Damato BE, Hiscott P. Palliative vitrectomy for intraocular metastasis from cutaneous melanoma. Eye. 2002;16:660–2.

Shen T, Liu R, Lin J, et al. Pars plana vitrectomy and evisceration resulting in death due to misdiagnosis of retinoblastoma in children: a review of 3 cases. Medicine. 2015;94(32):e1338. https://doi.org/10.1097/MD.0000000000001338.

Shields CL, Shields JA, De Potter P, et al. Plaque radiotherapy for the management of uveal metastasis. Arch Ophthalmol. 1997a;115:203–9.

Shields CL, Shields JA, Gross NE, et al. Survey of 520 eyes with uveal metastases. Ophthalmology. 1997b;104:1265–76.

Shome D, Jayadev C, Gadgil D, et al. Systemic chemotherapy and tamoxifen induced regression of choroidal metastasis from a breast carcinoma in a male. Indian J Ophthalmol. 2007;55:475–7.

Tsina EK, Lane AM, Zacks DN, et al. Treatment of metastatic tumors of the choroid with proton beam irradiation. Ophthalmology. 2005;112:337–43.

Vianna RN, Pena R, Muralha A, et al. Transpupillary thermotherapy in the treatment of choroidal metastasis from breast carcinoma. Int Ophthalmol. 2004;25:23–6.

Yang CJ, Tsai YM, Tsai MJ, et al. The effect of chemotherapy with cisplatin and pemetrexed for choroidal metastasis of non-squamous cell carcinoma. Cancer Chemother Pharmacol. 2014;73:199–205.

Choroidal Hemangioma

4

Duangnate Rojanaporn

4.1 Introduction

Choroidal hemangioma is a benign vascular harmatoma of the choroid, which is classified into two types, circumscribed choroidal hemangioma and diffuse choroidal hemangioma. Circumscribed choroidal hemangioma is an isolated solitary tumor without systemic association, whereas diffuse choroidal hemangioma is usually associated with Sturge-Weber syndrome. However, there are few cases reports of circumscribed choroidal hemangioma in Sturge-Weber syndrome patients (Scott et al. 1991; Cheung et al. 2000; Shields et al. 2001).

4.2 Circumscribed Choroidal Hemangioma

4.2.1 Clinical Features

Circumscribed choroidal hemangioma is considered to be congenital in origin and commonly asymptomatic. Therefore, circumscribed choroidal hemangioma is usually diagnosed in adulthood during routine eye examination or when the tumor causes visual symptoms (Shields and Shields 2015). In the largest published case series of 200 patients with circumscribed choroidal hemangioma, the mean age of diagnosis was 45 years. Most patients presented with decreased visual acuity (81%). Other symptoms were visual field defect (7%), metamorphopsia (3%), floaters (2%), progressive hypermetropia (1%), photopsia (1%), and pain (1%). The mean tumor size was 6.7 mm in diameter and 3.1 mm in thickness (Shields et al. 2001). Circumscribed choroidal hemangioma classically appears as unilateral, solitary, round or oval, orange-red elevated choroidal mass located posterior to equator, usually near and temporal to optic disc (Witschel and Font 1976) (Figs. 4.1a, 4.2a and 4.3a). This tumor can cause visual impairment from hyperopic shift with subsequent amblyopia or by producing macular abnormalities such as subretinal fluid (Fig. 4.2a, c), cystoid macular edema, retinoschisis, retinal detachment, and overlying retinal pigment epithelial alterations such as retinal pigment epithelial hyperplasia (Fig. 4.3a, b) and retinal pigment epithelial fibrous metaplasia (Shields et al. 2001).

4.2.2 Diagnosis

4.2.2.1 Fundus Photograph

The distinctive feature of circumscribed choroidal hemangioma is its color of orange-red, which is quite similar to surrounding choroid. This may cause the examiner to overlook the tumor on fundus photograph (Fig. 4.1a). Careful clinical examination to see choroidal elevation and pigmented appearance around the tumor base (caused by tumor compression to surrounding choroid) is helpful to identify the tumor (Witschel and Font 1976; Shields et al. 2001).

4.2.2.2 Fluorescein Angiography

Fluorescein angiography of circumscribed choroidal hemangioma typically shows hyperfluorescence in prearterial or arterial phase, with diffuse intense staining and leakage in the late phase (Shields et al. 2001) (left image Fig. 4.3c–e).

4.2.2.3 Indocyanine Green Angiography

Indocyanine green angiography of circumscribed choroidal hemangioma is unique and pathognomonic. The tumor classically displays early intense hyperfluorescence, followed by moderate hyperfluorescence in the mid phase and moderate hypofluorescence with late "washout" phenomenon, leaving a central hypofluorescent region surrounded by rim of hyperfluorescence (Arevalo et al. 2000; Shields et al. 2001) (right image Fig. 4.3c–e).

D. Rojanaporn (✉)
Department of Ophthalmology, Faculty of Medicine, Ramathibodi Hospital, Mahidol University, Bangkok, Thailand
e-mail: duangnate.roj@mahidol.ac.th

D. Rojanaporn (ed.), *Ocular Oncology*, https://doi.org/10.1007/978-981-13-2336-2_4

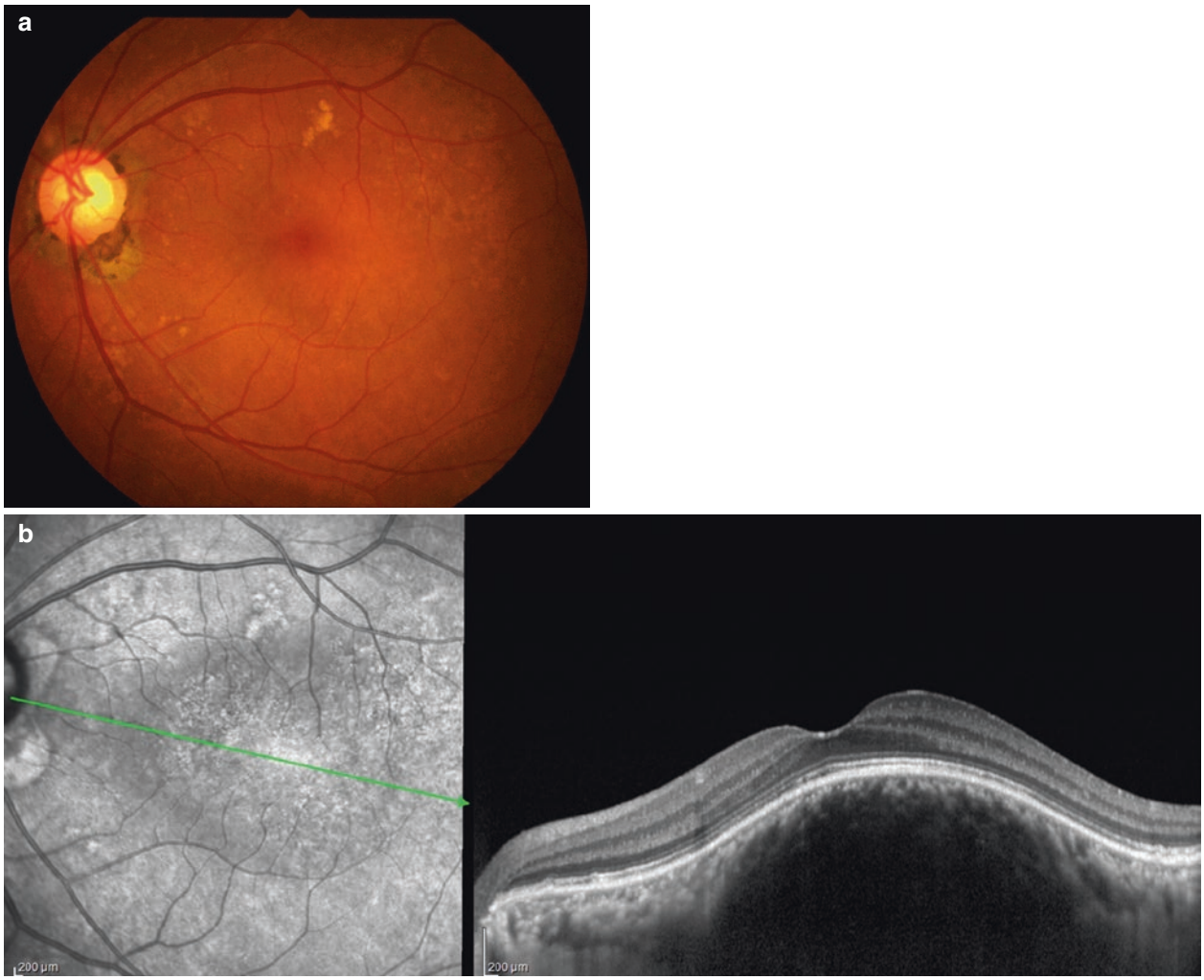

Fig. 4.1 A 55-year-old female with circumscribed choroidal hemangioma. Fundus photograph showing slightly elevated circumscribed choroidal hemangioma in the macula (**a**). EDI-OCT showing choroidal mass with smooth elevated anterior tumor contour, preservation of choriocapillaris, and expansion of medium and large choroidal vessels (**b**)

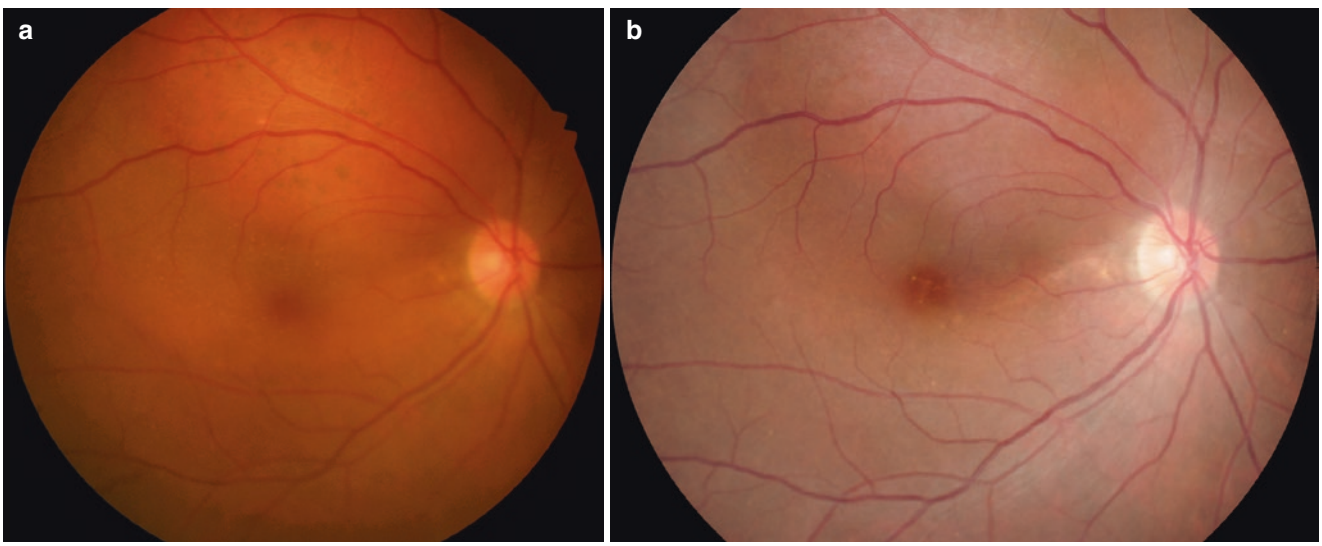

Fig. 4.2 A 50-year-old female with circumscribed choroidal hemangioma. Fundus photograph showing circumscribed choroidal hemangioma with retinal pigment epithelial alteration overlying tumor surface and subretinal fluid involving macula (**a**). EDI-OCT showing subretinal fluid in the macula (**c**), irregular and thickening of RPE with subretinal fluid over the tumor (**d**). After single session of photodynamic therapy, subretinal fluid was completely resolved (**b**, fundus photograph; **e**, EDI-OCT of macula; **f**, EDI-OCT of tumor)

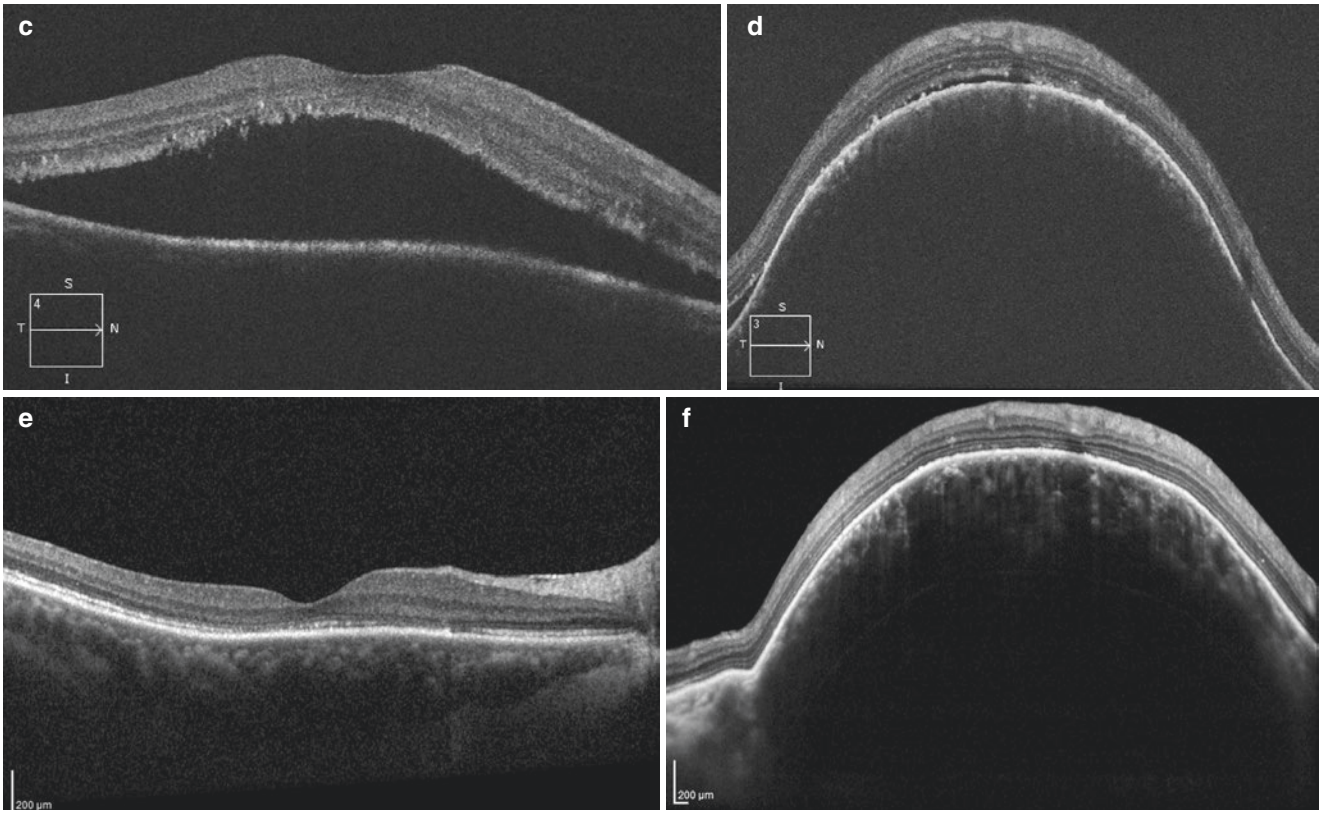

Fig. 4.2 (continued)

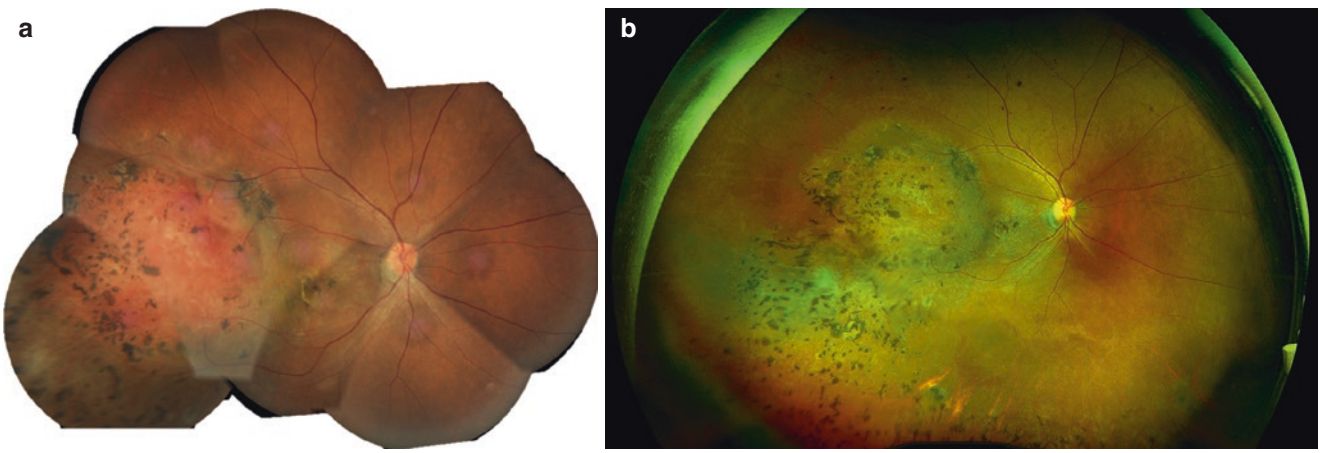

Fig. 4.3 A 69-year-old female with circumscribed choroidal hemangioma. Montage fundus photograph (**a**) and Optos image (**b**) showing large circumscribed choroidal hemangioma with marked retinal pigment epithelial alteration overlying tumor surface, in macula, and in inferior retina. Fundus fluorescein angiography (FFA) (left image **c**–**e**) showing tumor hyperfluorescence in early phase (**c**), with diffuse intense staining in mid phase (**d**) and late phase (**e**). Indocyanine green angiography (ICG) (right image **c**–**e**) showing tumor hyperfluorescence in early phase (**c**), with diffuse staining in mid phase (**d**) and tumor hypofluorescence in the center with surrounding hyperfluorescent rim in late phase (washout phenomenon) (**e**). Ultrasonography of the tumor showing acoustically dense, dome-shaped choroidal mass on B-scan (**f**) with high internal reflectivity on A-scan (**g**)

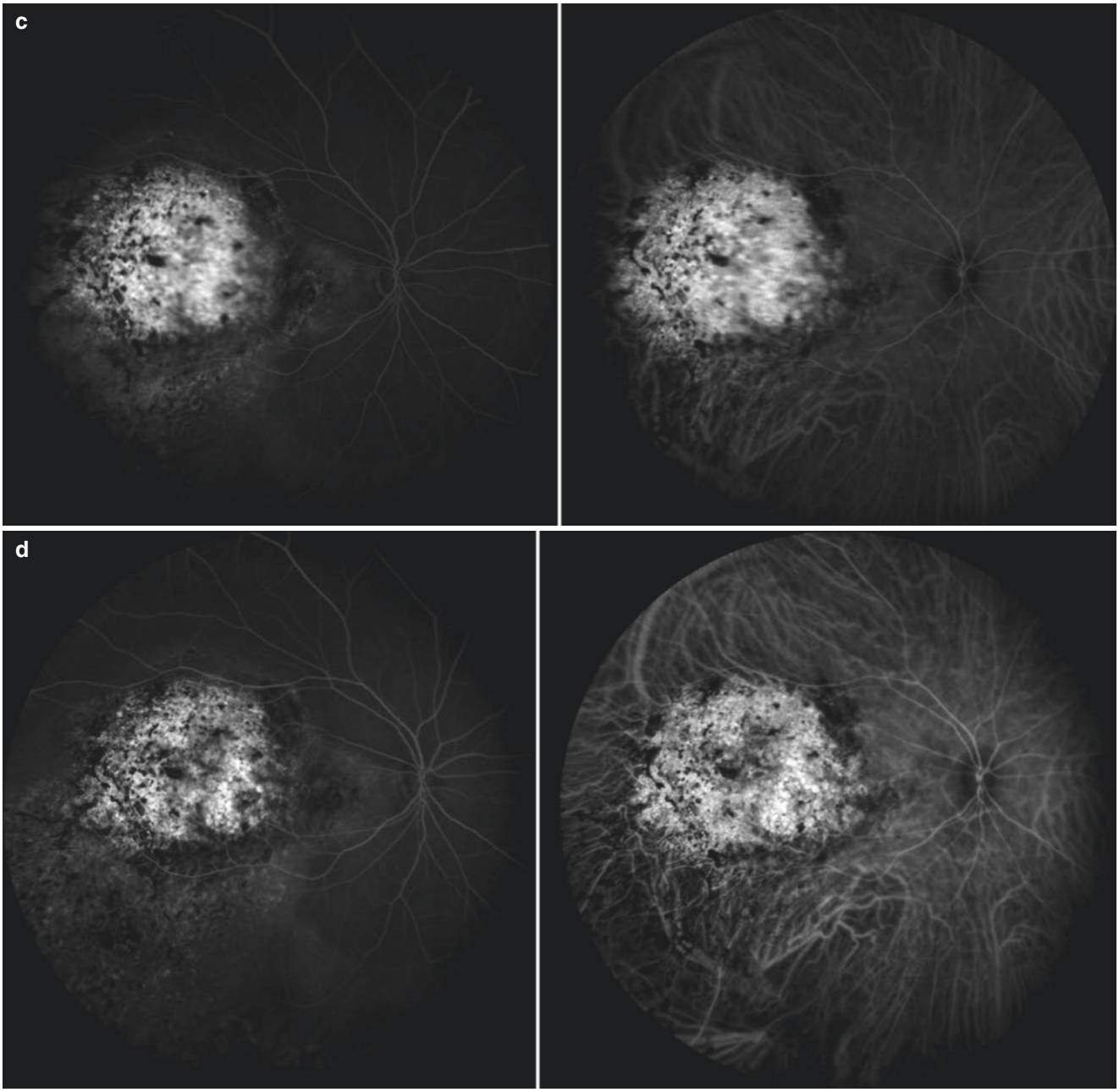

Fig. 4.3 (continued)

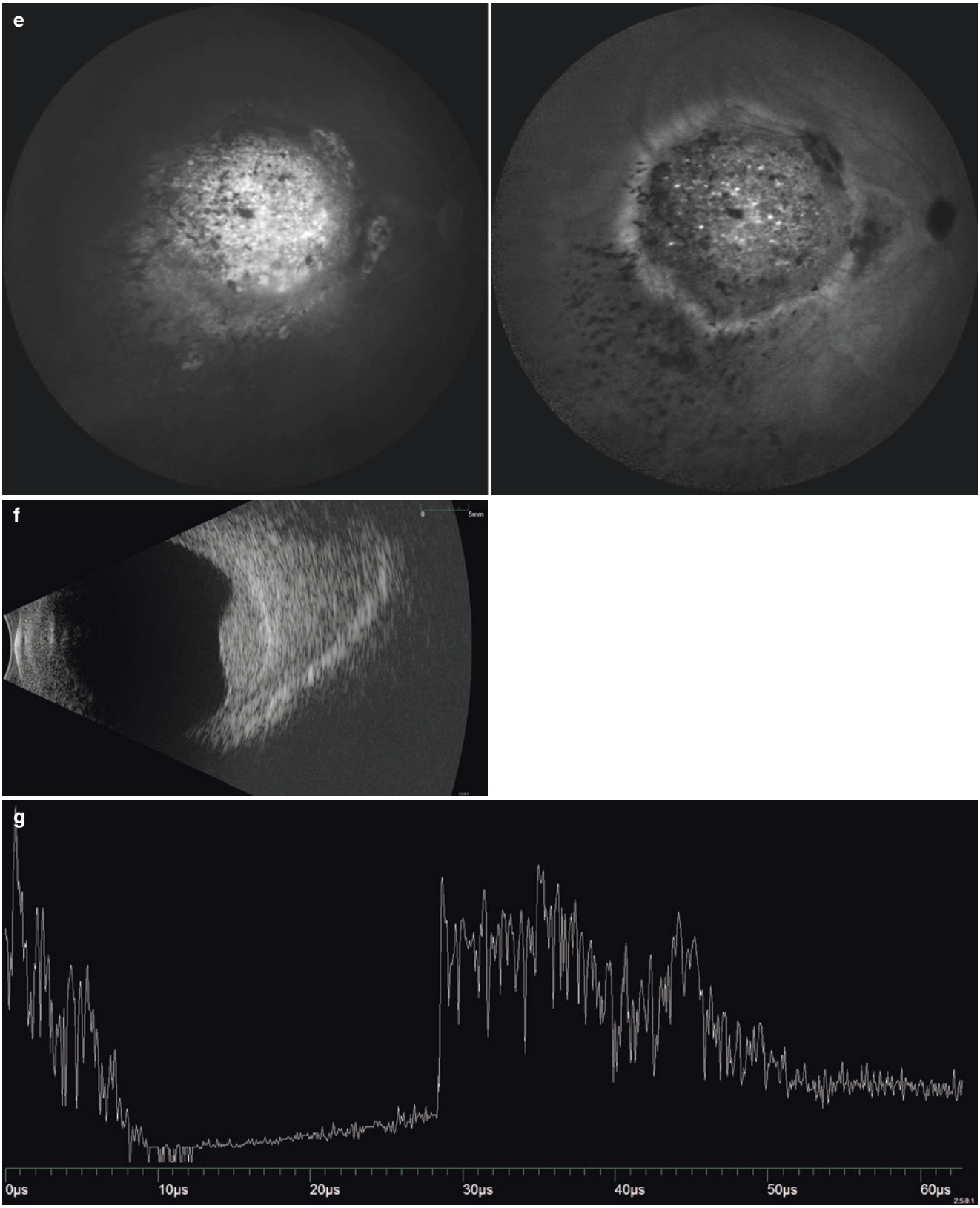

Fig. 4.3 (continued)

4.2.2.4 Ultrasonography

The ultrasonographic features of circumscribed choroidal hemangioma are characteristic. The tumor typically appears as an elevated dome-shaped mass with acoustic solidity on B-scan (Fig. 4.3f) and high initial spike with high internal reflectivity on A-scan (Fig. 4.3g) (Shields et al. 2001).

4.2.2.5 Optical Coherence Tomography (OCT)

OCT is useful to detect and monitor subretinal fluid, macular edema, and secondary changes in the retina and retinal pigment epithelium associated with circumscribed choroidal hemangioma (Shields et al. 2005) (Fig. 4.2c–f). Moreover, enhanced-depth imaging OCT (EDI-OCT) can be used to differentiate circumscribed choroidal hemangioma from other choroidal tumors, as it displays unique features of smooth, gradual dome-shaped anterior tumor contour with expansion of the medium and large choroidal vessels without compression of choriocapillaris (Torres et al. 2011; Rojanaporn et al. 2015) (Figs. 4.1b and 4.2d, f).

4.2.2.6 Fundus Autofluorescence

Circumscribed choroidal hemangioma shows bright hyperautofluorescence in fresh hemangioma and dark hypoautofluorescence in those following therapy or those with chronic retinal pigment epithelium hyperplasia and atrophy (Ramasubramanian et al. 2010).

4.2.2.7 Magnetic Resonance Imaging (MRI)

MRI of choroidal hemangioma typically shows hyperintensity in contrast to vitreous on T-1 weighted images and hyperintensity of isointensity on T2-weighted images. The tumor also shows enhancement with gadolinium contrast (Shields et al. 2001).

4.2.3 Differential Diagnosis

The differential diagnosis of circumscribed choroidal hemangioma includes choroidal nevus, amelanotic choroidal malignant melanoma, choroidal metastasis, choroidal osteoma, central serous chorioretinopathy, and posterior scleritis (Shields et al. 2001; Mashayekhi and Shields 2003; Karimi et al. 2015). The characteristic color of circumscribed choroidal hemangioma is orange-red color, unlike amelanotic choroidal malignant melanoma which is more often yellow-tan and choroidal metastasis which usually creamy-yellow (Shields et al. 2001). However, choroidal metastases from renal cell carcinoma, thyroid carcinoma, and carcinoid tumor can appear orange in color, similar to circumscribed choroidal hemangioma (Shields et al. 1997). Circumscribed choroidal hemangioma is almost always unilateral and solitary, whereas choroidal metastasis may be multifocal or bilateral. Circumscribed choroidal hemangioma is usually dome shape, never attaining a mushroom shape like choroidal malignant melanoma or plateau shape like choroidal metastases. On ultrasonography, circumscribed choroidal hemangioma showed acoustic solidity with high internal reflectivity, in contrast to choroidal malignant melanoma which showed acoustic hollowness with low to medium internal reflectivity. Fluorescein angiography and indocyanine green angiography of circumscribed choroidal hemangioma are characteristic and helpful to differentiate circumscribed choroidal hemangioma from other simulating lesions, as described earlier in Sect. 4.2. Enhanced-depth imaging OCT is a noninvasive tool to differentiate circumscribed choroidal hemangioma from other choroidal tumors. EDI-OCT of circumscribed choroidal hemangioma displays smooth, gradual dome-shaped anterior tumor contour with expansion of medium- and large-sized choroidal vessels without choriocapillaris compression, in contrast to choroidal nevus and choroidal malignant melanoma which show compression of choriocapillaris and choroidal metastasis which shows lumpy bumpy anterior tumor contour (Rojanaporn et al. 2015).

4.2.4 Management

The goal of management of circumscribed choroidal hemangioma is preservation or improvement of vision by reducing subretinal fluid and macular edema before irreversible retina or RPE changes. It is based on tumor size, location, and visual symptoms.

4.2.4.1 Laser Photocoagulation

Argon, xenon, and diode laser photocoagulation are effective to reduce subretinal fluid and improve visual acuity in circumscribed choroidal hemangioma (Anand et al. 1989; Lanzetta et al. 1995; Shields et al. 2001). However, laser photocoagulation does not reduce tumor size and produced scar which leads to scotoma in laser treatment area (Tsipursky et al. 2011).Currently, laser photocoagulation is rarely used to treat circumscribed choroidal hemangioma.

4.2.4.2 Transpupillary Thermotherapy (TTT)

Transpupillary thermotherapy with 810 diode laser, large spot size, and long exposure can lead to tumor regression and ceasing tumor leakage in circumscribed choroidal hemangioma (Gunduz 2004). TTT is effective in small- to medium-sized tumor (<10 mm in diameter and < 4 mm in thickness) (Garcia-Arumi et al. 2000). Transpupillary thermotherapy produces chorioretinal scar and also can cause thermal papillitis (Shields et al. 2002); therefore, it is not a proper treatment in circumscribed choroidal hemangioma in macular region or adjacent to optic disc (Garcia-Arumi et al. 2000). To enhance the heat uptake, indocyanine green dye can be given prior to TTT (Kamal et al. 2000).

4.2.4.3 Photodynamic Therapy (PDT)

Photodynamic therapy is currently the most widely used treatment for circumscribed choroidal hemangioma. The main advantage of PDT is its selectivity and minimal disruption and damage to adjacent normal tissue. PDT is typically performed with standard dose of intravenous verteporfin (6 mg/m^2), standard intensity (600 mW/cm^2), and standard or double duration (83–166 s) of 689 nm laser (Karimi et al. 2015). The baseline tumor thickness in previous cases series on PDT for circumscribed choroidal hemangioma was less than 4 mm (Karimi et al. 2015). Usually one session of photodynamic therapy can effectively reduce tumor size, reduce subretinal fluid and macular edema, and improve visual acuity in patients with circumscribed choroidal hemangioma (Jurklies et al. 2003; Singh et al. 2004; Blasi et al. 2010; Zhang et al. 2010; Tsipursky et al. 2011; Karimi et al. 2015) (Fig. 4.2a–f).

4.2.4.4 Radiotherapy

Various types of radiotherapy have been reported to be effective in circumscribed choroidal hemangioma. These includes low-dose external beam radiotherapy (Schilling et al. 1997), proton beam radiotherapy (Zografos et al. 1998; Frau et al. 2004; Levy-Gabriel et al. 2009), and gamma knife radiosurgery (Kong et al. 2007). Plaque brachytherapy allows more localized treatment of the tumor and minimizes radiation complications. Effective tumor control has been reported in brachytherapy with cobalt-60 (Zografos et al. 1996), ruthenium-106 (Naseripour et al. 2017), iodine-125 (Shields et al. 2001), and palladium-103 (Aizman et al. 2004). Due to its potential radiation complication, radiotherapy is reserved for large tumor or tumor with extensive retinal detachment, which are difficult to treat with PDT.

4.2.4.5 Intravitreal Anti-VEGF

The role of VEGF and choroidal hemangioma remains unclear. Few case reports have suggested that intravitreal bevacizumab can lead to resolution of subretinal fluid and retinal edema in patients with circumscribed choroidal hemangioma (Sagong et al. 2009; Mandal et al. 2011).

4.2.4.6 Systemic Propranolol

The effect of oral propranolol for circumscribed choroidal hemangioma has been shown in few case report with variable outcomes (Sanz-Marco et al. 2011; Tanabe et al. 2013). Further studies are required.

4.3 Diffuse Choroidal Hemangioma

4.3.1 Clinical Features

Diffuse choroidal hemangioma is usually associated with Sturge-Weber syndrome (SWS). Systemic manifestations of SWS include facial angiomatosis or nevus flammeus (port-wine stain) (Fig. 4.4a) and leptomeningeal hemangioma. Approximately 50% of patients with SWS has ocular pathology, which are eyelid port-wine stain, abnormal conjunctival and scleral vessels, vascular malformations in trabecular meshwork, glaucoma, diffuse choroidal hemangioma, and circumscribed choroidal hemangioma (rare) (Mantelli et al. 2016). Diffuse choroidal hemangioma classically shows a dark red color or "tomato ketchup" appearance of the fundus (Fig. 4.4b), in contrast to orange or bright red color of normal fundus (Fig. 4.4c). Associated retinal findings include retinal edema, retinal pigment epithelial alterations, mildly dilated and tortuous retinal vessels, exudative retinal detachment, and secondary neovascular glaucoma (Witschel and Font 1976; Mantelli et al. 2016; Shields and Shields 2015).

4.3.2 Diagnosis

The diagnosis of diffuse choroidal hemangioma can be made clinically. The patient with diffuse choroidal hemangioma typically shows ipsilateral facial and eyelid port-wine stain on external eye examination (Fig. 4.4a). Dilated fundus examination in both eyes can highlight the difference in background fundus color, which shows dark red "tomato ketchup" appearance in eyes with diffuse choroidal hemangioma (Fig. 4.4b) and orange or bright red color in normal eye (Fig. 4.4c). Furthermore, the absence of normal choroidal vascular pattern in diffuse choroidal hemangioma can guide the diagnosis and identify the area of tumor involvement. Ultrasonography and fundus angiography can be used to confirm the diagnosis. On ultrasonography, diffuse choroidal hemangioma displays markedly generalized choroidal thickening with acoustic solidity on B-scan and high internal reflectivity on A-scan. On fundus fluorescein angiography, diffuse choroidal hemangioma displays similar leakage pattern to circumscribed choroidal hemangioma but with more widespread involvement (Shields and Shields 2015).

4.3.3 Management

Several therapeutic methods have been reported to treat diffuse choroidal hemangioma. The majority of the patients were treated effectively with low-dose radiotherapy including external beam radiotherapy (Schilling et al. 1997), proton beam radiotherapy (Zografos et al. 1998), and stereotactic radiotherapy (Kong et al. 2007). Few case report of diffuse choroidal hemangioma showed tumor regression with resolution of subretinal fluid with plaque brachytherapy (Kubicka-Trzaska et al. 2015). Photodynamic therapy have shown to be effective in few case reports in patients with diffuse choroidal hemangioma (Tsipursky et al. 2011). There

Fig. 4.4 A 22-year-old female with Sturge-Weber syndrome and diffuse choroidal hemangioma. Face photograph showing port-wine stain skin lesion (**a**). Fundus photograph showing diffuse choroidal hemangioma and glaucomatous optic nerve head in the right eye (**b**) and normal fundus in the left eye (**c**). EDI-OCT of the macula showing diffuse choroidal thickening with expansion of choroidal vessels in the right eye (**d**) and normal choroid in the left eye (**e**)

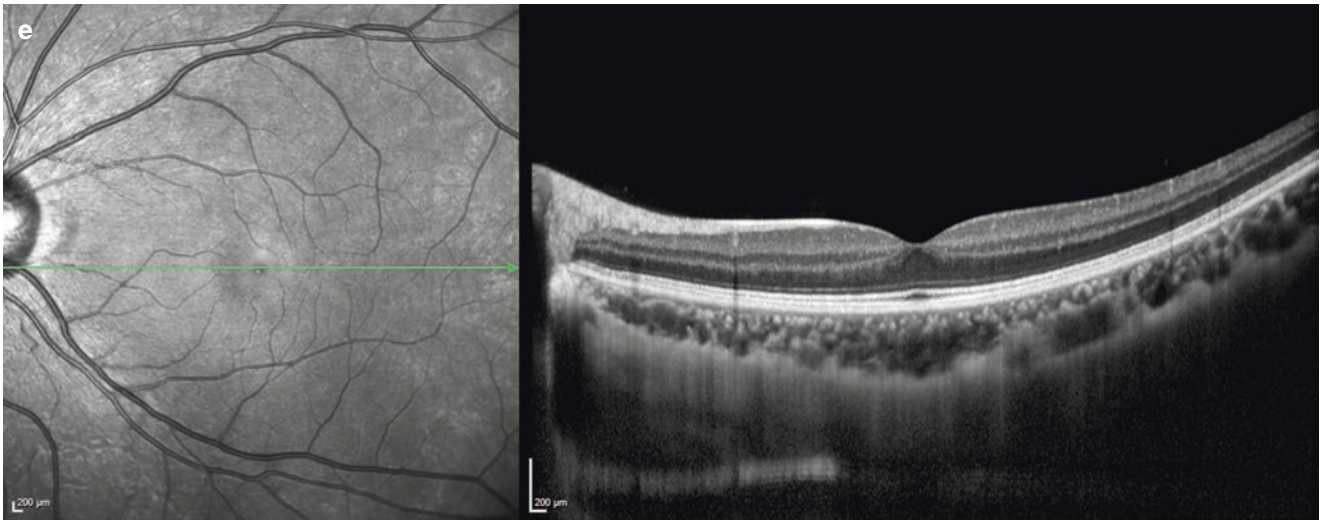

Fig. 4.4 (continued)

were also few case reports of resolution of exudative retinal detachment in diffuse choroidal hemangioma following the use of systemic oral propranolol (Arevalo et al. 2011; Thapa and Shields 2013; Dave et al. 2016).

References

Aizman A, Finger PT, Shabto U, et al. Palladium 103 (103Pd) plaque radiation therapy for circumscribed choroidal hemangioma with retinal detachment. Arch Ophthalmol. 2004;122:1652–6.

Anand R, Augsburger JJ, Shields JA. Circumscribed choroidal hemangiomas. Arch Ophthalmol. 1989;107:1338–42.

Arevalo JF, Shields CL, Shields JA, et al. Circumscribed choroidal hemangioma: characteristic features with indocyanine green videoangiography. Ophthalmology. 2000;107:344–50.

Arevalo JF, Arias JD, Serrano MA. Oral propanolol for exudative retinal detachment in diffuse choroidal hemangioma. Arch Ophthalmol. 2011;129:1373–5.

Blasi MA, Tiberti AC, Scupola A, et al. Photodynamic therapy with verteporfin for symptomatic circumscribed choroidal hemangioma: five-year outcomes. Ophthalmology. 2010;117:1630–7.

Cheung D, Grey R, Rennie I. Circumscribed choroidal haemangioma in a patient with Sturge Weber syndrome. Eye (Lond). 2000;14:238–40.

Dave T, Dave VP, Shah G, et al. Diffuse choroidal hemangioma masqueradingas central serous chorioretinopathy treated with oral propanolol. Retin Cases Brief Rep. 2016;10:11–4.

Frau E, Rumen F, Noel G, et al. Low-dose proton beam therapy for circumscribed choroidal hemangiomas. Arch Ophthalmol. 2004;122:1471–5.

Garcia-Arumi J, Ramsay LS, Guraya BC. Transpupillary thermotherapy for circumscribed choroidal hemangiomas. Ophthalmology. 2000;107:351–6.

Gunduz K. Transpupillary thermotherapy in the management of circumscribed choroidal hemangioma. Surv Ophthalmol. 2004;49:316–27.

Jurklies B, Anastassiou G, Ortmans S, et al. Photodynamic therapy using verteporfin in circumscribed choroidal haemangioma. Br J Ophthalmol. 2003;87:84–9.

Kamal A, Watts AR, Rennie IG. Indocyanine green enhanced transpupillary thermotherapy of circumscribed choroidal haemangioma. Eye (Lond). 2000;5:701–5.

Karimi S, Nourinia R, Mashayekhi A. Circumscribed Choroidal Hemangioma. J Ophthalmic Vis Res. 2015;10:320–8.

Kong DS, Lee JI, Kang SW. Gamma knife radiosurgery for choroidal hemangioma. Am J Ophthalmol. 2007;144:319–22.

Kubicka-Trzaska A, Karska-Basta I, Oleksy, et al. Management of diffuse choroidal hemangioma in Sturge-Weber syndrome with Ruthenium-106 plaque radiotherapy. Graefes Arch Clin Exp Ophthalmol. 2015;253:2015–9.

Lanzetta P, Virgili G, Ferrari E, et al. Diode laser photocoagulation of choroidal hemangioma. Int Ophthalmol. 1995;19:239–47.

Levy-Gabriel C, Rouic LL, Plancher C, et al. Long-term results of low-dose proton beam therapy for circumscribed choroidal hemangiomas. Retina. 2009;29:170–5.

Mandal S, Naithani P, Venkatesh P, et al. Intravitreal bevacizumab (avastin) for circumscribed choroidal hemangioma. Indian J Ophthalmol. 2011;59:248–51.

Mantelli F, Bruscolini A, La Cava M, et al. Ocular manifestations of Sturge-Weber syndrome: pathogenesis, diagnosis, and management. Clin Ophthalmol. 2016;10:871–8.

Mashayekhi A, Shields CL. Circumscribed choroidal hemangioma. Curr Opin Ophthalmol. 2003;14:142–9.

Naseripour M, Maleki A, Astaraki A, et al. Ruthenium-106 brachytherapy in the treatment of circumscribed choroidal hemangioma. Retina. 2017;38:1024–30.

Ramasubramanian A, Shields CL, Harmon SA, et al. Autofluorescence of choroidal hemangioma in 34 consecutive eyes. Retina. 2010;30:16–22.

Rojanaporn D, Kaliki S, Ferenczy SR, et al. Enhanced depth imaging optical coherence tomography of circumscribed choroidal hemangioma in 10 consecutive cases. Middle East Afr J Ophthalmol. 2015;22:192–7.

Sagong M, Lee J, Chang W. Application of intravitreal bevacizumab for circumscribed choroidal hemangioma. Korean J Ophthalmol. 2009;23:127–31.

Sanz-Marco E, Gallego R, Diaz-Llopis M. Oral propranolol for circumscribed choroidal hemangioma. Case Rep Ophthalmol. 2011;2:84–90.

Schilling BW, Poon TC, Indebetouw G, et al. Three-dimensional holographic fluorescence microscopy. Opt Lett. 1997;22:1506–8.

Scott TA, Augsburger JJ, Brady LW, et al. Low dose ocular irradiation for diffuse choroidal hemangiomas associated with bullous nonrhegmatogenous retinal detachment. Retina. 1991;11:389.

Shields JA, Shields CL. Intraocular tumors: an atlas and textbook. 3rd ed. Philadelphia: Wolters Kluwer; 2015.

Shields CL, Shields JA, Gross NE, et al. Survey of 520 eyes with uveal metastases. Ophthalmology. 1997;104:1265–76.

Shields CL, Honavar SG, Shields JA, et al. Circumscribed choroidal hemangioma: clinical manifestations and factors predictive of visual outcome in 200 consecutive cases. Ophthalmology. 2001;108:2237–48.

Shields CL, Shields JA, Perez N, et al. Primary transpupillary thermotherapy for small choroidal melanoma in 256 consecutive cases: outcomes and limitations. Ophthalmology. 2002;109:225–34.

Shields CL, Materin MA, Marr BP, et al. Resolution of advanced cystoid macular edema following photodynamic therapy for choroidal hemangioma. Ophthalmic Surg Lasers Imaging. 2005;36:237–9.

Singh AD, Kaiser PK, Sears JE, et al. Photodynamic therapy of circumscribed choroidal haemangioma. Br J Ophthalmol. 2004;88:1414–8.

Tanabe H, Sahashi K, Kitano T, et al. Effects of oral propranolol on circumscribed choroidal hemangioma: a pilot study. JAMA Ophthalmol. 2013;131:1617–22.

Thapa R, Shields CL. Oral propanolol therapy for management of exudative retinal detachment from diffuse choroidal hemangioma in Sturge-Weber syndrome. Eur J Ophthalmol. 2013;23:922–4.

Torres VL, Brugnoni N, Kaiser PK, et al. Optical coherence tomography enhanced depth imaging of choroidal tumors. Am J Ophthalmol. 2011;151:586–93.

Tsipursky MS, Golchet PR, Jampol LM. Photodynamic therapy of choroidal hemangioma in sturge-weber syndrome, with a review of treatments for diffuse and circumscribed choroidal hemangiomas. Surv Ophthalmol. 2011;56:68–85.

Witschel H, Font RL. Hemangioma of the choroid. A clinicopathologic study of 71 cases and a review of the literature. Surv Ophthalmol. 1976;20:415–31.

Zhang Y, Liu W, Fang Y, et al. Photodynamic therapy for symptomatic circumscribed macular choroidal hemangioma in Chinese patients. Am J Ophthalmol. 2010;150:710–5.

Zografos L, Bercher L, Chamot L, et al. Cobalt-60 treatment of choroidal hemangiomas. Am J Ophthalmol. 1996;121:190–9.

Zografos L, Egger E, Bercher L, et al. Proton beam irradiation of choroidal hemangiomas. Am J Ophthalmol. 1998;126:261–8.

Choroidal Osteoma

5

Tero T. Kivelä

5.1 Introduction

Choroidal osteoma, a benign tumor of mature bone, first appeared in a textbook in 1963 but was misdiagnosed as a calcified choroidal hemangioma (Reese 1963). A second case was presented in 1975 in the Verhoeff Society by Van Dyk and published in 1978 by Williams, Font, Van Dyk, and Riekhof (Williams et al. 1978). A little earlier, Gass, Guerry, Jack, and Harris had written about this case, adding clinical descriptions of three others they had identified from photographs at the Bascom Palmer Eye Institute (Gass et al. 1978). They established choroidal osteoma as an entity: a benign yet growing osseous tumor, located in the juxtapapillary choroid of healthy patients who were predominantly young females. The following year, Gass published already on 15 patients with choroidal osteoma, including four bilateral tumors (Gass 1979).

The importance of choroidal osteomas derives from the fact that they can lead to loss of central vision if they extend under the foveola and deossify, a process involving decalcification, shrinkage, disruption of the retinal pigment epithelium (RPE), and, often, formation of a choroidal neovascular membrane, first documented in 1968 (Trimble et al. 1988). Osteomas are easy to diagnose using a combination of ophthalmoscopy and ultrasonography, while optical coherence tomography (Shields et al. 2015a) and fundus autofluorescence imaging (Sisk et al. 2013) are useful adjuncts in assessing their impact on vision. No known treatment can prevent the initial growth and the later deossification of choroidal osteomas, but the choroidal neovascular membranes over them, if any, usually regress with anti-vascular endothelial growth factor therapy (Mansour et al. 2014).

T. T. Kivelä (✉)
Department of Ophthalmology, University of Helsinki and Helsinki University Hospital, Helsinki, Finland
e-mail: tero.kivela@helsinki.fi

5.2 Etiopathogenesis

The histogenesis of choroidal osteomas is unresolved. Because they are initially asymptomatic, it is not known at which age they first appear, but the youngest patients described have been 3 years (Mizota et al. 1998; Wilson et al. 2002), 4 years (Süsskind et al. 2014), 5 years (Eting and Savir 1992; Aylward et al. 1998), and 6 years old (Fava et al. 1980; Pellegrini et al. 2014; Heichel et al. 2016). The youngest children in whom a choroidal osteoma has been documented to emerge in a previously normal fundus were 3–12 years old and under ophthalmological follow-up for unrelated disease (Kline et al. 1982; Trimble and Schatz 1983; Eting and Savir 1992; Wilson et al. 2002). Additional osteomas have appeared in a child at the age of 9 years (Noble 1990). The fact that the majority of patients are young adults (Aylward et al. 1998; Shields et al. 2005) suggests that choroidal osteomas are congenital and developmental in origin but may not be clinically detectable before they have grown postnatally: they may be osseous choristomas with a twist. Familial, typically bilateral osteomas in siblings and sometimes in their parent hint to a genetic influence (Cunha 1984; Noble 1990; Eting and Savir 1992; Tsuchihashi et al. 2005).

According to an alternative theory, a cytokine such as a bone morphogenetic protein induces a choroidal mesenchymal stem cell or pericyte, a cell type capable of both angiogenic and osteogenic differentiation, to proliferate and to differentiate into an osteoblast (Munteanu et al. 2013). An inflammatory etiology also has been proposed as an alternative (Katz and Gass 1983) but appears very unlikely, given that choroidal osteomas are rarely associated with any signs or even a history of an inflammatory disorder. Because of the preponderance of females with choroidal osteomas, hormonal factors also have been suspected in the past (Gass 1979).

Once a choroidal osteoma has emerged, its faith probably is controlled by the opposing activities of osteoblasts and osteoclasts. The former secrete osteoid that becomes remodeled into bone spicules and trabeculae that generate

D. Rojanaporn (ed.), *Ocular Oncology*, https://doi.org/10.1007/978-981-13-2336-2_5

primary spongy bone and, later, lamellar bone, explaining the growth of most choroidal osteomas. The latter are thought to drive later deossification and shrinkage—indicating loss of bone, not just decalcification (Shields et al. 2015a, b)—that typically is seen in choroidal osteomas when they age (Shields et al. 2005). Compromised intrinsic blood circulation of a deossifying osteoma and, possibly, of the adjacent choroid might induce secretion of vascular endothelial growth factor, which together with coinciding disruption of the RPE and Bruch's membrane over the tumor might contribute to the formation of the frequently emerging choroidal neovascular membrane (Foster et al. 2003; Sisk et al. 2013; Yoshikawa and Takahashi 2015).

5.3 Clinical Features

5.3.1 Incidence

Choroidal osteomas are infrequent but more common than what might be judged from older medical literature. With the advent of open access publishing, case reports and case series appear regularly: between 2010 and 2017, over 135 patients were reported in PubMed, and only a fraction of osteomas diagnosed in retinal and ocular oncology services will ever be published. In our service, we diagnose approximately one case per year, suggesting an incidence in the order of one in five million.

5.3.2 Age

The median age at presentation of a patient with a choroidal osteoma, calculated for 135 patients reported from 2010 to 2017, is 28 years, 25 years for males and 29 years for females (Fig. 5.1). Of the 135 patients, the youngest was 4 years of age, 26% were younger than 18 years, 16% were older than 45 years, and the oldest one was 72 years of age. These estimates correspond with 25 years in the largest referral-based series of 61 patients (Shields et al. 2005).

5.3.3 Gender and Race

Choroidal osteomas are more common in women who represented 63% of the 135 patients reported from 2010 to 2017, which corresponds to a 2:1 female/male ratio. This percentage is a close match with 67% in the largest referral-based series (Shields et al. 2005). No racial predilection is evident among reported patients.

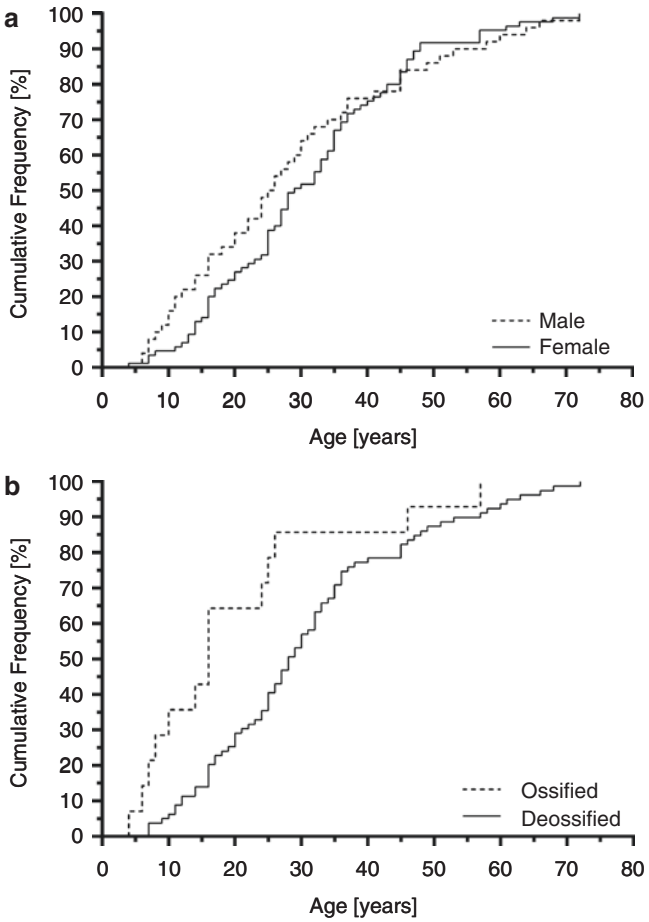

Fig. 5.1 Cumulative frequency of having a choroidal osteoma diagnosed plotted according to (**a**) gender and (**b**) presence or absence of deossification for 135 patients reported from 2010 to 2017 in the literature. Deossified choroidal osteomas are diagnosed later than ossified ones

5.3.4 Location and Laterality

Choroidal osteomas occur almost exclusively in the posterior pole of the eye (Figs. 5.2, 5.3, 5.4, 5.5 and 5.6), preferably in a juxta-, peri-, or circumpapillary location either on the nasal or temporal side, and they often involve or later grow under the foveola (Aylward et al. 1998; Shields et al. 2005; Sisk et al. 2013; Pellegrini et al. 2014; Shields et al. 2015a, b). They were bilateral in 21% (Fig. 5.2) and unilateral in 79% (Fig. 5.3) among 73 patients with laterality reported between 2010 and 2017, in good agreement with 25 and 21% in the two large referral-based series with 36 and 61 patients, respectively (Aylward et al. 1998; Shields et al. 2005). Although a rare occurrence, osteomas can be multifocal (MirNaghi et al. 2015) or additional lesions may appear over time (Chen et al. 2006; Sambricio et al. 2015).

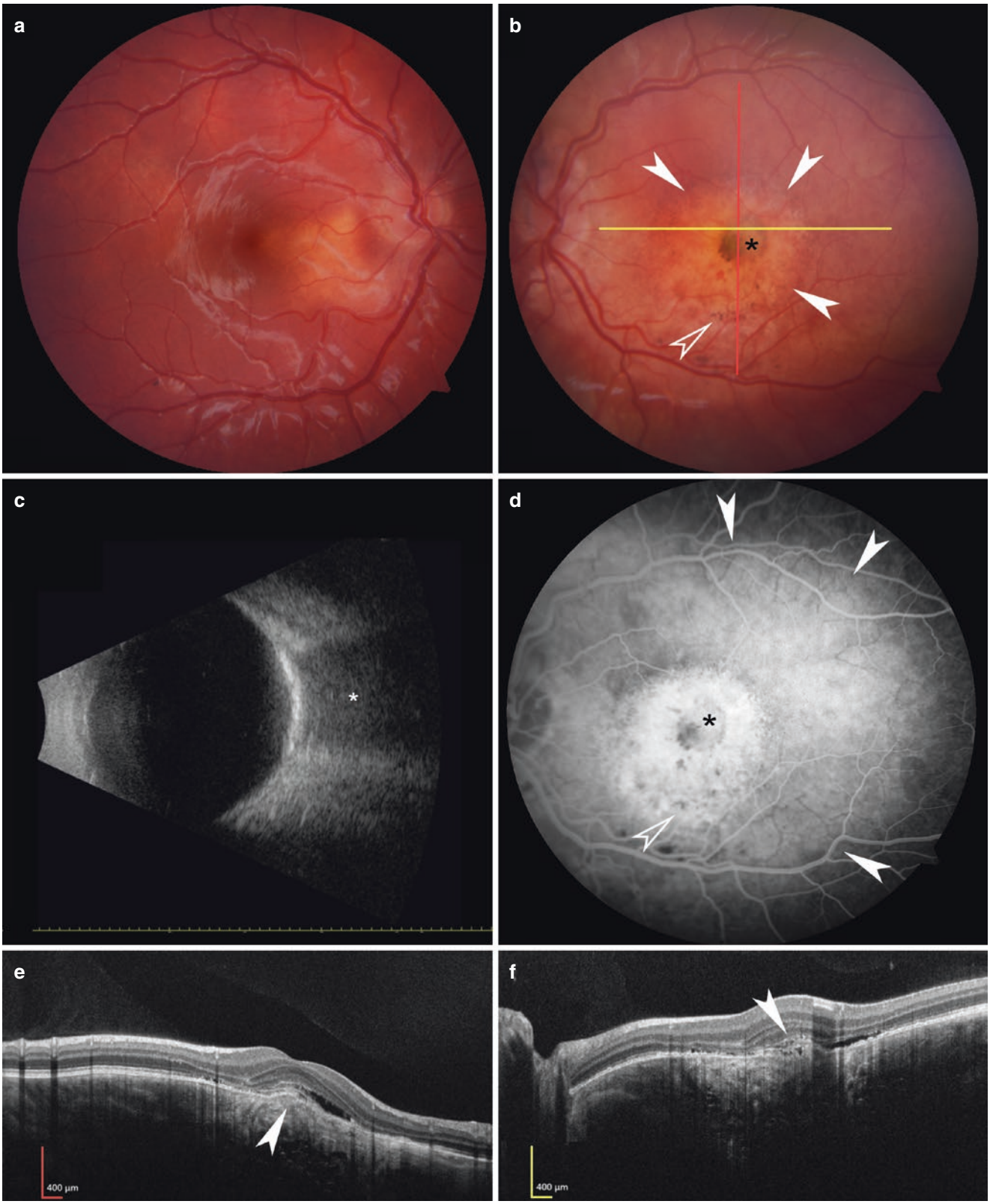

Fig. 5.2 Bilateral choroidal osteoma in a 7-year-old female. (**a**) One year after failing a vision screen, a fully ossified small osteoma of orange color is seen in the papillomacular area. Vision was 20/20. (**b**) A larger osteoma with a yellowish central deossified region (*arrowheads*), pigment mottling (*open arrowhead*), and a central pigmented nodule (*asterisk*) are seen. Vision was 20/30. (**c**) The osteoma is highly reflective and casts an acoustic shadow (*asterisk*) on ultrasonography. (**d**) The full extent of the osteoma (*arrowheads*) is revealed in a late frame of a fluorescein angiogram in which mottled (*open arrowhead*) and largely atrophic retinal pigment epithelium (RPE) over the deossifying part of the tumor is hyperfluorescent because of a window defect. The subretinal nodule stains but does not leak (*asterisk*). (**e**, **f**) Optical coherence tomography shows a subretinal bulge (*arrowhead*) with disrupted RPE and outer retinal disturbance

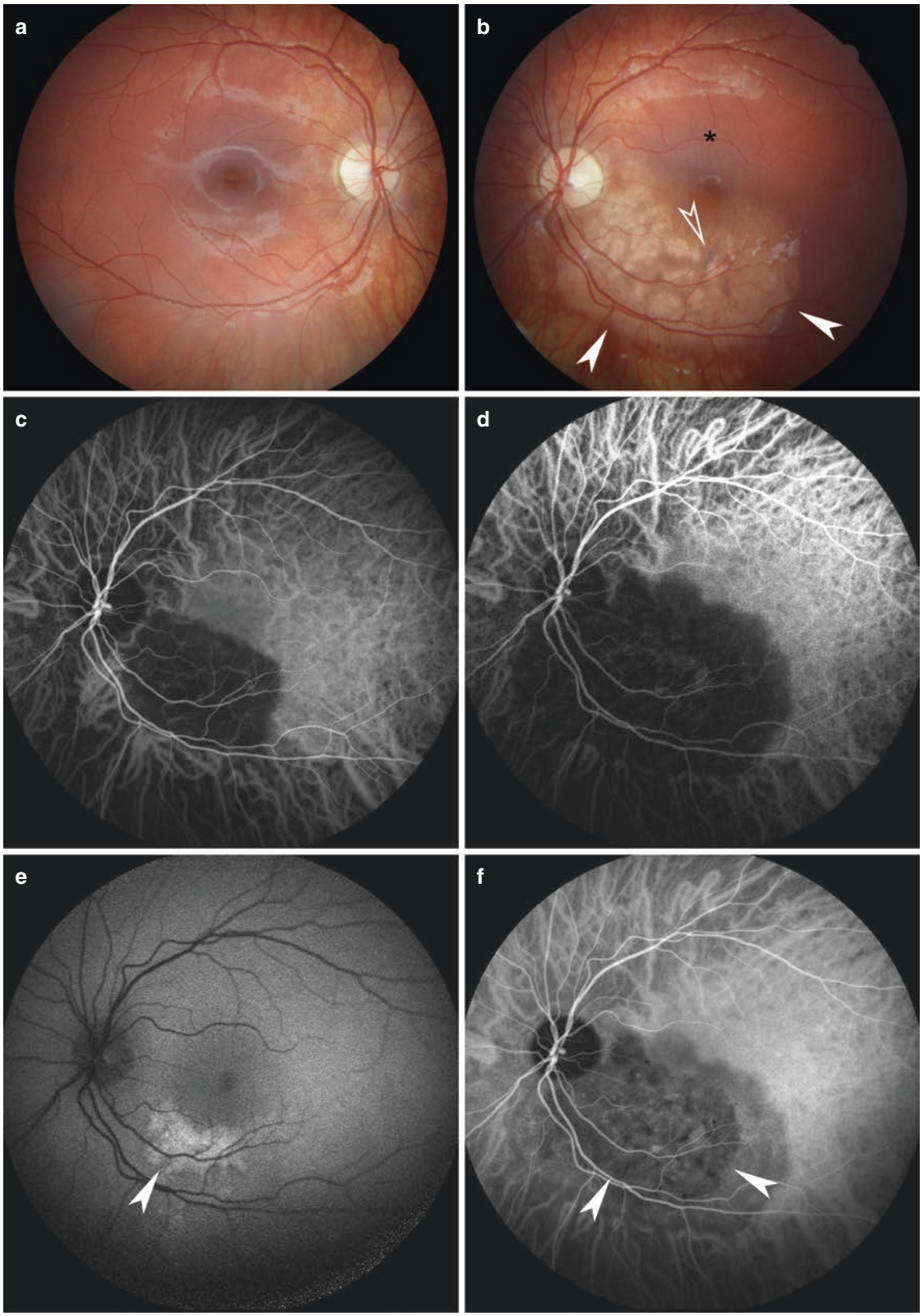

Fig. 5.3 Unilateral growing choroidal osteoma in an 11-year-old female. (**a**) Normal right eye. (**b**) Two years after experiencing transient metamorphopsia, a partially deossified perifoveal osteoma is seen inferotemporally (*arrowheads*). Note mottling of pigment (*open arrowhead*) and more yellowish area of retinal pigment epithelial (RPE) atrophy in its center. Vision was 20/25. (**c**, **d**) Early frames of fluorescein angiograms highlight growth to more than double its initial size within the preceding 2 years. (**e**) Two years earlier, fundus autofluorescence imaging showed a patch of hyperautofluorescence (*arrowhead*) as a sign of stress in the RPE from early leakage related to emerging deossification. (**f**) Indocyanine green angiography highlights the RPE atrophy and mottling over the deossified central part of the osteoma (arrowheads), whereas the peripheral still ossified part is relatively hypofluorescent within intact RPE

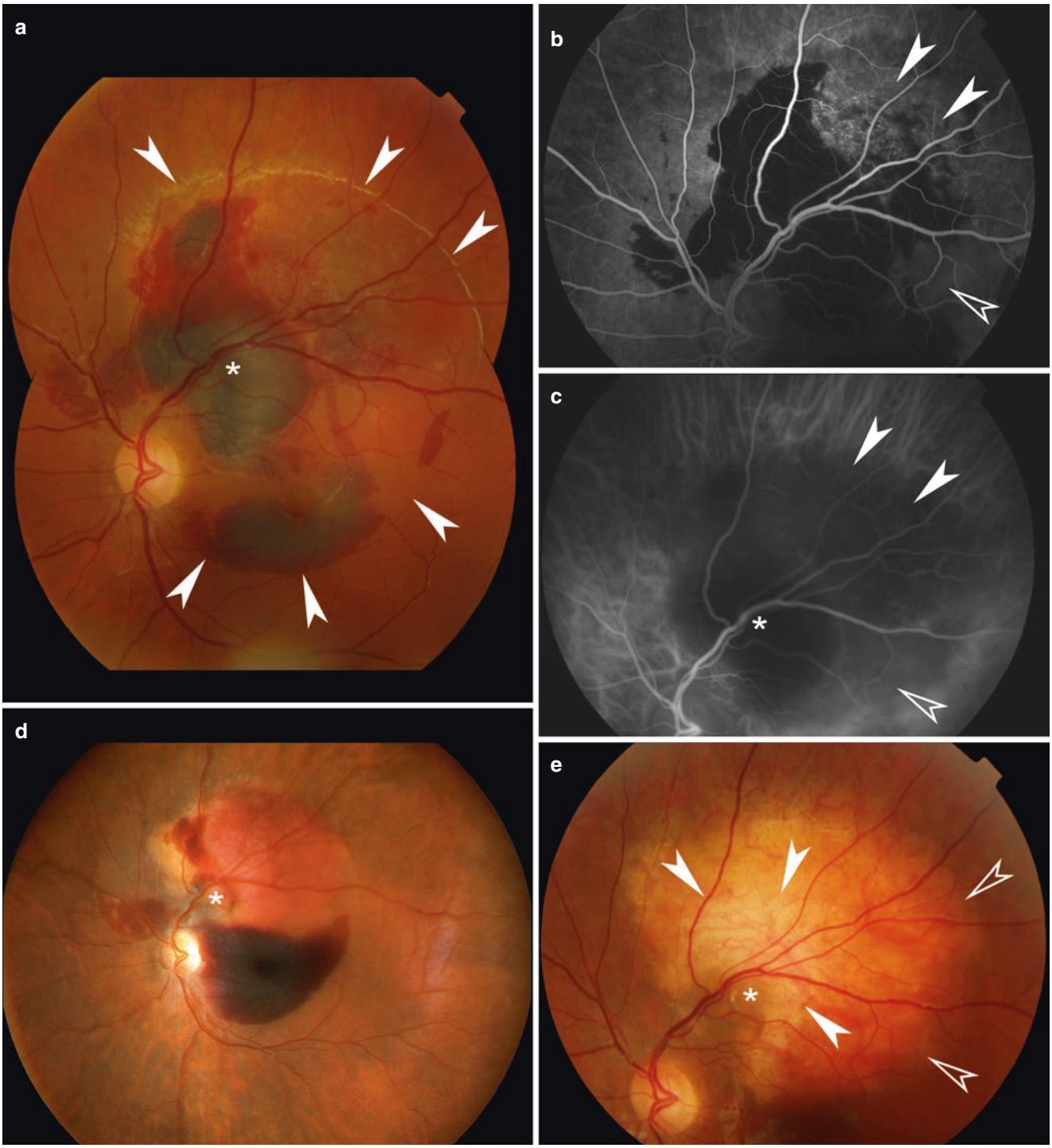

Fig. 5.4 Subretinal hemorrhage from an osteoma in an 18-year-old female. (**a**) One day after experiencing a sudden loss of vision, a hemorrhagic retinal detachment (*arrowheads*) largely hides an osteoma. The densest clot (*asterisk* in **a**–**e**) suggests the site of bleeding. Vision was 20/100. (**b**) Pinpoint hyperfluorescence and mottled retinal pigment epithelium over a deossifying part of the osteoma (*arrowheads*) not covered by the subretinal blood, whereas the ossified part (*open arrowhead*) is silent. (**c**) Both parts remain silent in an indocyanine green angiogram. (**d**) Three weeks later, the bleeding has settled in the dependent part of the detachment. Vision was 20/70. (**e**) Five months later, the bleeding has resolved spontaneously. The whitish deossified part of the osteoma highlighted by atrophy of the retinal pigment epithelium is seen (*arrowheads*), surrounded by the still ossified yellow-orange rim (*open arrowheads*). The site of the bleeding remains slightly elevated, suggesting a break in Bruch's membrane (*asterisk*).Vision was 20/20

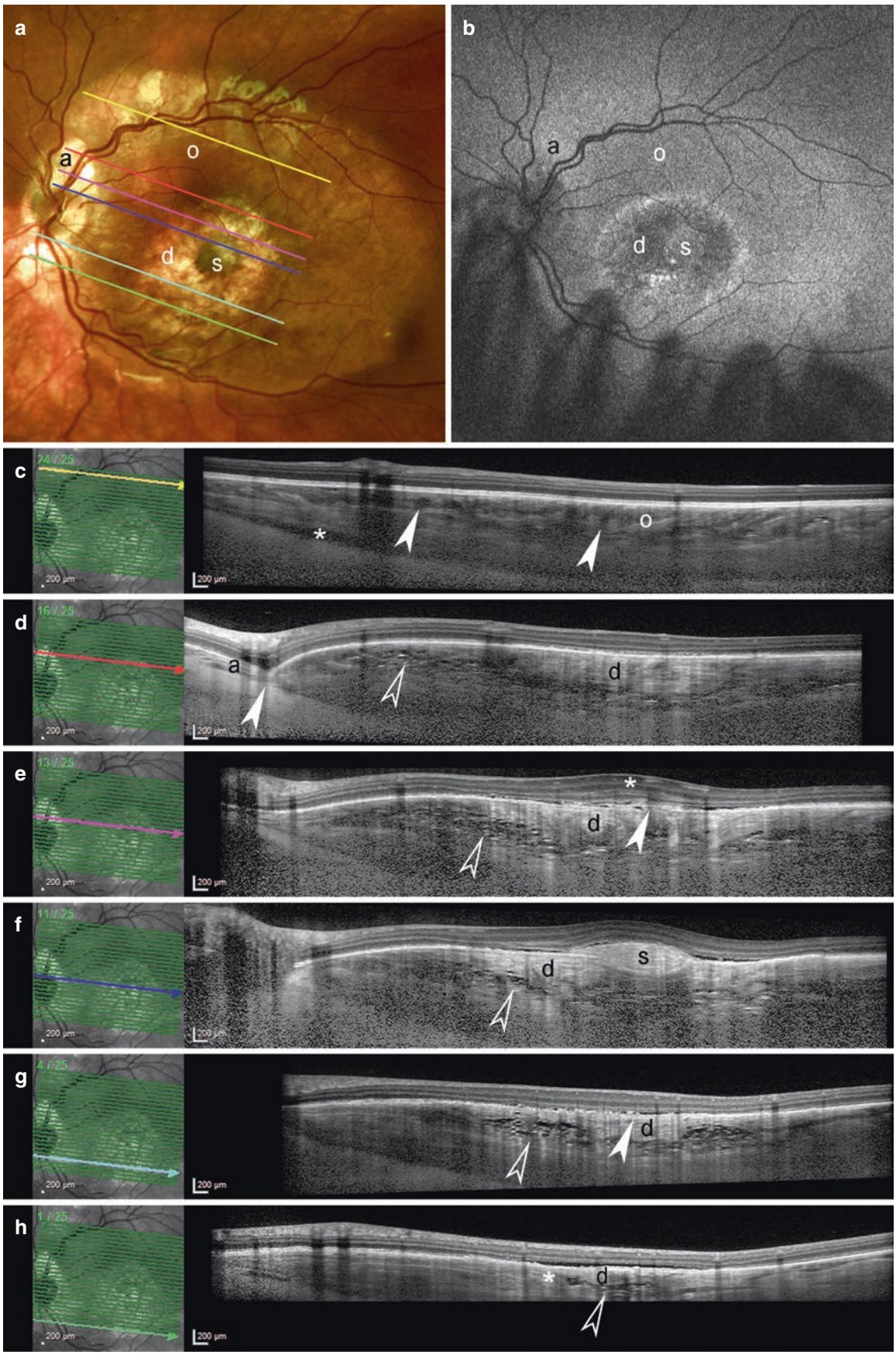
a
o
d
s
b
a
o
d
s
c
24 / 25
200 µm
*
o
d
16 / 25
a
d
e
13 / 25
*
d
f
11 / 25
d
s
g
4 / 25
d
h
1 / 25
*
d

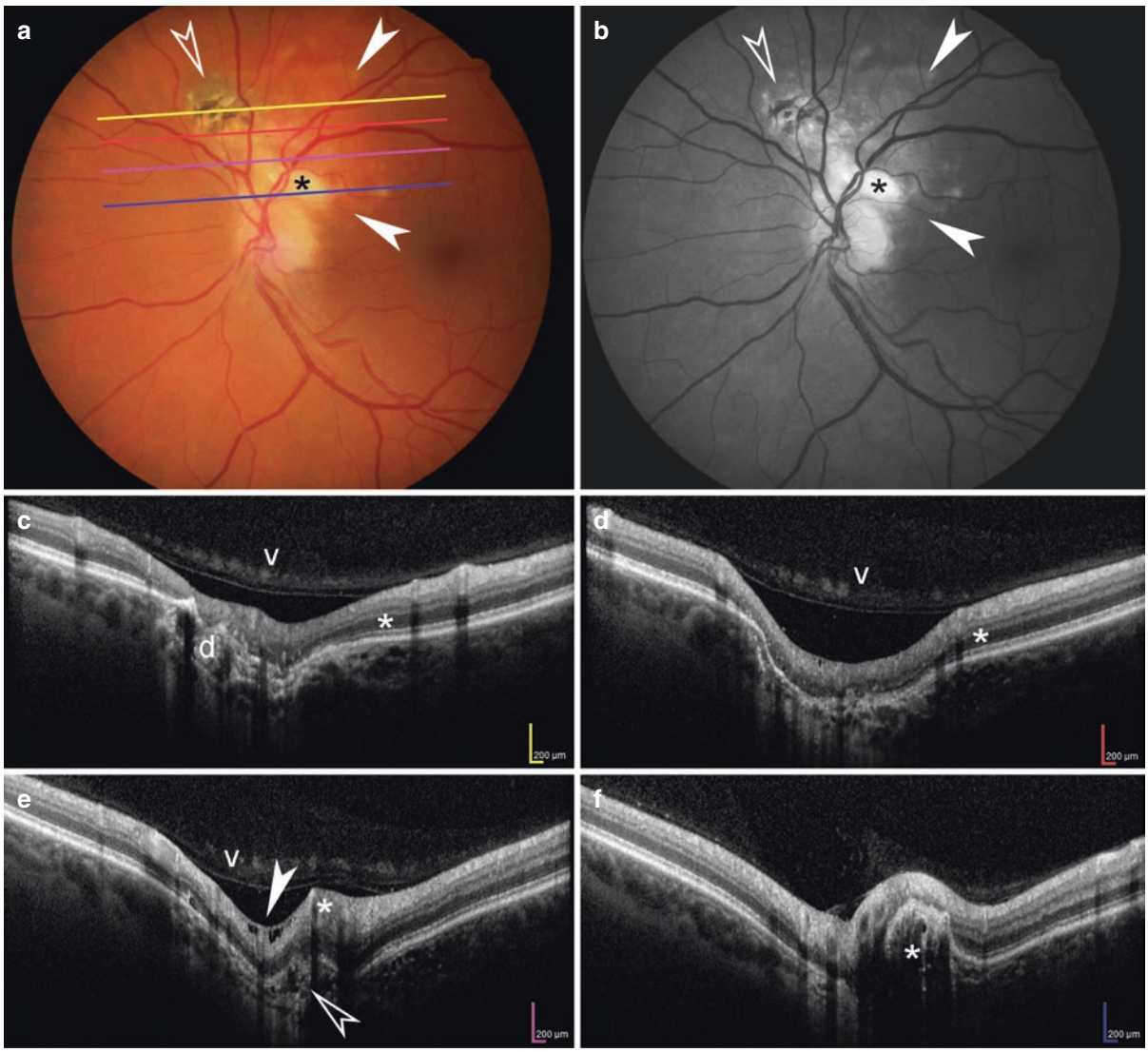

Fig. 5.6 An ancient osteoma with a focal choroidal excavation in a 58-year-old female with 20/20 vision. (**a**) The decalcified osteoma (*arrowheads*) is located superior to the optic disk and shows proliferation (*open arrowhead*) and atrophy of the overlying retinal pigment epithelium and a whitish nodule (*asterisk*) adjacent to the disk. (**b**) The margins of the osteoma are better visualized in a red-free image. (**c–f**) Optical coherence tomography (the color of the size bars corresponds to the location markers in the color fundus image; note the three times exaggerated vertical scale to highlight detail) shows a typical dense hyperreflective decalcified area (*d*) in the superior part of the osteoma with loss of the outer layers that are preserved in the adjacent retina (*asterisk* in **c** and **d**) and a focal choroidal excavation in the central and inferior part of the osteoma associated with a focal retinoschisis (*arrowhead*) and disorganization of the outer retina (*open arrowhead*) from traction caused by the overhanging large retinal vessels (*asterisk* in **e**) and a protuberant nodule (*asterisk* in **f**). Note overhanging vitreous membrane (*v* in **c–e**)

Fig. 5.5 An osteoma in a 7-year-old female with 20/40 vision in her left eye in a vision screen. (**a**) The osteoma occupies the posterior pole extending to slightly beyond the temporal vascular arcades as imaged by a wide-field scanning laser. Its peripheral part is ossified (*o*), and whitish mottled central part is undergoing deossification (*d*). Note peripapillary atrophic (*a*) areas and a parafoveolar subretinal (*s*) membrane in the center of the osteoma. (**b**) The ossified (*o*) part and subretinal nodule (*s*) are mildly hyperautofluorescent; the deossifying part (*d*) is relatively hypoautofluorescent from damage to the retinal pigment epithelium but bordered with a circle of hyperautofluorescence corresponding to the advancing rim of deossification with accumulation of lipofuscin in the pigment epithelial cells. Note that the peripapillary choroidal atrophy (*a*) has maintained the pigment epithelium. (**c**) On enhanced death imaging optical coherence tomography, the superficial layers of the ossified (*o*) portion has a multilayered wavy mostly horizontal lamellar structure with relatively hyporeflective intervening material that gives it a sponge-like appearance. Note apparent round vascular channels (*arrowheads*) and retained choroid (*asterisk*) close to the margin of the osteoma. (**d–h**) The deossified part (*d*) is hyperreflective and more densely packed and is surrounded by lamellar hyperreflective speckles (*open arrowhead*) in a hyporeflective matrix in the adjacent ossified part. Note damaged retinal pigment epithelium (*arrowhead* in **e** and **g**) and irregularity of photoreceptors with some intraretinal edema (*asterisk* in **e**), a hyperreflective subretinal membrane (*s* in **f**) that breaches the retinal pigment epithelium with shadowing of the underlying osteoma, and depression at the lower margin of the deossifying part (*asterisk* in **h**) with minor subretinal fluid. The greatest thickness of the osteoma was 1200 µm. Colors of the scanning lines in (**a**) correspond with **c–h**)

5.3.5 Symptoms and Signs

Unless the osteoma is serendipitously detected during a routine eye examination (Sisk et al. 2013; Süsskind et al. 2014), patients with a choroidal osteoma present after they experience visual loss related to deossification (Shields et al. 2015a, b; Pellegrini et al. 2014). Many patients become symptomatic because they develop a choroidal neovascular membrane or subretinal bleeding (Fig. 5.4) in which case they are seen within a few days of the onset of vision loss (Rao and Gentile 2010; Kubota-Taniai et al. 2011; Mercé et al. 2012; Koylu et al. 2014; Agarwal et al. 2014; Najafabadi et al. 2015; Shen et al. 2017). Photopsia, metamorphopsia, and a visual field defect also can be noted (Munteanu et al. 2013; Kamalden et al. 2014; Empeslidis et al. 2014; Dinah and Sandinha 2014; Shields et al. 2015a, b; Pellegrini et al. 2014). Others are seen after several months of vague or gradually developing visual symptoms that result from progressive subfoveal extension of the osteoma (Fig. 5.3), its slow deossification, or both (Empeslidis et al. 2014; Dinah and Sandinha 2014; Kamalden et al. 2014; Hussain et al. 2015; Lekha et al. 2015).

An ossified choroidal osteoma and the ossified portion of a partially deossified tumor, which can be either central or peripheral (Shields et al. 2005), are orange in color (Figs. 5.2, 5.3 and 5.4), likely reflecting the presence of an intact RPE over whitish bony tissue (Gass et al. 1978; Gass 1979; Yoshikawa and Takahashi 2015). The margins of the tumor appear sharp but often are scalloped, giving the osteoma a geographic or amoeboid shape. Overlying larger choroidal or intratumoral vessels may be visible (Sisk et al. 2013). With deossification of the underlying tumor, the RPE degenerates, resulting in a yellowish or whitish color with pigment dispersion and mottling (Figs. 5.2, 5.3, 5.4 and 5.5) over the deossified part (Trimble et al. 1988; Trimble and Schatz 1991; Aylward et al. 1998; Shields et al. 2005; Sisk et al. 2013; Kamalden et al. 2014; Empeslidis et al. 2014; MirNaghi et al. 2015; Yoshikawa and Takahashi 2015). Deossification is usually spontaneous, but it can follow treatment for choroidal neovascularization (CNV) (Trimble and Schatz 1991; Shields et al. 2005; Shields et al. 2008; Song et al. 2010; Hussain et al. 2015).

Serous retinal detachment overlying choroidal osteomas, if present, results from atrophy and disruption of the RPE, a CNV, or both. A CNV over an osteoma is visible as a grayish patch (Fig. 5.3) very often accompanied with focal subretinal bleeding (Rao and Gentile 2010; Morris et al. 2011; Mercé et al. 2012; Lekha et al. 2015; Hussain et al. 2015; Shen et al. 2017) and sometimes with reactive proliferation of the RPE (Sisk et al. 2013; Gupta et al. 2014; Yoshikawa and Takahashi 2015; Takkar et al. 2017) or bleeding under it (Kubota-Taniai et al. 2011).

Of 93 patients with appropriate documentation published from 2010 to 2017, 15% had a totally ossified choroidal osteoma at a median age of 16 years (range, 4–57) as comparted to 85% of patients with evidence of at least partial deossification of their tumor at a median age of 28 years (range, 7–63), suggesting that deossification might take on average about one decade to emerge (Fig. 5.1). These percentages are biased, however, because a report is more likely when symptoms related to the deossification have appeared.

5.3.6 Size

Choroidal osteomas measure from 3 to 20 mm in basal diameter, with a median of 7–8 mm (Shields et al. 2005; Freton and Finger 2012; Shields et al. 2015a, b; Papastefanou et al. 2016; Xuan et al. 2018). The diameter as measured from fundus photographs is on average 1.2 mm smaller than that measured by ultrasonography (Freton and Finger 2012) because its margins often are in part embedded and hidden within the adjacent choroid. The median thickness of the tumor is 1.3–1.5 mm as measured with ultrasonography, with a range from 0.1 to 4.0 mm (Shields et al. 2005; Freton and Finger 2012; Shields et al. 2015a, b; Papastefanou et al. 2016). Measurements taken with optical coherence tomography (OCT) are smaller because they exclude the retina, ranging from 0.1 to 1.7 mm with a median between 0.5 and 0.9 mm in several small series (Yoshikawa and Takahashi 2012; Pellegrini et al. 2014; Dinah and Sandinha 2014; Shields et al. 2015a, b; Yoshikawa and Takahashi 2015; de Mello et al. 2016).

Many if not most osteomas demonstrate slow growth centrifugally over several months to years (Palamar et al. 2012; Empeslidis et al. 2014; Süsskind et al. 2014), measured to be approximately 1 mm^2 per year in one particular case in which the growth also was somewhat faster when the patient approached adolescence (Kamalden et al. 2014) and a median of 0.37 mm per year (range, 0.01–1.15 mm) in a series of 13 growing choroidal osteomas (Shields et al. 2005). Occasionally, more rapidly growing choroidal osteomas (Fig. 5.3) have been reported in young children (Mizota et al. 1998). Deossification will not reduce the diameter of an osteoma, and growth may continue in other parts of the lesion, but the deossified part regresses in thickness (Fig. 5.6) and may even become excavated (Shields et al. 2005; Pierro et al. 2017; Chawla et al. 2017).

5.4 Examination

5.4.1 Ultrasonography

Both ophthalmoscopy and ultrasonography are necessary and almost always also sufficient for diagnosing a choroidal osteoma. A calcified osteoma is visible as a thin, highly reflective choroidal lesion with shadowing of the orbital structures

behind the tumor (Fig. 5.2c), giving the appearance of a virtual second optic nerve if the tumor is peripapillary (Rao and Gentile 2010; Freton and Finger 2012; Palamar et al. 2012; Altpeter et al. 2013; Munteanu et al. 2013; Süsskind et al. 2014; Kamalden et al. 2014; Empeslidis et al. 2014; Marty et al. 2014; Gupta et al. 2014; Lekha et al. 2015; Sambricio et al. 2015; Heichel et al. 2016). The tumor is still visible if the gain is lowered between 25 and 50 dB (Behera and Das 2015; Mihailovic et al. 2017). Deossified areas may not be more reflective than normal choroid, however, and they do not cast an acoustic shadow, and if the osteoma is thin, it may not even thicken the choroid enough to be visible by ultrasonography (Freton and Finger 2012; Sisk et al. 2013); in these rare cases, OCT is helpful in making the diagnosis (Dinah and Sandinha 2014).

5.4.2 Fluorescein and Indocyanine Green Angiography

Fluorescein angiography is necessary only if a CNV is suspected (Figs. 5.2d and 5.4b). It shows early patchy hyperfluorescence (Figs. 5.3d and 5.4b) and late diffuse staining of the tumor (Fig. 5.2d) (Palamar et al. 2012; Munteanu et al. 2013; Süsskind et al. 2014; Kamalden et al. 2014; Empeslidis et al. 2014; Hayashi et al. 2014; Marty et al. 2014; Gupta et al. 2014; Lekha et al. 2015; Hussain et al. 2015; Najafabadi et al. 2015). An ossified osteoma with an intact but thinned overlying RPE can show only minor hyperfluorescence because of a relative window effect (Fig. 5.3c) (MirNaghi et al. 2015). Window defects and stippled to patchy hypofluorescence from RPE atrophy and clumps with partial loss of choriocapillaris are seen in deossified areas (Fig. 5.2d) (Sisk et al. 2013; Kamalden et al. 2014). A choroidal neovascular membrane, if present, is visible as a patch of early hyperfluorescence and late leakage, often with blocked fluorescence from focal subretinal bleeding (Navajas et al. 2012; Jang et al. 2012; Wu et al. 2012; Sisk et al. 2013; Gupta et al. 2014; Süsskind et al. 2014; Hayashi et al. 2014; Lekha et al. 2015; Hussain et al. 2015).

On indocyanine green angiography, a choroidal osteoma is initially hypofluorescent but develops diffuse fine multifocal hyperfluorescence (Fig. 5.3f) that may become more confluent in late images (Agarwal et al. 2014; MirNaghi et al. 2015). Some osteomas remain hypofluorescent throughout (Fig. 5.4c), possibly because of compression or frank atrophy of the choriocapillaris (Altpeter et al. 2013; Hayashi et al. 2014; Empeslidis et al. 2014). A choroidal neovascular membrane is visualized more often as compared with fluorescein angiography (Kubota-Taniai et al. 2011; Pellegrini et al. 2014; Agarwal et al. 2014; Shen et al. 2017).

5.4.3 Optical Coherence Tomography

Choroidal osteomas have characteristic features on OCT imaging (Fig. 5.5). Their contour can be flat, dome-shaped, or undulating (Shields et al. 2015a). They vary from hyporeflective to hyperreflective, and the reflectivity often is inhomogeneous (Freton and Finger 2012). The over- or underlying choroid, if retained, is compressed if the osteoma elevates the retina; however, some osteomas are thin enough not to alter retinal contour (Freton and Finger 2012). Choroidal osteomas are transparent to infrared light, causing minimal optical shadowing (Pellegrini et al. 2014). Using enhanced-depth imaging (EDI), the posterior surface of the tumor can be traced, and the sclerochoroidal junction is usually visible (Pellegrini et al. 2014; Hayashi et al. 2014; Hussain et al. 2015). A hyperreflective line toward adjacent choroid may be visible (Navajas et al. 2012; Erol et al. 2013). The mnemonic "To See Osteoma" was proposed to memorize two of its most typical OCT characteristics: T for the optical transparency, S for spongy internal structure, and O for osteoma (Pellegrini et al. 2014).

The ossified portion of a choroidal osteoma (Fig. 5.5c) has a multilayered, bony, horizontal lamellar structure that gives it a sponge- or lattice-like reflective appearance (Navajas et al. 2012; Freton and Finger 2012; Mercé et al. 2012; Erol et al. 2013; Pellegrini et al. 2014; Hayashi et al. 2014; Shields et al. 2015a; Hussain et al. 2015; Sambricio et al. 2015; MirNaghi et al. 2015). The most hyperreflective lamellae have been interpreted as cement lines, and the intervening areas of low reflectivity between reflective lines and blocks of lamellar bone may represent Haversian and Volkmann's vascular canals of cortical bone (Freton and Finger 2012; Pellegrini et al. 2014; Shields et al. 2015a). Layers with multiple tiny hyperreflective dots or speckles in a hyporeflective matrix also are characteristic and may represent compact (cortical) or trabecular (spongy) bone with different degrees of calcification (Navajas et al. 2012; Freton and Finger 2012; Hayashi et al. 2014; Pellegrini et al. 2014; Shields et al. 2015a; Hussain et al. 2015). Retinal structures over an ossified tumor appear to be preserved (Navajas et al. 2012; Palamar et al. 2012; Erol et al. 2013).

The deossified portion of an osteoma (Fig. 5.5d–g) initially develops more irregular, denser lamellar reflective pattern without hyporeflective channels and, frequently, an irregular surface contour that may elevate, bulge, and even extend through the RPE as a heterogeneously reflective mound (Navajas et al. 2012; Yoshikawa and Takahashi 2012; Sisk et al. 2013; Sambricio et al. 2015; Hayashi et al. 2014; Kamalden et al. 2014). The deossified area tends to enlarge centrifugally (Navajas et al. 2012; Yoshikawa and Takahashi 2012; Hayashi et al. 2014), and at the same time they tend to atrophy in the center, becoming shrunken, sometimes forming crater relative to the adjacent still calcified portions of the

tumor, likely reflecting bone resorption through osteoclastic activity (Mercé et al. 2012; Sisk et al. 2013; Kamalden et al. 2014; Dinah and Sandinha 2014; Shields et al. 2015a; Yoshikawa and Takahashi 2015; Kumar 2017). A focal choroidal excavation can eventually develop (Fig. 5.4), leading to a focal tractional retino- or foveoschisis or consecutive anisometropia in some cases (Heichel et al. 2016; Introini et al. 2016; Chawla et al. 2017; Cheng et al. 2017; Pierro et al. 2017).

The outer retina over a deossified osteoma usually shows focal to diffuse disorganization of photoreceptor outer segments (Figs. 5.1e and 5.5e), disruption of the external limiting membrane, and breaching of the inner and outer segment junction (Navajas et al. 2012; Freton and Finger 2012; Erol et al. 2013; Sisk et al. 2013; Hayashi et al. 2014; Kamalden et al. 2014; Pellegrini et al. 2014; Sambricio et al. 2015; Hussain et al. 2015; MirNaghi et al. 2015). These irregularities may extend to the outer nuclear layer (Pellegrini et al. 2014). Outer retinal tubulations (Xuan et al. 2018), intraretinal cystic edema, and subretinal fluid in the absence of a choroidal neovascular membrane (Fig. 5.1e, f) because of dysfunction of the RPE pump may be seen (Marty et al. 2014; Empeslidis et al. 2014). Disruption, atrophy, or hyperplasia of the RPE (Figs. 5.1e and 5.5e) is typically present (Freton and Finger 2012; Hayashi et al. 2014), and Bruch's membrane may be deformed or ruptured (Hayashi et al. 2014). The choriocapillaris is thin, and the medium caliber vessels in Sattler's layer are irregular or are obliterated, whereas the large caliber vessels in Haller's layer can be preserved (Pellegrini et al. 2014; Hayashi et al. 2014; Hussain et al. 2015; MirNaghi et al. 2015).

A choroidal neovascular membrane, if present, is visualized as a hyperreflective layer over the RPE (Navajas et al. 2012; Erol et al. 2013; Hayashi et al. 2014; Saitta et al. 2015; Hussain et al. 2015; MirNaghi et al. 2015; Yoshikawa and Takahashi 2015; Shen et al. 2017; de Mello et al. 2016). Serous retinal detachment (Freton and Finger 2012; Gupta et al. 2014; Pellegrini et al. 2014; Hayashi et al. 2014; Dinah and Sandinha 2014; Najafabadi et al. 2015; Hussain et al. 2015; Yoshikawa and Takahashi 2015) and intraretinal edema also are present (Pellegrini et al. 2014; Gupta et al. 2014; Yoshikawa and Takahashi 2015).

En face OCT angiography can document a CNV as an irregular vascular signal at the level of the outer retina, the choriocapillaris, and the hyperreflective layer over RPE that overlies a choroidal osteoma (Azad et al. 2016; Szelog et al. 2016; Shen et al. 2017; Cennamo et al. 2017; Mihailovic et al. 2017; Pierro et al. 2017; Grisolia et al. 2018; Xuan et al. 2018).

5.4.4 Fundus Autofluorescence Imaging

Fundus autofluorescence imaging is helpful in estimating damage to the RPE in the foveal area (Figs. 5.1e and 5.5b). Osteomas may show areas with hypoautofluorescence, isoautofluorescence, and hyperautofluorescence, often in a patchy pattern if deossification has taken place (Sisk et al. 2013; Najafabadi et al. 2015; Kuma 2017). A ring of hyperautofluorescence from metabolically stressed RPE may be seen along the margin of the osteoma (Fig. 5.4) surrounding a central area of isoautofluorescence or heterogeneous autofluorescence (Ascaso and Villen 2011; Hassani et al. 2011; Mayer et al. 2011; Marty et al. 2014). Visual acuity is normal with foveal isoautofluorescence but subnormal in eyes with foveal hypoautofluorescence (Sisk et al. 2013; Sambricio et al. 2015).

Ossified areas show either preserved isoautofluorescence (Fig. 5.1e) or mild relative hyperautofluorescence (Fig. 5.5b) so that the osteoma often is almost invisible (Sisk et al. 2013; Erol et al. 2013; Hayashi et al. 2014; Sambricio et al. 2015; MirNaghi et al. 2015). Lipofuscin flecks occasionally may be seen as hyperautofluorescence over the tumor (Sisk et al. 2013).

Deossified areas may show initially hyperautofluorescence (Fig. 5.1e) and later hypoautofluorescence with scattered hyperautofluorescence (Fig. 5.5b) from stressed and damaged RPE, respectively (Sisk et al. 2013; Erol et al. 2013; Hayashi et al. 2014; Marty et al. 2014; Sambricio et al. 2015; MirNaghi et al. 2015). Hyperautofluorescent spots or a reticular diffuse hyperautofluorescence may be seen in areas with serous detachment, possibly resulting from outer segment elongations of photoreceptors containing retained visual pigments and, eventually, lipofuscin (Sisk et al. 2013; Hayashi et al. 2014; Erol et al. 2013). Mild residual autofluorescence possibly corresponding to fibrous metaplasia of the RPE may be retained over long-standing decalcified osteomas (Navajas et al. 2012).

5.4.5 Computed Tomography and Magnetic Resonance Imaging

Computed tomography of the orbit shows a choroidal osteoma as a flat hyperdense plaque at the posterior pole of the eye (Song et al. 2010; Karanjia et al. 2010; Kubota-Taniai et al. 2011; Palamar et al. 2012; Erol et al. 2013; Yiu and Young 2013; MirNaghi et al. 2015; Bessho et al. 2017; Mihailovic et al. 2017). This examination is to be avoided, however, because it provides no additional information compared with ultrasonography while unnecessarily exposing the patient to ionizing radiation. A decalcified osteoma will not be visible (Marty et al. 2014).

A choroidal osteoma shows high signal intensity in T1-weighted magnetic resonance images and low intensity in T2-weighted images; it enhances with gadolinium (DePotter et al. 1991; Verma et al. 2000; Bessho et al. 2017).

5.5 Differential Diagnosis

Choroidal osteomas must be differentiated from other choroidal lesions that are calcified and will thus mimic it in ultrasonography. The most common of these is sclerochoroidal calcification, which typically affects adults and elderly patients with a mean age of 69 years (range, 32–95) and is located along the vascular arcades or between them and the equator in 90% of patients (Shields et al. 2015a, b), and metaplastic bone is a phthisical eye (Munteanu et al. 2013). More rare lesions to be differentiated from osteomas include a calcified choroidal hemangioma (Munteanu et al. 2013), a calcified choroidal melanoma (Gianniou et al. 2017), and a calcified posterior scleral choristoma in the organoid nevus syndrome; the latter can appear very similar to a choroidal osteoma (Traboulsi et al. 1999).

5.6 Histopathology

Choroidal osteomas are not managed surgically and thus histopathological reports are scarce. The tumor in two enucleated eyes consisted of dense bony trabeculae connected to each other and separated by wide marrow spaces with loose vacuolated stroma, young mesenchymal cells, cavernous vascular channels and small capillaries, numerous osteocytes, prominent cement lines, osteoblasts especially adjacent to a largely attenuated choriocapillaris, occasional osteoclasts, and an overlying degenerative RPE and a serous retinal detachment (Reese 1963; Gass et al. 1978; Williams et al. 1978). Several of these features are recapitulated in recent OCT images (Navajas et al. 2012; Freton and Finger 2012; Shields et al. 2015a). Partial hyalinization was additionally present in one surgically resected, apparently partially decalcified choroidal osteoma (Bessho et al. 2017).

5.7 Management

There is no need to treat an asymptomatic choroidal osteoma. Therapy is directed toward controlling subretinal fluid arising from disrupted RPE and toward CNV, if present.

5.7.1 Observation

Ossified choroidal osteomas are observed, and they can remain quiescent for many years or even decades without loss of vision, and, when they deossify, the process does not always extend to the center of the macula (Hasanreisoglu et al. 2015; Empeslidis et al. 2014; MirNaghi et al. 2015). Rarely, even a subretinal bleeding can spontaneously resolve without leaving behind an active choroidal neovascular membrane (Koylu et al. 2014) (Fig. 5.3).

5.7.2 Calcium Supplementation

Calcium supplementation in an effort to delay deossification has been prescribed, but evidence for its efficacy has not been published (Voluck et al. 2011).

5.7.3 Anti-vascular Endothelial Growth Factor Agents

One to three intravitreal injections of 1.25 mg bevacizumab (Table 5.1) has almost consistently resulted in regression of a CNV associated with a choroidal osteoma, albeit often with a short follow-up time (Mansour et al. 2014; Pandey and Guruprasad 2010; Pérez Aragón et al. 2010; Rao and Gentile 2010; Song et al. 2010; Kubota-Taniai et al. 2011; Mercé et al. 2012; Agarwal et al. 2014; Süsskind et al. 2014). It also has sometimes been effective in resolving subretinal fluid in the absence of a demonstrable CNV (Song et al. 2010; Vayalambrone and Misra 2012; Carle et al. 2014; Najafabadi et al. 2015), but treatment for subretinal fluid may not prevent a CNV from developing (Hayashi et al. 2014).

Results comparable with those obtained with intravitreal injection of bevacizumab have been achieved with 0.5 mg of ranibizumab (Table 5.1), a drug which is theoretically safer than bevacizumab in children (Wu et al. 2012; Mansour et al. 2014; Gupta et al. 2014; Lekha et al. 2015; Schuh et al. 2017; Sarigül Sezenöz et al. 2017). In one report, switching from bevacizumab and ranibizumab to 2.0 mg aflibercept induced regression of a CVN unresponsive to the former medications (Saitta et al. 2015).

Late recurrences more than 5 years after initial regression of a CNV induced with anti-vascular endothelial growth factor agents can occur (Lekha et al. 2015). In a multicenter review of 18 eyes with a choroidal osteoma treated with bevacizumab, ranibizumab, or both, the visual acuity improved a median of three lines, a result that was maintained after 2 years (Mansour et al. 2014). Like with other treatment modalities, it has been speculated that anti-vascular endothelial growth factor agents

Table 5.1 Primary monotherapy for choroidal osteoma published from 2010 to 2017

Author	Age (years)	Indication	Injections	Outcome	Follow-up (months)
Bevacizumab					
Ayachit 2010	27	CNV	Single	Regression	6
Rao 2010	24	CNV	3, monthly	Regression	5
Song 2010	46	CVN	2, PRN	Regression	23
Song 2010	29	SRF	3, PRN	Resolution	7
Song 2010	36	SRF	2, PRN	Resolution	6
Song 2010	40	SRF	Single	Response	2
Pérez Aragón 2010	12	CNV	3, PRN	Regression	12
Kubota-Taniai 2011	12	CNV	2, PRN	Regression	24
Vayalambrone 2012	11	SRF	3, monthly	Resolution	24
Mercé 2012	11	CNV	3, PRN	Regression	4
Agarwal 2014	10	CNV	3, monthly	Regression	12
Najafabadi 2015	20	SRF	Single	Resolution	18
Hussain 2015	45	CNV	9	Unresponsive	
Saitta 2015	45	CNV	2, monthly	Unresponsive	
Yoshikawa 2015	34	CNV	2, PRN	Regression	44
Yoshikawa 2015	53	CNV	Single	Regression	56
Yoshikawa 2015	14	CNV	3, PRN	Unresponsive	
MirNaghi 2015	32	CNV	3, monthly	Regression	9
Papastefanou 2016	36	CNV	10, PRN	Regression	15
Papastefanou 2016	27	CNV	4, PRN	Regression	12
Papastefanou 2016	32	CNV	5, PRN	Regression	12
Papastefanou 2016	66	CNV	3, PRN	Regression	4
Papastefanou 2016	17	CNV	5, PRN	Regression	7
Papastefanou 2016	21	CNV	5, PRN	Regression	10
Papastefanou 2016	58	CNV	3, PRN	Regression	3
Papastefanou 2016	72	CNV	7, PRN	Regression	9
Cheng 2017	51	CNV	Single	Regression	84
Takkar 2017	35	CNV	3, monthly	Regression	12
Ranibizumab					
Wu 2012	57	CNV	3, monthly	Regression	14
Gupta 2014	9	CNV	3, PRN	Regression	30
Carle 2014	20	SRF	6	Resolution	12
Lekha 2015	30	CNV	3, monthly	Regression	60*
Saitta 2015	45	CNV	3, monthly	Unresponsive	
Shen 2017	25	CNV	2, monthly	Regression	1
Cennamo 2017	75	CNV	3, monthly	Regression	12
Schuh 2017	28	CNV	6, monthly	Unresponsive	
Aflibercept					
Saitta 2015	45	CNV	3, monthly	Regression	10†
Sarigül Sezenöz 2017	47	CNV	3 + 1, monthly	Regression	24

CNV, choroidal neovascular membrane; *PRN*, pro re nata; *SRF*, subretinal fluid without neovascular membrane; * Late recurrence; † After failed bevacizumab and ranibizumab

might in some cases augment the deossification process (Cheng et al. 2017).

5.7.4 Laser Therapy

Although argon and krypton laser photocoagulation have been applied in the past to eradicate a CNV over a choroidal osteoma, this treatment is now only of historical interest (Aylward et al. 1998). The same applies to transpupillary thermotherapy (TTT) described in a few case reports in which it was successful (Sharma et al. 2004; Shukla et al. 2006; Yahia et al. 2008).

Photodynamic therapy (PDT) with verteporfin has been used to eradicate choroidal neovascular membranes associated with osteomas, frequently in combination with anti-vascular endothelial growth factor agents (Morris et al. 2011; Jang et al. 2012; Mansour et al. 2014; Khan et al. 2014). PDT may have a role in eradicating a CNV that does not respond to treatment with anti-vascular endothelial growth factor agents (Hussain et al. 2015).

All forms of laser treatment cause focal deossification in the treated volume (Trimble and Schatz 1991; Shields et al. 2005; Shields et al. 2008; Song et al. 2010; Hussain et al. 2015). Theoretically, this is an option for aborting the growth of an extrafoveal choroidal osteoma that approaches

toward the fovea, but this approach is considered hazardous because of a risk of an iatrogenic subretinal bleeding or CNV (Shields et al. 2008; Palamar et al. 2012).

5.7.5 Radiotherapy

Proton beam irradiation at a dose on 20 cobalt gray equivalents to induce regression of an enlarging perifoveal choroidal osteoma in a young child was followed by development of a CNV with loss of reading vision in spite of inducing regression of the CNV with bevacizumab (Süsskind et al. 2014).

5.7.6 Vitreoretinal Surgery

Endoresection of one extrafoveal choroidal osteoma in a procedure originally planned to biopsy the tumor to exclude an amelanotic melanoma (Bessho et al. 2017) and surgical removal of a CNV associated with a choroidal osteoma (Foster et al. 2003) have been performed only once and are as such highly experimental procedures.

5.8 Prognosis

Choroidal osteomas can remain asymptomatic for extended periods and are benign tumors that pose no hazard to life. Visual prognosis is variable and depends on the location, uni- or bilaterality, and the individual tendency to grow and deossify and the presence or absence of a CNV after deossification has commenced (Shields et al. 2005; Yoshikawa and Takahashi 2015). Prognosis is usually excellent for extrafoveal and ossified tumors, guarded for ossified subfoveal and most perifoveal tumors, and poor for those osteomas that have extended subfoveally and deossify.

References

Agarwal M, Kantha M, Mayor R, et al. Bilateral choroidal osteoma with choroidal neovascular membrane treated with bevacizumab in a child. Middle East Afr J Ophthalmol. 2014;21:265–7.

Altpeter EK, Süsskind D, Bartz-Schmidt KU, et al. Unklarer parapapillärer Tumor im Kindesalter. Ophthalmologe. 2013;110:986–9.

Ascaso FJ, Villen L. Fundus autofluorescence imaging findings in choroidal osteoma. Retina. 2011;31:1004–5.

Aylward GW, Chang TS, Pautler SE, et al. A long-term follow-up of choroidal osteoma. Arch Ophthalmol. 1998;116:1337–41.

Azad SV, Takkar B, Venkatesh P, et al. Swept source: optical coherence tomography angiography features of choroidal osteoma with choroidal neovascular membrane. BMJ Case Rep. 2016:2016.

Behera M, Das MK. A case of choroidal osteoma in a 10-year-old child. Int Med Case Rep J. 2015;8:273–5.

Bessho H, Imai H, Azumi A. The histopathological finding of the surgically extracted atypical dome-shaped choroidal osteoma. Case Rep Ophthalmol Med. 2017;2017:2874823.

Carle MV, Chu TG, Liao D, et al. Successful use of anti-VEGF treatment for subretinal hemorrhage and fluid in a young patient with choroidal osteoma. Ophthalmic Surg Lasers Imaging Retina. 2014;45:169–71.

Cennamo G, Romano MR, Iovino C, et al. OCT angiography in choroidal neovascularization secondary to choroidal osteoma. Acta Ophthalmol. 2017;95:e152–4.

Chawla R, Azad SV, Takkar B, et al. Nonconforming deep focal choroidal excavation in a patient with choroidal osteoma: a diagnostic dilemma. Ophthalmic Surg Lasers Imaging Retina. 2017;48:944–7.

Chen J, Lee L, Gass JD. Choroidal osteoma: evidence of progression and decalcification over 20 years. Clin Exp Optom. 2006;89:90–4.

Cheng YC, Shen JH, Chao AN, et al. Later development of posterior staphyloma in choroidal osteoma with choroidal neovascularization. Retina. 2017;37:e95–6.

Cunha SL. Osseous choristoma of the choroid. A familial disease. Arch Ophthalmol. 1984;102:1052–4.

DePotter P, Shields JA, Shields CL, et al. Magnetic resonance imaging in choroidal osteoma. Retina. 1991;11:221–3.

Dinah C, Sandinha T. Enhanced depth imaging as an adjunctive tool in the diagnosis of decalcified choroidal osteoma. Eye (Lond). 2014;28:356–8.

Empeslidis T, Imrani U, Konidaris V, et al. Diagnosis and monitoring of choroidal osteoma through multimodal imaging. Case Rep Med. 2014;2014:393804.

Erol MK, Coban DT, Ceran BB, et al. Enhanced depth imaging optical coherence tomography and fundus autofluorescence findings in bilateral choroidal osteoma: a case report. Arq Bras Oftalmol. 2013;76:189–91.

Eting E, Savir H. An atypical fulminant course of choroidal osteoma in two siblings. Am J Ophthalmol. 1992;113:52–5.

Fava GE, Brown GC, Shields JA, et al. Choroidal osteoma in a 6-year-old child. J Pediatr Ophthalmol Strabismus. 1980;17:203–5.

Foster BS, Fernandez-Suntay JP, Dryja TP, et al. Surgical removal and histopathologic findings of a subfoveal neovascular membrane associated with choroidal osteoma. Arch Ophthalmol. 2003;121:273–6.

Freton A, Finger PT. Spectral domain-optical coherence tomography analysis of choroidal osteoma. Br J Ophthalmol. 2012;96:224–8.

Gass JD. New observations concerning choroidal osteomas. Int Ophthalmol. 1979;1:71–84.

Gass JD, Guerry RK, Jack RL, et al. Choroidal osteoma. Arch Ophthalmol. 1978;96:428–35.

Gianniou C, Zografos L, Hrbacek J, et al. Kalzifiziertes nicht pigmentiertes Aderhautmelanom: fallbericht einer seltenen Entität. Klin Monatsbl Augenheilkd. 2017;234:608–10.

Grisolia ABD, de França Martins M, Demirci H. Imaging of neovascular membrane over a choroidal osteoma by OCT angiography. Ophthalmology. 2018;125:236.

Gupta A, Gopal L, Sen P, et al. Long-term results of intravitreal ranibizumab for osteoma-related choroidal neovascularization in a child. Oman J Ophthalmol. 2014;7:78–80.

Hasanreisoglu M, Shields JA, Mashayekhi A, et al. Bilateral choroidal osteoma: visual acuity at 45-year follow-up. Retin Cases Brief Rep. 2015;9:239–41.

Hassani RT, Terrada C, Puech M, et al. Ostéome choroïdien compliqué de néovascularisation: aspects en OCT spectral-domain. J Fr Ophtalmol. 2011;34:349–52.

Hayashi Y, Mitamura Y, Egawa M, et al. Swept-source optical coherence tomographic findings of choroidal osteoma. Case Rep Ophthalmol. 2014;5:195–202.

Heichel J, Bredehorn-Mayr T, Stuhlträger U, et al. Manifestation eines bilateralen chorioidalen Osteoms im Kindesalter. Ophthalmologe. 2016;113:160–3.

Hussain R, Anantharaman G, Rajesh B, et al. Real-time in vivo micromorphology and histopathology of choroidal osteoma using enhanced depth imaging. Indian J Ophthalmol. 2015;63:453–5.

Introini U, Casalino G, Parodi MB, et al. Diagnostic and therapeutic challenges. Retina. 2016;36:422–7.
Jang JH, Kim KH, Lee SJ, et al. Photodynamic therapy combined with intravitreal bevacizumab in a patient with choroidal neovascularization secondary to choroidal osteoma. Korean J Ophthalmol. 2012;26:478–80.
Kamalden TA, Lingam G, Sundar G. Bone remodeling in choroidal osteoma monitored by fundus photography and spectral-domain optical coherence tomography. Ocul Oncol Pathol. 2014;1: 13–8.
Karanjia R, Gale JG, ten Hove MW. Macular choroidal osteoma with progressive widespread outer-retinal dysfunction. Can J Ophthalmol. 2010;45:179–80.
Katz RS, Gass JD. Multiple choroidal osteomas developing in association with recurrent orbital inflammatory pseudotumor. Arch Ophthalmol. 1983;101:1724–7.
Khan MA, DeCroos FC, Storey PP, et al. Outcomes of anti-vascular endothelial growth factor therapy in the management of choroidal neovascularization associated with choroidal osteoma. Retina. 2014;34:1750–6.
Kline LB, Skalka HW, Davidson JD, et al. Bilateral choroidal osteomas associated with fatal systemic illness. Am J Ophthalmol. 1982;93:192–7.
Koylu MT, Gokce G, Uysal Y, et al. Spontaneous resolution of subretinal hemorrhage secondary to choroidal osteoma unassociated with choroidal neovascularization. Case Rep Ophthalmol Med. 2014;2014:823953.
Kubota-Taniai M, Oshitari T, Handa M, et al. Long-term success of intravitreal bevacizumab for choroidal neovascularization associated with choroidal osteoma. Clin Ophthalmol. 2011;5:1051–5.
Kumar V. Choroidal osteoma and pattern dystrophy of retinal pigment epithelium. Int Ophthalmol. 2017.
Lekha T, Renuka NS, Prasad HN. Anti-vascular endothelial growth factors for choroidal neovascularization secondary to choroidal osteoma: long-term results. Oman J Ophthalmol. 2015;8:185–7.
Mansour AM, Arevalo JF, Al Kahtani E, et al. Role of intravitreal antivascular endothelial growth factor injections for choroidal neovascularization due to choroidal osteoma. J Ophthalmol. 2014;2014:210458.
Marty AS, Debats F, Kodjikian L, et al. Imagerie multimodale d'un ostéome choroïdien décalcifié. J Fr Ophtalmol. 2014;37:745–7.
Mayer C, Glaser E, Khoramnia R. Sehstorungen bei auffalligem Fundusbefund. Ophthalmologe. 2011;108:379–83.
de Mello PC, Berensztejn P, Brasil OFM. Enhanced depth imaging optical coherence tomography of choroidal osteoma with secondary neovascular membranes: report of two cases. Arq Bras Oftalmol. 2016;79:197–9.
Mercé E, Korobelnik JF, Delyfer MN, et al. Néovascularisation choroïdienne sur un ostéome choroïdien: traitement par bévacizumab et suivi par OCT spectral-domain. J Fr Ophtalmol. 2012;35:508–13.
Mihailovic N, Alnawaiseh M, Merte RL, et al. OCT-angiographische Darstellung einer choroidalen Neovaskularisation infolge eines Aderhautosteoms. Ophthalmologe. 2017;114:843–7.
MirNaghi M, Nasser S, SeyedehMaryam H, et al. Bilateral multifocal choroidal osteoma with choroidal neovascularization. Case Rep Ophthalmol Med. 2015;2015:346415.
Mizota A, Tanabe R, Adachi-Usami E. Rapid enlargement of choroidal osteoma in a 3-year-old girl. Arch Ophthalmol. 1998;116:1128–9.
Morris RJ, Prabhu VV, Shah PK, et al. Combination therapy of low-fluence photodynamic therapy and intravitreal ranibizumab for choroidal neovascular membrane in choroidal osteoma. Indian J Ophthalmol. 2011;59:394–6.
Munteanu M, Munteanu G, Giuri S, et al. Ossification of the choroid: three clinical cases and literature review of the pathogenesis of intraocular ossification. Romanian J Morphol Embryol. 2013;54: 871–7.
Najafabadi FF, Hendimarjan SM, Zarrin Y, et al. Intravitreal Bevacizumab for Management of Choroidal Osteoma without Choroidal neovascularization. J Ophthalmic Vis Res. 2015;10:484–6.
Navajas EV, Costa RA, Calucci D, et al. Multimodal fundus imaging in choroidal osteoma. Am J Ophthalmol. 2012;153:890–895 e893.
Noble KG. Bilateral choroidal osteoma in three siblings. Am J Ophthalmol. 1990;109:656–60.
Palamar M, Uretmen O, Gündüz K. Transient subretinal hemorrhage after photodynamic therapy of subfoveal choroidal osteoma. Retin Cases Brief Rep. 2012;6:166–8.
Pandey N, Guruprasad A. Choroidal osteoma with choroidal neovascular membrane: successful treatment with intravitreal bevacizumab. Clin Ophthalmol. 2010;4:1081–4.
Papastefanou VP, Pefkianaki M, Al Harby L, et al. Intravitreal bevacizumab monotherapy for choroidal neovascularisation secondary to choroidal osteoma. Eye (Lond). 2016;30:843–9.
Pellegrini M, Invernizzi A, Giani A, et al. Enhanced depth imaging optical coherence tomography features of choroidal osteoma. Retina. 2014;34:958–63.
Pérez Aragón AJ, Toribio García M, Delgado Alonso E, et al. Osteoma coroideo y neovascularizacion coroidea: causa rara de ceguera en el adolescente. An Pediatr (Barc). 2010;72:436–7.
Pierro L, Marchese A, Gagliardi M, et al. Choroidal excavation in choroidal osteoma complicated by choroidal neovascularization. Eye (Lond). 2017;31:1740–3.
Rao S, Gentile RC. Successful treatment of choroidal neovascularization complicating a choroidal osteoma with intravitreal bevacizumab. Retin Cases Brief Rep. 2010;4:303–5.
Reese AB. Tumors of the eye. 2nd ed. New York: Hoeber; 1963.
Saitta A, Nicolai M, Neri P, et al. Rescue therapy with intravitreal aflibercept for choroidal neovascularization secondary to choroidal osteoma non-responder to intravitreal bevacizumab and ranibizumab. Int Ophthalmol. 2015;35:441–4.
Sambricio J, Fernández-Reyes M, De-Lucas-Viejo B, et al. A second new choroidal osteoma in the same eye: differences between them with new imaging techniques. Case Rep Ophthalmol Med. 2015;2015:684956.
Sarigül Sezenöz A, Akça Bayar S, Yilmaz G. Choroidal osteoma and secondary choroidal neovascularization treated with ranibizumab. Turk J Ophthalmol. 2017;47:243–6.
Schuh A, Foerster P, Priglinger S, et al.. Newly occurring loss of visual acuity in choroidal osteoma. Ophthalmologe. 2017.
Sharma S, Sribhargava N, Shanmugam MP. Choroidal neovascular membrane associated with choroidal osteoma (CO) treated with trans-pupillary thermo therapy. Indian J Ophthalmol. 2004;52:329–30.
Shen C, Yan S, Du M, et al. Assessment of choroidal osteoma complicating choroidal neovascularization by optical coherence tomography angiography. Int Ophthalmol. 2017;38(2):787–92.
Shields CL, Sun H, Demirci H, et al. Factors predictive of tumor growth, tumor decalcification, choroidal neovascularization, and visual outcome in 74 eyes with choroidal osteoma. Arch Ophthalmol. 2005;123:1658–66.
Shields CL, Materin MA, Mehta S, et al. Regression of extrafoveal choroidal osteoma following photodynamic therapy. Arch Ophthalmol. 2008;126:135–7.
Shields CL, Arepalli S, Atalay HT, et al. Choroidal osteoma shows bone lamella and vascular channels on enhanced depth imaging optical coherence tomography in 15 eyes. Retina. 2015a;35:750–7.
Shields CL, Hasanreisoglu M, Saktanasate J, et al. Sclerochoroidal calcification: clinical features, outcomes, and relationship with hypercalcemia and parathyroid adenoma in 179 eyes. Retina. 2015b;35:547–54.
Shukla D, Tanawade RG, Ramasamy K. Transpupillary thermotherapy for subfoveal choroidal neovascular membrane in choroidal osteoma. Eye (Lond). 2006;20:845–7.

Sisk RA, Riemann CD, Petersen MR, et al. Fundus autofluorescence findings of choroidal osteoma. Retina. 2013;33:97–104.

Song JH, Bae JH, Rho MI, et al. Intravitreal bevacizumab in the management of subretinal fluid associated with choroidal osteoma. Retina. 2010;30:945–51.

Süsskind D, Altpeter EK, Moser L, et al. Proton beam radiotherapy of progressive pediatric choroidal osteoma: first experience. Can J Ophthalmol. 2014;49:e123–7.

Szelog JT, Bonini Filho MA, Lally DR, et al. Optical coherence tomography angiography for detecting choroidal neovascularization secondary to choroidal osteoma. Ophthalmic Surg Lasers Imaging Retina. 2016;47:69–72.

Takkar B, Azad SV, Gangwe AB. Successful management of choroidal neovascular membrane secondary to choroidal osteoma with intravitreal bevacizumab. Saudi J Ophthalmol. 2017;31:120–1.

Traboulsi EI, Zin A, Massicotte SJ, et al. Posterior scleral choristoma in the organoid nevus syndrome (linear nevus sebaceus of Jadassohn). Ophthalmology. 1999;106:2126–30.

Trimble SN, Schatz H. Choroidal osteoma after intraocular inflammation. Am J Ophthalmol. 1983;96:759–64.

Trimble SN, Schatz H. Decalcification of a choroidal osteoma. Br J Ophthalmol. 1991;75:61–3.

Trimble SN, Schatz H, Schneider GB. Spontaneous decalcification of a choroidal osteoma. Ophthalmology. 1988;95:631–4.

Tsuchihashi T, Murayama K, Saito T, et al. Midperipheral mottling pigmentation with familial choroidal osteoma. Retina. 2005;25:63–8.

Vayalambrone D, Misra A. Paediatric choroidal osteoma treated with ranibizumab. BMJ Case Rep. 2012;2012.

Verma L, Venkatesh P, Lakshmaiah NC, et al. Osseous choristoma of the choroid. Indian J Ophthalmol. 2000;48:135–7.

Voluck MR, Say EA, Shields CL. Progressive growth of bilateral choroidal osteomas in a child. J Pediatr Ophthalmol Strabismus. 2011;48:e66–8.

Williams AT, Font RL, Van DJ, et al. Osseous choristoma of the choroid simulating a choroidal melanoma. Association with a positive 32P test. Arch Ophthalmol. 1978;96:1874–7.

Wilson MW, Moshfeghi DM, Haik BG, et al. Choroidal osteoma in a patient with contralateral persistent hyperplastic primary vitreous. Retina. 2002;22:358–60.

Wu ZH, Wong MY, Lai TY. Long-term follow-up of intravitreal ranibizumab for the treatment of choroidal neovascularization due to choroidal osteoma. Case Rep Ophthalmol. 2012;3:200–4.

Xuan Y, Zhang Y, Wang M, et al. Multimodal fundus imaging of outer retinal tubulations in choroidal osteoma patients. Retina. 2018;38:49–59.

Yahia SB, Zaouali S, Attia S, et al. Serous retinal detachment secondary to choroidal osteoma successfully treated with transpupillary thermotherapy. Retin Cases Brief Rep. 2008;2:126–7.

Yiu G, Young LH. Choroidal osteomas. JAMA Ophthalmol. 2013;131:124.

Yoshikawa T, Takahashi K. Decalcified choroidal osteoma found in the retina. Clin Ophthalmol. 2012;6:1823–5.

Yoshikawa T, Takahashi K. Long-term outcomes of intravitreal injection of bevacizumab for choroidal neovascularization associated with choroidal osteoma. Clin Ophthalmol. 2015;9:429–37.

Retinal Vascular Tumors

6

Jose J. Echegaray, Rubens Belfort Neto, and Arun D. Singh

6.1 Introduction

Vascular tumors of the retina generally include four distinct lesions: retinal capillary hemangioma, retinal cavernous hemangioma, racemose hemangioma, and vasoproliferative tumor of the retina. A main differentiation point between these entities arises by classifying them as either congenital in origin or acquired during the lifetime. The congenital retinal vascular tumors include the retinal cavernous hemangioma and the racemose hemangioma. From an ultrastructural standpoint, the vasculature components of these tumors maintain the integrity of endothelial tight junctions throughout life. Clinically, this translates into a lack of exudation or leakage irrespective of the depth of the tumor. In turn, the acquired tumors, retinal capillary hemangioma, and vasoproliferative tumor lack tight junctions and commonly present clinically with an exudative component.

This chapter will discuss the clinical features, diagnostic evaluation, management, and prognosis of the abovementioned tumors with the exception of the vasoproliferative tumor, which will be discussed in Chap. 7. It is important to delineate the differences in clinical presentation and angiographic features between these tumors in order to manage them appropriately.

J. J. Echegaray
Cole Eye Institute, Cleveland Clinic Foundation, Cleveland, OH, USA
e-mail: echegaj@ccf.org

R. B. Neto
Ocular Oncology Service, Department of Ophthalmology, Federal University of São Paulo, São Paulo, SP, Brazil
e-mail: rubens@belfort.med.br

A. D. Singh (✉)
Cole Eye Institute, Cleveland Clinic Foundation, Cleveland, OH, USA

Taussig Cancer Institute, Cleveland Clinic Foundation, Cleveland, OH, USA
e-mail: singha@ccf.org

6.2 Retinal Capillary Hemangioma

6.2.1 Clinical Features

Retinal capillary hemangiomas (RCH) are generally classified based on location (peripheral or juxtapapillary), morphology (endophytic, exophytic, and sessile), its effects on the retina (exudative form and tractional form), and their relationship to von Hippel-Lindau (VHL) disease (with or without VHL disease). Most patients with RCH will present with a solitary tumor, with up to one-third of patients showing multiple tumors. Around 50% of patients will present with bilateral involvement. The association of RCH to VHL is well known with a mean age of presentation of 25 years in those with VHL (Singh et al. 2001). In turn, patients with a RCH that do not have a diagnosis of VHL will present at a later average age of 48 years (Singh et al. 2001).

Typically, a symptomatic patient with a RCH will complain of progressive loss of vision and/or flashes. However, many patients with eccentric lesions may not complain of symptoms and may commonly be diagnosed as an incidental finding in a routine ophthalmic exam. The most common findings on a fundus examination will be of a well-circumscribed, orange-red retinal mass with associated feeder vessels and accompanying lipid exudation (Fig. 6.1). Retinal hemorrhages are only identified in less than 3% of cases (Webster et al. 1999). More commonly, these tumors are located in the temporal quadrants. The finding of engorged retinal vessels arising from the optic disc on ophthalmoscopic view of the posterior pole should arise suspicion for a peripheral RCH and warrant a thorough peripheral examination. In turn, juxtapapillary tumors may not show vessel engorgement in association with the tumor.

The natural history of RCH can vary from spontaneous regression, stability, or progression. Disease progression has been proposed to generally go from early detection of a solitary tumor that may turn into an exudative lesion, which may develop a retinal detachment, and later evolve into end-stage disease with blinding neovascular glaucoma and painful

D. Rojanaporn (ed.), *Ocular Oncology*, https://doi.org/10.1007/978-981-13-2336-2_6

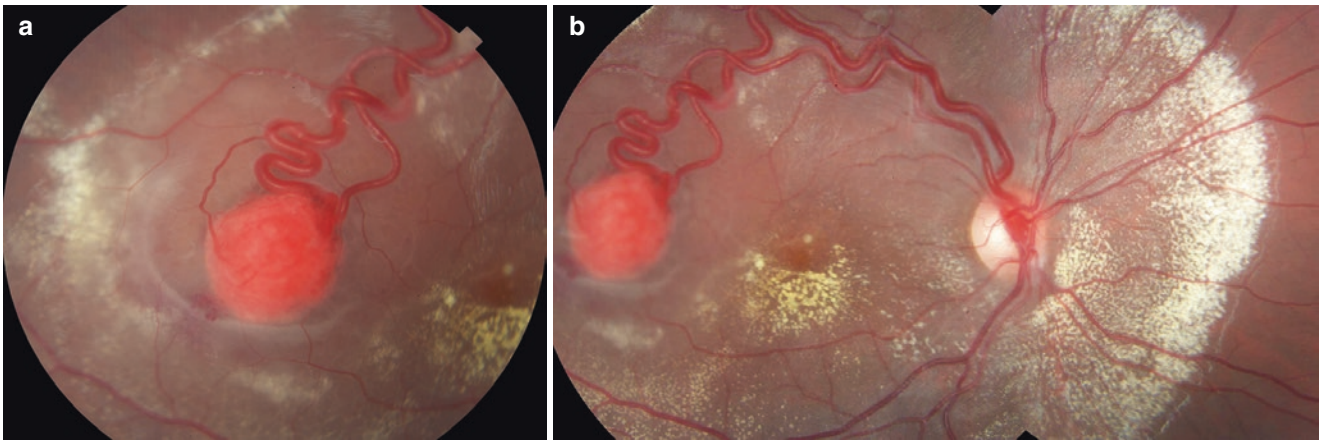

Fig. 6.1 Retinal capillary hemangioma. A well-circumscribed, orange-red retinal mass (**a**). Note prominent feeder vessels and accompanying lipid exudation (**b**)

phthisis. The initial findings at the moment of lesional detection will likely drive the selection of an appropriate treatment regimen.

6.2.2 Diagnosis

In addition to ophthalmoscopy, fluorescein angiography (FA) may aid in the diagnosis of a RCH. The most common findings will be of prominent hyperfluorescence of the tumor in the early stages of the study with associated late leakage. Angiography helps to delineate the tumor margins and provides a map of the tumor feeder vessels by identifying the feeding artery and feeding vein at different stages of the study. This anatomic map facilitates treatment planning.

6.2.3 Management

The appropriate treatment for a RCH is determined by the findings on initial presentation and/or evidence of disease progression, specifically as to the location, size, and presence of subretinal fluid and tractional components. In addition, identifying the presence of multiple tumors and estimating visual potential of the eye are of paramount importance in committing to a treatment plan.

Initial observation may be considered for a RCH, if the solitary tumor is small in size (<500 μm), if there is lack of exudation or tractional retinal detachment, and if there is no threat to the patient's vision. In addition, if the RCH is located in the juxtapapillary region, observation may be a reasonable course of action given the known history of stability of these lesions. Also, a lack of feeder vessels and presence of gliosis in association with the lesion may represent a regressing tumor, for which observation should be employed.

The mainstay of therapy for most RCH is laser photocoagulation (Singh et al. 2001; Singh et al. 2002b). Laser photocoagulation has been reported to be 91% effective when the RCH measures up to 4.5 mm in size and increases to 100% if the tumor is small in size (up to 1.5 mm in diameter) (Singh et al. 2002b). Laser can be employed directly into the tumor or may target a feeder vessel, as indicated by findings on fluorescein angiography. A combination of both, targeting the tumor and its feeder vessel, is another alternative. The resolution of fluid, tumor shrinkage, or change in color from red to pale pink generally represents therapeutic response and clinical resolution without the need to achieve complete tumor obliteration.

When the RCH is located anteriorly, if the tumor measures more than 3.0 mm in size, or if there is presence of moderate amount of subretinal fluid that may limit laser intake, cryotherapy may be an appropriate option (Singh et al. 2002b). As with laser photocoagulation, cryotherapy is most effective when the tumor measures less than 1.5 mm in diameter. Cryotherapy is not recommended when the tumor is juxtapapillary. Recently, there have been reports of successful treatment of RCH with photodynamic therapy by inducing occlusion of peripheral and juxtapapillary lesions (Schmidt-Erfurth et al. 2002; Bakri et al. 2005; Sachdeva et al. 2010). However, it was reported that visual stabilization or improvement was only present in half of cases with worsening epiretinal membranes in up to a half of cases, requiring further surgery (Sachdeva et al. 2010).

Episcleral plaque brachytherapy is another tool in the arsenal to treat RCH that are greater than 4 mm in size and show poor response to cryotherapy and laser photocoagulation (Singh et al. 2001; Singh et al. 2002b). The reported mean apical dose for RCH when treated with Iodine-125 plaque is 34 Gy prescribed to the apex of the lesion (range 22 Gy–41 Gy) (Singh et al. 2002b). Low-dose external beam

radiotherapy has also been reported as rescue therapy in recalcitrant cases (Raja et al. 2004). Intravitreal anti-VEGF therapy may serve as an adjuvant therapy to reduce exudation in combination of laser photocoagulation or cryotherapy, especially in cases of juxtapapillary RCH and small peripheral lesions (Slim et al. 2014). However, anti-VEGF monotherapy has not been shown significant benefits on the RCH size per se (Wong et al. 2008). For eyes with secondary tractional retinal detachments or total exudative detachments, pars plana vitrectomy with possible endodiathermy or endophotocoagulation of feeder vessels may serve to stabilize these cases (Avci et al. 2017).

6.2.4 Systemic Associations

It is well known that RCH is associated with Von Hippel-Lindau (VHL) disease, a syndrome that commonly manifests with vascular tumors in the retina and the central nervous system (CNS). Since RCH is the most common initial manifestation in VHL patients, knowing how to diagnose this condition is of paramount importance to every ophthalmologist. Additional systemic manifestations include cerebellar hemangiomas, renal cell carcinoma, and pancreatic tumors and cysts. Examination of these patients should be extended into immediate relatives, given its association with the VHL gene on chromosome 3p2526 and autosomal dominant inheritance (Stolle et al. 1998; Singh et al. 2002a). Genetic testing for VHL gene is commercially available.

6.3 Retinal Cavernous Hemangioma

6.3.1 Clinical Features

Cavernous hemangioma of the retina (CHR) is considered a rare form of congenital retinal hamartoma that is commonly sporadic and of equal gender distribution (Wang and Chen 2017). However, a subset of patients has shown an autosomal dominant hereditary pattern in association with cerebral cavernous malformations. The age of presentation has been reported to range between 1 and 55 years of age, with recent reports showing that 70% of cases present between 7 and 40 years of age with a mean age of presentation of 21 years (Messmer et al. 1983; Wang and Chen 2017). Ophthalmoscopically, CHR appear as peripheral solitary clusters of grape-like saccular thin-walled channels with associated retinal gliosis (Fig. 6.2). These tumors are usually small in size, measuring approximately 1–2 disc diameters. Ultrastructurally, the saccular channels are lined by non-fenestrated endothelium, which explains the lack of exudation evident on clinical exam. Another characteristic clinical feature of CHR is its independence from

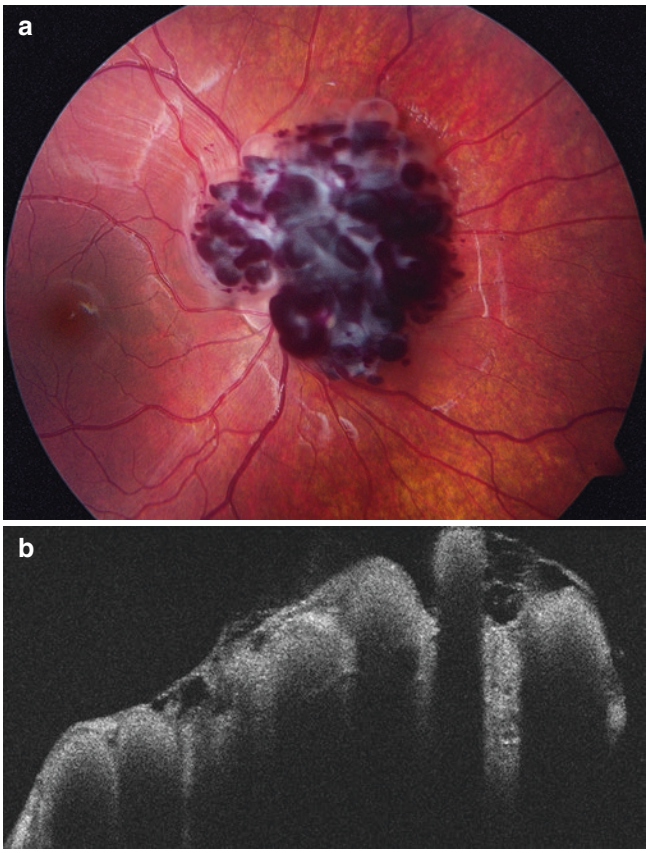

Fig. 6.2 Retinal cavernous hemangioma. A cluster of grape-like saccular vascular channels (**a**) that are thin walled when examined by OCT (**b**)

the surrounding retinal circulation, evident by the relatively unaffected retinal vasculature overlying and surrounding the lesion and the lack of any feeder vessels. Patients with CHR are generally asymptomatic. Those with visual complaints usually involve the macula or have associated vitreous hemorrhage.

6.3.2 Diagnosis

Fluorescein angiography can aid in the diagnosis of CHR with a relatively early hypofluorescence and delayed lesional dye filling, representing the low-flow system of the cavernous vascular channels. In the venous phase of the study, hyperfluorescent caps may be evident within the saccular channels, representing gravitational plasma-erythrocytic separation. There is a lack of fluorescein leakage, consistent with the non-fenestrated vascular channels that form these tumors. OCT scan through the tumor may illustrate preretinal and epiretinal membranes that form bridges between the saccular channels (Pringle et al. 2009). Contraction of these membranes is believed to cause subretinal or vitreous hemorrhage, which has been reported in 25% of cases (Wang and Chen 2017).

6.3.3 Management

Generally, patients with CHR are observed since most are asymptomatic and the tumors are generally non-progressive with a lack of exudation that would otherwise cause vision loss. Those that progress may show an increase of gliosis and thrombosis.

6.3.4 Systemic Associations

Although most cases of CHR are sporadic, few cases have been associated with a familial syndrome in association with cerebral cavernous hemangiomas. It has been suggested that bilateral CHR cases strongly correlate with familial history (Wang and Chen 2017). Patients with cerebral hemangiomas may warrant close follow-up, due to the possibility of seizures, intracranial hemorrhages, and death (Dobyns et al. 1987; Wang and Chen 2017).

6.4 Racemose Hemangioma

6.4.1 Clinical Features

Racemose hemangiomas (Wyburn-Mason syndrome) are sporadic congenital arteriovenous malformations that are usually identified incidentally in ophthalmoscopic examination in asymptomatic patients or in children with amblyopic eyes. The average age of presentation has been reported to be 23 years (Qin et al. 2014). Ophthalmoscopy discloses vascular malformations subdivided according to severity (Fig. 6.3). Group I features major vessels of the arteriovenous malformation joined by a capillary plexus. Group II lesions lack the intermediate capillary plexus. Group III is the most severe having significant dilation and tortuosity of the malformed vasculature. There is usually a lack of lipid exudation or retinal feeder vessels. Over time, these lesions may show an increase in tortuosity, vessel occlusion, and ischemia with subsequent development of neovascular glaucoma (Augsburger et al. 1980).

6.4.2 Diagnosis

Fluorescein angiography illustrates the arteriovenous malformation and may aid in further classifying the lesion by identifying the presence or absence of an intervening capillary plexus. A lack of differentiation between the arterial and venous components of the malformation on angiography is characteristic of group III lesions.

6.4.3 Management

Retinal arteriovenous malformations are generally not treatable. Secondary complications such as vitreous hemorrhage or neovascular glaucoma may be treated accordingly.

6.4.4 Systemic Associations

The association of racemose hemangioma with cerebral arteriovenous malformations has been established as Wyburn-Mason syndrome. Approximately 30% of patients with retinal manifestations also have concomitant cerebral involvement

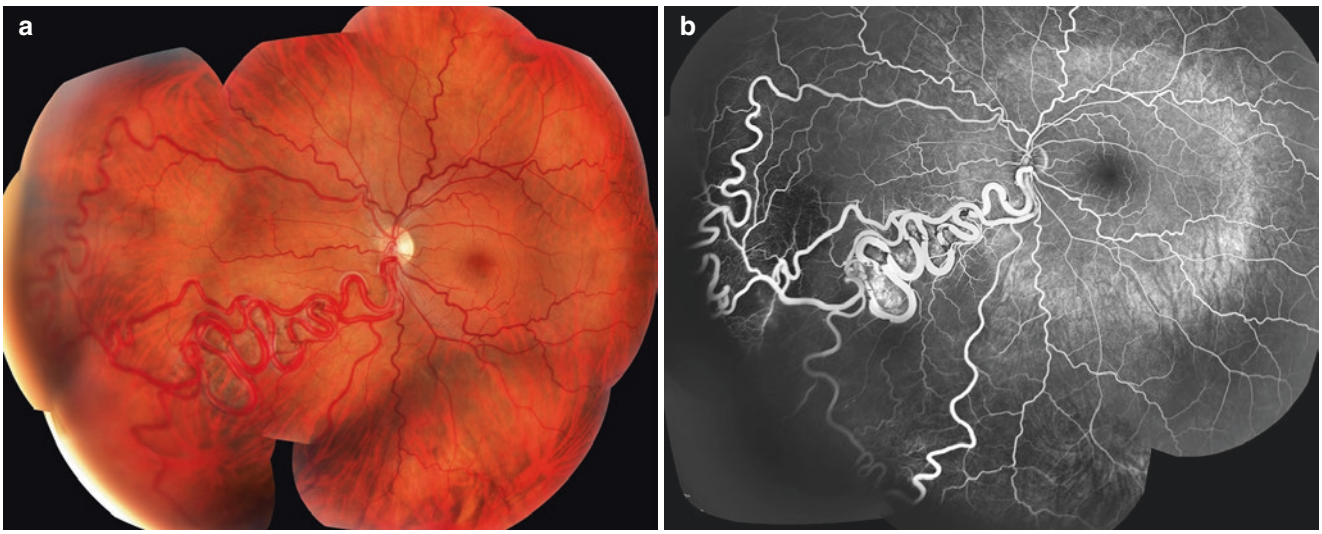

Fig. 6.3 Racemose hemangioma. Retinal arteriovenous malformation lacking intermediate capillary plexus (**a**). The vessels maintain endothelial tight junctions as suggested by absence of leakage on fluorescein angiogram (**b**)

(Ponce et al. 2001). Intracranial malformations involving the optic chiasm may present with neuro-ophthalmic manifestations. Associated cerebral hemorrhages may present with symptoms such as headaches, nuchal rigidity, or loss of consciousness. Patients identified with retinal arteriovenous malformation by an ophthalmologist should be evaluated for early detection of concomitant cerebral malformations.

References

Augsburger JJ, Goldberg RE, Shields JA, et al. Changing appearance of retinal arteriovenous malformation. Albrecht von Graefes Archiv fur klinische und experimentelle Ophthalmologie Albrecht Von Graefes. Arch Klin Exp Ophthalmol. 1980;215:65–70.

Avci R, Yilmaz S, Inan UU, et al. Vitreoretinal surgery for patients with severe exudative and proliferative manifestations of retinal capillary hemangioblastoma because of von hippel-lindau disease. Retina. 2017;37:782–8.

Bakri SJ, Sears JE, Singh AD. Transient closure of a retinal capillary hemangioma with verteporfin photodynamic therapy. Retina. 2005;25:1103–4.

Dobyns WB, Michels VV, Groover RV, et al. Familial cavernous malformations of the central nervous system and retina. Ann Neurol. 1987;21:578–83.

Messmer E, Laqua H, Wessing A, et al. Nine cases of cavernous hemangioma of the retina. Am J Ophthalmol. 1983;95:383–90.

Ponce FA, Han PP, Spetzler RF, et al. Associated arteriovenous malformation of the orbit and brain: a case of Wyburn-Mason syndrome without retinal involvement. Case report. J Neurosurg. 2001;95:346–9.

Pringle E, Chen S, Rubinstein A, et al. Optical coherence tomography in retinal cavernous haemangioma may explain the mechanism of vitreous haemorrhage. Eye (Lond). 2009;23:1242–3.

Qin XJ, Huang C, Lai K. Retinal vein occlusion in retinal racemose hemangioma: a case report and literature review of ocular complications in this rare retinal vascular disorder. BMC Ophthalmol. 2014;14:101. https://doi.org/10.1186/1471-2415-14-101.

Raja D, Benz MS, Murray TG, et al. Salvage external beam radiotherapy of retinal capillary hemangiomas secondary to von Hippel-Lindau disease: visual and anatomic outcomes. Ophthalmology. 2004;111:150–3.

Sachdeva R, Dadgostar H, Kaiser PK, et al. Verteporfin photodynamic therapy of six eyes with retinal capillary haemangioma. Acta Ophthalmol. 2010;88(8):e334–40. https://doi.org/10.1111/j.1755-3768.2010.02008.x.

Schmidt-Erfurth UM, Kusserow C, Barbazetto IA, et al. Benefits and complications of photodynamic therapy of papillary capillary hemangiomas. Ophthalmology. 2002;109:1256–66.

Singh AD, Shields CL, Shields JA, et al. von Hippel-Lindau disease. Surv Ophthalmol. 2001;46:117–42.

Singh AD, Ahmad NN, Shields CL. Solitary retinal capillary hemangioma: lack of genetic evidence for von Hippel-Lindau disease. Ophthalmic Genet. 2002a;23:21–7.

Singh AD, Nouri M, Shields CL, et al. Treatment of retinal capillary hemangioma. Ophthalmology. 2002b;109:1799–806.

Slim E, Antoun J, Kourie HR, et al. Intravitreal bevacizumab for retinal capillary hemangioblastoma: a case series and literature review. Can J Ophthalmol. 2014;49:450–7.

Stolle C, Glenn G, Zbar B, et al. Improved detection of germline mutations in the von Hippel-Lindau disease tumor suppressor gene. Hum Mutat. 1998;12:417–23.

Wang W, Chen L. Cavrnous hemangioma of the retina: a comprehensive review of the literature (1934-2015). Retina. 2017;37:611–21.

Webster AR, Maher ER, Moore AT. Clinical characteristics of ocular angiomatosis in von Hippel-Lindau disease and correlation with germline mutation. Arch Ophthalmol. 1999;117:371–8.

Wong WT, Liang KJ, Hammel K, et al. Intravitreal ranibizumab therapy for retinal capillary hemangioblastoma related to von Hippel-Lindau disease. Ophthalmology. 2008;115:1957–64.

Vasoproliferative Tumors of the Retina

7

Duangnate Rojanaporn

7.1 Introduction

Vasoproliferative tumors (VPT) are benign vascular tumors of the fundus which has distinct characteristics. It was firstly termed "presumed acquired retinal hemangiomas" by Shields and colleagues (Shields et al. 1983), who described 12 patients with nonfamilial, unilateral, solitary, vascular mass of the sensory retina. In 1995, they further studied a larger series of 103 patients with similar appearance and found that many of these vascular masses may not be true hemangioma and some lesions involved not only the retina but also retinal pigment epithelium and choroid. Therefore, they renamed these lesions as "vasoproliferative tumors of the ocular fundus" (Shields et al. 1995).

Poole Perry and colleagues reported histopathological findings in four enucleated patients with vasoproliferative tumors and found that the lesions were composed of glial cells with paucity of microvessels. They proposed that "reactive retinal astrocytic tumors" is more appropriate term (Poole Perry et al. 2013). However, their cases represented the end stage of vasoproliferative tumor, and in clinical practice, vasoproliferative tumor is a vascular mass in the early stages. Therefore, the term vasoproliferative tumor is more acceptable and has been used widely in the literature (Shields et al. 2013).

7.2 Clinical Features

Vasoproliferative tumor generally appears as an ill-defined elevated yellow-orange or pink-red retinal mass in peripheral fundus (Shields et al. 1995; Heimann et al. 2000; Shields et al. 2013), with normal or dilated feeding retinal artery and drainage vein. These vessels are normal or slightly dilated and tortuous, in contrast to those of retinal capillary hemangioma (retinal hemangioblastoma) associated with Von Hippel-Lindau syndrome (Shields et al. 1995; Heimann et al. 2000) (Fig. 7.1).

In the largest case series that reviewed clinical features of 334 vasoproliferative tumors in 275 patients, 59% were female, with the mean age of 44 years. The majority of tumors located in peripheral fundus between equator to ora serrata (73%), and in inferotemporal quadrant (67%). The peripheral location of vasoproliferative tumors were also reported in other studies (Heimann et al. 2000; Anastassiou et al. 2006). Characteristically, VPT produces exudates and subretinal fluid around the tumor and extends toward posterior pole, with adjacent retinal pigment epithelial alterations around the tumor (Shields et al. 1995; Heimann et al. 2000; Shields et al. 2013) (Figs. 7.1a, 7.2a, 7.3a, and 7.4c).

Although VPT is a peripheral benign tumor, it can produce visual symptoms in large number of cases due to its associated findings, such as anterior chamber cells, vitreous cells, macular exudates, macular edema, epiretinal membrane, and vitreous hemorrhage (Shields et al. 1995; Heimann et al. 2000; Anastassiou et al. 2006; Shields et al. 2013). Iris neovascularization and neovascular glaucoma rarely occurred (Shields et al. 1995; Heimann et al. 2000; Shields et al. 2013).

7.3 Classification

Vasoproliferative tumors are classified into two types, the primary or idiopathic type and the secondary type, which had associated ocular diseases (Shields et al. 1995). Most of VPTs are primary (80%). When compared to primary VPT, secondary VPTs were more often bilateral, multiple, and larger. The important similar features of primary and secondary VPT were their peripheral location in inferotemporal quadrant, tumor thickness, epimacular membrane, macular subretinal fluid, and macular exudates (Shields et al. 2013).

D. Rojanaporn (✉)
Department of Ophthalmology, Faculty of Medicine, Ramathibodi Hospital, Mahidol University, Bangkok, Thailand
e-mail: duangnate.roj@mahidol.ac.th

D. Rojanaporn (ed.), *Ocular Oncology*, https://doi.org/10.1007/978-981-13-2336-2_7

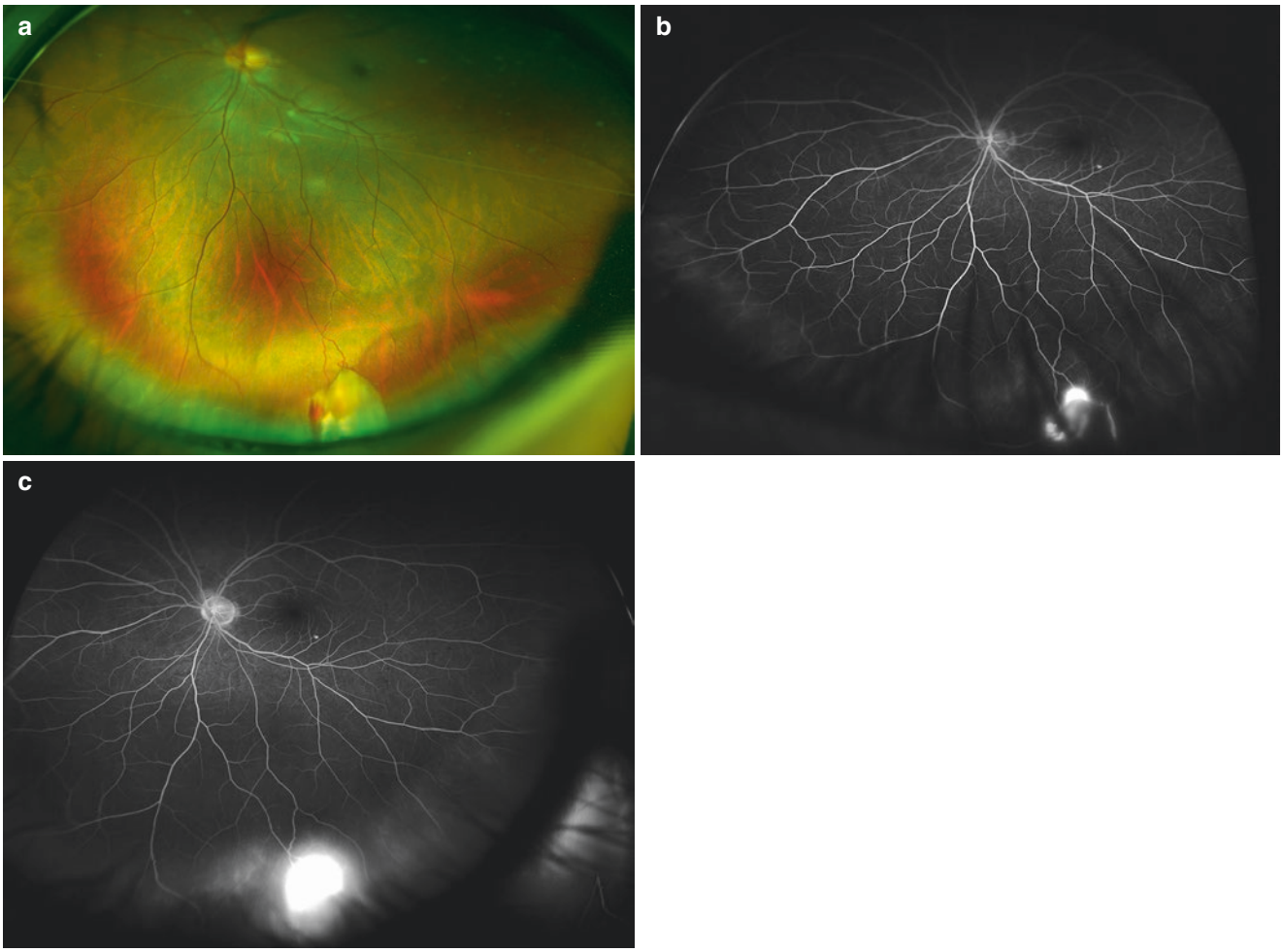

Fig. 7.1 A 32-year-old male with primary vasoproliferative tumor. Optos image showing vasoproliferative tumor in peripheral inferotemporal quadrant with retinal hemorrhages and retinal exudates adjacent to the tumor (**a**). The feeding arteriole and drainage vein are nondilated and slightly tortuous (**a**–**c**). Fluorescein angiography showing hyperfluorescence of the tumor in early phase (**b**) with leakage in late phase (**c**)

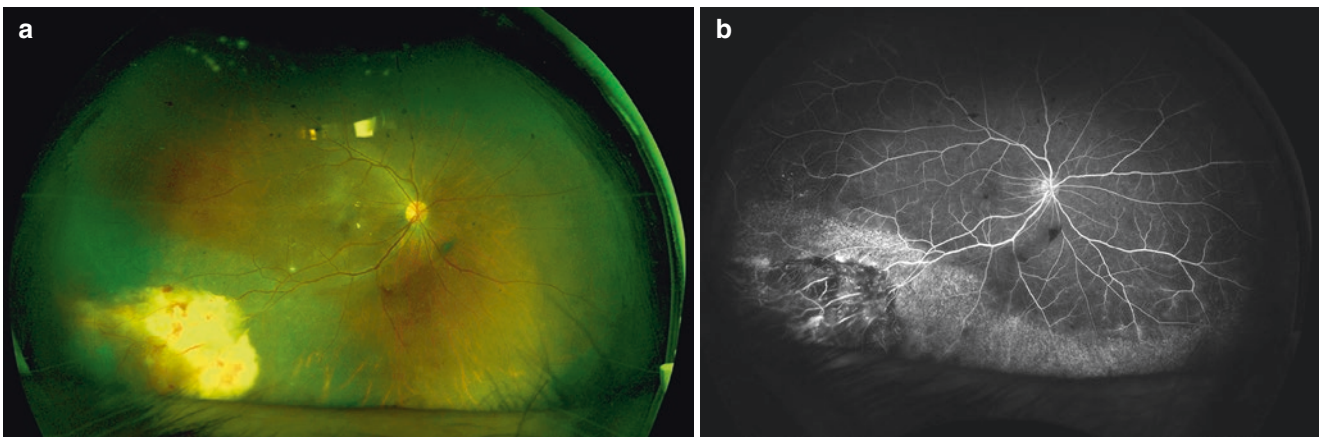

Fig. 7.2 A 53-year-old male with primary vasoproliferative tumor. Optos image showing vasoproliferative tumor in peripheral inferotemporal quadrant with retinal pigment epithelial changes, retinal hemorrhages, and massive subretinal exudates around the tumor (**a**). Fluorescein angiography showing hyperfluorescence of the tumor in early phase (**b**) with leakage in late phase (**c**, **d**). Ultrasonography of the tumor showing acoustically dense plateau-shaped retinal mass on B scan (**e**) with high internal reflectivity on A scan (**f**). Optical coherence tomography of the macula showing epiretinal membrane (**g**). After cryotherapy, subretinal exudates and retinal hemorrhages were reduced (**h**)

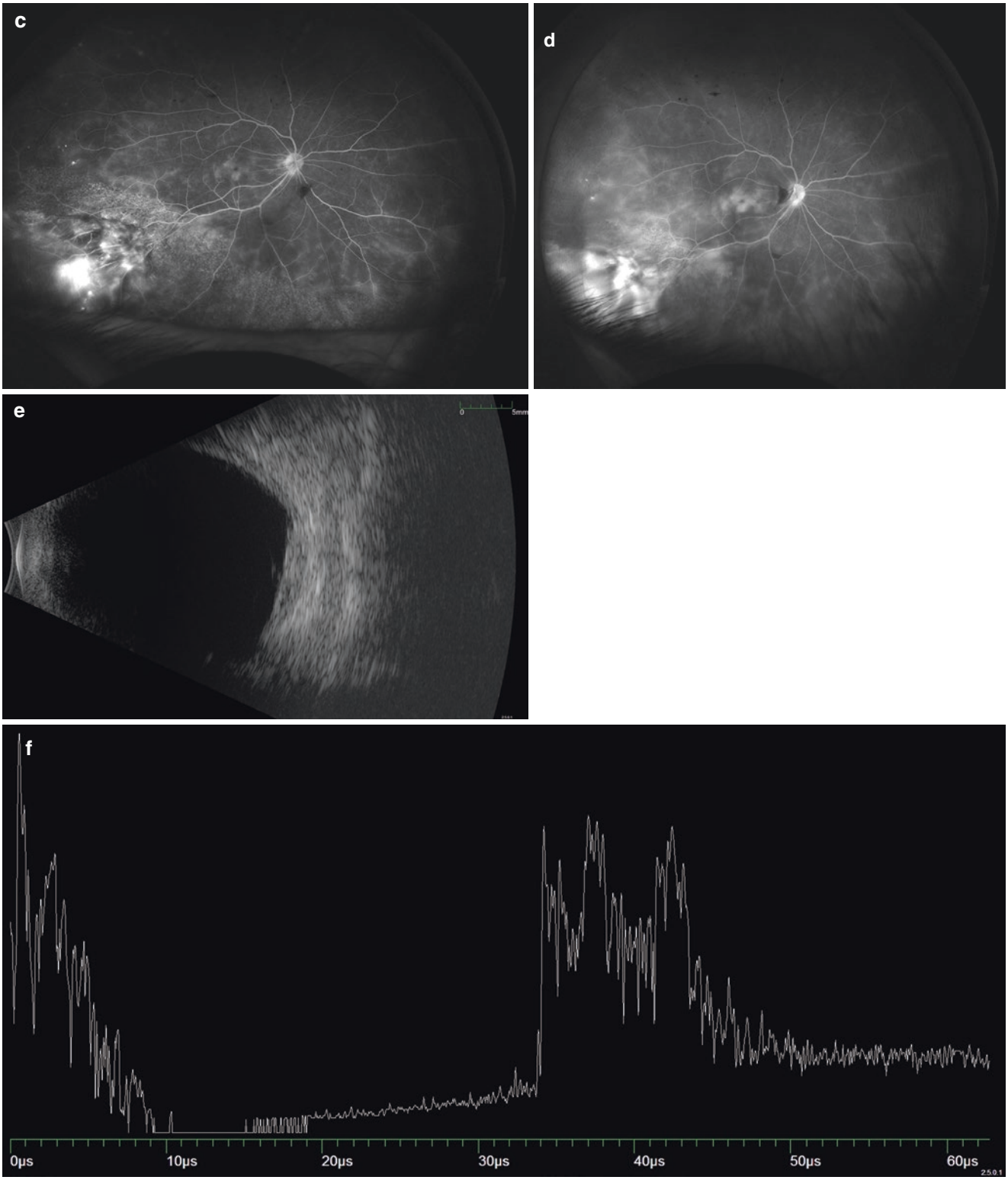

Fig. 7.2 (continued)

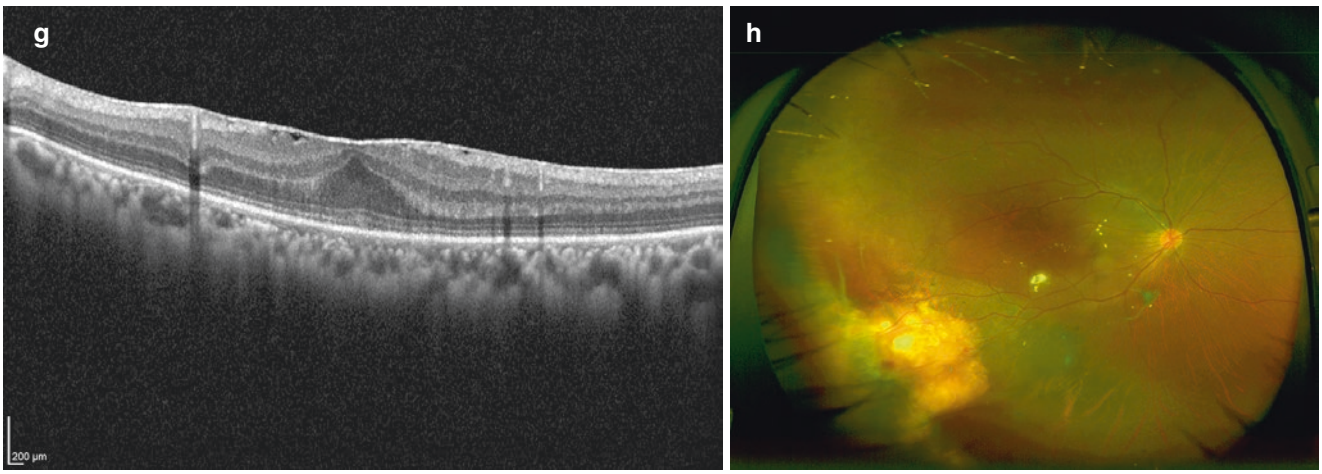

Fig. 7.2 (continued)

7.3.1 Primary Vasoproliferative Tumor

Primary or idiopathic vasoproliferative tumor accounted for 80% of all VPT. There was no associated ocular disease in this group of patients. Associated systemic diseases were hypertension (20%), diabetes mellitus (5%), and hypercholesterolemia (13%). It is characteristically unilateral (96%), solitary (95%), and located between equator and ora serrata (77%) in inferotemporal quadrant (66%) (Shields et al. 2013) (Figs. 7.1a–c and 7.2a–h).

7.3.2 Secondary Vasoproliferative Tumor

Secondary vasoproliferative tumor accounted for 20% of all VPT. Associated systemic diseases were similar to primary VPT (Shields et al. 2013). Various ocular diseases have been reported to be associated with secondary VPT. Common associated ocular diseases are retinitis pigmentosa, pars planitis, Coats disease, previous retinal detachment repair, peripheral retinal vasculitis, and toxoplasmosis (Shields et al. 1995; Heimann et al. 2000; Anastassiou et al. 2006; Shields et al. 2013) (Figs. 7.3a–f and 7.4a–f).

7.4 Diagnosis

It is important for ophthalmologists to perform detailed peripheral fundus examination in patients with epimacular membrane, macular edema, or macular exudates, to avoid overlooking peripheral VPT. The unique clinical features of VPT which are the tumor color of yellow-orange-red; peripheral location, especially inferotemporal quadrant; associated exudative changes and pigmentary changes around the tumor (Figs. 7.1a, 7.2a, 7.3a, and 7.4a, c); and associated macular edema or epimacular membrane (Fig. 7.2g) make it easy to recognize the tumor.

Ancillary investigations can confirm the diagnosis of VPT.

7.4.1 Fluorescein Angiography

Fluorescein angiography can be helpful in the initial diagnosis of VPT. Due to the peripheral location of VPT, wide-filed angiography can give more details of the tumor. VPT usually shows hyperfluorescence in arterial phase (92%), venous phase (96%), with leakage (40%) or hyperfluorescence (56%) in late phase. Feeder artery and drainage vein are generally normal (43%) or mildly dilated (57%) (Shields et al. 2013) (Figs. 7.1b, c, 7.2b–d, 7.3c–f, and 7.4d, e).

7.4.2 Ultrasonography

VPT generally shows acoustically dense (87%), irregular (16%) or dome-shaped (81%) mass without choroidal excavation (Shields et al. 2013). On A scan ultrasonography, it generally shows medium to high internal reflectivity (Shields et al. 1983; Shields et al. 1995) (Fig. 7.2e, f).

7.4.3 Optical Coherence Tomography

Imaging of VPT with OCT is difficult due to its peripheral location. However, macular changes can occur in a large number of patients with VPT and can cause visual disability.

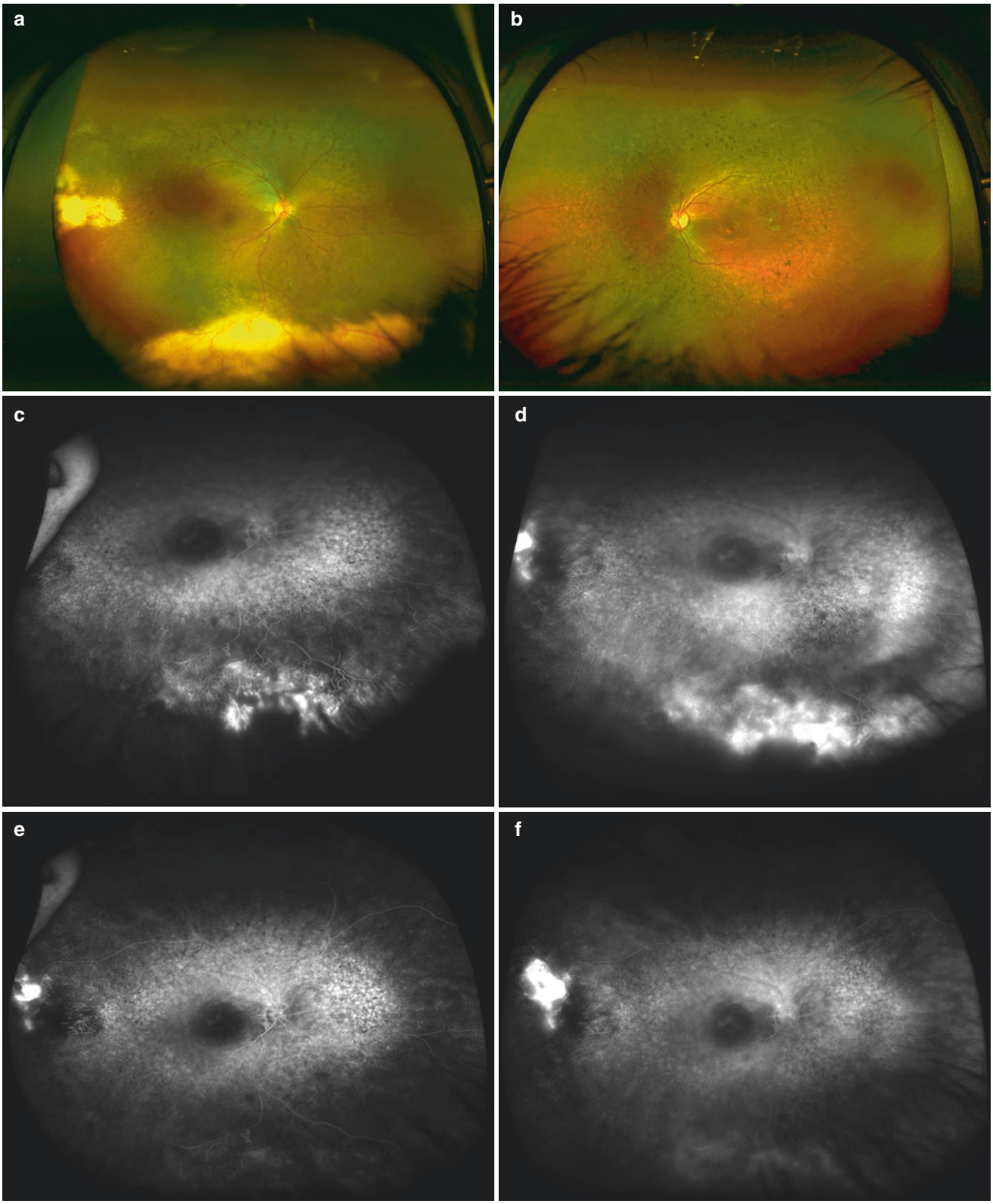

Fig. 7.3 A 18-year-old female with retinitis pigmentosa and secondary vasoproliferative tumors. Optos image showing pigmentary retinopathy in the midperiphery and vasoproliferative tumors in peripheral temporal and inferior quadrant with subretinal exudates around the tumor and retinal hemorrhages over the tumor. The feeding arterioles and drainage venules are normal (temporal tumor) and nondilated and mildly tortuous (inferior tumors) (**a**). The left eye has pigmentary retinopathy in the midperiphery without vasoproliferative tumor (**b**). Fluorescein angiography showing hyperfluorescence of the tumor in early phase (**c**, **e**) with leakage in late phase (**d**, **f**)

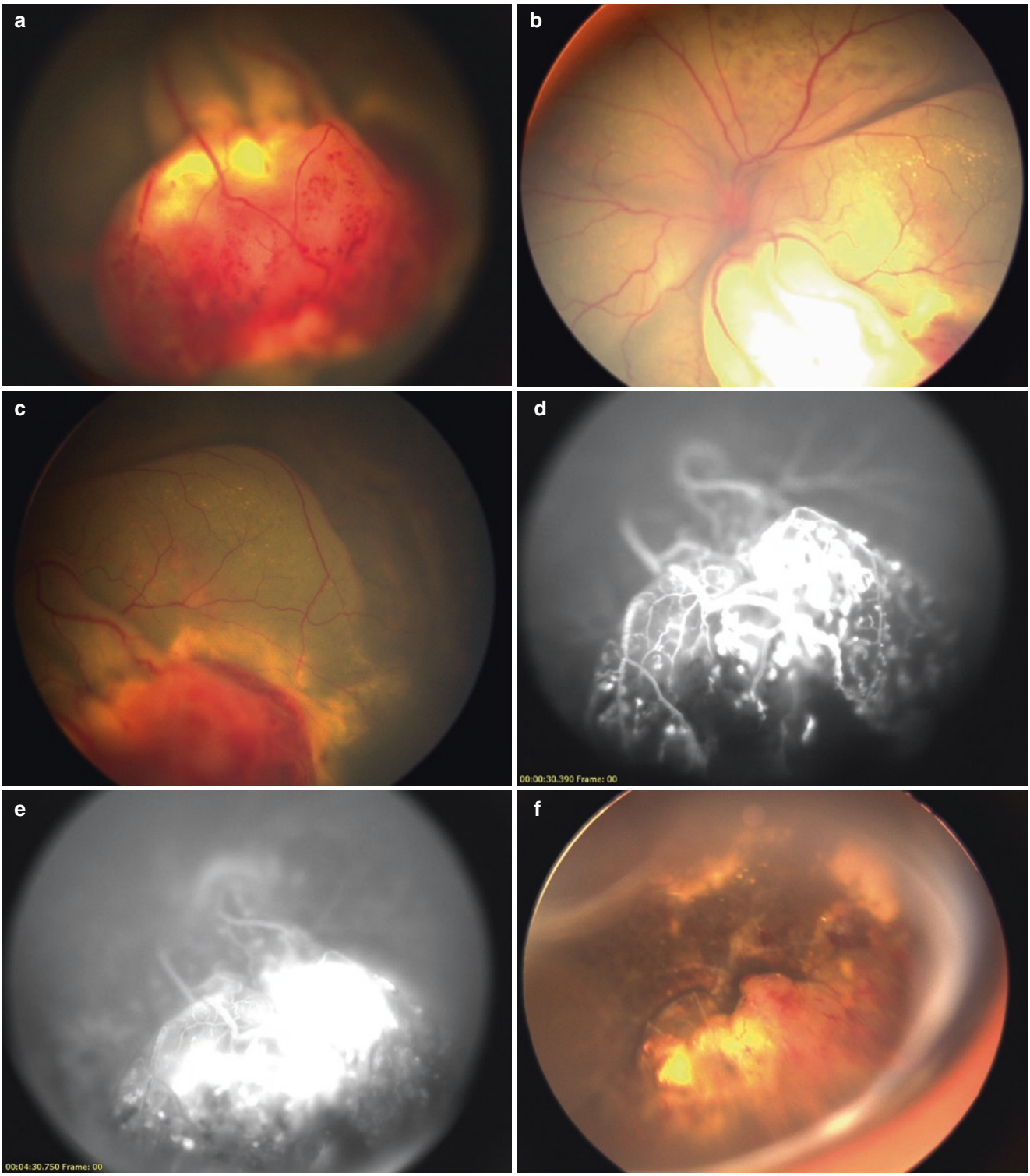

Fig. 7.4 A 13-year-old boy with Coats disease and secondary vasoproliferative tumor. Retcam image showing vasoproliferative tumor in peripheral inferior quadrant with retinal telangiectasia over tumor surface (**a**), total exudative retinal detachment (**b**), and subretinal exudates around the tumor (**c**). Fluorescein angiography showing retinal telangiectasia over tumor surface with hyperfluorescence of the tumor in early phase (**d**) with leakage in late phase (**e**). After intravitreal steroid injection and brachytherapy with Ruthenium-106 plaque, the tumor was regressed; exudative retinal detachment and subretinal exudates were resolved (**f**)

Common macular changes associated with VPT include subretinal fluid (24%), macular exudates (23%), and epimacular membrane (12%) (Shields et al. 2013). OCT is useful to detect these macular changes, plan the proper treatment, and evaluate the treatment results (Heimann et al. 2013) (Fig. 7.2g).

7.5 Differential Diagnosis

Retinal capillary hemangioma may mimic VPT due to its color, highly vascularization, and exudative changes around the tumor. But the feeder vessels in VPT are normal or slightly dilated and tortuous (Fig. 7.1a–c), in contrast to those of retinal capillary hemangioblastoma, which are markedly dilated and tortuous (see Chap. 6). The location of VPT is usually periphery, whereas retinal capillary hemangiomas locate from optic disc, posterior fundus, to peripheral fundus. The presence of systemic conditions and family history of Von Hippel-Lindau disease can guide the diagnosis of retinal capillary hemangioma.

Peripheral exudative hemorrhagic chorioretinopathy can cause peripheral exudates, hemorrhage, or exudative retinal detachment like VPT. The lack of feeder vessels and hypofluorescence on fluorescein angiography (due to blockage of blood) in PEHCR can distinguish it from VPT (see Chap. 13).

Amelanotic choroidal malignant melanoma in peripheral location may be confused with VPT. On Ultrasonography, VPT generally shows acoustic solidity in contrast to melanoma, which generally shows acoustic hollowness (see Chap. 2).

7.6 Management

Decision for management of VPT is based on visual symptoms, tumor size, tumor location, and other associated vitreoretinal findings.

7.6.1 Observation

Asymptomatic and stable VPT can be carefully observed. Treatment is recommended in cases with progressive exudation, retinal detachment, vitreous hemorrhage, or remote macular changes (Shields et al. 1995; McCabe and Mieler 1996).

7.6.2 Cryotherapy

Cryotherapy is an effective treatment for small VPT (less than 2 mm in thickness) (Heimann et al. 2000). Cryotherapy with double freeze-thaw technique (Manjandavida et al. 2014), or triple freeze-thaw technique (Heimann et al. 2000; Garcia-Arumi et al. 2015), had been described with favorable results (Fig. 7.2a, h). Repeated treatment may be required, especially in thick tumor (>2 mm in thickness). However, excessive cryotherapy can lead to progression of exudation and total exudative retinal detachment (Heimann et al. 2000). Cryotherapy might have additional benefit on epimacular membrane associated with VPT. Spontaneous release of EMM has been reported following the treatment of VPT with cryotherapy (Manjandavida et al. 2014).

7.6.3 Laser Photocoagulation

Laser photocoagulation can be applied to VPT by slit lamp laser or endolaser photocoagulation during vitrectomy. Laser photocoagulation with 532 nm laser selectively applied to peripheral telangiectasia and afferent feeder vessels has been reported to lead to complete resorption of subretinal fluid (100%), and subretinal exudates (97%) in 30 patients with primary VPT at mean follow-up of 3 years. (Krivosisc et al. 2014).

7.6.4 Transpupillary Thermotherapy (TTT)

Few case reports have shown the resolution of exudative retinal detachment and macular edema in VPT patients following transpupillary thermotherapy (Nomura et al. 2009), or indocyanine green-mediated photothrombosis (Bertelli and Pernter 2009).

7.6.5 Photodynamic Therapy (PDT)

Several case reports and cases series have shown the favorable results of PDT in VPT. In the largest case series of 24 patients with VPT treated with standard protocal of PDT with Verteporfin, the majority of patients had complete tumor regression (76%), resolution of exudation (76%), and visual gain or stabilization (92%) at the mean follow-up of 2 years. Similar to the previous cases report, they also found limited success of PDT in VPT with extensive exudative maculopathy (Blasi et al. 2006; Hussain et al. 2015).

7.6.6 Brachytherapy

Brachytherapy is an effective treatment for larger VPT (more than 2 or 2.5 mm in thickness) (Heimann et al. 2000; Anastassiou et al. 2006; Cohen et al. 2008; Brockmann et al. 2016) (Fig. 7.4a, f). The advantage of brachytherapy is its ability to treat the entire tumor with ease and safety due to peripheral location of VPT, and less likely to cause massive

exudation or hemorrhage following the treatment (Heimann et al. 2000; Anastassiou et al. 2006). Ruthenium-106 brachytherapy with apex dose of 80–10 Gray (Heimann et al. 2000; Anastassiou et al. 2006; Brockmann et al. 2016) and Iodine-125 brachytherapy with apex dose of 40 Gray (Cohen et al. 2008) have been reported to successfully control VPT and tumor-associated exudation in 72–97% of cases. Greater tumor diameter (>7.5 mm) and larger tumor basal area (>40 mm^2) increased the risk of persistent or recurrent tumor activity (Brockmann et al. 2016). Complications such as cataract, radiation retinopathy, radiation maculopathy, vitreous hemorrhage, and neovascular glaucoma may occurred following the treatment (Heimann et al. 2000; Anastassiou et al. 2006; Cohen et al. 2008; Brockmann et al. 2016).

7.6.7 Intravitreal Anti-VEGF

The strong immunoreactivity for VEGF in resected VPT tumor tissue has been reported (Saito et al. 2013). Tumor regression and resolution of macular edema following intravitreal anti-VEGF monotherapy have been reported in small VPT (Kenawy et al. 2007; Saito et al. 2013). However, the majority of patients, especially in larger tumor, required additional treatment, such as laser photocoagulation, cryotherapy, or brachytherapy, for long-term tumor control (Saito et al. 2013; Rogers et al. 2014).

7.6.8 Pars Plana Vitrectomy

Pars plana vitrectomy is indicated in VPT with epiretinal membrane, vitreous hemorrhage, rhegmatogenous retinal detachment, and tractional retinal detachment (Shields et al. 1995; Shields et al. 2013; Rogers et al. 2014; Garcia-Arumi et al. 2015).

7.6.9 Tumor Resection

Tumor resection may be required in selected cases of VPT. A small number of patients with VPT have been treated successfully with transcleral resection (Irvine et al. 2000), or transvitreal endoresection (Gibran 2008; Yeh and Wilson 2010; Rogers et al. 2014).

7.6.10 Systemic Antitumor Necrosis Factor (TNF)

A single case report of a patient with bilateral VPT and unilateral macular edema was treated with systemic infliximab for his systemic condition. After systemic infliximab, VPT in both eyes were regressed, and macular edema was improved (Japiassu et al. 2008).

References

Anastassiou G, Bornfeld N, Schueler AO, et al. Ruthenium-106 plaque brachytherapy for symptomatic vasoproliferative tumours of the retina. Br J Ophthalmol. 2006;90:447–50.

Bertelli E, Pernter H. Vasoproliferative retinal tumor treated with indocyanine green-mediated photothrombosis. Retin Cases Brief Rep. 2009;3:266–71.

Blasi MA, Scupola A, Tiberti AC, et al. Photodynamic therapy for vasoproliferative retinal tumors. Retina. 2006;26:404–9.

Brockmann C, Rehak M, Heufelder J, et al. Predictors of Treatment Response of Vasoproliferative Retinal Tumors to Ruthenium-106 Brachytherapy. Retina. 2016;36:2384–90.

Cohen VM, Shields CL, Demirci H, et al. Iodine I 125 plaque radiotherapy for vasoproliferative tumors of the retina in 30 eyes. Arch Ophthalmol. 2008;126:1245–51.

Garcia-Arumi J, Distefano LN, Fonollosa A, et al. Management of vision-threatening complications of vasoproliferative tumors of the retina. Ophthalmic Res. 2015;54:34–40.

Gibran SK. Trans-vitreal endoresection for vasoproliferative retinal tumours. Clin Exp Ophthalmol. 2008;36:712–6.

Heimann H, Bornfeld N, Vij O, et al. Vasoproliferative tumours of the retina. Br J Ophthalmol. 2000;84:1162–9.

Heimann H, Jmor F, Damato B. Imaging of retinal and choroidal vascular tumours. Eye (Lond). 2013;27:208–16.

Hussain RN, Jmor F, Damato B, et al. Verteporfin Photodynamic Therapy for the Treatment of Retinal Vasoproliferative Tumors. Ophthalmology. 2015;122:2361–3.

Irvine F, O'Donnell N, Kemp E, et al. Retinal vasoproliferative tumors: surgical management and histological findings. Arch Ophthalmol. 2000;118:563–9.

Japiassu RM, Brasil OF, Cunha AL, et al. Regression of vasoproliferative tumor with systemic infliximab. Ophthalmic Surg Lasers Imaging. 2008;39:348–9.

Kenawy N, Groenwald C, Damato B. Treatment of a vasoproliferative tumour with intravitreal bevacizumab (Avastin). Eye (Lond). 2007;21:893–4.

Krivosisc V, Massin P, Desjardins L, et al. Management of idiopathic vasoproliferative tumor with laser photocoagulation. Am J Ophthalmol. 2014;158:154–61.

Manjandavida FP, Shields CL, Kaliki S, et al. Cryotherapy-induced release of epiretinal membrane associated with retinal vasoproliferative tumor: analysis of 16 cases. Retina. 2014;34:1644–50.

McCabe CM, Mieler WF. Six-year follow-up of an idiopathic retinal vasoproliferative tumor. Arch Ophthalmol. 1996;114:617.

Nomura Y, Tamaki Y, Tsuji H, et al. Transpupillary thermotherapy for vasoproliferative retinal tumor. Retin Cases Brief Rep. 2009;3:358–60.

Poole Perry LJ, Jakobiec FA, Zakka FR, et al. Reactive retinal astrocytic tumors (so-called vasoproliferative tumors): histopathologic, immunohistochemical, and genetic studies of four cases. Am J Ophthalmol. 2013;155:593–608.

Rogers C, Damato B, Kumar I, et al. Intravitreal bevacizumab in the treatment of vasoproliferative retinal tumours. Eye (Lond). 2014;28:968–73.

Saito W, Kase S, Fujiya A, et al. Expression of vascular endothelial growth factor and intravitreal anti-VEGF therapy with bevacizumab in vasoproliferative retinal tumors. Retina. 2013;33:1959–67.

Shields JA, Decker WL, Sanborn GE, et al. Presumed acquired retinal hemangiomas. Ophthalmology. 1983;90:1292–300.
Shields CL, Shields JA, Barrett J, et al. Vasoproliferative tumors of the ocular fundus. Classification and clinical manifestations in 103 patients. Arch Ophthalmol. 1995;113:615–23.
Shields CL, Kaliki S, Al-Dahmash S, et al. Retinal vasoproliferative tumors: comparative clinical features of primary vs secondary tumors in 334 cases. JAMA Ophthalmol. 2013;131:328–34.
Yeh S, Wilson DJ. Pars plana vitrectomy and endoresection of a retinal vasoproliferative tumor. Arch Ophthalmol. 2010;128:1196–9.

Astrocytic Hamartoma of the Retina

8

Andrew W. Stacey and Mandeep S. Sagoo

8.1 Introduction

Retinal astrocytic hamartomas (RAH), also known as retinal astrocytomas, are tumors of retinal glial cells, arising from astrocytes in the nerve-fiber layer. The lesions are benign in nature and are thought to be congenital in origin. They are often diagnosed incidentally during routine examination and rarely cause any symptoms. They can be solitary or multifocal and often show no change in decades of follow-up. Rarely, RAH can exhibit unusual characteristics such as rapid growth, neovascularization, retinal exudation, and retinal detachment. There are no reports of metastasis of RAH (Shields et al. 2006).

RAH are often associated with systemic phacomatoses such as tuberous sclerosis complex (TSC) and, more rarely, neurofibromatosis type 1 (NF1). RAH can also arise spontaneously in otherwise normal individuals. In these cases the lesions can be referred to as solitary retinal astrocytomas, though many other names have been used in the literature including acquired retinal astrocytoma, astrocytic hamartoma of the retina not associated with TSC, atypical retinal astrocytic hamartoma, and spontaneous retinal astrocytoma (Reeser et al. 1978).

The pathogenesis of RAH is not entirely clear. Hamartomas occurring in the developing retina may be caused by mutations in the TSC1 or TSC2 gene which would lead to unregulated growth of undifferentiated glioneurocytes. Tuberin and hamartin, encoded by TSC1 and TSC2, respectively, are found in retinal astrocytes and play a role in cell cycle regulation via the PDGF-signaling pathway (Pusateri and Margo 2014).

The diagnosis of RAH, particularly in a patient without a history of TSC or neurofibromatosis, can be very challenging. One must distinguish this lesion from other simulating lesions including: retinal capillary hemangiomas, choroidal osteomas, retinoblastoma, and other choroidal and retinal lesions. Clinical exam and clinical imaging can be very helpful and lead to a correct diagnosis in the majority of cases. Biopsy is rarely necessary to make a diagnosis or RAH.

8.2 Associated Syndromes

TSC is a dominantly inherited disorder with a variable phenotype that includes brain astrocytoma, cutaneous angiofibromas, cutaneous depigmented macules (ash-leaf sign), renal angiomyolipoma, and other hamartomas and has also been termed Bourneville's disease. TSC is genetically heterogeneous with two major loci: 9q34 (TSC1), and 16p13 (TSC2). The gene at each locus has been identified, and both are tumor suppressor genes. TSC1 encodes the protein hamartin and TSC2, tuberin. RAH are one of the major diagnostic features of TSC occurring in about a third of patients (De Waele et al. 2015).

NF1 is an autosomal dominant genetic disease associated with a gene mutation on the NF1 gene (chromosome 17). Common systemic findings in NF1 include café au lait spots, cutaneous neurofibromas, and epilepsy. Ocular findings in NF1 include eyelid plexiform neurofibromas, Lisch nodules, and RAH (Williams et al. 2009). The incidence of RAH in NF1 is not known. Neurofibromatosis Type 2, a separate dominantly inherited genetic disorder due to mutations in the NF2 gene on chromosome 22, is also associated with retinal hamartomas, but these are combined hamartomas of the retina and retinal pigmented epithelium and are not of the astrocytic type (Evans 2009).

A. W. Stacey
Department of Ophthalmology, University of Washington, Seattle, WA, USA

M. S. Sagoo (✉)
Ocular Oncology Service, Moorfields Eye Hospital, London, UK

Retinoblastoma Service, Royal London Hospital, London, UK

UCL Institute of Ophthalmology, London, UK

D. Rojanaporn (ed.), *Ocular Oncology*, https://doi.org/10.1007/978-981-13-2336-2_8

8.3 Clinical Features

RAH are often noted incidentally on routine examination and rarely cause visual symptoms. RAH can be solitary or multifocal, unilateral or bilateral, and calcified or non-calcified. They arise from the inner sensory retina and can involve any layer of the retina. RAH can present in a wide variety of clinical phenotypes. There are three main categories of lesions: calcified, non-calcified, and lesions displaying both characteristics. Calcified lesions show multiple, small spherical calcific beads and are often white in color (Fig. 8.1a, b). These lesions are often referred to as "mulberry"-shaped due to their clinical appearance. Non-calcified, or "feathery," lesions can take on a more yellow or grey color (Fig. 8.1c, d). These lesions can be very subtle and nearly invisible on clinical examination. Lesions can also display features of both calcified and feathery lesions (Fig. 8.1e, f).

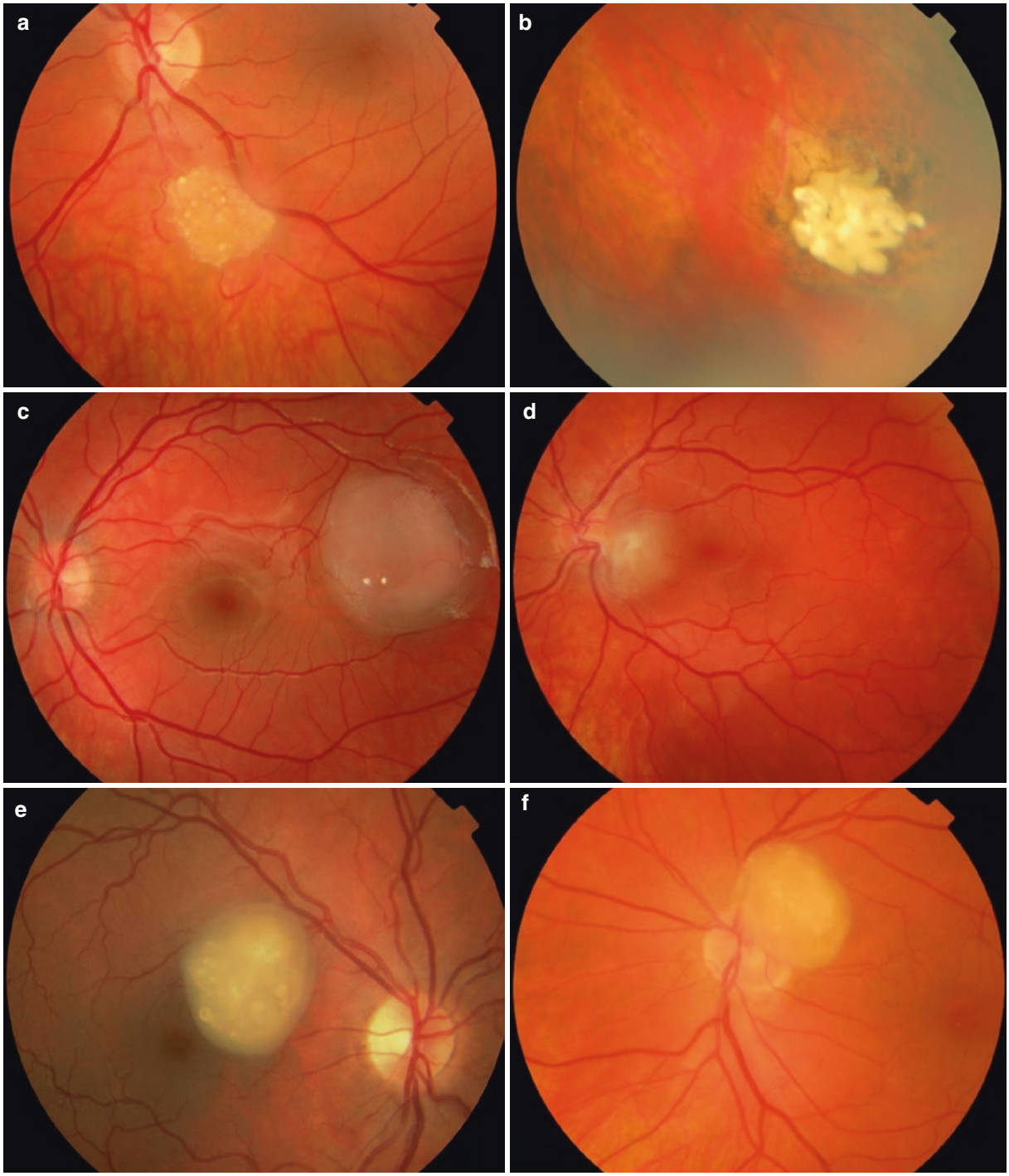

Fig. 8.1 (**a**, **b**) Calcified retinal astrocytic hamartoma, (**c**, **d**) Non-calcified, "feathery," astrocytic hamartoma. (**e**, **f**) Lesion with both calcified and feathery features

The vast majority of RAH remain stable without any progression for many years (Zimmer-Galler and Robertson 1995). Most RAH lesions are circumscribed and demonstrate little effect to the surrounding retina. While the lesions can exhibit intrinsic vascularity, they do not recruit feeder vessels as do other retinal lesions (e.g., retinoblastoma and retinal capillary hemangiomas) (Fig. 8.2). Rarely, RAH can undergo changes including hemorrhage, retinal exudation, total serous retinal detachment, neovascular glaucoma, and even globe perforation (Shields et al. 2004)

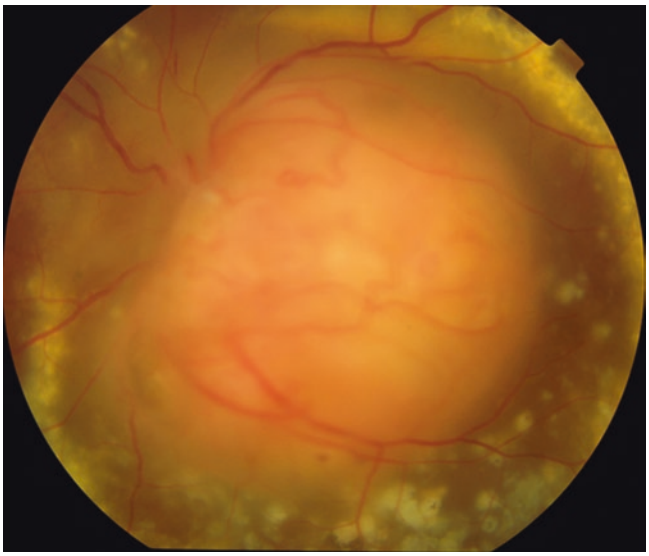

Fig. 8.2 Color fundus photograph of a large astrocytic hamartoma, exhibiting a white calcified mass, without dilated feeder vessels but with exudation and retinal detachment

8.4 Imaging and Diagnosis

When RAH is found in association with a systemic disease such as TSC, the diagnosis can be straightforward. Often these lesions are found in the periphery of patients with known systemic disease who are referred for routine screening examination. Differentiating RAH from other retinal lesions can be more complicated in patients without history of systemic phacomatoses. Clinical imaging tools can be helpful for distinguishing RAH from other lesions of the retina and choroid (Semenova et al. 2015).

Fundus autofluorescence (FAF) can aid in mapping the footprint of the RAH (Fig. 8.3b). FAF is highly sensitive for identifying RAH and often shows hyperautofluorescence in the lesion. Fundus fluorescein angiography (FFA) is useful for evaluating intrinsic vascularity in RAH (Fig. 8.3c). RAH often exhibits vast networks of small intrinsic vessels, but would not be expected to demonstrate enlarged feeder vessels, in contrast to retinal capillary hemangioma (hemangioblastoma) and retinoblastoma. FFA occasionally reveals late leakage within the lesion which may correspond to subretinal fluid on examination. Optical coherence tomography (OCT) provides information about the thickness of a lesion, the location of the lesion within the retina, and whether there are vitreous seeds or vitreoretinal traction (Fig. 8.3d). In smaller, posterior lesions OCT can be used to follow the thickness of the tumor over time. Ultrasonography is useful in identifying

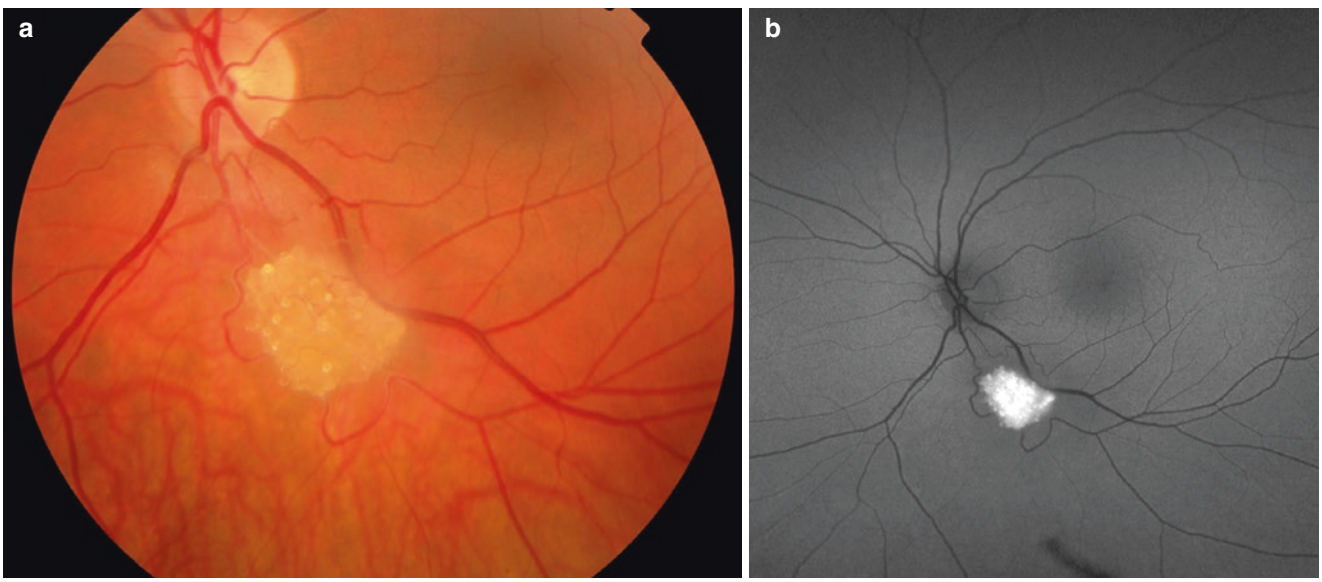

Fig. 8.3 A series of clinical imaging of a calcified, cystic retinal astrocytic hamartoma. (**a**) Color image of lesion presented in Fig. 8.1a. (**b**) Fundus autofluorescence of the same lesion demonstrating hyperautofluorescence. (**c**) Fluorescein angiogram demonstrating intrinsic vascularity in the lesion. (**d**) Enhanced depth ocular coherence tomography demonstrating a mass in the inner and middle retinal layers as well as subtle vitreous traction to the apex of the lesion. (**e**) Ultrasound B scan of an eye with a retinal astrocytic hamartoma. Note the hyperechoic retinal mass, with posterior shadowing

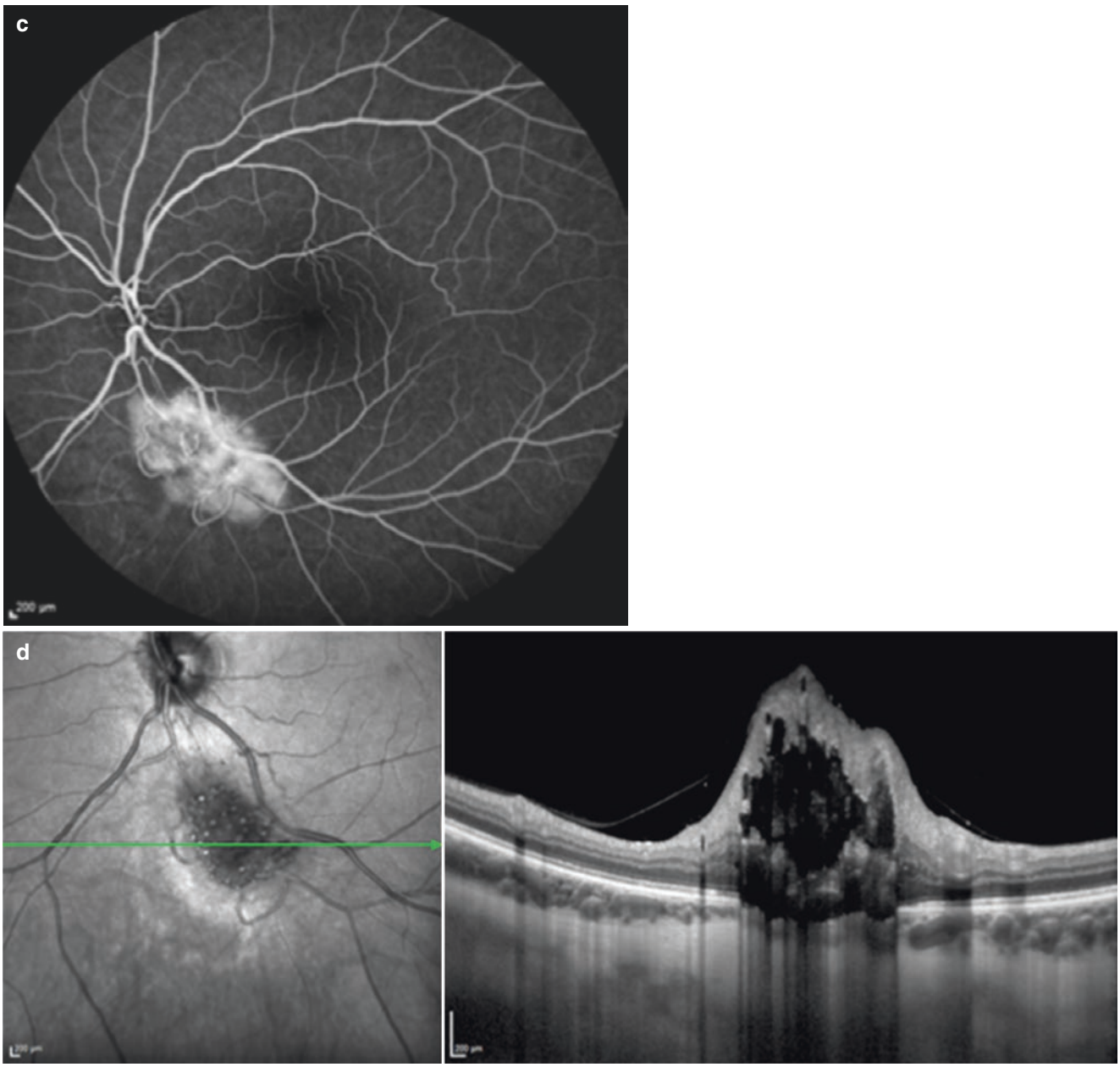

Fig. 8.3 (continued)

Fig. 8.3 (continued)

intrinsic calcification and monitoring the thickness of larger or peripheral lesions (Fig. 8.3e).

Occasionally the diagnosis of RAH is not clear and a biopsy can be performed for formal diagnosis. Due to advances in clinical imaging noted above, the need for biopsy is rare, and caution should be taken to avoid unnecessary inadvertant biopsies of aggressive neoplasia such as retinoblastoma. Fine needle aspiration biopsies as well as endoresections have been successfully performed on RAH and have led to positive diagnoses. Diagnostic or therapeutic enucleation can be considered in cases of aggressive lesions where RAH is on a differential diagnosis with malignant neoplasms such as retinoblastoma or melanoma (Shields et al. 2004).

8.5 Management

Patients who are found to have multifocal or bilateral RAH should be evaluated for systemic diseases including TSC or NF1. All patients found to have RAH should be evaluated with serial examinations over time for the presence of aggressive features including retinal hemorrhages, exudation, retinal detachment, and vitreous traction or seeding, as in Fig. 8.3. Even lesions without any aggressive features at the time of presentation need to be monitored over time as a small proportion of these lesions show progressive calcification or spontaneous development of aggressive features. Clinical imaging can aid in diagnosis and long-term monitoring of RAH.

When lesions are found to have aggressive features, an expanded differential diagnosis should be considered given the rarity of progression of RAH. In an aggressive variant, the course of such lesions can be progressive, with enlargement, vitreous hemorrhage and neovascular glaucoma. These cases can mimic retinoblastoma in children and may require enucleation in selected cases.

If a diagnosis of RAH is assured, options for treatment include laser photocoagulation, photodynamic therapy, or external beam radiotherapy. Vitrectomy may be necessary to treat traction and retinal detachments occurring secondary to aggressive RAH. Recently, the mammalian target of rapamycin (mTOR) signaling pathway has been targeted in the treatment of systemic astrocytomas via mTOR inhibitors (sirolimus and everolimus) (Curatolo and Moavero 2012). These drugs have shown early promise in halting the progression of aggressive RAH and can be considered in these situations.

8.6 Conclusion

RAH can occur sporadically or in combination with systemic illness. The course of RAH is typically benign and visual prognosis is very good. However, these lesions need to be monitored over time given the small chance of marked progression.

References

Curatolo P, Moavero R. mTOR inhibitors in tuberous sclerosis complex. Curr Neuropharmacol. 2012;10:404–15.

De Waele L, Lagae L, Mekahli D. Tuberous sclerosis complex: the past and the future. Pediatr Nephrol Berl Ger. 2015;30:1771–80.

Evans DGR. Neurofibromatosis type 2 (NF2): a clinical and molecular review. Orphanet J Rare Dis. 2009;4:16. https://doi.org/10.1186/1750-1172-4-16.

Pusateri A, Margo CE. Intraocular astrocytoma and its differential diagnosis. Arch Pathol Lab Med. 2014;138:1250–4.

Reeser FH, Aaberg TM, Van Horn DL. Astrocytic hamartoma of the retina not associated with tuberous sclerosis. Am J Ophthalmol. 1978;86:688–98.

Semenova E, Veronese C, Ciardella A, et al. Multimodality imaging of retinal astrocytoma. Eur J Ophthalmol. 2015;25:559–64.

Shields JA, Eagle RC, Shields CL, Marr BP. Aggressive retinal astrocytomas in four patients with tuberous sclerosis complex. Trans Am Ophthalmol Soc. 2004;102:139–47; discussion 147–148

Shields CL, Benevides R, Materin MA, Shields JA. Optical coherence tomography of retinal astrocytic hamartoma in 15 cases. Ophthalmology. 2006;113:1553–7.

Williams VC, Lucas J, Babcock MA, et al. Neurofibromatosis type 1 revisited. Pediatrics. 2009;123:124–33.

Zimmer-Galler IE, Robertson DM. Long-term observation of retinal lesions in tuberous sclerosis. Am J Ophthalmol. 1995;119:318–24.

Intraocular Lymphoma

9

Hiroshi Goto

9.1 Introduction

Intraocular lymphoma is a rare and highly malignant disease. The so-called primary intraocular lymphoma (PIOL) may occur prior or subsequent to primary central nervous system lymphoma (PCNSL).

Intraocular lymphoma is easily to be misdiagnosed as intraocular inflammatory diseases such as uveitis, and the issue of masquerade syndrome tends to delay diagnosis and treatment. Visual function is often well-preserved unless the lesion involves the macula or optic nerve. However, CNS lymphoma occurs in 65–90% of the patients with intraocular lymphoma (Baehring et al. 2005; Chan and Gonzales 2007), and the prognosis of survival is poor with 5-year survival rate of approximately 60% (Kimura et al. 2012), although long-term survival has been improved recently.

Intraocular lymphomas are broadly divided into primary oculo-CNS lymphomas that arise primarily in the eye and CNS and secondary intraocular lymphomas which are ocular lesions disseminated from systemic lymphomas during the course of disease. Primary intraocular lymphomas comprise primary vitreoretinal lymphoma (PVRL) and primary uveal lymphoma (PUL) (Coupland et al. 2009). Primary uveal lymphoma is an extremely rare disease and is usually a low-grade lymphoma equivalent to extranodal marginal zone B-cell lymphoma. Intraocular lymphoma secondary to disseminated systemic disease is usually confined to the choroid, unlike primary intraocular lymphoma that mostly involves the retina.

The background for the increased attention being drawn to intraocular lymphoma is the growing recognition of intraocular lymphoma and CNS lymphoma among oncologists, neurologists, and ophthalmologists, resulting in an increase in number of definitively diagnosed cases. However, even after subtracting the effect of this background, there is an actual annual increase in number of patients during the past 20 or 30 years.

Intraocular lymphoma affects elderly patients, usually over 60 years of age (Coupland et al. 2009; Kimura et al. 2012). Eighty to ninety percent of the patients with intraocular lymphoma develop bilateral disease, although initial presentation is unilateral (Coupland et al. 2009; Kimura et al. 2012).

9.2 Etiopathogenesis

Most of the intraocular lymphomas are of B-cell origin histopathologically equivalent to diffuse large B-cell lymphoma (DLBCL), and they are classified as high-grade lymphomas. Etiopathogenesis of intraocular lymphoma is unknown due to the lack of samples obtained from the intraocular tissue, although extensive studies of PCNSL have been conducted. In general, it is extremely rare for PCNSL and PIOL to manifest or recur outside the CNS in their natural history, demonstrating a unique tropism for the CNS and eye. The mechanisms involved in the migration of lymphoma cells in the CNS and eye constitute a major issue to understand the pathogenesis of these diseases (Chan et al. 2011).

The origin of the tumor cells in PCNSL and PIOL is also unknown. One possibility is that a malignant clone of B cells of systemic origin might evolve to express selective, specific adhesion molecules that facilitate homing to CNS and eye. Many studies suggested that certain chemokines which regulate leukocyte trafficking, proliferation, and adhesion are associated with PCNSL as well as PIOL (Chan et al. 2011).

9.3 Clinical Features

The clinical features of intraocular lymphoma are generally classified into two phenotypes: lesion formed by retinal as well as subretinal infiltration and vitreous opacification consisted of infiltration of mainly lymphoma cells. Many patients

H. Goto (✉)
Department of Ophthalmology, Tokyo Medical University, Tokyo, Japan
e-mail: goto1115@tokyo-med.ac.jp

D. Rojanaporn (ed.), *Ocular Oncology*, https://doi.org/10.1007/978-981-13-2336-2_9

present with a mixture of these two types. Papilledema with subretinal infiltration surrounding optic disc and retinal vasculitis are also occasionally experienced.

9.3.1 Features of Retinal and Subretinal Lesion

Lymphoma cells infiltrate at the retinal pigment epithelium and gradually make patchy mass underneath retinal pigment epithelium, which is clinically recognized as yellowish-white lesions in color (Fig. 9.1). In the initial disease stage, tiny infiltrates like small exudates can be seen. These lesions increase in number and size over time and become slightly elevated. Subretinal infiltrates fuse and expand, forming a widespread lesion in the fundus (Fig. 9.2). Characteristic brownish pigment dots and/or line are often observed in the yellowish-white lesions. Subretinal lesions may reduce in size or become atrophic over time with or without treatment (Fig. 9.3). Once these atrophic changes involve the macular area, significant disturbance of visual acuity may occur, although it is not common (Fig. 9.4).

On fluorescein angiography, various findings indicating damage of the retinal pigment epithelium by infiltrating lymphoma cells can be observed. Hypofluorescence, as a result of blockade by subretinal lesion, as well as granular or patchy hyperfluorescence, and late staining due to disturbance at the level of retinal pigment epithelium are some of the typical findings (Fig. 9.5). Even though ophthalmoscopic

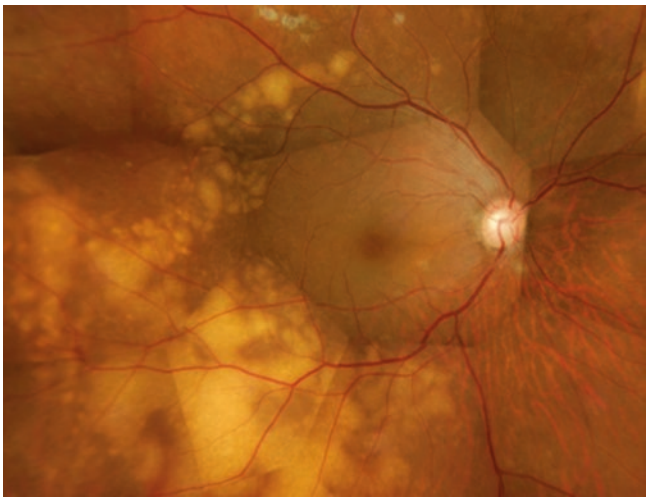

Fig. 9.1 Typical ocular findings of intraocular lymphoma with yellowish-white lesions composed of subretinal infiltration of lymphoma cells

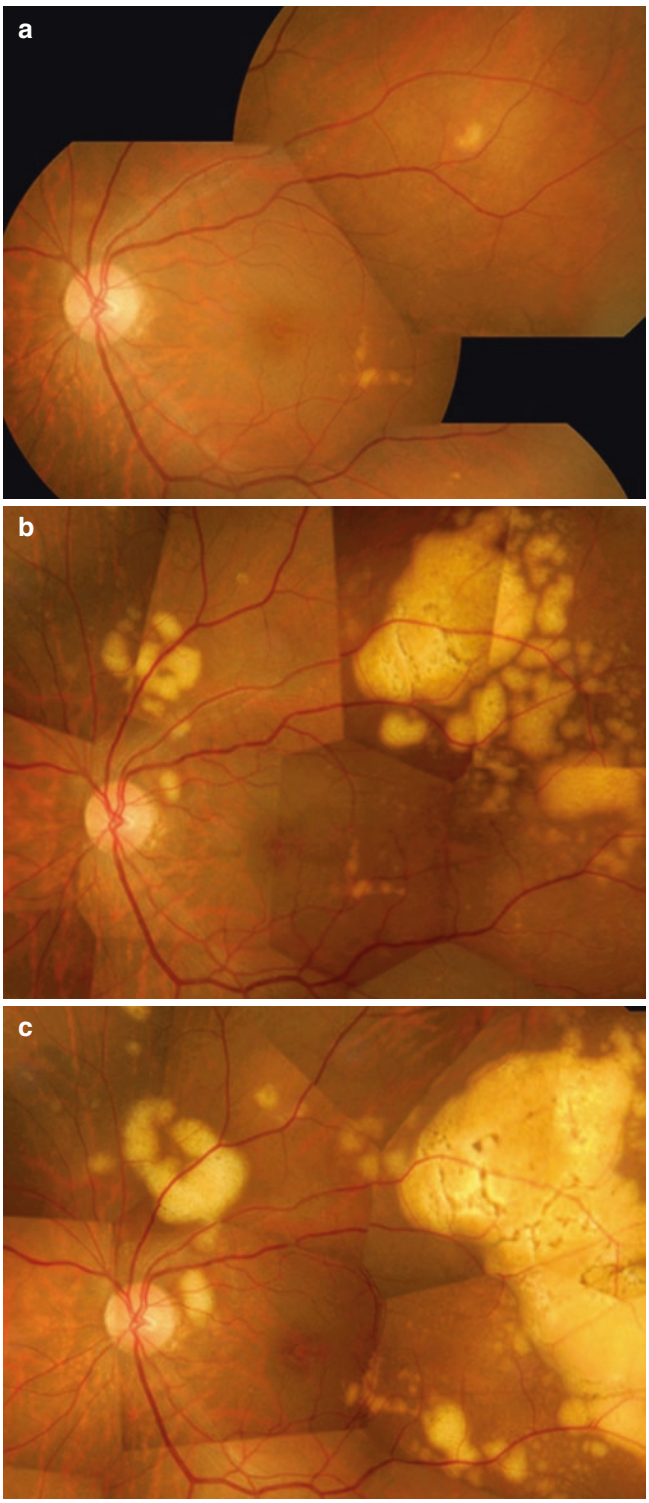

Fig. 9.2 Time course of intraocular lymphoma manifesting subretinal infiltration. In the early stage, small exudative lesions are observed (**a**). The subretinal lesions increase in number gradually and tend to fuse (**b**) and finally form a widespread infiltrative lesion (**c**). Note the brownish pigment dots and line in the yellowish-white lesion

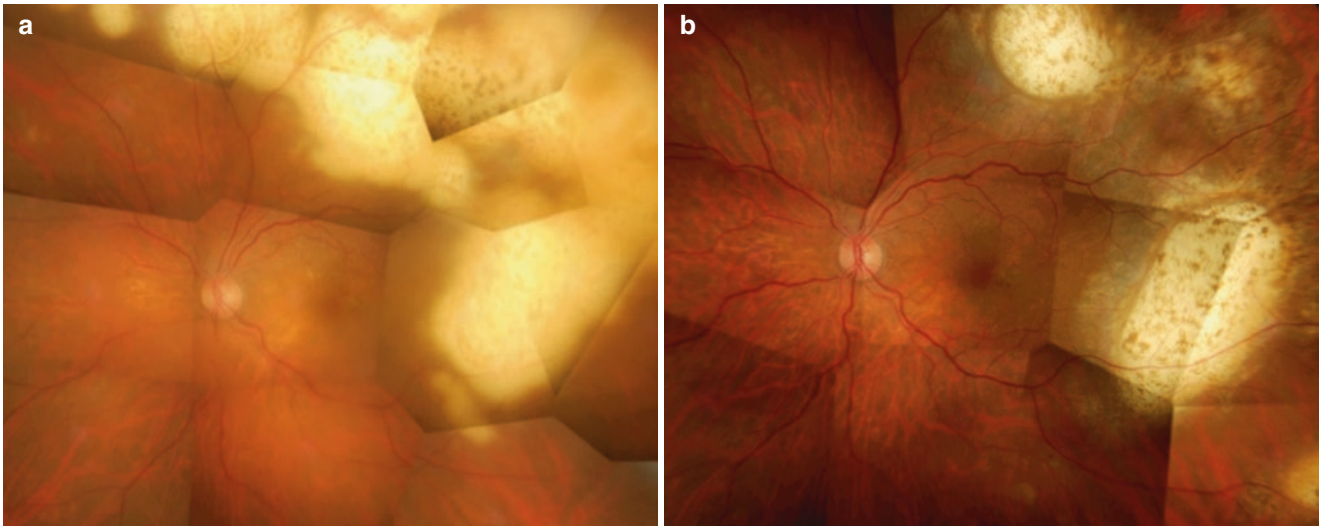

Fig. 9.3 Irrespective of treatment or no treatment, subretinal lesions (**a**) gradually become atrophic forming scars with time (**b**)

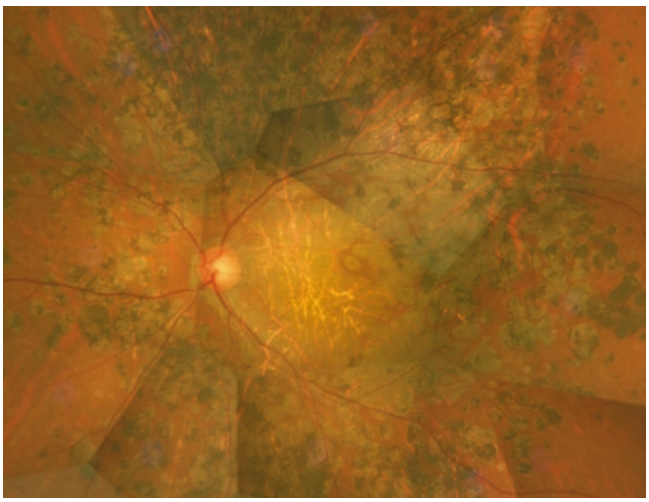

Fig. 9.4 Diffuse atrophic changes after disappearing of subretinal lesions involving the macular area

examination reveals no obvious abnormalities, fluorescein angiography may depict pathological changes (Fig. 9.6).

Optical coherent tomography (OCT) can detect granular lesions at retinal pigment epithelium level in the early disease stage and subretinal lesions between the retinal pigment epithelium and Bruch's membrane (Fig. 9.7) reflecting histopathological features (Whitcup et al. 1993). OCT may be useful in the diagnosis and monitoring of the progression or regression of intraocular lymphoma with retinal involvement (Liu et al. 2012). Fundus autofluorescence (FAF) is also useful in the assessment of disease activity (Casady et al. 2014) (Fig. 9.8).

Although rare, sheathing of retinal vessels resembling retinal vasculitis may be observed (Fig. 9.9). The sheathing may arise from infiltration of lymphoma cells to the vascular wall, while reactive vasculitis is also a possibility. Unlike uveitis, cystoid macular edema is rarely seen in intraocular lymphoma (Velez et al. 2002).

Retinal hemorrhage is uncommon at the initial onset of intraocular lymphoma or during the early stage of primary disease, but hemorrhage may be found during relapse or in untreated cases in which the disease has advanced. When retinal hemorrhage is present with yellowish-white infiltrative lesions, differentiation from *Cytomegalovirus retinitis* and other conditions is necessary (Fig. 9.10).

Recently, Pan et al. reported paraneoplastic cloudy vitelliform submaculopathy as a form of lymphoma-associated retinopathy which precedes the diagnosis of PIOL or PCNSL (Pang et al. 2014) (Fig. 9.11).

9.3.2 Features of Vitreous Opacification

Vitreous opacification is caused by lymphoma cells and reactive inflammatory cells infiltrating the vitreous cavity. The opacities are composed of many cells in sheets and clumps (Fig. 9.12). A characteristic opacity spreading radially from the posterior pole of the fundus toward the periphery is occasionally observed (Fig. 9.13). Despite the presence of severe vitreous opacification, good corrected visual acuity is often preserved.

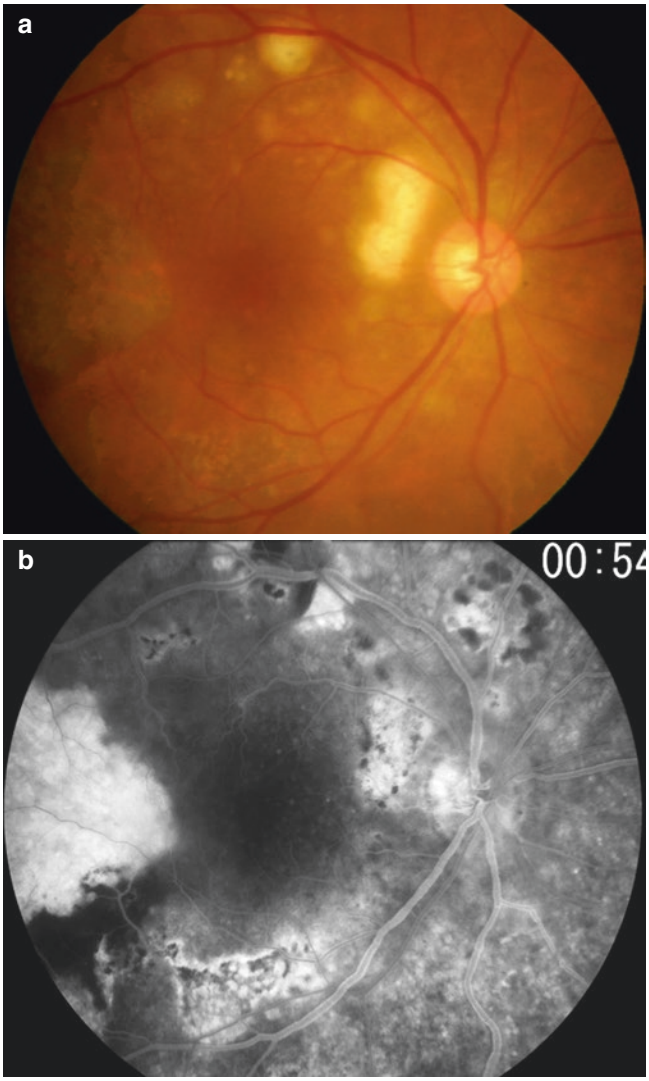

Fig. 9.5 Ophthalmoscopic examination reveals typical subretinal lesions and atrophy of retinal pigment epithelium (**a**). Note the hypofluorescence and hyperfluorescence on fluorescein angiography (**b**)

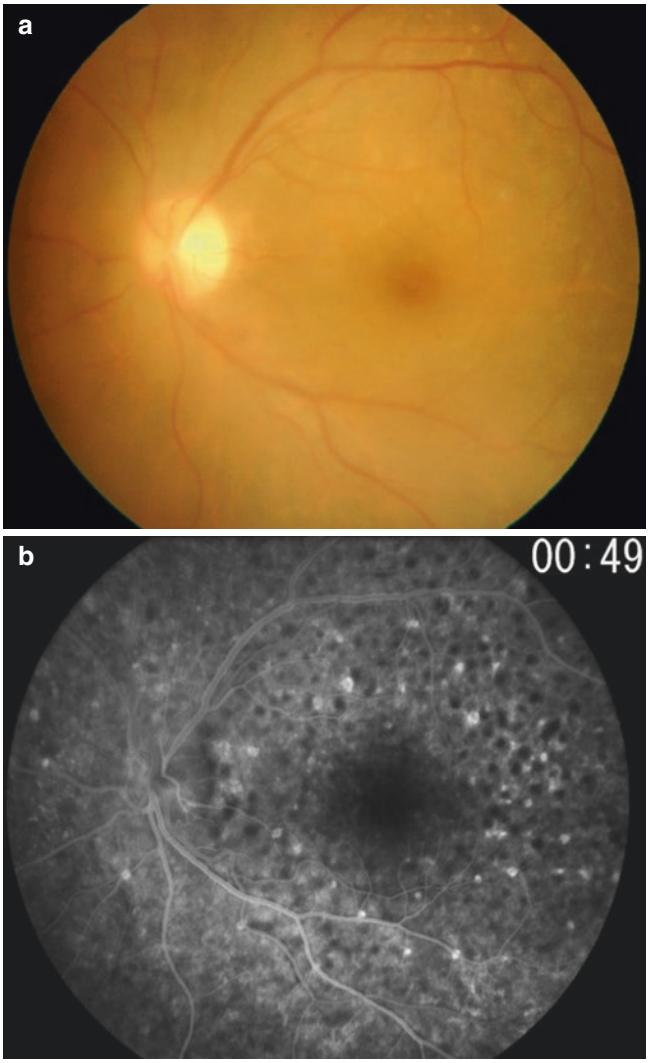

Fig. 9.6 Ophthalmoscopic examination reveals no obvious abnormalities except for diffuse vitreous opacification (**a**). Fluorescein angiography depicts multiple hypofluorescence or hyperfluorescence (**b**)

9.3.3 Findings in the Anterior Segment

Many patients with intraocular lymphoma have little or no anterior segment inflammation, especially at the early stage of disease. During relapse, however, cell infiltration in the anterior chamber together with fine, coarse, and reticular keratic precipitates often with spinous margin may be present (Fig. 9.14).

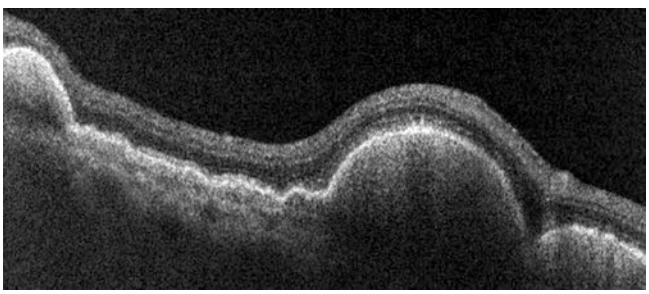

Fig. 9.7 Optical coherent tomography (OCT) detects the presence of lesions beneath the retinal pigment epithelium

9.4 Management

A consensus has not been reached regarding the recommended treatment for intraocular lymphoma. Especially, when onset of ocular lesion precedes CNS lesion, whether systemic chemotherapy and external beam radiotherapy (EBRT) are prophylactic against onset of CNS lesion remain controversial. Nevertheless, it is generally agreed that there is currently no prophylactic method that completely prevents the onset of CNS lymphoma subsequent to intraocular lymphoma. A study demonstrated that treatment of ocular symptoms did not improve the survival outcome of CNS

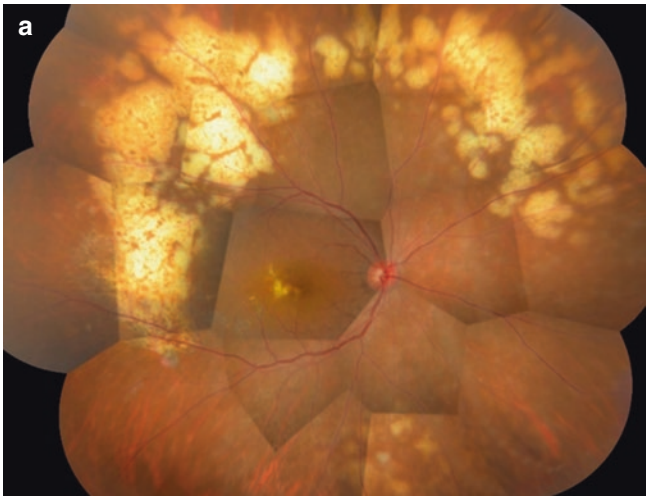

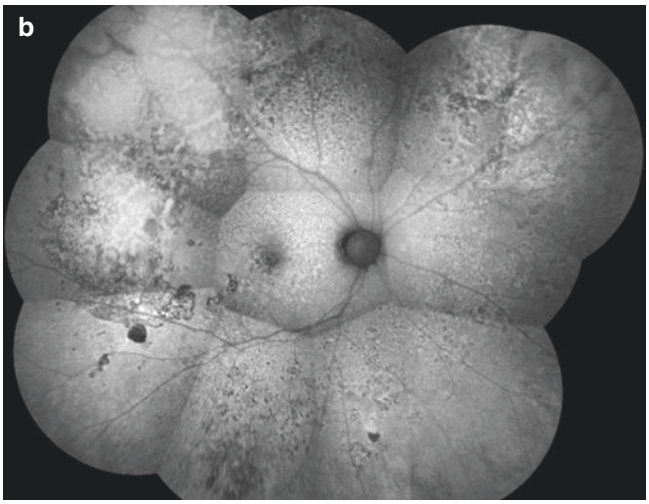

Fig. 9.8 Disseminated subretinal lesions of intraocular lymphoma (**a**). Fundus autofluorescence depicts diffuse hyper- as well as hypofluorescence (**b**)

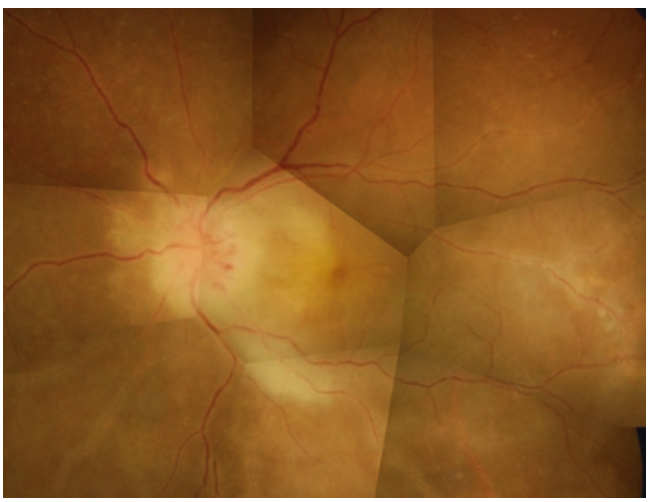

Fig. 9.9 Note the sheathing of retinal vessels with papilledema and dense subretinal lesion surrounding optic disc

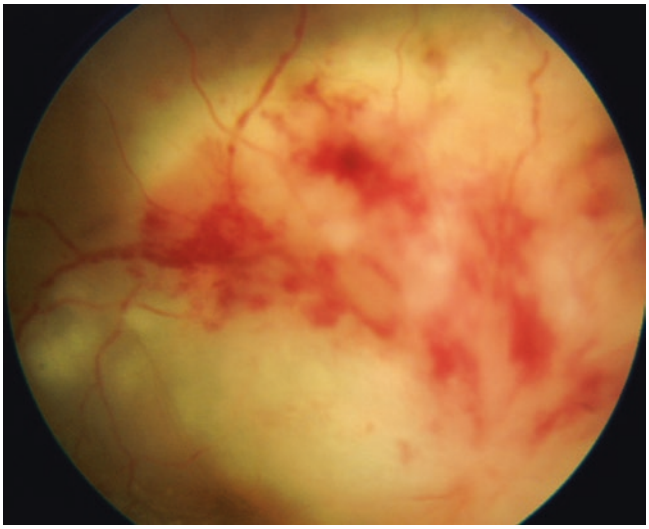

Fig. 9.10 In a case with hemorrhage accompanied by severe subretinal lesion, differentiation from infectious uveoretinitis such as *Cytomegalovirus retinitis* is required

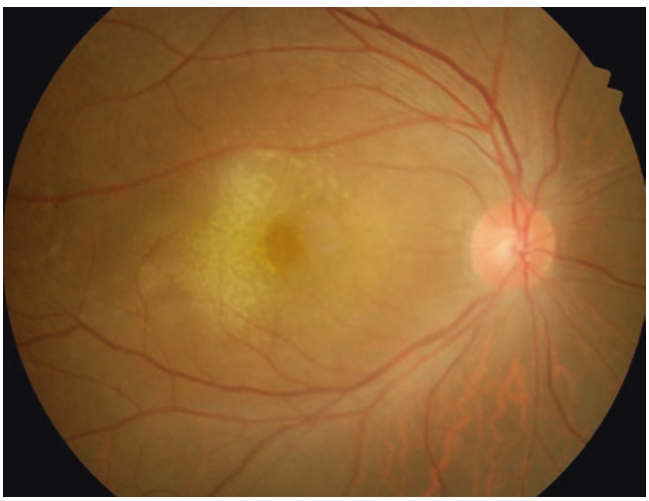

Fig. 9.11 So-called paraneoplastic cloudy vitelliform submaculopathy. Note the vitelliform yellowish lesion in the macular area

lymphoma (Grimm et al. 2008). However, this result was obtained from an uncontrolled study, and therefore may not conclusively demonstrate whether or not local ocular therapy has an impact on survival (Chan et al. 2011). Recent multicenter study showed the use of systemic chemotherapy was not proven to prevent CNSL and was associated with more severe adverse effects compared with local treatment. (Riemens et al. 2015).

9.4.1 Radiotherapy

External beam radiotherapy is one of the most effective treatments for ocular lesions (Berenbom et al. 2007).

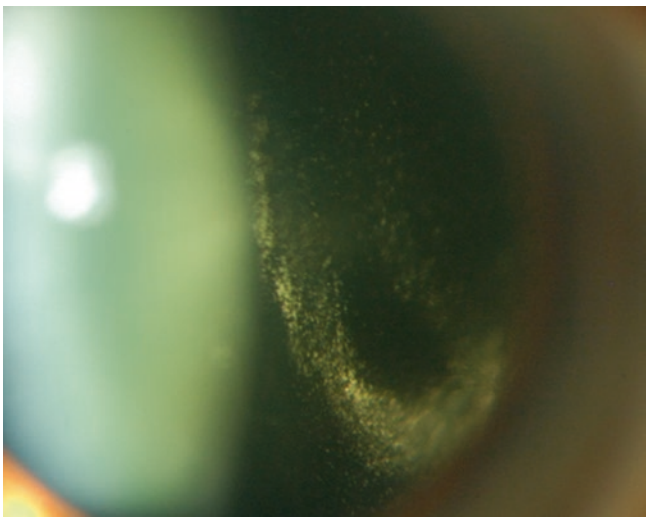

Fig. 9.12 Intraocular lymphoma observed by slit lamp manifesting vitreous opacification composed of many cells in sheets and clumps

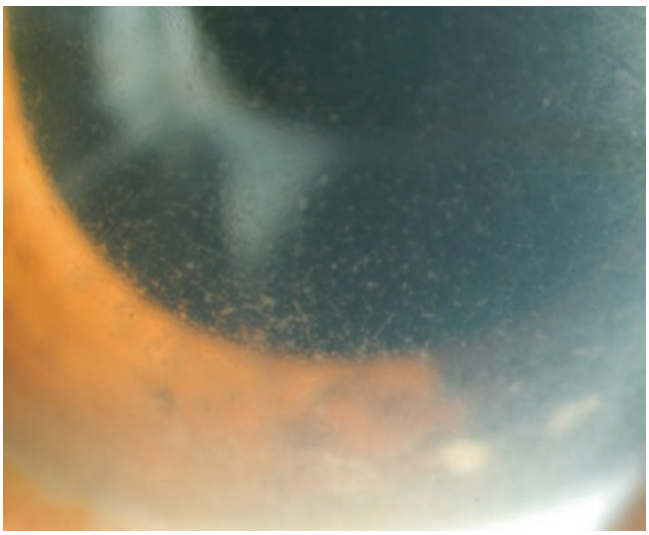

Fig. 9.14 Cells in the anterior chamber together with coarse and reticular keratic precipitates are observed at the time of relapse

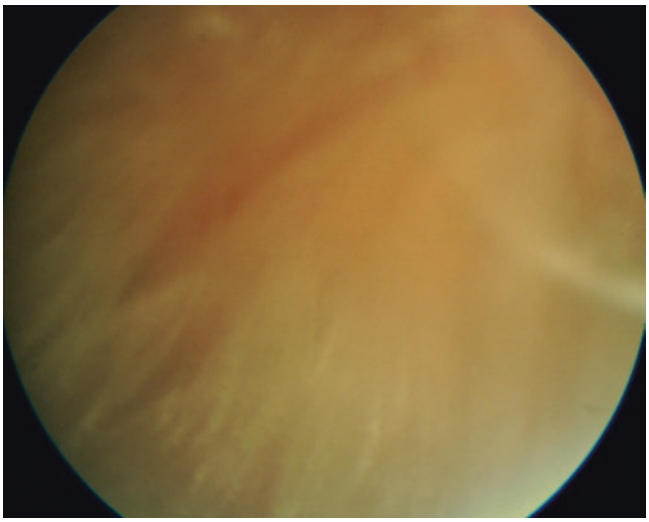

Fig. 9.13 Funduscopic examination shows characteristic vitreous opacification in sheets spreading radially

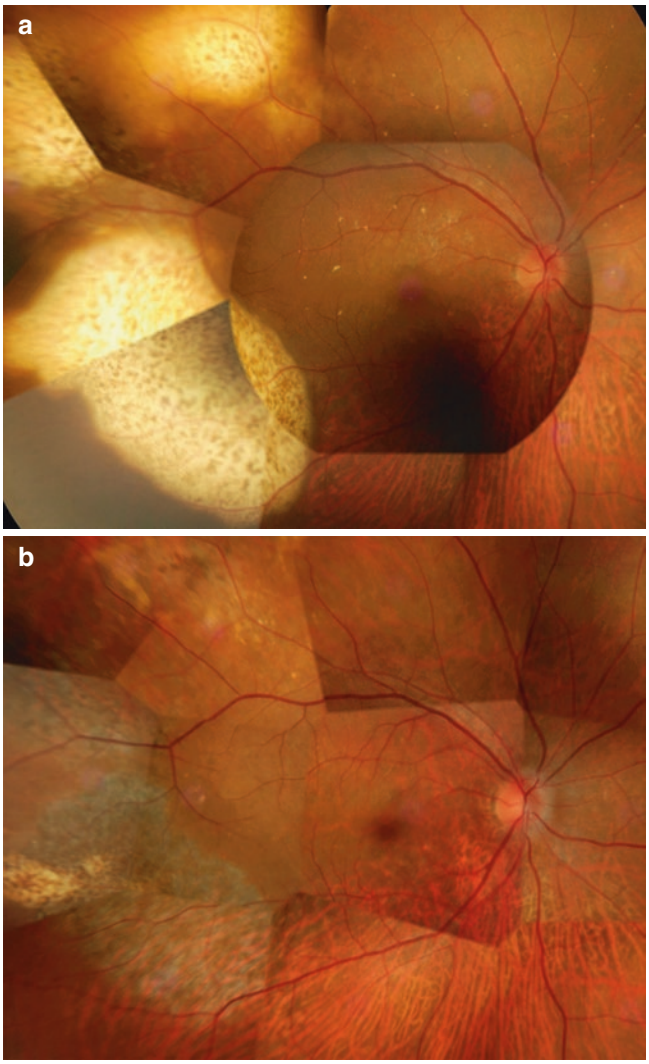

Fig. 9.15 Intraocular lymphoma before (**a**) and after (**b**) local external beam radiotherapy

Especially, bilateral involvement is a good indication for EBRT. A total of 30–40 Gy is delivered in 15–20 interrupted fractions (1.5–2.0 Gy per fraction) with lateral beams. Subretinal or retinal lesions gradually shrink shortly after irradiation is initiated or after irradiation is completed and become atrophied and scarred (Fig. 9.15). The 2-year overall and disease-free survival rates were reported to be 74 and 58%, respectively, after radiotherapy, but prophylactic cranial irradiation did not prevent intracranial recurrence (Isobe et al. 2006).

Although EBRT to the eyeball carry risks including dermatitis, corneal epithelial damage, cataract, and radiation retinopathy, most of these effects are acceptable and treatable. Serious visual impairment may occur due to chorioretinal atrophy extending to the posterior pole of the fundus;

however, this is not solely due to the adverse effect of radiation, but the retinal lesion per se may also play a role.

While there is no dispute that radiotherapy to the eyeball is effective in controlling the disease, relapse often occurs after radiotherapy in a certain percentage of cases. Especially with the improved long-term survival among patients, a high rate of relapse is observed nowadays, often necessitating local and systemic chemotherapy which will be described below. Recent study reveals that 3-year overall survival, progression-free survival, and local control rates were 89, 49, and 95% over a median of 36 months of observation, respectively. However, 55% of patients had intracranial relapse at a median of 28 months after initiation of radiotherapy (Mikami et al. 2013).

9.4.2 Local Chemotherapy

9.4.2.1 Methotrexate

Local chemotherapy by intravitreal injection of methotrexate (MTX) has been used widely either as primary therapy as an alternative to ocular radiation therapy or as treatment for relapse after radiation therapy (Fishburne et al. 1997; de Smet et al. 1999). Especially, unilateral involvement and previous treatment with EBRT are good indications (Chan et al. 2011). A dose of 400 μg of MTX is injected intravitreally twice weekly for 4 weeks and then weekly for 1 month, followed by monthly injections for 1 year (Fishburne et al. 1997).

When treatment is conducted following this protocol, clinical remission is achieved after a mean of 6.4 ± 3.4 (range, 2–16) injections of MTX (Frenkel et al. 2008). Intravitreal injection of MTX may have adverse effects including conjunctival injection and disturbance of the corneal epithelium. Most of the adverse effects are transient; however, there are cases of severe corneal damage causing difficulties to continue treatment. Apart from the original regimen, various modifications of intravitreal MTX injection have been attempted, such as reducing the number of injections or extending the dosing interval appropriately according to clinical improvement (Rajagopal and Harbour 2011).

9.4.2.2 Rituximab

The efficacy of intravitreal injection of anti-CD20 monoclonal antibody, also known as rituximab, has been reported (Kitzmann et al. 2007). Rituximab is a useful treatment for cases unresponsive to intravitreal MTX injection and cases intolerable to repeated MTX injections due to adverse events. The lack of serious adverse reactions is another merit of rituximab. On the other hand, several problems remain unsolved including the dosage, and dosing interval and treatment duration have not been established.

9.4.3 Systemic Chemotherapy

Intravenous injection of high dose of the antimetabolic drug MTX (HD-MTX therapy; 8 g/mm) is commonly used for the treatment of oculo-CNS lymphoma, especially CNS lymphoma, because of the capability of HD-MTX to cross the blood-brain barrier. However, low concentrations of MTX are obtained in the eye and cerebrospinal fluid after treatment with intravenous HD-MDX, and disease may relapse (Batchelor et al. 2003). Therefore, complete remission of intraocular lymphoma is difficult to achieve with systemic chemotherapy alone and usually requires local therapy.

Combined modality therapy using high-dose methotrexate and whole-brain radiotherapy has been reported to improve the survival rate of CNS lymphoma (Abrey et al. 1998). On the other hand, in elderly patients aged over 60 years, the possibility of a high incidence of delayed treatment-related neurotoxicity caused by combined therapy has been suggested (Prica et al. 2012). Therefore, for the treatment of CNS lymphoma, the strategy of initial systemic therapy with HD-MTX followed by whole-brain irradiation in unresponsive and relapse cases is being used more commonly.

References

Abrey LE, DeAngelis LM, Yahalom J. Long-term survival in primary CNS lymphoma. J Clin Oncol. 1998;16:859–63.

Baehring JM, Androudi S, Longtine JJ, et al. Analysis of clonal immunoglobulin heavy chain rearrangements in ocular lymphoma. Cancer. 2005;104:591–7.

Batchelor TT, Kolak G, Ciordia R, et al. High-dose methotrexate for intraocular lymphoma. Clin Cancer Res. 2003;9:711–5.

Berenbom A, Davila RM, Lin HS, et al. Treatment outcomes for primary intraocular lymphoma: implications for external beam radiotherapy. Eye. 2007;21:1198–201.

Casady M, Faia L, Nazemzadeh M, et al. Fundus autofluorescence patterns in primary intraocular lymphoma. Retina. 2014;34:366–72.

Chan CC, Gonzales JA. Primary intraocular lymphoma. Singapore: World Scientific; 2007.

Chan CC, Rubenstein JL, Coupland SE, et al. Primary vitreoretinal lymphoma: a report from an international primary central nervous system lymphoma collaborative group symposium. Oncologist. 2011;16:1589–99.

Coupland SE, Chan CC, Smith J. Pathophysiology of retinal lymphoma. Ocul Immunol Inflamm. 2009;17:227–37.

Fishburne BC, Wilson DJ, Rosenbaum JT, et al. Intravitreal methotrexate as an adjunctive treatment of intraocular lymphoma. Arch Ophthalmol. 1997;115:1152–6.

Frenkel S, Hendler K, Siegal T, et al. Intravitreal methotrexate for treating vitreoretinal lymphoma: 10 years of experience. Br J Ophthalmol. 2008;92:383–8.

Grimm SA, McCannel CA, Omuro AM, et al. Primary CNS lymphoma with intraocular involvement: International PCNSL Collaborative Group Report. Neurology. 2008;71:1355–60.

Isobe K, Ejima Y, Tokumaru S, et al. Treatment of primary intraocular lymphoma with radiation therapy: a multi-institutional survey in Japan. Leuk Lymphoma. 2006;47:1800–5.

Kimura K, Usui Y, Goto H, et al. Clinical features and diagnostic significance of the intraocular fluid of 217 patients with intraocular lymphoma. Jpn J Ophthalmol. 2012;56:383–9.

Kitzmann AS, Pulido JS, Mohney BG. Intraocular use of rituximab. Eye. 2007;21:1524–7.

Liu TY, Ibrahim M, Bittencourt M, et al. Retinal optical coherence tomography manifestations of intraocular lymphoma. J Ophthal Inflamm Infect. 2012;2:215–8.

Mikami R, Nakayama H, Goto H, et al. Preliminary results of radiotherapy for primary intraocular non-Hodgkin lymphoma. Leuk Lymphoma. 2013;54:2181–4.

Pang CE, Shields CL, Jumper JM, et al. Paraneoplastic cloudy vitelliform submaculopathy in primary vitreoretinal lymphoma. Am J Ophthalmol. 2014;158:1253–61.

Prica A, Chan K, Cheung MC. Combined modality therapy versus chemotherapy alone as an induction regimen for primary central nervous system lymphoma: a decision analysis. Br J Haematol. 2012;158:600–7.

Rajagopal R, Harbour JW. Diagnostic testing and treatment choices in primary vitreoretinal lymphoma. Retina. 2011;31:435–40.

Riemens A, Bromberg J, Touitou V, et al. Treatment strategies in primary vitreoretinal lymphoma: a 17-center European collaborative study. JAMA Ophthalmol. 2015;133:191–7.

de Smet MD, Vancs VS, Kohler D, et al. Intravitreal chemotherapy for the treatment of recurrent intraocular lymphoma. Br J Ophthalmol. 1999;83:448–51.

Velez G, Chan CC, Csaky KG. Fluorescein angiographic findings in primary intraocular lymphoma. Retina. 2002;22:37–43.

Whitcup SM, de Smet MD, Rubin BI, et al. Intraocular lymphoma. Clinical and histopathologic diagnosis. Ophthalmology. 1993;100:1399–406.

Retinoblastoma

10

Carol L. Shields and Sara E. Lally

10.1 Introduction

Retinoblastoma is the most common intraocular cancer of childhood (Shields and Shields 2015; JA and CL 1992; Kivela 2009; Ramasubramanian and Shields 2012a). This malignancy represents approximately 4% of all pediatric malignancies and carries a fairly high survival rate in developed nations. There has been a tremendous progress in retinoblastoma management over the past 20 years in the United States of America (USA) and abroad.

10.2 Demographics

It is estimated that 250–300 new cases of retinoblastoma are diagnosed in the USA each year and 7000 cases worldwide. This serious ocular malignancy can manifest with painless leukocoria, and if unrecognized and untreated, retinoblastoma can lead to death within 1–2 years (Shields and Shields 2015; JA and CL 1992). Advanced disease with massive tumor, invasive into surrounding structures, is at greatest risk for metastasis. Worldwide, survival parallels economic development as retinoblastoma survival is approximately 30% in Africa, 60% in Asia, 80% in Latin America, and >97% in Europe and North America (Kivela 2009). The reason for the poor survival in undeveloped nations relates to late detection of advanced retinoblastoma, often presenting with orbital invasion or metastatic disease and the lack of chemotherapy.

10.3 Clinical Features

The clinical features of retinoblastoma vary depending on the extent of tumor. In the USA, an evaluation of 1265 patients by Abramson et al. from New York, revealed that the most common presenting signs included leukocoria (56%), strabismus (24%), and poor vision (8%) (Abramson et al. 1998) (Fig. 10.1). Further study on a cohort of 1196 eyes by our team in Philadelphia found median age at presentation of 15 months with 51% male and 49% female and 53% unilateral and 47% bilateral (Epstein et al. 2003). However, in the remainder of the world, the features can differ. From Sudan (Ali et al. 2011), buphthalmos (56%) and leukocoria (32%) were most common, and from Mali in Africa (Boubacar et al. 2010), proptosis (55%), leukocoria (38%), strabismus (6%), and buphthalmos (2%) were found.

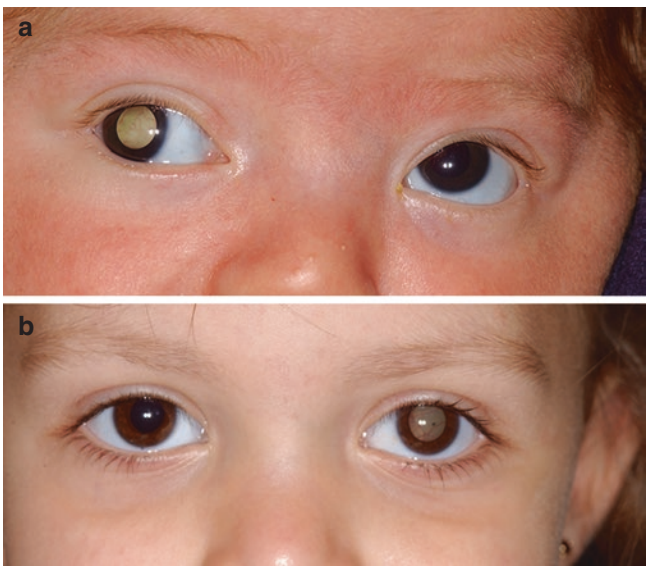

Fig. 10.1 Retinoblastoma presenting with leukocoria. (**a**) Leukocoria from retinoblastoma in a 3 month old. (**b**) Leukocoria from retinoblastoma in a 3 year old

C. L. Shields (✉) · S. E. Lally
Wills Eye Hospital, Philadelphia, PA, USA

Department of Ophthalmology, Thomas Jefferson University, Philadelphia, PA, USA
e-mail: carol@shields.md; sara@shields.md

D. Rojanaporn (ed.), *Ocular Oncology*, https://doi.org/10.1007/978-981-13-2336-2_10

The clinical manifestations of retinoblastoma vary. Small retinoblastomas under 2 mm in basal dimension appears ophthalmoscopically as a subtle, transparent, or slightly translucent lesion in the sensory retina (Shields and Shields 2015; JA and CL 1992; Shields and Shields 2010). Slightly larger tumors lead to dilated retinal blood vessels and foci of chalk-like calcification. Larger tumors often present with leukocoria, but any size tumor can produce leukocoria.

Retinoblastoma growth patterns include intraretinal, endophytic, and exophytic. Intraretinal tumors are limited to the retina. Endophytic tumors grow from the retina inward toward the vitreous cavity, with free-floating vitreous seeds, often simulating endophthalmitis. Exophytic retinoblastoma grows from the retina deep into the subretinal space and produce progressive retinal detachment, with the retina often displaced anteriorly behind a clear lens resembling Coats disease or other forms of exudative retinal detachment. Occasionally retinoblastoma can assume a diffuse infiltrating pattern, characterized by a flat infiltration of the retina without an obvious mass (Shields et al. 2008). In such cases, the diagnosis can be more challenging and simulate uveitis or endophthalmitis. Less frequently, the presenting feature can be pseudohypopyon due to tumor seeding in the anterior chamber, hyphema secondary to iris neovascularization, vitreous hemorrhage, or signs of orbital cellulitis.

10.4 Classification

There have been several classifications (Ramasubramanian and Shields 2012b; Shields et al. 2004; Linn Murphree 2005; Shields and Shields 2006) proposed for intraocular retinoblastoma including the Reese-Ellsworth classification, Essen classification, and Philadelphia classification. The current classification is the International Classification of Retinoblastoma (Linn Murphree 2005; Shields and Shields 2006) based predominantly on the presence and extent of subretinal and vitreous tumors seeds (Table 10.1) (Fig. 10.2).

10.5 Diagnostic Testing

Accurate diagnosis in a child with suspected retinoblastoma is accomplished by taking a detailed history, physical evaluation, external ocular examination, slit-lamp biomicroscopy, and binocular indirect ophthalmoscopy with scleral depression. This is typically performed in the office and then under anesthesia to determine precisely the number and location of all tumors. The diagnosis is established by the classic appearance of the retinal tumors by an experienced examiner. Needle biopsy confirmation is not performed due to risk for tumor seeding.

Table 10.1 The international classification of retinoblastoma

Group	Philadelphia version Quick reference using ABCDE	Philadelphia version[a]	Los Angeles version[b]
A	SmAll rb	Rb ≤ 3 mm	Rb ≤ 3 mm, at least 3 mm from the foveola and 1.5 mm from optic nerve. No seeding.
B	Bigger rb Macular rb Juxtapapillary rb Subretinal fluid	Rb > 3 mm or • Macular location or • Juxtapapillary location [<1.5 mm to disc] or • SRF present	Eyes with no vitreous or subretinal seeding and retinal tumors of any size or location not included in group A. Small cuff of subretinal fluid ≤ 5 mm from tumor margin
C	Contained (focal) seeds	Rb with • SRS ≤3 mm from Rb or • VS ≤3mm from Rb	Eyes with focal vitreous or subretinal seeding and discrete tumor of any size or location. Seeding must be local, fine and limited so as to be theoretically treatable with a radioactive plaque. Up to one quadrant subretinal fluid may be present.
D	Diffuse seeds	Rb with • SRS >3 mm from Rb or • VS >3mm from Rb	Eyes with diffuse vitreous or subretinal seeding and/or massive, nondiscrete endophytic or exophytic disease. Seeding more extensive than Group C. Retinal detachment > 1 quadrant.
E	Extensive rb	Rb with • Size >50% of globe or • Neovascular glaucoma or • Opaque media or • Invasion of optic nerve, choroid, sclera, orbit, anterior chamber	Massive Rb with anatomic or functional destruction of the eye with one or more of the following • Neovascular glaucoma • Massive intraocular hemorrhage • Aseptic orbital cellulitis • Tumor anterior to anterior vitreous face • Tumor touching lens • Diffuse infiltrating tumor • Phthisis or pre-phthisis

Rb retinoblastoma, *SRF* subretinal fluid, *SRS* subretinal seeds, *VS* vitreous seeds adapted from

[a]Murphree AL. Intraocular retinoblastoma: the case for a new group classification. Ophthalmol Clin North Am 2005;18:41-53

[b]Shields CL, Shields JA. Basic understanding of current classification and management of retinoblastoma. Curr Opin Ophthalmol 2006;17:228-34

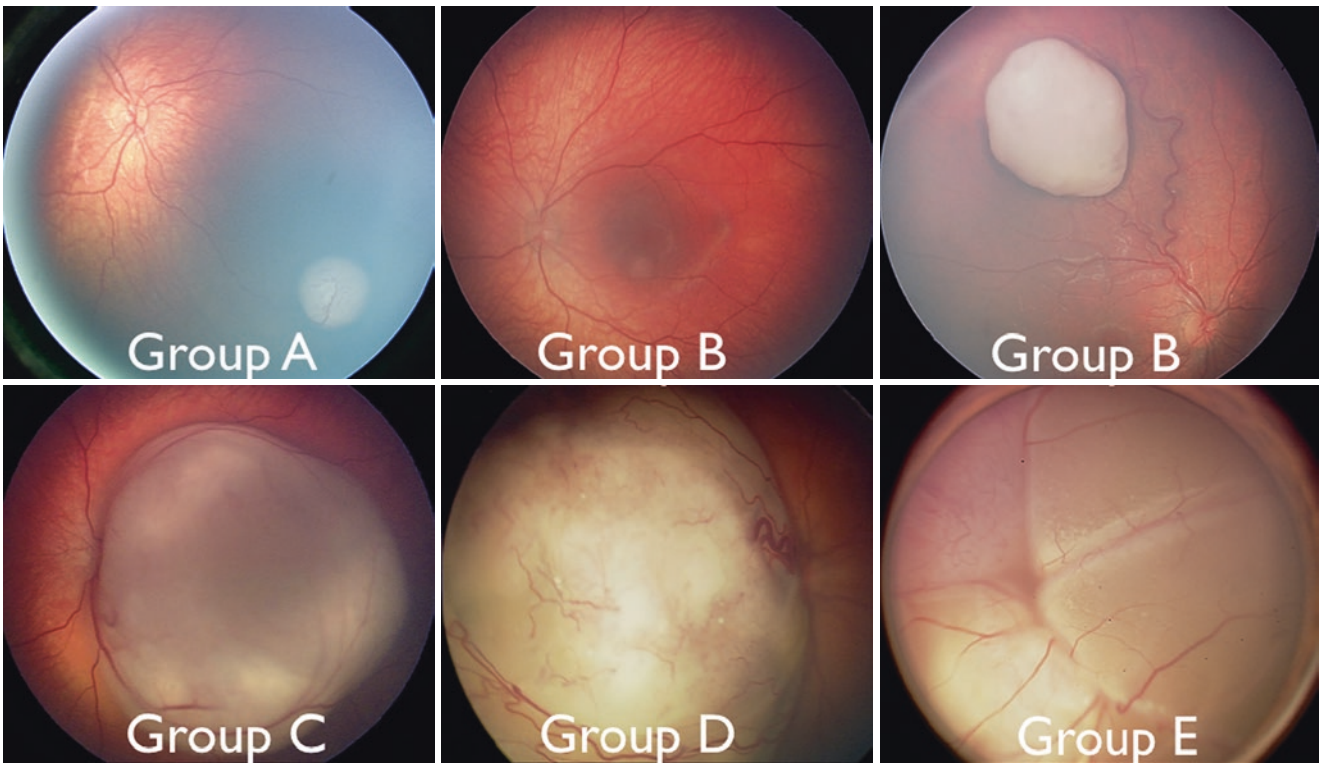

Fig. 10.2 International Classification of Retinoblastoma (see Table 10.1). Group A. Tumor of slightly <3 mm in diameter and outside macula. Group B. Tumor within macula. Group B. Tumor of >3 mm in diameter outside the macular region. Group C. Tumor with surrounding subretinal fluid and trace subretinal seeds, within 3 mm of the mass. Group D. Tumor with large retinoblastoma and extensive subretinal seeds, greater than 3 mm from the mass. Group E. Tumor with large retinoblastoma and total retinal detachment up against the posterior lens surface

Ancillary diagnostic studies can be helpful in confirming the diagnosis of retinoblastoma (Shields and Shields 2015; JA and CL 1992). Ultrasonography is the first test for confirmation of retinoblastoma and demonstrates an intraocular mass, often with intrinsic calcification and orbital shadowing. About 5–10% of retinoblastomas show no intrinsic calcification (Fig. 10.3). Fluorescein angiography shows early vascularity and late hyperfluorescence of the tumor. Optical coherence tomography (OCT) is useful for detection of subclinical (invisible) retinoblastoma and for judging the status of the foveola during and after therapy. Additionally, OCT is useful in the follow-up of patients to assess macular anatomy (Cao et al. 2014; Saktanasate et al. 2015; Park et al. 2017). Magnetic resonance imaging (MRI) is of value in assessment of the optic nerve, orbit, and brain. Computed tomography (CT) can confirm the intraocular calcified tumor (Fig. 10.4).

10.6 Genetics

Retinoblastoma affects approximately one infant in 15,000–20,000 live births in the USA each year (Shields and Shields 2015; Kivela 2009; Ramasubramanian and Shields 2012a). Retinoblastoma is classified in four different ways: familial or sporadic, bilateral or unilateral, heritable or nonheritable, and germline or somatic. Our preference is germline or somatic. Both bilateral and familial retinoblastomas are a result of germline mutation and are thus a heritable tumor. Unilateral sporadic retinoblastoma shows germline mutation in 10–15% of cases.

The retinoblastoma gene is located on the long arm of chromosome 13 (13q14) and acts as a recessive suppressor gene. It is a large 4.73 kilobase message. An intact gene protects against expression of retinoblastoma. In germline cases of retinoblastoma, all cells in the body have a mutation and are predisposed to possible tumor development. This explains the high incidence of second nonocular tumors, such as osteosarcoma, soft tissue sarcoma, and cutaneous melanoma, seen in patients with familial retinoblastoma or bilateral sporadic retinoblastoma. By contrast, in somatic mutation retinoblastoma, there is no predisposing mutation, so most children manifest only one tumor and carry little risk for other cancers.

10.6.1 13q Syndrome

The 13q deletion syndrome can manifest with several phenotypic abnormalities. Many patients have minimal or no visible abnormality. The characteristic findings include dysmorphic

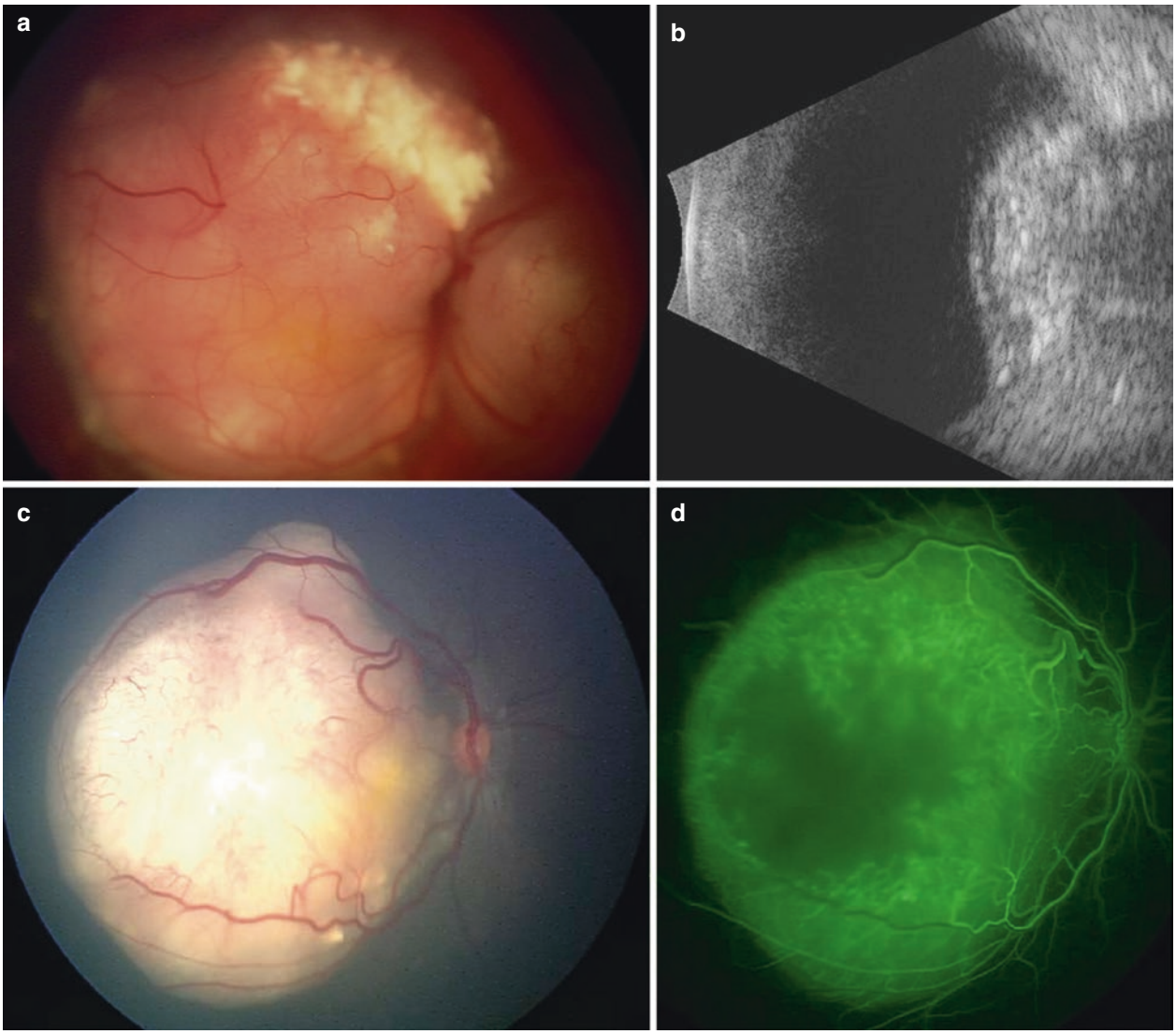

Fig. 10.3 Imaging of retinoblastoma. (**a**) Fundus photography demonstrating nonpigmented retinal tumor involving the macula and showing (**b**) dense calcification with tumor shadowing on ultrasonography. (**c**) Fundus photography demonstrating macular retinoblastoma with (**d**) fluorescein angiography documenting intrinsic fluorescence

Fig. 10.4 Computed tomography of retinoblastoma showing the dense, calcified mass within the right globe

features such as microcephaly, broad prominent nasal bridge, hypertelorism, microphthalmos, epicanthus, ptosis, protruding upper incisors, micrognathia, short neck with lateral folds, large prominent low set ears, facial asymmetry, imperforate anus, genital malformations, perineal fistula, hypoplastic or absent thumbs, toe abnormalities, and psychomotor and mental retardation. The midface of patients with 13q deletion is notable for prominent eyebrows, broad nasal bridge, bulbous tipped nose, large mouth, and thin upper lip.

10.7 Management

Management of retinoblastoma is complex and involves a balance of patient life with globe salvage and ultimate visual potential (Shields and Shields 2015;

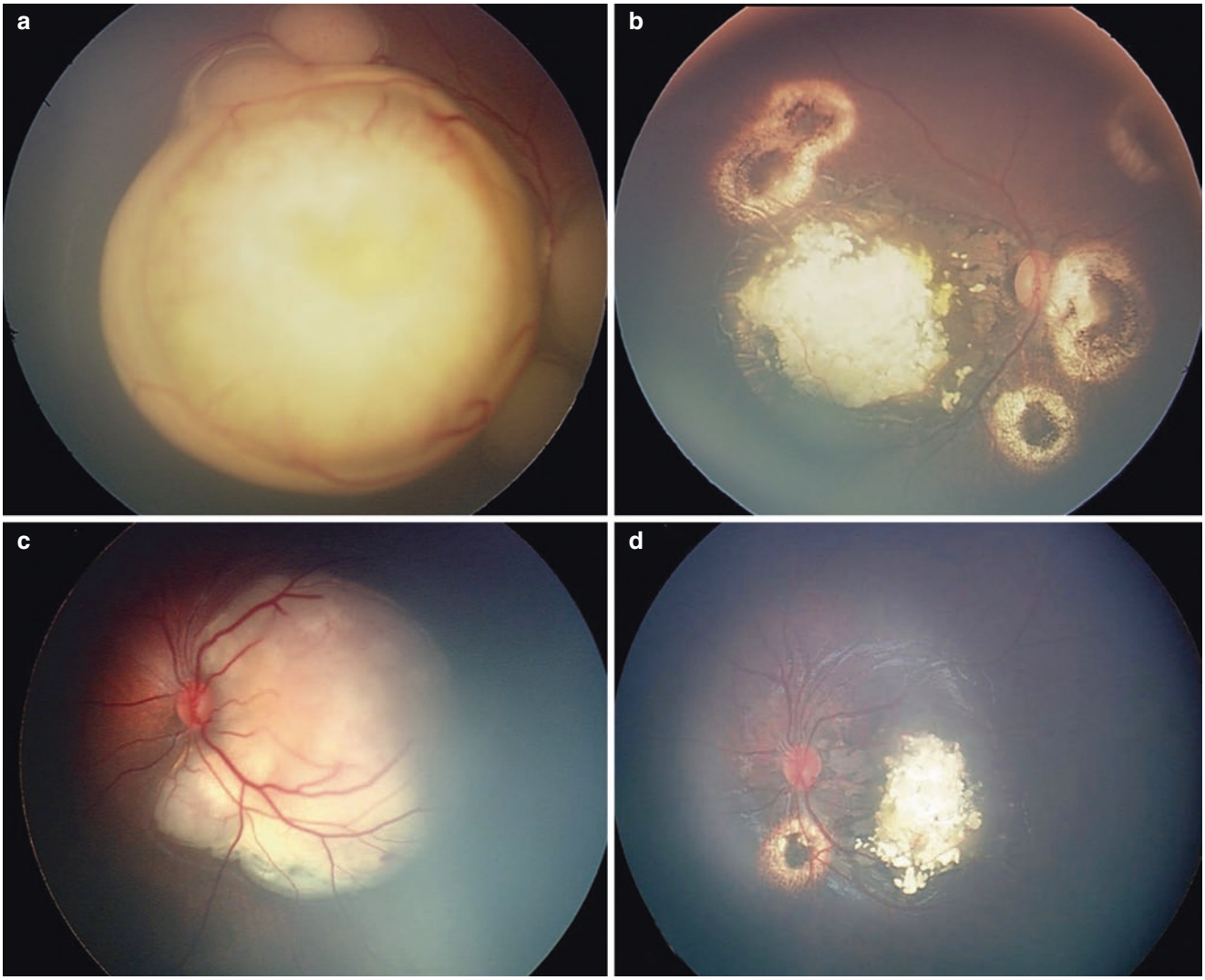

Fig. 10.5 Intravenous chemotherapy (chemoreduction) for retinoblastoma. Intravenous chemotherapy (**a**) before and (**b**) after chemoreduction for multifocal retinoblastoma. Intravenous chemotherapy (**c**) before and (**d**) after chemoreduction for macular retinoblastoma

Shields and Shields 1992; Shields and Shields 2010; Ramasubramanian and Shields 2012b; Shields et al. 2014; Shields et al. 2013a; Stathopoulos et al. 2017). There are numerous tools for management including enucleation, radiotherapy by teletherapy (external beam radiotherapy [EBRT]) or brachytherapy (plaque radiotherapy), chemotherapy using various delivery routes (intravenous, intra-arterial, intravitreal, and sub-Tenon's fascia), and chemotherapy protocols and focal treatments with laser photocoagulation, transpupillary thermotherapy, cryotherapy, and plaque radiotherapy (Shields et al. 2014; Shields et al. 2013a; Stathopoulos et al. 2017; Abramson et al. 2015) (Figs. 10.5, 10.6 and 10.7). Chemotherapy remains the most common method for conservative globe salvage (Abramson et al. 2015).

10.8 Prognosis

Children with retinoblastoma are at risk for three important life-threatening problems including metastasis from retinoblastoma, intracranial neuroblastic malignancy (trilateral retinoblastoma), and second primary cancers.

Retinoblastoma metastasis, when it occurs, generally develops within 1 year of the diagnosis of the intraocular tumor. Those at greatest risk for metastasis show features of retinoblastoma invasion beyond the lamina cribrosa in the optic nerve, in the choroid (>2 mm dimension), sclera, orbit, or anterior chamber (Honavar et al. 2002; Kaliki et al. 2011; Kaliki et al. 2013; Shields et al. 1994; Shields et al. 1993) (Figs. 10.8 and 10.9). Eyes with invasion of the optic nerve or choroid generally demonstrate large retinoblastoma over 15 mm, greatest

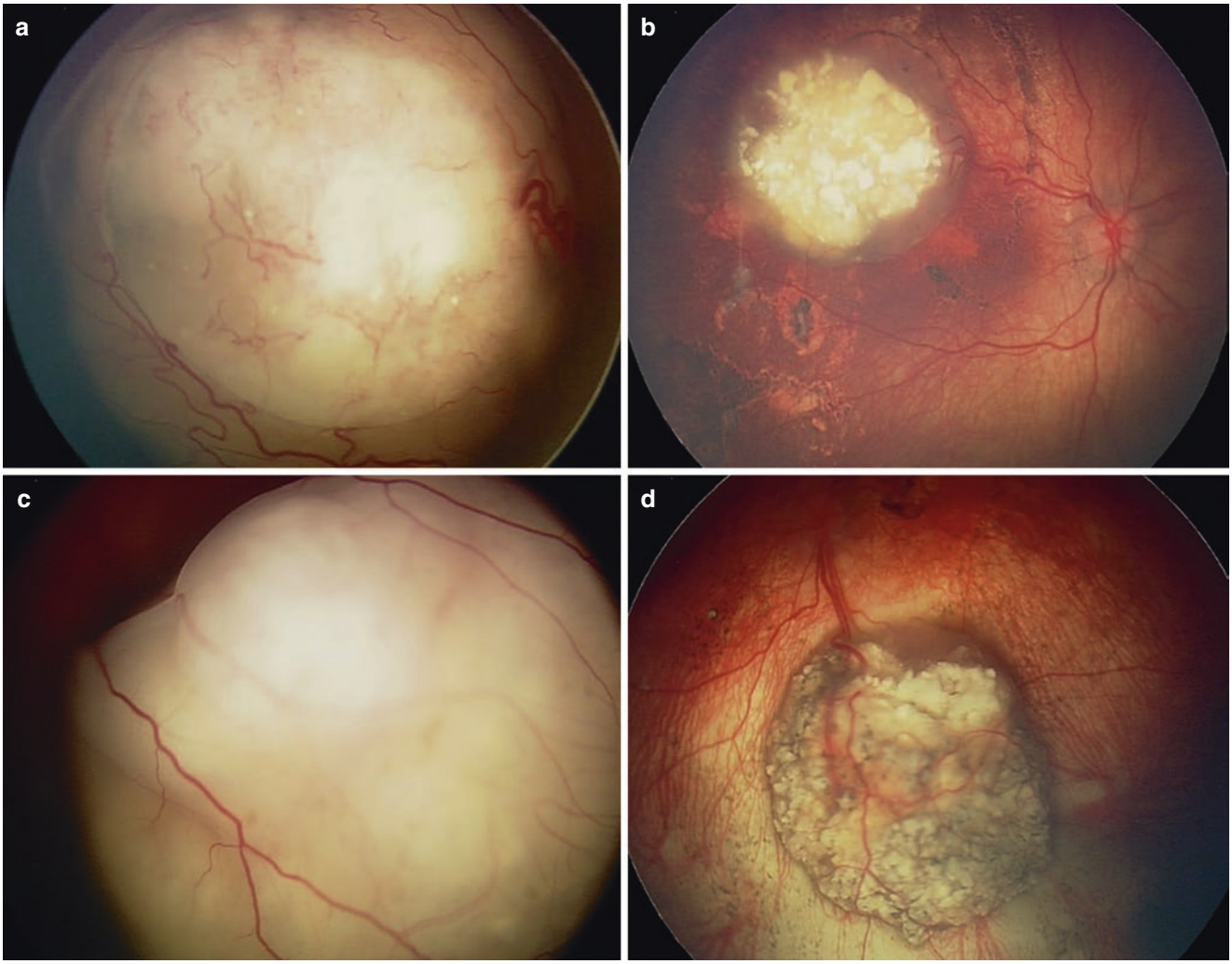

Fig. 10.6 Intra-arterial chemotherapy for retinoblastoma. Intra-arterial chemotherapy (**a**) before and (**b**) after therapy for macular retinoblastoma. Intra-arterial chemotherapy (**c**) before and (**d**) after therapy for inferior retinoblastoma

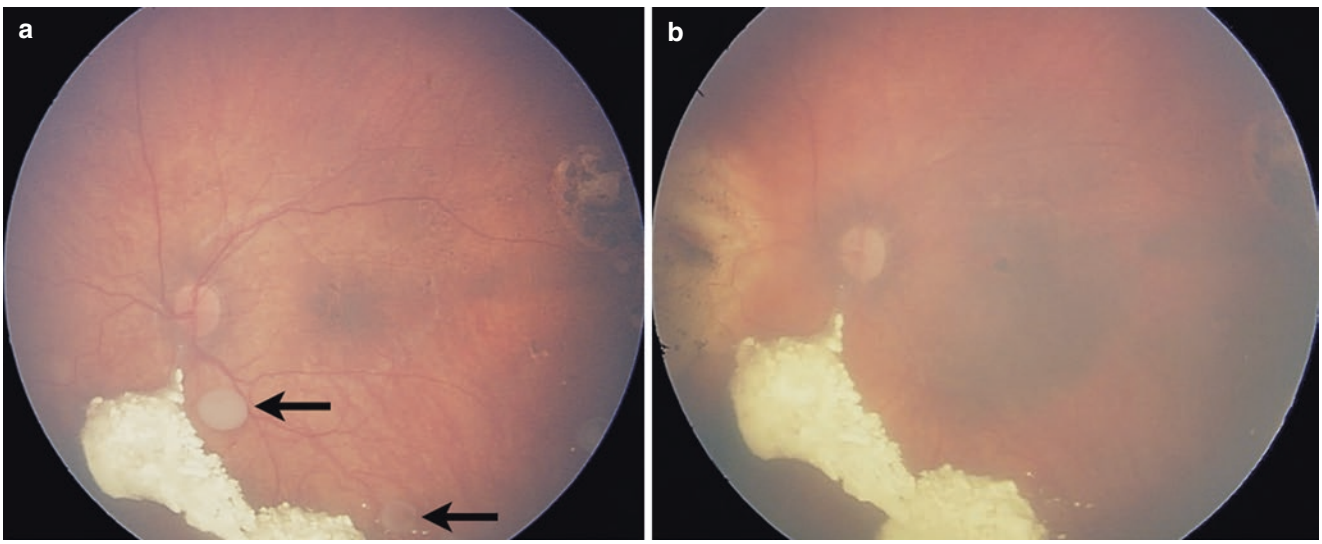

Fig. 10.7 Intravitreal chemotherapy for retinoblastoma vitreous seeds. Intravitreal chemotherapy (**a**) before and (**b**) after therapy for recurrent vitreous seeds from retinoblastoma

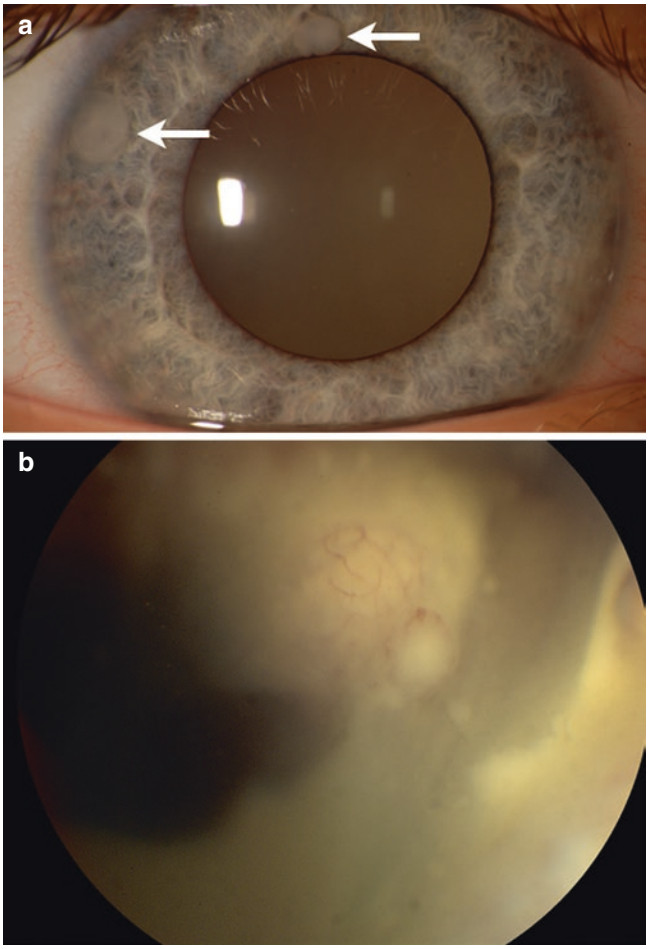

Fig. 10.8 Management of high-risk anterior chamber seeds from retinoblastoma. A young boy with visual blur was found to have (**a**) anterior chamber seeding from (**b**) massive posterior retinoblastoma with vitreous hemorrhage

dimension along with elevated intraocular pressure and total retinal detachment (Shields et al. 1994; Shields et al. 1993). Patients with invasive retinoblastoma should be treated with chemotherapy (vincristine, etoposide, and carboplatin) for 6 months to prevent metastases (Kaliki et al. 2011).

Trilateral retinoblastoma is a neuroblastic intracranial malignancy in children with germline retinoblastoma and presents as pineoblastoma or other parasellar tumors (Bader et al. 1980; Kivela 1999; Shields et al. 2001). The pineoblastoma is identical to retinoblastoma from an embryologic and pathologic standpoint. Trilateral retinoblastoma is found in 5–15% of children with germline retinoblastoma; however, the incidence is decreasing due to avoidance of radiotherapy and the use of neoadjuvant chemotherapy (Shields et al. 2001).

Genetically related second cancers are another risk in retinoblastoma survivors. Children with retinoblastoma have approximately 5% chance of developing another malignancy during the first 10 years of follow-up, 18% during 20 years, and 26% within 30 years (Abramson et al. 1979). The 30-year cumulative incidence is about 35% or even higher for those patients who received radiation therapy (external beam therapy) as compared to an incidence rate of 6% for those patients who avoided radiation. Osteogenic sarcoma of the femur is most common. Patients who survive a second tumor are at risk for a third, fourth, and even fifth nonocular tumor (Abramson et al. 2001).

10.9 Pseudoretinoblastoma

The diagnosis of retinoblastoma is based on characteristic clinical features of a yellow-white retinal mass often with surrounding subretinal fluid, subretinal seeding, and vitreous

Fig. 10.9 Management of high-risk optic nerve and brain invasion from retinoblastoma. A young boy with loss of vision was found to have possible Coats disease and later suspected to have (**a**) leukocoria from retinoblastoma with (**b**) optic nerve and (**c**) brain invasion

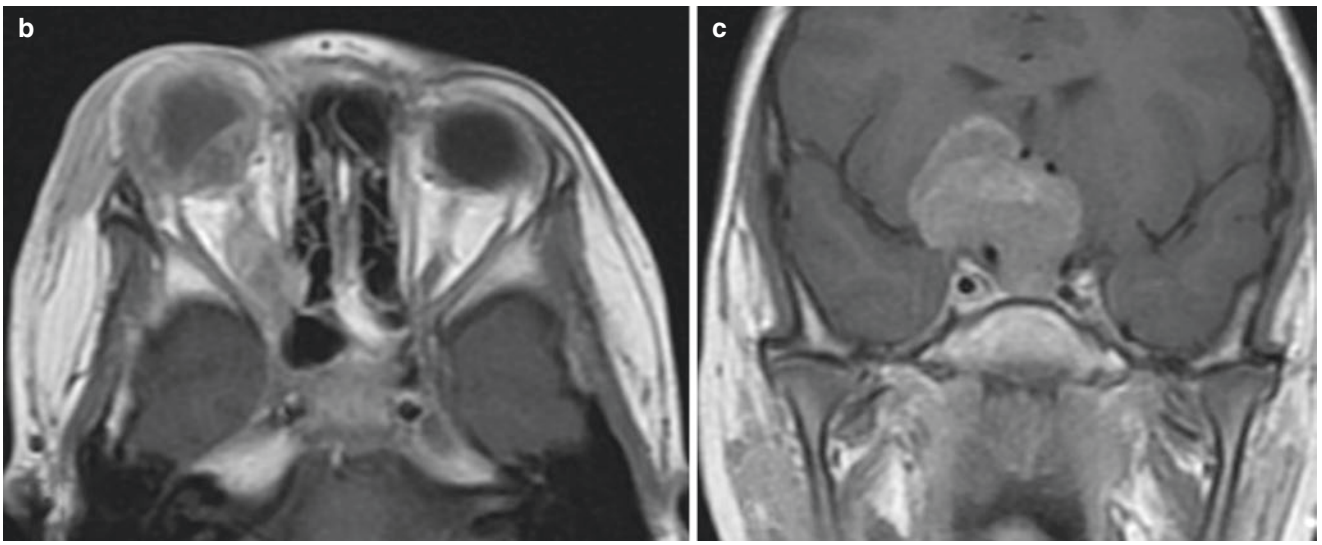

Fig. 10.9 (continued)

seeding. Ancillary testing can confirm the diagnosis. Fine-needle aspiration biopsy or open biopsy of retinoblastoma is not performed due to risk for local tumor dissemination. The diagnosis is established based on classic clinical features alone.

There are several lesions that can simulate retinoblastoma, and they are termed pseudoretinoblastoma. In a large series of 2775 eyes referred with possible retinoblastoma, retinoblastoma was confirmed in 2171 (78%) eyes and a simulating lesion (pseudoretinoblastoma) in 604 (22%) (Shields et al. 2013b) (Table 10.2). Overall, the leading pseudoretinoblastoma included Coats disease (40%), persistent fetal vasculature (PFV) (26%), and vitreous hemorrhage (5%). The pseudoretinoblastomas differed based on age at presentation. Of patients age ≤1 year, PFV (49%) was the most common pseudoretinoblastoma, whereas in children >2 years, Coats disease (60%) was most common (Tables 10.2).

10.10 Summary

In summary, the management of retinoblastoma begins with establishing the correct diagnosis and choosing appropriate therapy. There are several pediatric conditions that can simulate retinoblastoma. Chemotherapy is the most common conservative treatment for retinoblastoma using intravenous, intra-arterial, or intravitreal routes. In general, most children with bilateral retinoblastoma receive intravenous chemotherapy (chemoreduction) for ocular tumor control and preven-

Table 10.2 Pseudoretinoblastoma in 604 children

Pseudoretinoblastoma diagnosis	All ages $n = 604$ (%)
Coats disease	244 (40)
Persistent fetal vasculature PFV	158 (26)
Vitreous hemorrhage	27 (5)
Toxocariasis	22 (4)
Familial exudative vitreoretinopathy FEVR	18 (3)
Rhegmatogenous retinal detachment	18 (3)
Coloboma	17 (3)
Astrocytic hamartoma	15 (2)
Combined hamartoma	15 (2)
Endogenous endophthalmitis	10 (2)
Myelinated nerve fibers	9 (1)
Congenital cataract	8 (1)
Peripheral uveoretinitis	7 (1)
Retinopathy of prematurity	7 (1)
Non-rhegmatogenous retinal detachment	5 (<1)
Medulloepithelioma	4 (<1)
X-linked retinoschisis	4 (<1)
Vitreoretinal tuft	3 (<1)
Incontinentia pigmenti	2 (<1)
Juvenile xanthogranuloma	2 (<1)
Norrie's disease	2 (<1)
Vasoproliferative tumor	2 (<1)
Choroidal osteoma	1 (<1)
Morning glory disc anomaly	1 (<1)
Retinal capillary hemangioma	1 (<1)
Retrolental fibrosis	1 (<1)
Toxoplasmosis	1 (<1)

Adapted from Shields CL, Schoenfeld E, Kocher K, et al. Lesions simulating retinoblastoma (pseudoretinoblastoma) in 604 cases. Ophthalmology 2013;120:311-6

tion of metastasis, pinealoblastoma, and long-term second cancers. For unilateral retinoblastoma, intra-arterial chemotherapy provides excellent control with minimal systemic effect. Sub-Tenon's chemotherapy is used in conjunction with chemoreduction to enhance dose at the eye in advanced cases. Intravitreal chemotherapy is currently reserved for those eyes with recurrent vitreous seeds following incomplete control with other methods. Plaque radiotherapy is an excellent salvage method for recurrence following chemotherapy. Eyes with advanced retinoblastoma, particularly if unilateral or considered high-risk for metastasis should be managed with enucleation.

References

Abramson DH, Ronner HJ, Ellsworth RM. Second tumors in nonirradiated bilateral retinoblastoma. Am J Ophthalmol. 1979;87:624–7.

Abramson DH, Frank CM, Susman M, et al. Presenting signs of retinoblastoma. J Pediatr. 1998;132:505–8.

Abramson DH, Melson MR, Dunkel IJ, et al. Third (fourth and fifth) nonocular tumors in survivors of retinoblastoma. Ophthalmology. 2001;108:1868–76.

Abramson DH, Shields CL, Munier FL, et al. Treatment of retinoblastoma in 2015: agreement and disagreement. JAMA Ophthalmol. 2015;133:1341–7.

Ali AA, Elsheikh SM, Elhaj A, et al. Clinical presentation and outcome of retinoblastoma among children treated at the National Cancer Institute (NCI) in Gezira, Sudan: a single institution experience. Ophthalmic Genet. 2011;32:122–5.

Bader JL, Miller RW, Meadows AT, et al. Trilateral retinoblastoma. Lancet. 1980;2:582–3.

Boubacar T, Fatou S, Fousseyni T, et al. A 30-month prospective study on the treatment of retinoblastoma in the Gabriel Toure Teaching Hospital, Bamako, Mali. Br J Ophthalmol. 2010;94:467–9.

Cao C, Markovitz M, Ferenczy S, et al. Hand-held spectral-domain optical coherence tomography of small macular retinoblastoma in infants before and after chemotherapy. J Pediatr Ophthalmol Strabismus. 2014;51:230–4.

Epstein JA, Shields CL, Shields JA. Trends in the management of retinoblastoma: evaluation of 1,196 consecutive eyes during 1974 to 2001. J Pediatr Ophthalmol Strabismus. 2003;40:196–203.

Honavar SG, Singh AD, Shields CL, et al. Postenucleation adjuvant therapy in high-risk retinoblastoma. Arch Ophthalmol. 2002;120:923–31.

Kaliki S, Shields CL, Shah SU, et al. Postenucleation adjuvant chemotherapy with vincristine, etoposide, and carboplatin for the treatment of high-risk retinoblastoma. Arch Ophthalmol. 2011;129:1422–7.

Kaliki S, Shields CL, Rojanaporn D, et al. High-risk retinoblastoma based on international classification of retinoblastoma: analysis of 519 enucleated eyes. Ophthalmology. 2013;120:997–1003.

Kivela T. Trilateral retinoblastoma: a meta-analysis of hereditary retinoblastoma associated with primary ectopic intracranial retinoblastoma. J Clin Oncol. 1999;17:1829–37.

Kivela T. The epidemiological challenge of the most frequent eye cancer: retinoblastoma, an issue of birth and death. Br J Ophthalmol. 2009;93:1129–31.

Linn Murphree A. Intraocular retinoblastoma: the case for a new group classification. Ophthalmol Clin N Am. 2005;18:41–53.

Park K, Sioufi K, Shields CL. Clinically invisible retinoblastoma recurrence in an infant. Retin Cases Brief Rep. 2017. https://doi.org/10.1097/icb.0000000000000555.

Ramasubramanian A, Shields CL. Epidemiology and magnitude of the problem. Epidemiology and magnitude of the problem. Retinoblastoma. New Delhi, India: Jaypee Brothers Medical Publishers; 2012a.

Ramasubramanian A, Shields CL. Staging and treatment strategies. In: Epidemiology and magnitude of the problem. Retinoblastoma. New Delhi, India: Jaypee Brothers Medical Publishers; 2012b.

Saktanasate J, Vongkulsiri S, Khoo CT. Invisible retinoblastoma. JAMA Ophthalmol. 2015;133(7):e151123. https://doi.org/10.1001/jamaophthalmol.2015.1123.

Shields CL, Shields JA. Basic understanding of current classification and management of retinoblastoma. Curr Opin Ophthalmol. 2006;17(3):228–34.

Shields CL, Shields JA. Retinoblastoma management: advances in enucleation, intravenous chemoreduction, and intra-arterial chemotherapy. Curr Opin Ophthalmol. 2010;21:203–12.

Shields JA, Shields CL. Intraocular tumors: an atlas and textbook. 3rd ed. Philadelphia: Wolters Kluwer; 2015.

Shields CL, Shields JA, Baez KA, et al. Choroidal invasion of retinoblastoma: metastatic potential and clinical risk factors. Br J Ophthalmol. 1993;77:544–8.

Shields CL, Shields JA, Baez K, et al. Optic nerve invasion of retinoblastoma. Metastatic potential and clinical risk factors. Cancer. 1994;73:692–8.

Shields CL, Meadows AT, Shields JA, et al. Chemoreduction for retinoblastoma may prevent intracranial neuroblastic malignancy (trilateral retinoblastoma). Arch Ophthalmol. 2001;119:1269–72.

Shields CL, Mashayekhi A, Demirci H, et al. Practical approach to management of retinoblastoma. Arch Ophthalmol. 2004;122(5):729–35. https://doi.org/10.1001/archopht.122.5.729.

Shields CL, Ghassemi F, Tuncer S, et al. Clinical spectrum of diffuse infiltrating retinoblastoma in 34 consecutive eyes. Ophthalmology. 2008;115:2253–8.

Shields CL, Fulco EM, Arias JD, et al. Retinoblastoma frontiers with intravenous, intra-arterial, periocular, and intravitreal chemotherapy. Eye (Lond). 2013a;27:253–64.

Shields CL, Schoenberg E, Kocher K, et al. Lesions simulating retinoblastoma (pseudoretinoblastoma) in 604 cases: results based on age at presentation. Ophthalmology. 2013b;120:311–6.

Shields CL, Lally SE, Leahey AM, et al. Targeted retinoblastoma management: when to use intravenous, intra-arterial, periocular, and intravitreal chemotherapy. Curr Opin Ophthalmol. 2014;25:374–85.

Shields JA, Shields CL. A text and Atlas Philadelphia. In: In intraocular tumors. Philadelphia: Wolters Kluwer; 1992.

Stathopoulos C, Say EAT, Shields CL. Intra-arterial and intravitreal chemotherapy for retinoblastoma. Curr Ophthalmol Rep. 2017;5:73–84.

Tumors and Related Lesions of the Retinal Pigmented Epithelium

11

Carol L. Shields and Jerry A. Shields

11.1 Introduction

There are a variety of pigment epithelial tumors, including benign and malignant types. Some are considered congenital such as congenital hypertrophy of the retinal pigment epithelium (CHRPE) (solitary and multifocal), congenital simple hamartoma, and torpedo maculopathy. Some are presumed acquired such as adenoma and adenoma of the pigment epithelium. These lesions can clinically simulate malignant tumors, particularly malignant melanoma of the iris, ciliary body, and choroid (Shields and Shields 2015; Shields and Shields 2017a, b, c).

True tumors that arise in the pigmented epithelium have been called adenomas and adenocarcinomas, depending on whether they have benign or malignant histopathologic features. Because they arise from neuroepithelium and do not usually arise from glandular structures, some consider it more appropriate to use the terms benign and malignant epithelioma, rather than adenoma or adenocarcinoma (Shields and Shields 2017a). However the latter are well established and will be used here.

11.2 Solitary Congenital Hypertrophy of the Retinal Pigment Epithelium (CHRPE)

11.2.1 Introduction

Solitary CHRPE is a well-known, common fundus condition believed to be congenital, but with median age at diagnosis at 45 years, with late diagnosis probably related to the peripheral, asymptomatic location in a somewhat hidden location (Shields et al. 2003a; Gass 1989; Chamot et al. 1993). CHRPE is usually a solitary lesion with no predilection for race.

The term CHRPE has also been applied to a different multifocal fundus condition, namely, pigmented ocular fundus lesions (POFL) that are associated with familial adenomatous polyposis (FAP) and colon cancer (Traboulsi 2005; Traboulsi et al. 1987). However, there are important differences in CHRPE and POFL that should be understood. Classic solitary CHRPE is round, with lacunae and not associated with FAP (Shields et al. 1992). POFL (described later in this chapter under Pigmented Ocular Fundus Lesions) demonstrate an ellipsoid configuration, multifocality, and "fish-tail" appearance, suggestive of remote FAP.

11.2.2 Clinical Features

Shields et al. published a review of 330 cases of solitary CHRPE that provided information regarding clinical features of this condition, including the appearance as a well-demarcated flat fundus mass ranging from a black homogeneous lesion (88%), usually with typical depigmented lacunae, to a completely depigmented lesion (12%) (Shields et al. 2003a) (Figs. 11.1, 11.2, 11.3, and 11.4). Most CHRPE are located in the midperipheral or peripheral fundus. Only 2% are found in the macular or peripapillary region. The median basal diameter is 4.5 mm. Well-defined depigmented foci, called lacunae, are present in 43% of pigmented CHRPE. The lacunae can enlarge slowly over long period of time (Fig. 11.4). Most solitary CHRPE (74–83%) show gradual increase in diameter over 10–20-year follow-up (Shields et al. 2003a; Chamot et al. 1993).

Rarely (<2%) CHRPE can spawn a nodular growth pattern with transformation into RPE adenoma or adenocarcinoma (Shields et al. 2000). The nodule acquires a retinal feeding artery and draining vein and produces yellow intraretinal exudation and occasional exudative retinal detachment. The mass can represent either a benign or malignant process.

C. L. Shields (✉) · J. A. Shields (✉)
Ocular Oncology Service, Wills Eye Hospital, Philadelphia, PA, USA

Department of Ophthalmology, Thomas Jefferson Unversity, Philadelphia, PA, USA

D. Rojanaporn (ed.), *Ocular Oncology*, https://doi.org/10.1007/978-981-13-2336-2_11

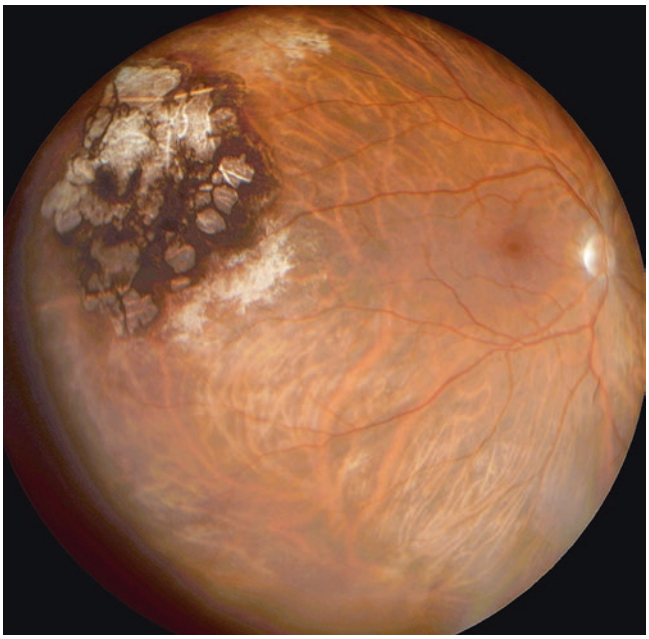

Fig. 11.1 Congenital hypertrophy of the retinal pigment epithelium (CHRPE) features. Wide-angle view documenting CHRPE with numerous intrinsic lacunae

11.2.3 Diagnosis

Fluorescein angiography (FA) and indocyanine green angiography (ICGA) show blockage of fluorescence/cyanescence throughout the angiogram. Transmission of choroidal fluorescence through the lacunae can be noted. Ultrasonography shows a flat, echodense lesion of <1 mm thickness. Visual field results typically reveal a mild relative or absolute scotoma corresponding to the lesion. Optical coherence tomography (OCT) shows overlying outer retinal thinning, abrupt loss of photoreceptors, slightly thickened RPE, and relative shadowing of underlying choroid (Fung et al. 2014; Shields et al. 2006; Shields et al. 2014) (Fig. 11.2). Fundus autofluorescence (FAF) shows absolute lack of lipofuscin with a dark appearance (Shields et al. 2007; Almeida et al. 2013) (Figs. 11.2 and 11.3).

11.2.4 Management

The management for solitary CHRPE is a simple periodic observation. If a small nodular growth should evolve, it can often be observed for a period of time because progression is

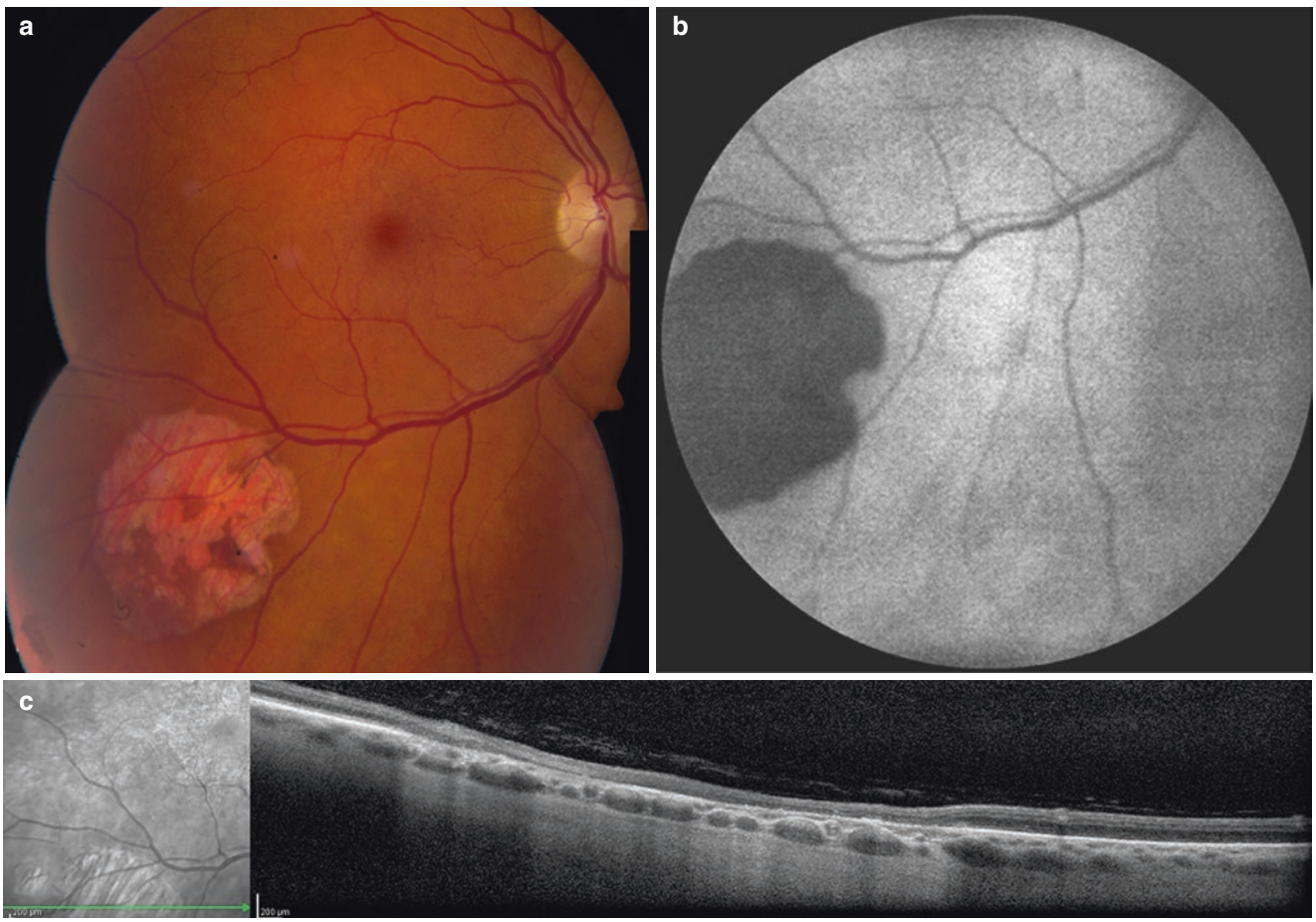

Fig. 11.2 Congenital hypertrophy of the retinal pigment epithelium (CHRPE) imaging. (**a**) CHRPE with nearly complete lacunae, (**b**) showing abrupt hypoautofluorescence, and (**c**) flat surface with slight retinal thinning and transmission of light through the lesion

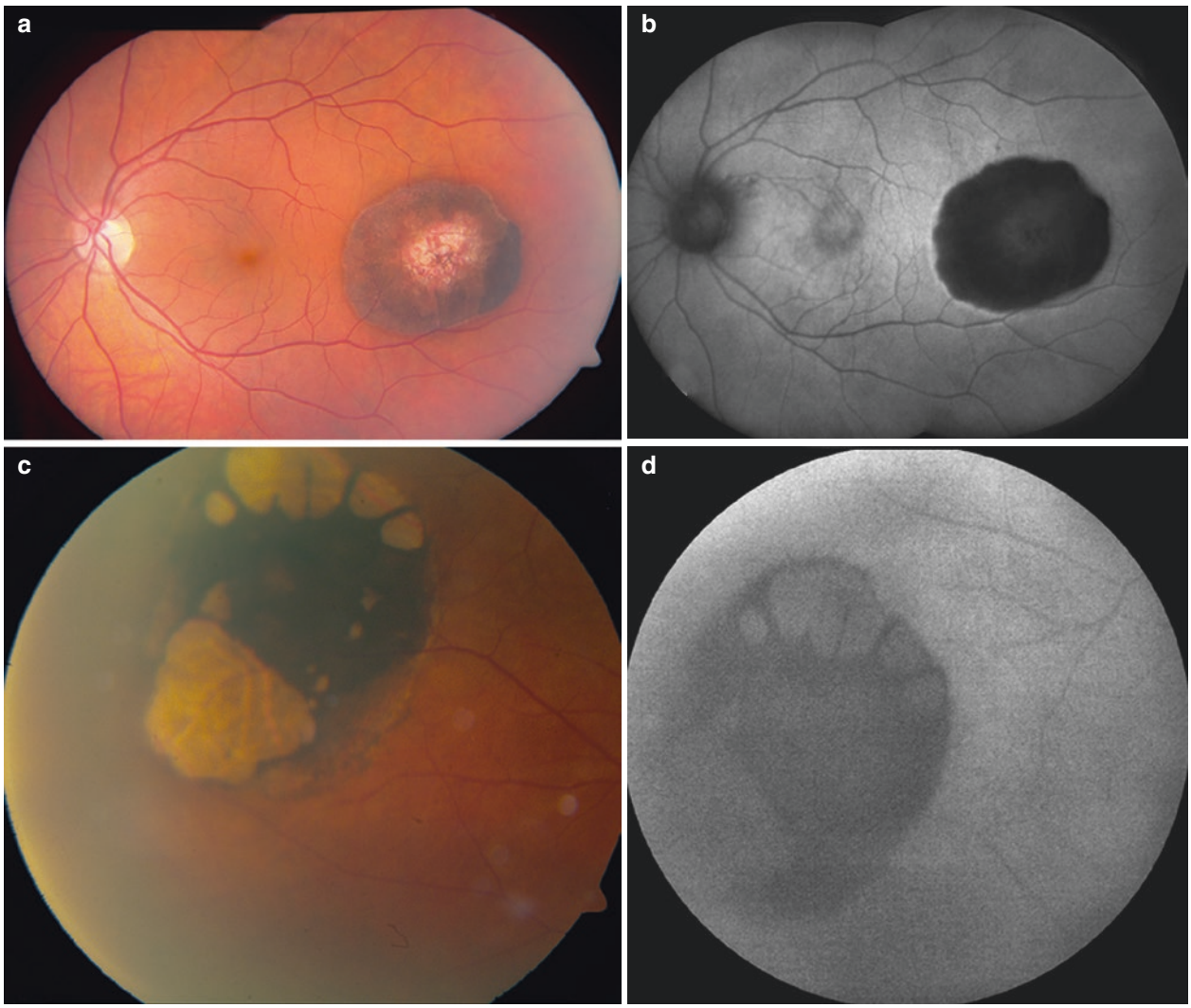

Fig. 11.3 Congenital hypertrophy of the retinal pigment epithelium (CHRPE) autofluorescence. (**a**) CHRPE with central lacunae (**b**) showing abrupt hypoautofluorescence and surround ring of hyperautofluorescence. (**c**) CHRPE with prominent lacunae (**d**) showing abrupt hypoautofluorescence nearly isoautofluorescence from unmasking of the scleral autofluorescence

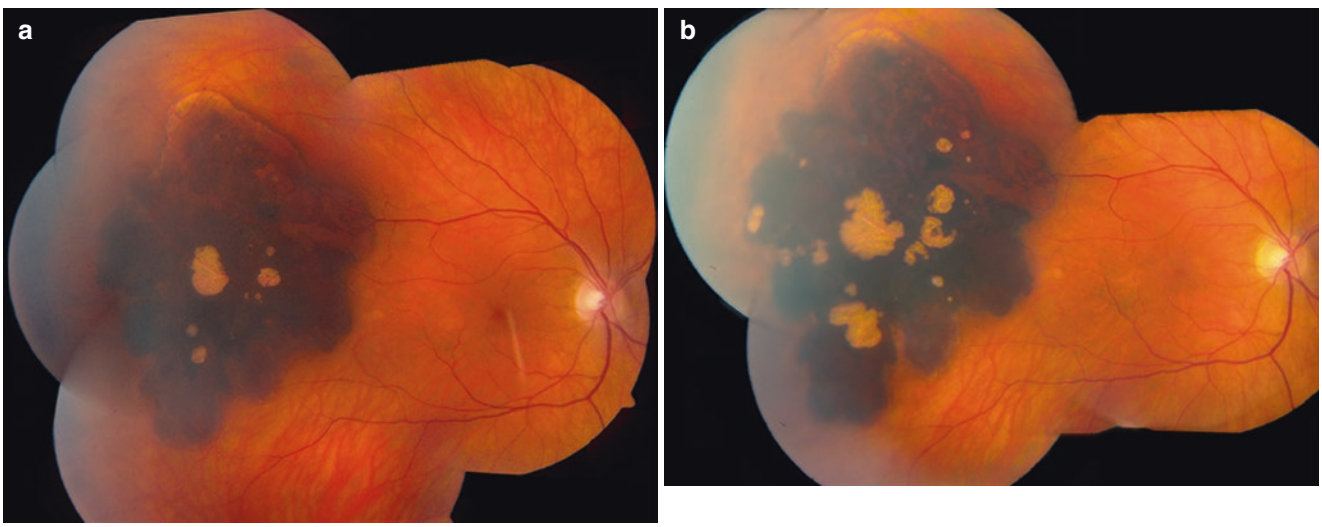

Fig. 11.4 Congenital hypertrophy of the retinal pigment epithelium (CHRPE) flat enlargement. (**a**) CHRPE at initial examination and (**b**) several years later with obvious enlargement inferiorly and temporally

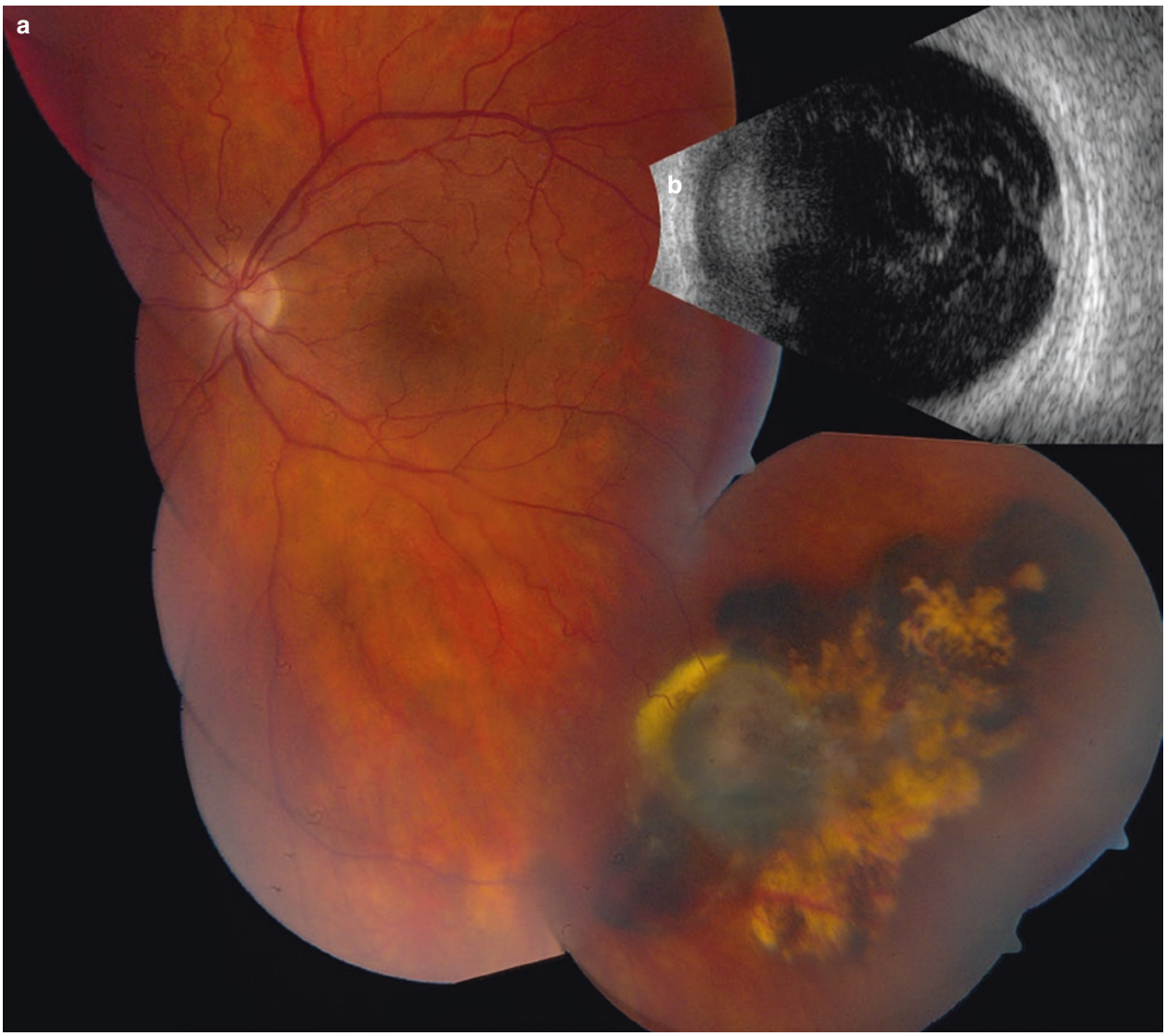

Fig. 11.5 Congenital hypertrophy of the retinal pigment epithelium (CHRPE) growth to adenoma. (**a**) CHRPE base and nearly central elevated nodule, surrounded by exudation, and classified as adenoma and (**b**) confirmed as echodense on ultrasonography

very slow, and this does not usually affect the patient's visual acuity (Fig. 11.5). If the nodule produces exudation or subretinal fluid, laser photocoagulation, thermotherapy, photodynamic therapy, or cryotherapy can be considered. If the nodule produces epiretinal membrane in the macular region, pars plana vitrectomy and membrane peeling can be considered.

11.3 Multifocal Congenital Hypertrophy of the Retinal Pigment Epithelium (Congenital Grouped Pigmentation: Bear Tracks)

11.3.1 Introduction

The multifocal variant of CHRPE is a nonhereditary, sporadic condition. There are usually no related ocular or systemic abnormalities.

11.3.2 Clinical Features

Multifocal CHRPE is characterized by numerous well-delineated, flat, slate-gray lesions in a sector distribution or involving the entire fundus (Fig. 11.6). Each group consists of from 3 to 30 individual round or oval pigmented lesions that vary from 0.1 to 3 mm in diameter, with smaller lesions posteriorly and larger lesions more peripherally (Shields and Shields 2015; Shields and Shields 2017a, c). Each lesion is similar in appearance to solitary CHRPE but generally smaller and without lacunae. Sometimes all lesions are nonpigmented, in which they have been called "polar bear tracks." These lesions remain stable.

Multifocal CHRPE, not associated with FAP (Shields et al. 1992), can be confused with POFL, a condition associated with FAP, Gardner syndrome, and familial colon cancer. Multifocal CHRPE has a regular distribution with round homogenous appearance, whereas POFL has a more haphaz-

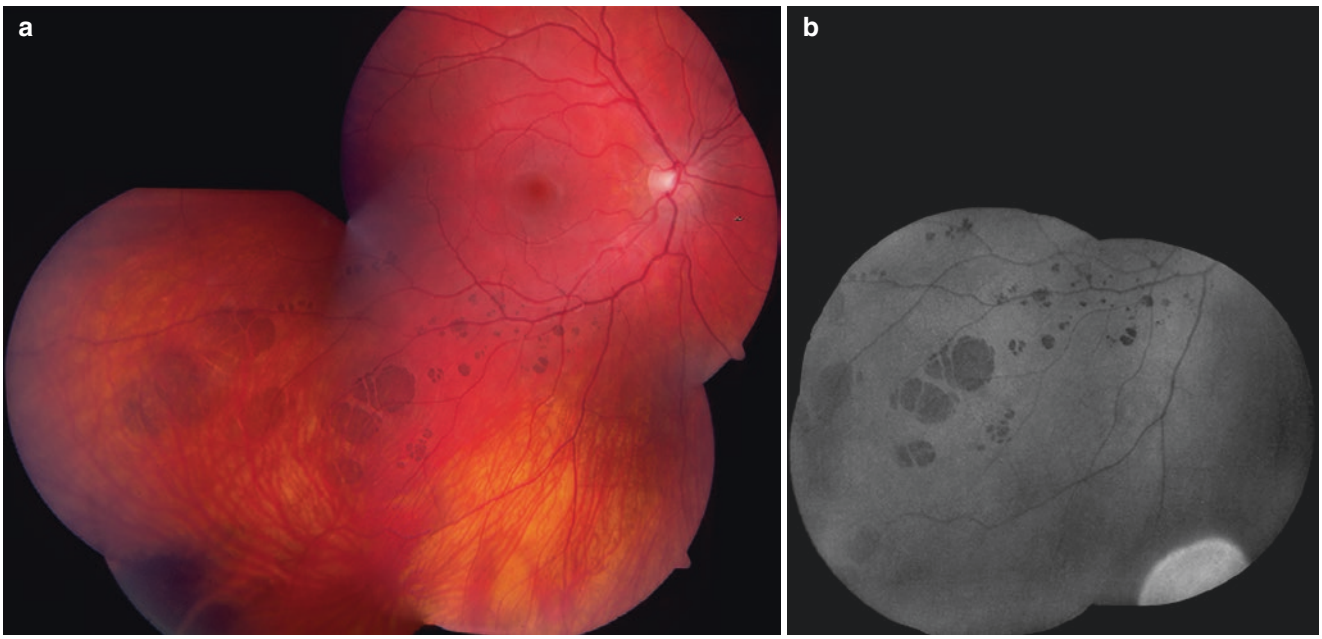

Fig. 11.6 Congenital hypertrophy of the retinal pigment epithelium (CHRPE) multifocal type. (**a**) Multifocal CHRPE in sectoral distribution and (**b**) remaining hypoautofluorescent on imaging

ard distribution, with irregular borders, and "fish-tail" depigmentation.

11.3.3 Diagnostic Approaches

FA demonstrates hypofluorescence of each lesion, OCT shows a flat lesion with focal outer retinal atrophy and photoreceptor loss, and FAF documents the lesions with hypoautofluorescent.

11.3.4 Management

Multifocal CHRPE requires no treatment and can be observed as part of routine ocular examination.

11.4 Pigmented Ocular Fundus Lesions Associated with Familial Adenomatous Polyposis and Gardner Syndrome

11.4.1 Introduction

Pigmented ocular fundus lesions (POFL) have a strong association with FAP, an autosomal dominant condition in which nearly 100% of patients develop colon cancer at a young age (Traboulsi 2005; Traboulsi et al. 1987). About 70% of patients with FAP have these characteristic RPE lesions, and this serves as a benign marker for a potentially life-threatening familial colon cancer.

11.4.2 Clinical features

POFL demonstrate characteristic features with irregular margins, sometimes pinpoint in size and sometimes larger, randomly dispersed in the fundus, and with an irregular depigmented tail, forming a "fish-tail," "comma," or "comet" configuration (Fig. 11.7). It has been proposed that the presence of four or more such lesions is diagnostic of FAP, but some patients have many more, even hundreds of lesions bilaterally.

11.4.3 Diagnosis

These lesions are best imaged with FA that demonstrates blockage from pigment. Some lesions are so tiny that they are only visible on FA.

11.4.4 Management

The management of POFL is a periodic observation as the eye lesions remain stable. However, the patient should be examined by periodic colonoscopy for colonic polyps of FAP and warned about the high risk for colon cancer. Genetic evaluation for the adenomatous polyposis coli (APC) gene is warranted.

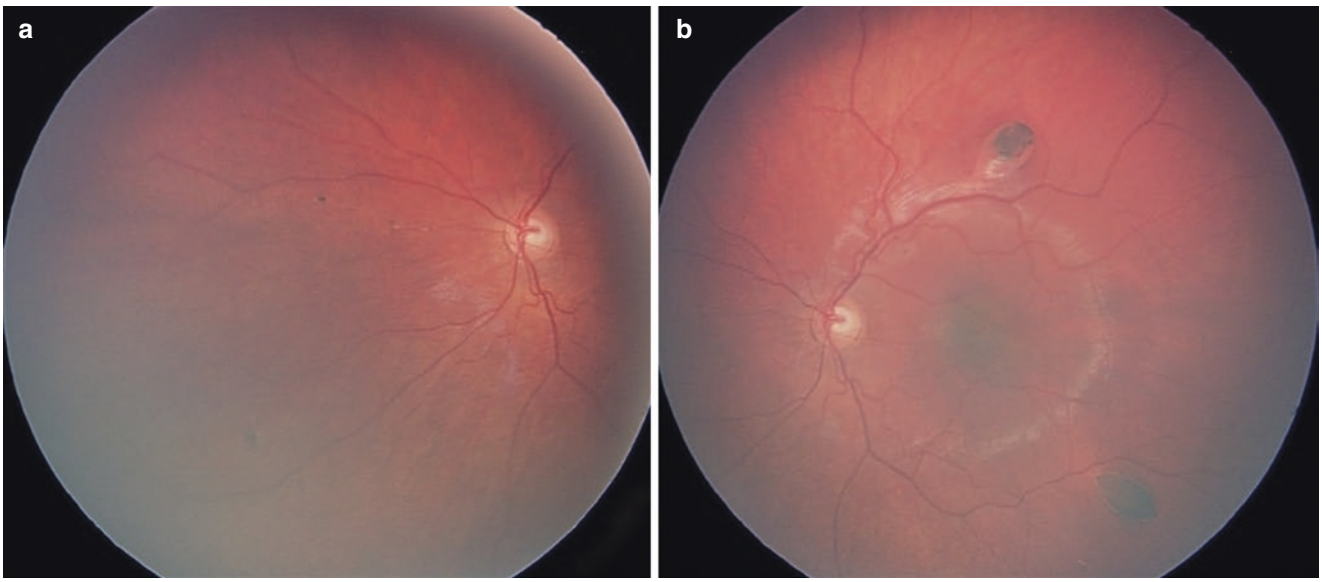

Fig. 11.7 Pigmented ocular fundus lesions (POFL) associated with familial adenomatous polyposis. (**a**) POFL ranging from tiny black dots to (**b**) prominent black spots at the level of the RPE and with fish-tail configuration in a child with positive adenomatous polyposis coli (APC) gene testing

11.5 Combined Hamartoma of the Retina and Retinal Pigment Epithelium

11.5.1 Introduction

Combined hamartoma of the retina and retinal pigment epithelium is a fundus lesion that has a fairly characteristic feature that can sometimes show variability (Gass 1973; Schachat et al. 1984; Shields et al. 2008; Arepalli et al. 2014; Shields et al. 2005a; Stallman 2002; Mason 3rd 2002; Cohn et al. 2009). This mass is believed to be congenital and nonhereditary, but there are a few documented cases of acquired lesions. Patients with this tumor should be evaluated for neurofibromatosis type 2, Gorlin-Goltz syndrome, Potter's syndrome, juvenile nasopharyngeal angiofibroma, the branchio-oculofacial syndrome, and others (Shields et al. 2008).

11.5.2 Clinical Features

The characteristic fundus finding of combined hamartoma is an ill-defined gray-green retinal mass with prominent intrinsic tortuous vessels that straighten and stretch more peripherally, as if the retina is drawn into posterior traction (Figs. 11.8 and 11.9). Glial tissue on the surface of the lesion is noted. Most tumors are located on or adjacent to the optic disc, but they can be found in the periphery.

Combined hamartoma can vary widely in size, ranging from a small lesion 1 mm in diameter to a mass lesion >10 mm in diameter. Visual acuity is variable, depending on the tumor size and location and the amount of retinal traction. In one analysis of 77 eyes, the mean initial Snellen visual acuity for macular versus extramacular tumors was 20/320 versus 20/80 and at 4 years follow-up was 20/800 versus 20/125, demonstrating the profound effect this tumor has on vision (Shields et al. 2008). Most patients that come to clinical attention base on poor visual acuity on school examination. Amblyopia can result from tumors in the macular area as well as foveal ectopia from traction.

In either location, the abnormal tortuous retinal blood vessels show characteristic straightening as they pass anterior to the lesion toward the peripheral fundus. A peripheral lesion can cause retinal dragging, creating a "dragged disc" appearance. Combined hamartoma can be associated with peripheral retinal ischemia and secondary peripheral neovascularization. Combined hamartoma is generally stable, but glial proliferation can lead to retinal traction. Other complications, such as retinal exudation and vitreous hemorrhage, can occur.

11.5.3 Diagnosis

On FA, combined hamartoma demonstrates markedly abnormal retinal blood vessels within the mass and gradual late staining (Fig. 11.9). OCT shows an irregular lesion with vitreoretinal traction into a "sawtooth" or "folded" pattern that

Fig. 11.8 Combined hamartoma of the retina and retinal pigment epithelium with posterior involvement. (**a**) White epiretinal membrane with dragging of retinal vessels toward the fovea in a child, showing (**b**) prominent retinal folding and epiretinal thickening on optical coherence tomography

replaces full-thickness retinal tissue (Arepalli et al. 2014; Shields et al. 2005a) (Fig. 11.8). OCTA demonstrates the corkscrew vessels with peripheral straightening (Sridhar et al. 2016).

11.5.4 Management

Most eyes with combined hamartoma have chronic retinal damage, and therapy is not of benefit. Amblyopia patching therapy can be helpful in some young children. Vitrectomy and membrane peeling has been employed in cases with vitreous hemorrhage and preretinal gliosis but is generally not useful if the lesion involves full thickness of the retina by OCT (Stallman 2002; Mason 3rd 2002; Cohn et al. 2009). OCT is important in judging visual potential.

11.6 Congenital Simple Hamartoma of the Retinal Pigment Epithelium

11.6.1 Introduction

Congenital simple hamartoma of the retinal pigment epithelium (RPE) is a congenital small, darkly pigmented, round mass, composed of RPE cells, and located in the perifoveal region. It is presumably composed exclusively of RPE cells and hence is classified as a simple rather than complex or combined hamartoma.

11.6.2 Clinical Features

Congenital simple hamartoma of the RPE appears clinically as a distinct solitary nodule that protrudes through the sen-

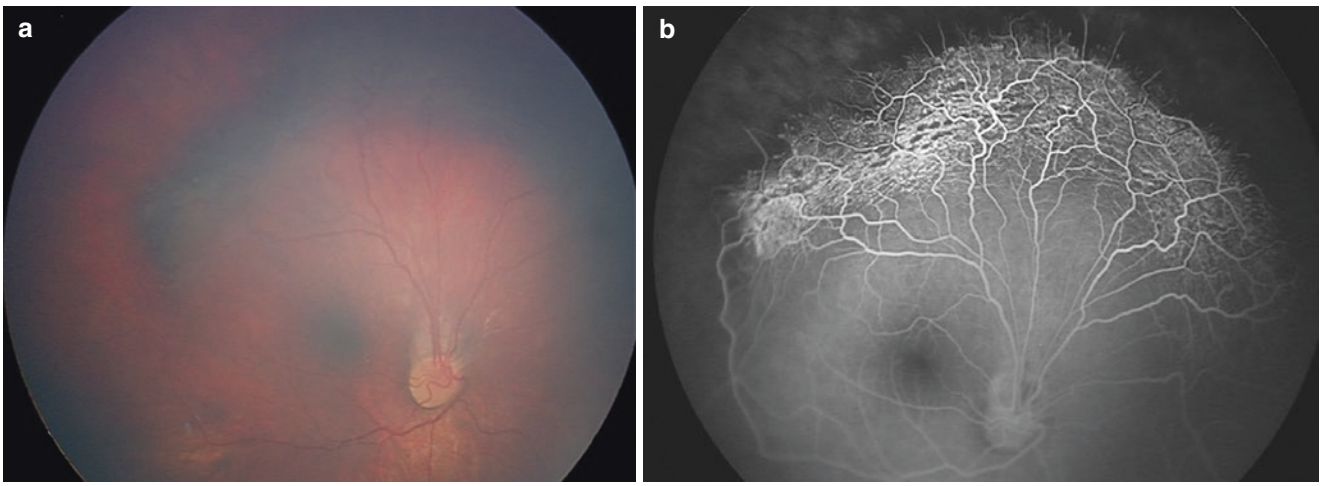

Fig. 11.9 Combined hamartoma of the retina and retinal pigment epithelium with peripheral involvement. (**a**) Gray epiretinal membrane with dragging of retinal vessels toward the superior region in a child and fluorescein angiography (**b**) documenting the retinal vessels with corkscrew contraction and peripheral retinal nonperfusion and straightened vessel

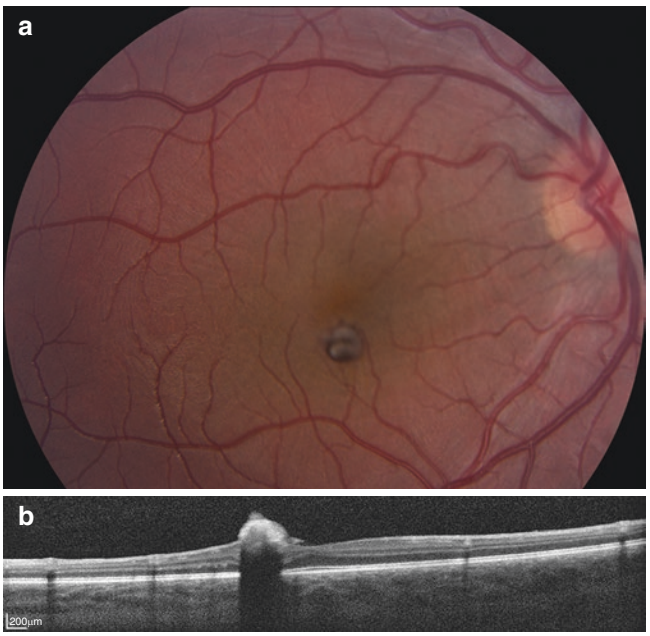

Fig. 11.10 Congenital simple hamartoma of the retinal pigment epithelium (RPE)—pigmented type. (**a**) Central, parafoveolar, pigmented congenital simple hamartoma of the RPE showing (**b**) classic elevation with abrupt shadowing on optical coherence tomography, immediately adjacent to the foveola

sory retina, sometimes into the vitreous cavity. Most reported cases have been <1 mm in diameter and approximately 1–2 mm in thickness, with tumor location within the macular region and often adjacent to the foveola (Figs. 11.10 and 11.11). It is possible that similar lesions could exist in the peripheral fundus but are not recognized or appreciated clinically. Based on a clinical series of five cases, associated features include minimally dilated retinal feeding artery and draining retinal vein (100%), adjacent mild retinal traction (80%), yellow retinal exudation (20%), and vitreous pigmented cells (20%) (Shields et al. 2003b).

11.6.3 Diagnosis

By FA, this congenital simple hamartoma is generally hypofluorescent throughout all phases. On ultrasonography, it appears as a tiny echodense perifoveal lesion. The best imaging modality is OCT as this mass shows characteristic features of abruptly elevated solid mass within the retina and extending as a dome into the vitreous cavity with complete deep optical shadowing (Shields et al. 2004).

11.6.4 Management

The management of congenital simple hamartoma of the RPE is periodic observation. Most lesions have remained stable.

11.7 Torpedo Maculopathy

11.7.1 Introduction

Torpedo maculopathy is a presumed congenital condition affecting the eye at the level of the retinal pigment epithelium with focal, well-circumscribed atrophy or hyperplasia in a torpedo-like configuration, with the head of the torpedo facing the foveola. This lesion tends to occur in the temporal macular region, adjacent to the foveola.

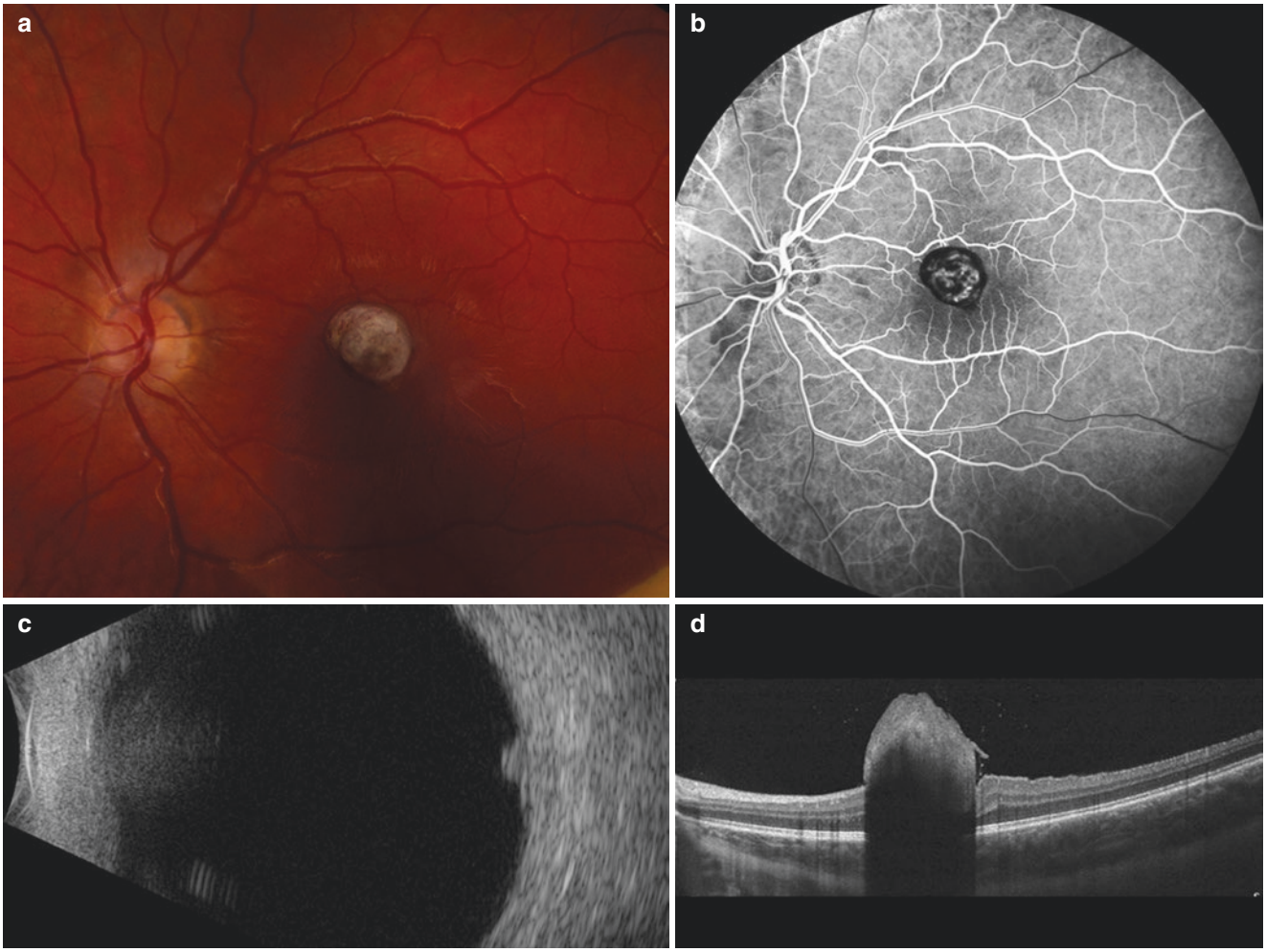

Fig. 11.11 Congenital simple hamartoma of the retinal pigment epithelium (RPE)—nonpigmented type. (**a**) Central, parafoveolar, minimally pigmented congenital simple hamartoma of the RPE showing (**b**) minimal fluorescence on angiography, (**c**) dome-shaped echodensity on ultrasonography, and (**d**) classic elevation with abrupt shadowing on optical coherence tomography, involving the foveola

11.7.2 Clinical Features

This unusual lesion is characterized by a torpedo-shaped focal loss of RPE and choroid in the temporal macular region, pointing toward the foveola (Fig. 11.12). Speculation on the pathogenesis related to focal in utero ocular developmental defect at the time of the fetal bulge (Roseman and Gass 1992; Shields et al. 2010; Golchet et al. 2010).

11.7.3 Diagnosis

By FA, the lesion appears hypofluorescent due to lack of choroidal flow. By ultrasonography, the lesion is flat. By OCT, this flat lesion demonstrates loss of outer retinal layers and RPE, often with a thin cleft under the retina draped over the defect (Golchet et al. 2010). By FAF, the mass is dark, implying loss of RPE cells.

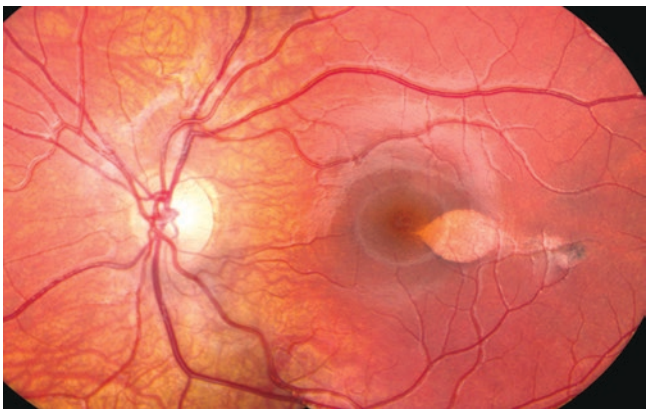

Fig. 11.12 Torpedo maculopathy showing abrupt depigmented torpedo-shaped retinal pigment epithelial abnormality heading toward the foveola and with depigmented tail

11.7.4 Management

There are no associated syndromes with this condition and the management is observation. There have been reports of congenital Zika virus infection that can produce torpedo-like scars in the macular region, so patients should be evaluated for that consideration. (de Paula Freitas et al. 2016)

11.8 Adenoma/Adenocarcinoma (Benign/Malignant Epithelioma) of the Iris Pigment Epithelium (IPE)

11.8.1 Introduction

Adenoma/adenocarcinoma of the iris pigment epithelium is rare. In some publications, the terms benign/malignant epithelioma is suggested to be more descriptive of these tumors as they arise from neuroepithelium, and there is no glandular structure. In a large single-center survey of 3680 iris tumors from an ocular oncology center, Shields et al. found only 35 (1%) were solid IPE tumors including adenoma (n = 31), adenocarcinoma (n = 1), and secondary invasion from medulloepithelioma from nonpigmented ciliary epithelium (n = 3) (Shields et al. 2012).

11.8.2 Clinical Features

Adenoma of the IPE is found on the posterior surface of the iris and typically located in the peripheral region, near the iridociliary junction, although it can originate near the pupillary margin. This mass is solitary, unilateral, abruptly elevated, and dark gray to black in color, and rarely yellow white in color (Fig. 11.13). The tumor surface is usually smooth and intrinsic vessels not seen. Adenoma can efface the iris stroma and erode through to the front surface of the iris, but, unlike melanoma, it does not originate in the iris stroma.

The main tumors in the differential diagnosis of adenoma of the IPE include iris nevus, iris or ciliary body melanoma, and cyst of the IPE (Shields et al. 2012; Shields et al. 1985). The uniform black color, site of origin behind the iris, and abruptly elevated margin should suggest the correct diagnosis. Rarely, malignant adenocarcinoma of the IPE is found, based on histopathologic features, and can risk local invasiveness but with minimal tendency for metastasis.

11.8.3 Diagnosis

Occasionally, it can be difficult to differentiate adenoma of the IPE from iris melanoma, nevus, melanocytoma, and IPE cyst, but the classic clinical features should suggest the diagnosis. In contrast to IPE cyst, adenoma blocks light with transillumination. Ultrasound biomicroscopy (UBM) documents an echogenic mass arising from the IPE and without cyst formation (Fig. 11.13). However, adenoma of the IPE can sometimes show tiny intrinsic cysts, best seen on anterior segment OCT and ultrasound biomicroscopy (UBM).

11.8.4 Management

Adenoma of the IPE has an indolent clinical course, so if asymptomatic, observation is advised. Those with documented growth can eventually require surgical removal, by iridectomy or iridocyclectomy. In a series of 20 cases of IPE

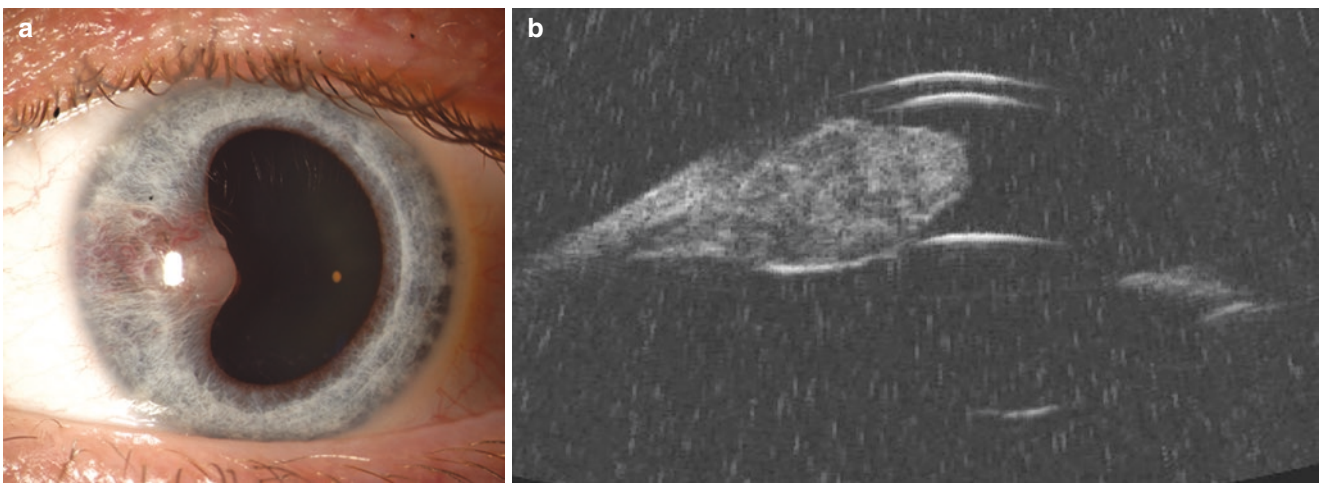

Fig. 11.13 Iris pigment epithelial adenoma. (**a**) Minimally pigmented solid vascular mass arising on the posterior iris surface, eroding through the iris stroma and (**b**) confirmed on ultrasound biomicroscopy as an echodense mass. Histopathology confirmed iris pigment epithelial adenoma

solid tumors, Shields et al. found that the tumor required iridocyclectomy in 2 and observation in 18, with the latter remaining stable on follow-up from 6 months to 9 years (Shields et al. 1999c).

11.9 Adenoma/Adenocarcinoma (Benign/Malignant Epithelioma) of the Ciliary Body Pigment Epithelium (CPE)

11.9.1 Introduction

Adenoma and adenocarcinoma can originate from the ciliary pigmented epithelium (CPE). This tumor has somewhat different clinical and histopathologic features than adenoma/adenocarcinoma of the IPE and RPE.

11.9.2 Clinical Features

In a series of eight patients with adenoma of CPE, Shields et al. found the referring diagnosis as presumed melanoma in seven and cyst in one (Shields et al. 1999a). This rare tumor is nearly always misdiagnosed. In our series, the tumor was unilateral in all cases, and mean age at diagnosis was 51 years (range 8–73 years).

Clinically, adenoma of the CPE is typically dark brown to black in color, dome-shaped, and with abruptly elevated margins. This tumor can have a slightly corrugated surface, visible behind the dilated pupil and producing lens subluxation. Even though it is usually benign cytologically, adenoma can grow slowly and invade the anterior chamber and produce secondary glaucoma, vitreous hemorrhage, and retinal detachment, similar to ciliary body melanoma.

11.9.3 Diagnosis

Ultrasonography reveals high internal reflectivity with A-scan and acoustic solidity with B-scan. By UBM, this mass appears solid and often can be seen to arise at the level of the CPE without deep ciliary body stromal involvement. Transillumination documents blockage of light from the tumor, but this feature is also seen with melanoma. Anterior segment OCT is generally not helpful due to shadowing from iris tissue. Diagnostic fine-needle aspiration biopsy can disclose pigment epithelial cells compatible with a tumor of the pigment epithelium (Shields et al. 1993).

11.9.4 Management

The management of adenoma/adenocarcinoma of the CPE varies with tumor size, extent, and activity. Generally, the tumor resembles ciliary body melanoma, and it is often difficult to differentiate from melanoma, so intervention is usually necessary, despite the fact that this tumor is often benign. We doubt that this tumor is sensitive to radiotherapy. For small asymptomatic adenomas, in which the diagnosis is fairly certain, periodic observation is employed. For larger tumors with secondary effects or documented to enlarge, surgical resection is considered (Shields et al. 1991). Larger tumors with secondary glaucoma and other complications may require enucleation. The prognosis for vision depends on the size and extent of the tumor, and the prognosis for life is excellent.

11.10 Adenoma/Adenocarcinoma (Benign/Malignant Epithelioma) of the Retinal Pigment Epithelium (RPE)

11.10.1 Introduction

Adenoma/adenocarcinoma of the RPE is quite uncommon. An acquired RPE neoplasm can be benign or malignant, but even the more malignant variant rarely, if ever, exhibits regional or distant metastasis. Because their clinical features and management are similar, benign and malignant types are discussed collectively here under the term adenoma of the RPE.

11.10.2 Clinical Features

Adenoma of the RPE is typically diagnosed in adulthood, at mean age of 53 years (range 28–79 years). In a series of 13 patients with adenoma of RPE, Shields et al. found the referring diagnosis as presumed melanoma in all cases; thus this tumor closely resembles malignant melanoma (Shields et al. 1999b; Shields et al. 2005b). Unlike uveal melanoma, this tumor appears to have no predilection for race. Although adenoma of the RPE usually occurs in an otherwise healthy eye, it can be found in an eye with prior CHRPE, inflammation, or trauma (Shields et al. 2009; Shields et al. 2001a). In such instances, the adenoma can arise from a prior reactive hyperplasia of the RPE (Shields et al. 2001b).

Clinically adenoma of the RPE is usually solitary and unilateral and begins as a small, deep retinal tumor of dark brown to black color (Figs. 11.14 and 11.15). This tumor grows slowly and invades the overlying sensory retina, at which time it often acquires a dilated retinal feeding artery and draining vein, similar to those seen with the retinal hemangioblastoma. Yellow intraretinal exudation can slowly accumulate and eventually reach the subretinal space, producing intraretinal and subretinal yellow exudation, a finding that would be extremely rare with choroidal melanoma. In rare instances in which the tumor remains untreated, it may

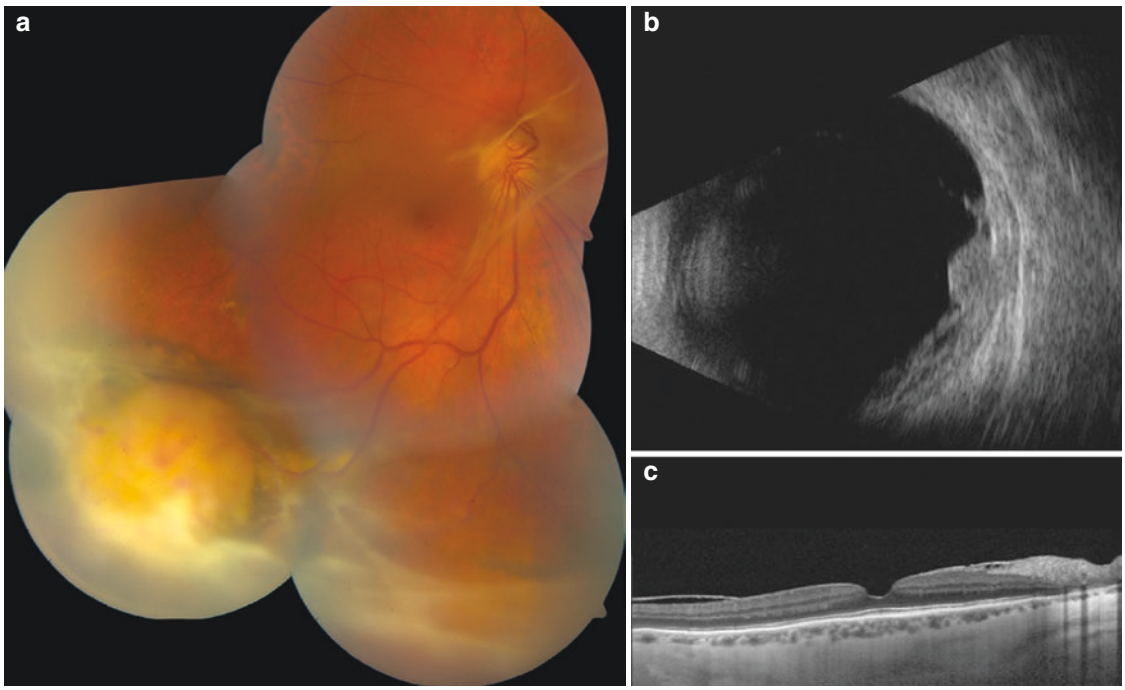

Fig. 11.14 Retinal pigment epithelial adenoma. (**a**) Nonpigmented vascular mass arising from congenital hypertrophy of the retinal pigment epithelium, with surrounding exudative retinopathy and vitreous fibrosis. (**b**) Ultrasonography confirms the echodense mass. (**c**) Optical coherence tomography confirms related epiretinal membrane

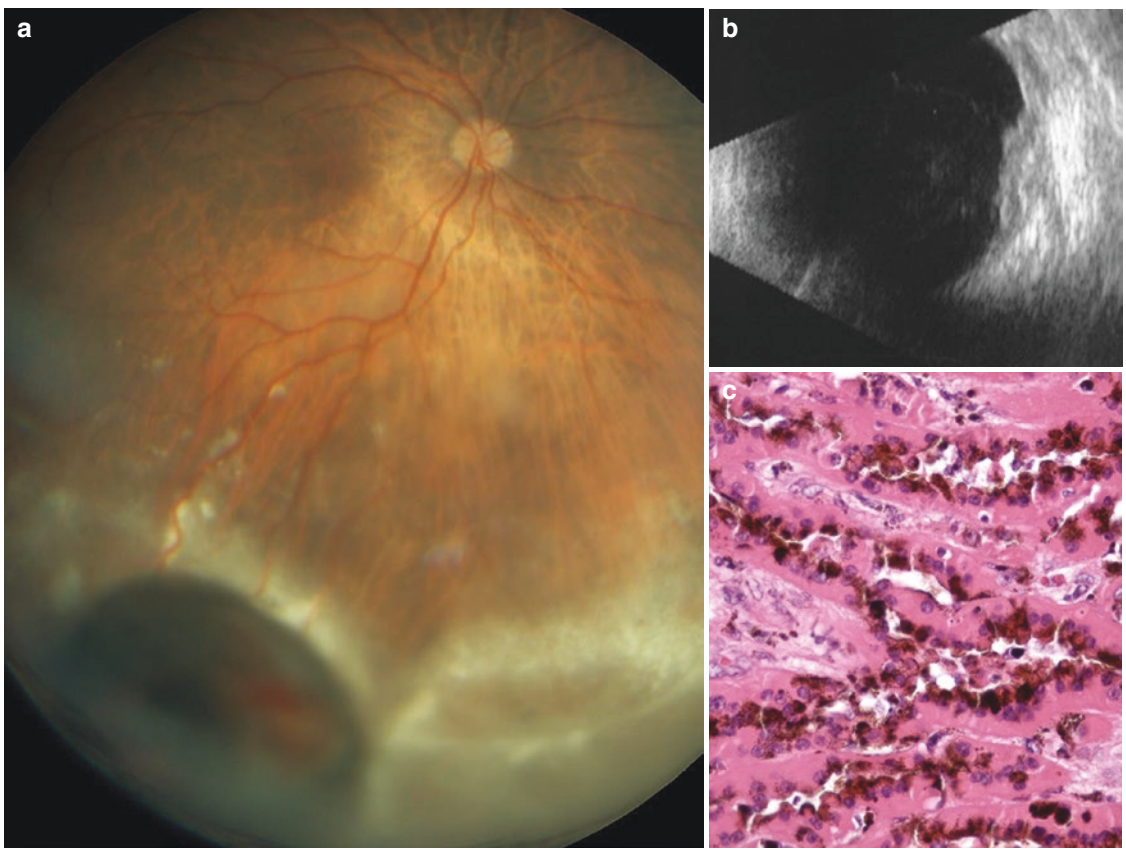

Fig. 11.15 Retinal pigment epithelial (RPE) adenocarcinoma. (**a**) Heavily pigmented retinal mass with surrounding exudative retinopathy. (**b**) Ultrasonography confirms the echodense mass. (**c**) Histopathology depicts bands of malignant epithelial cells with pigment, consistent with RPE adenocarcinoma

fill the globe and extend through the sclera to involve the orbital soft tissues. In some instances, adenoma of the RPE has arisen from solitary congenital hypertrophy of the RPE (Shields et al. 2009).

11.10.3 Diagnosis

This tumor can have a strong resemblance to choroidal melanoma, but there are differences in that adenoma can have a feeding retinal artery and vein, confirmed on FA, whereas melanoma generally has no retinal feeding vessels or at most only draining vein (Shields et al. 2005b). Fluorescein angiography shows early hypofluorescence and late minimal hyperfluorescence of adenoma, without visibility of choroidal vessels. Transillumination demonstrates a tumor shadow. Ultrasonography shows a characteristic abruptly elevated (derby hat configuration) and with medium to high internal reflectivity and acoustic solidity. Fine-needle aspiration biopsy can be performed to confirm cells compatible with an RPE adenoma.

11.10.4 Management

Treatment of adenoma of the RPE depends on tumor activity. If inactive and small, observation is advised. If the tumor is located anterior to the equator and shows growth, local resection by partial lamellar sclerouvectomy is provided versus plaque radiotherapy (Shields et al. 1991). If the adenoma is located posterior to the equator and produces symptomatic exudative retinal detachment, then laser treatment, thermotherapy, photodynamic therapy, or cryotherapy can be attempted.

References

Almeida A, Kaliki S, Shields CL. Autofluorescence of intraocular tumours. Curr Opin Ophthalmol. 2013;24:222–32.

Arepalli S, Pellegrini M, Ferenczy SR, et al. Combined hamartoma of the retina and retinal pigment epithelium: findings on enhanced depth imaging optical coherence tomography in eight eyes. Retina. 2014;34:2202–7.

Chamot L, Zografos L, Klainguti G. Fundus changes associated with congenital hypertrophy of the retinal pigment epithelium. Am J Ophthalmol. 1993;115:154–61.

Cohn AD, Quiram PA, Drenser KA, et al. Surgical outcomes of epiretinal membranes associated with combined hamartoma of the retina and retinal pigment epithelium. Retina. 2009;29:825–30.

Fung AT, Pellegrini M, Shields CL. Congenital hypertrophy of the retinal pigment epithelium: enhanced-depth imaging optical coherence tomography in 18 cases. Ophthalmology. 2014;121:251–6.

Gass JD. An unusual hamartoma of the pigment epithelium and retina simulating choroidal melanoma and retinoblastoma. Trans Am Ophthalmol Soc. 1973;71:171–83.

Gass JD. Focal congenital anomalies of the retinal pigment epithelium. Eye (Lond). 1989;3(Pt 1):1–18. https://doi.org/10.1038/eye.1989.2.

Golchet PR, Jampol LM, Mathura JR, et al. Torpedo maculopathy. Br J Ophthalmol. 2010;94:302–6.

Mason JO 3rd. Visual improvement after pars plana vitrectomy and membrane peeling for vitreoretinal traction associated with combined hamartoma of the retina and retinal pigment epithelium. Retina. 2002;22:824–5.

de Paula Freitas B, de Oliveira Dias JR, Prazeres J et al. Ocular findings in infants with microcephaly associated with presumed zika virus congenital infection in Salvador, Brazil. JAMA Ophthalmol. 2016.

Roseman RL, Gass JD. Solitary hypopigmented nevus of the retinal pigment epithelium in the macula. Arch Ophthalmol. 1992;110:1358–9.

Schachat AP, Shields JA, Fine SL, et al. Combined hamartomas of the retina and retinal pigment epithelium. Ophthalmology. 1984;91:1609–15.

Shields JA, Shields CL. Intraocular tumors: an atlas and textbook. 3rd ed. Philadelphia: Wolters Kluwer; 2015.

Shields CL, Shields JA. The American Society of retina specialists 2016 founders award lecture: retinal tumors: understanding clinical features, oct morphology, and therapy. J Vitreoretin Dis. 2017a;1:10–23.

Shields JA, Shields CL. The development of ocular oncology. Watching a dream come true. Asia Pac J Ophthalmol. 2017b;6:107–8.

Shields JA, Shields CL. Tumors and related lesions of the pigmented epithelium. Asia Pac J Ophthalmol. 2017c;6:215–23.

Shields CL, Shields JA, Cook GR, et al. Differentiation of adenoma of the iris pigment epithelium from iris cyst and melanoma. Am J Ophthalmol. 1985;100:678–81.

Shields JA, Shields CL, Shah P, Sivalingam V. Partial lamellar sclerouvectomy for ciliary body and choroidal tumors. Ophthalmology. 1991;98:971–83.

Shields JA, Shields CL, Shah PG, et al. Lack of association among typical congenital hypertrophy of the retinal pigment epithelium, adenomatous polyposis, and Gardner syndrome. Ophthalmology. 1992;99:1709–13.

Shields JA, Shields CL, Ehya H, et al. Fine-needle aspiration biopsy of suspected intraocular tumors. The 1992 Urwick Lecture. Ophthalmology. 1993;100:1677–84.

Shields JA, Shields CL, Gunduz K, et al. Adenoma of the ciliary body pigment epithelium: the 1998 Albert Ruedemann, Sr, memorial lecture, Part 1. Arch Ophthalmol. 1999a;117:592–7.

Shields JA, Shields CL, Gunduz K, et al. Neoplasms of the retinal pigment epithelium: the 1998 Albert Ruedemann, Sr, memorial lecture, Part 2. Arch Ophthalmol. 1999b;117:601–8.

Shields JA, Shields CL, Mercado G, et al. Adenoma of the iris pigment epithelium: a report of 20 cases: the 1998 Pan-American Lecture. Arch Ophthalmol. 1999c;117:736–41.

Shields JA, Shields CL, Singh AD. Acquired tumors arising from congenital hypertrophy of the retinal pigment epithelium. Arch Ophthalmol. 2000;118:637–41.

Shields JA, Shields CL, Eagle RC, et al. Adenocarcinoma arising from congenital hypertrophy of retinal pigment epithelium. Arch Ophthalmol. 2001a;119:597–602.

Shields JA, Shields CL, Slakter J, et al. Locally invasive tumors arising from hyperplasia of the retinal pigment epithelium. Retina. 2001b;21:487–92.

Shields CL, Mashayekhi A, Ho T, et al. Solitary congenital hypertrophy of the retinal pigment epithelium: clinical features and frequency of enlargement in 330 patients. Ophthalmology. 2003a;110:1968–76.

Shields CL, Shields JA, Marr BP, et al. Congenital simple hamartoma of the retinal pigment epithelium: a study of five cases. Ophthalmology. 2003b;110:1005–11.

Shields CL, Materin MA, Karatza EC, et al. Optical coherence tomography of congenital simple hamartoma of the retinal pigment epithelium. Retina. 2004;24:327–8.

Shields CL, Mashayekhi A, Dai VV, et al. Optical coherence tomographic findings of combined hamartoma of the retina and retinal pigment epithelium in 11 patients. Arch Ophthalmol. 2005a;123:1746–50.

Shields JA, Mashayekhi A, Ra S, Shields CL. Pseudomelanomas of the posterior uveal tract: the 2006 Taylor R. Smith Lecture. Retina. 2005b;25:767–71.

Shields CL, Materin MA, Walker C, et al. Photoreceptor loss overlying congenital hypertrophy of the retinal pigment epithelium by optical coherence tomography. Ophthalmology. 2006;113:661–5.

Shields CL, Pirondini C, Bianciotto C, et al. Autofluorescence of congenital hypertrophy of the retinal pigment epithelium. Retina. 2007;27:1097–100.

Shields CL, Thangappan A, Hartzell K, et al. Combined hamartoma of the retina and retinal pigment epithelium in 77 consecutive patients visual outcome based on macular versus extramacular tumor location. Ophthalmology. 2008;115:2246–52.

Shields JA, Eagle RC Jr, Shields CL, et al. Malignant transformation of congenital hypertrophy of the retinal pigment epithelium. Ophthalmology. 2009;116:2213–6.

Shields CL, Guzman JM, Shapiro MJ, et al. Torpedo maculopathy at the site of the fetal “bulge”. Arch Ophthalmol. 2010;128:499–501.

Shields CL, Kancherla S, Patel J, et al. Clinical survey of 3680 iris tumors based on patient age at presentation. Ophthalmology. 2012;119:407–14.

Shields CL, Pellegrini M, Ferenczy SR, et al. Enhanced depth imaging optical coherence tomography of intraocular tumors: from placid to seasick to rock and rolling topography--the 2013 Francesco Orzalesi Lecture. Retina. 2014;34:1495–512.

Sridhar J, Shahlaee A, Rahimy E, et al. Optical coherence tomography angiography of combined hamartoma of the retina and retinal pigment epithelium. Retina. 2016;36(7):e60–2. https://doi.org/10.1097/iae.0000000000000976.

Stallman JB. Visual improvement after pars plana vitrectomy and membrane peeling for vitreoretinal traction associated with combined hamartoma of the retina and retinal pigment epithelium. Retina. 2002;22:101–4.

Traboulsi EI. Ocular manifestations of familial adenomatous polyposis (Gardner syndrome). Ophthalmol Clin N Am. 2005;18:163–6.

Traboulsi EI, Krush AJ, Gardner EJ, et al. Prevalence and importance of pigmented ocular fundus lesions in Gardner's syndrome. N Engl J Med. 1987;316:661–7.

Retinal Metastasis

12

Sachin M. Salvi, Soyang E. Kim, and Arun D. Singh

12.1 Introduction

Metastatic lesions are the most common type of intraocular malignancy. In a study involving 741 patients, microscopic intraocular metastases were found on histopathology in 12.6% of patients who died from cancer (Eliassi-Rad et al. 1996).

Choroidal metastasis is the most common type of intraocular metastasis (covered in Chap. 3). A study involving 520 eyes showed that metastases to the eye can involve the choroid (88%), iris (9%), ciliary body (2%), optic disc (5%) and only rarely the retina (<1%) (Shields et al. 1997).

In contrast, there are only a few cases of retinal metastasis reported in the literature. Retinal metastasis was first reported in 1879 in a patient with cutaneous melanoma (Uhler 1940). Vajzovic and Mrutyunjaya reviewed 42 cases published between 1935 and 2012 (Vajzovic and Mruthyunjaya 2014).

We further identified 19 cases of retinal metastasis reported in 12 publications in the English literature between 2012 and 2017 (Shields et al. 2014; Singh et al. 2014; Breazzano and Barker-Griffith 2015; Gubbiotti et al. 2015; Taubenslag et al. 2015; Kanavati et al. 2016; Klufas et al. 2016; Nookala et al. 2016; Whalen et al. 2016; Praidou et al. 2017; Shaheen et al. 2017; Yalcinbayir et al. 2017). In our review of these cases reported over the last 5 years, the primary site was cutaneous melanoma in six patients (32%), lung cancer in four (21%), breast cancer in three (16%), oesophageal cancer in two (11%), colorectal cancer in one (5%), bladder cancer in one (5%) and liver cancer in one (5%), while the primary remained unknown in one patient (5%).

Details of the primary site by combining all data from 1935 to 2017 are presented in Table 12.1. Concluding from these reported 61 cases, we find that cutaneous melanoma followed by lung cancer and breast cancer is the most common primary cancers causing retinal metastasis.

Retinal metastases are not only exceedingly rare but also present a diagnostic challenge. They can often be mistaken for retinal pathology such as infective or inflammatory retinitis; unless a high index of suspicion for malignancy is maintained. Initial misdiagnosis may cause delay in treatment, progression of disease and visual loss.

Retinal metastases are usually unilateral (81% cases) and may have vitreous involvement. Patients have a known non-ocular primary malignancy in 90 percent of cases at presentation. Subsequent evaluation may identify a primary site on systemic screening after the ophthalmic presentation, though rarely no primary site may be found.

Patients with retinal metastasis carry a higher risk of brain metastasis as well as disseminated metastases and thus have poor prognosis. Retinal metastasis appears to be an end-stage finding, with malignancy entering the eye by a haematogenous route and presumably with diffuse dissemination to all organs (Shields et al. 2014).

Table 12.1 Primary site of tumour causing retinal metastasis reported in the literature in order of reducing frequency from 1935 to 2017

Primary tumour site	Number of reported cases	Percentage
Cutaneous	24	39
Lung	13	21
Breast	9	15
Gastrointestinal	6	10
Oesophageal	2	3
Colorectal	2	3
Unknown	2	3
Uterine	1	2
Bladder	1	2
Liver	1	2

S. M. Salvi · S. E. Kim
Sheffield Ocular Oncology Service, Royal Hallamshire Hospital, Sheffield, UK
e-mail: sachin.salvi@sth.nhs.uk; ella.kim@doctors.org.uk

A. D. Singh (✉)
Department of Ophthalmic Oncology, Cole Eye Institute, Cleveland Clinic, Cleveland, OH, USA
e-mail: singha@ccf.org

D. Rojanaporn (ed.), *Ocular Oncology*, https://doi.org/10.1007/978-981-13-2336-2_12

12.2 Clinical Features

Diagnosing retinal metastasis is challenging and requires a high index of suspicion. A thorough detailed history especially of any past or current malignancy and its management is important.

Patients usually present with reduced vision, floaters or eye pain depending on the size and site of the metastasis, vitreous involvement or intraocular inflammation. Some patients may also have metamorphopsia, photopsia or visual field defect especially if there is an associated retinal detachment.

Typically, retinal metastasis manifests as a unilateral yellow-white patch of retinal opacification, although these can occasionally be multifocal or bilateral (Fig. 12.1a). Retinal metastasis from cutaneous melanoma can appear brown, whereas those from metastatic carcinoma are usually the typical yellow-white (Mack and Jakobiec 1997).

There may be associated retinal haemorrhage and sub-retinal exudation. Rarely, retinal vasculitis may be noted (Manusow et al. 2014). With progression of the tumour, the intra-retinal opacification continues causing loss of retinal transparency. These coalescing patches of retinal opacification and associated retinal vascular ischaemic changes are often mistaken for necrotizing retinitis secondary to inflammatory or infectious aetiology such as cytomegalovirus or toxoplasmosis. Further progression may lead to sub-retinal fluid, retinal detachment or secondary glaucoma and painful blind eye.

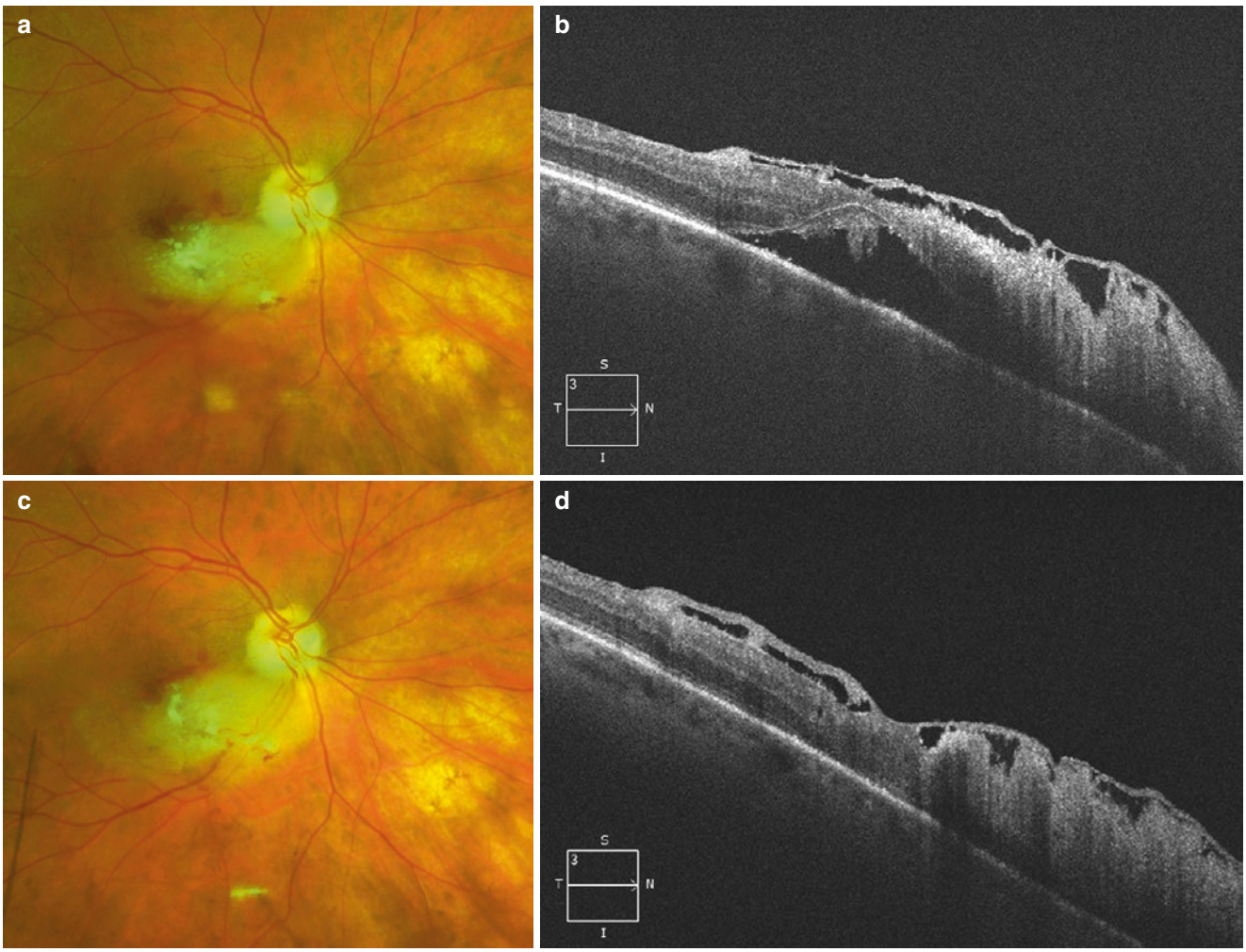

Fig. 12.1 Retinal metastasis: 74-year-old with previously treated non-small-cell lung cancer (11/2013) noted metamorphopsia of the right eye in 7/2015. Fundus examination revealed an elevated white intra-retinal lesion along the inferior temporal arcade which measured approximately 4 × 2 mm associated with lipid exudation but without evidence of intrinsic vessels. Intra-retinal haemorrhage at the posterior margins was observed. Overlying vitritis was absent (**a**). OCT through the lesion demonstrated an intra-retinal lesion with sub-retinal fluid (**b**). Initial workup for infectious aetiology was unremarkable, and after a PET scan was obtained, the patient was noted to have metastasis to the brain and clavicle; therefore suspicion for metastatic carcinoma to the retina was suspected. Patient was treated with whole-brain radiation (with inclusion of involved retina, completed in September 2015). Four weeks later, the lesion appeared smaller and less dense, and there is also resolution of associated SRF (**c**). OCT findings also suggested overall regression with resolution of SRF (**d**). Patient succumbed to metastases in January 2016

Unlike choroidal metastases, retinal metastases often have associated vitreous cellular activity. This vitreous involvement differs depending on the primary site. Vitreous infiltrates from cutaneous melanoma are usually large, golden-brown spherules, while those from metastatic carcinoma are usually non-pigmented. The presence of any spherules of vitreous infiltrates point towards the aetiology being neoplastic rather than inflammatory. Rarely, there may also be associated vitreous haemorrhage.

12.3 Differential Diagnosis

The rarity of retinal metastasis and its fundus appearance means that it is initially often mistaken to be caused by an alternative aetiology.

The majority of times, it is initially thought to be infectious or inflammatory retinitis caused by aetiologies such as toxoplasmosis, varicella zoster virus, herpes simplex virus, fungal or bacterial retinal abscess, granuloma or even lymphoproliferative disease. Due to the associated retinal and vitreous haemorrhage, it may be mistaken for vascular aetiology such as vascular occlusion, choroidal neovascular membrane, nerve fibre layer infarction, Coats' disease or haemangioma. Diffuse retinal involvement from cutaneous melanoma may be initially mistaken for choroidal melanoma or melanoma-associated retinopathy.

12.4 Diagnostic Techniques

Even though retinal metastasis can be a great masquerade, by maintaining a high index of suspicion and detailed history taking and examination, it can be confirmed by appropriate investigations.

12.4.1 Imaging

Fundus photographs: Wide-field photography such as Optos imaging will allow baseline imaging and monitoring of progression.

Fundus fluorescein angiography: Retinal metastasis typically shows focal tumour staining with intrinsic blood supply. The absence of leakage elsewhere will help differentiate from retinitis and other vascular aetiology.

Ultrasound B scan: Retinal thickening and any associated retinal detachment will be noted. B scan will also help to rule out any choroidal metastatic involvement and differentiate from choroidal melanoma. It will also demonstrate overlying vitreous changes.

Optical coherence tomography: OCT will often show the lesion involving either the outer retinal layer or full thickness of retina. It will also demonstrate any sub-retinal fluid or any associated exudates.

12.4.2 Biopsy

In patients with known primary malignancy and multi-organ metastases, the presence of retinal metastasis can be deducted from the clinical findings and imaging alone. In patients, who do not have systemic metastases or a known primary malignancy, definitive diagnosis can be achieved via direct biopsy of the retinal lesion. This can be in the form of fine-needle aspiration biopsy (FNAB) (Singh and Biscotti 2012) or vitrectomy-assisted retinal biopsy (Singh et al. 2014; Taubenslag et al. 2015; Praidou et al. 2017). Vitreous biopsy or vitrectomy alone may be useful in patients with heavy disease load in the vitreous. Histopathological examination with immunohistochemical staining will help confirm the diagnosis, and these findings can be compared to those from biopsy of the primary tumour.

12.5 Management

Once a diagnosis of retinal metastasis is made, further management depends on the severity of ophthalmic involvement, management of primary tumour and any systemic metastases, life expectancy and patient's preferences.

12.5.1 Systemic Management

It is important to liaise closely with the oncologist, primary care physician as well as palliative care team. Restaging of the patient may be necessary with whole-body PET (positron emission tomography) scan or CT chest abdomen and pelvis as well as MRI head and neck. Further systemic chemo/immune/biological therapy which may treat not only the retinal metastasis but also the systemic metastasis may be appropriate. Palliative care may be decided in patients who are too unwell for treatment, who refuse treatment and who have very limited life expectancy.

Rarely where patients are diagnosed with retinal metastasis but have no previous cancer diagnosis, referral to dermatologist to exclude skin melanoma, CT thorax to exclude lung cancer and a mammogram in females to exclude breast cancer may be necessary.

12.5.2 Local Management

Retinal metastases, which are extensive and multifocal and with associated retinal detachment and poor visual progno-

sis, are usually treated with palliative ocular radiotherapy. The treatment is provided in fractions with a typical dose of 30–37.5 grey (Gy) (Nookala et al. 2016; Whalen et al. 2016; Taubenslag et al. 2015). The advantage is the treatment can be provided fairly promptly and is effective, and any concomitant brain metastases can also be treated at the same time (Fig. 12.1c). The main disadvantage is visual loss, which is usually associated with the treatment.

Healthy patients with a solitary peripheral retinal metastatic lesion with good visual potential can be treated with plaque brachytherapy or photodynamic therapy (Rundle and Rennie 2006). Local excision of the lesion (Balestrazzi et al. 1995) can be attempted, but the high potential risk of retinal detachment and further surgical interventions should be kept in mind.

Enucleation surgery may be the only option in patients with a painful blind eye secondary to extensive ocular involvement from the metastasis. In some patients with poor overall prognosis, who are medically unfit for surgery, palliative pain management may be the only treatment to be provided.

Even though local control is usually achieved, systemic outcomes are overwhelmingly poor with metastasis-related deaths occurring between 1 month and 2 years in the majority of cases.

12.6 Conclusion

Retinal metastases are exceedingly rare. Cutaneous melanoma, lung cancer and breast cancer are the most common primary tumour sites. Retinal metastases may mimic retinitis. A high index of suspicion is needed. Biopsy may be required to confirm diagnosis. Multidisciplinary team approach is required. Systemic and/or local treatment may be necessary. Patients have poor long-term prognosis.

References

Balestrazzi E, Blasi MA, Marullo M, et al. Local excision of retinal metastasis from cutaneous melanoma. Eur J Ophthalmol. 1995;5:149–54.

Breazzano MP, Barker-Griffith AE. Features of cutaneous malignant melanoma metastatic to the retina and vitreous. Ocul Oncol Pathol. 2015;2:80–5.

Eliassi-Rad B, Albert DM, Green WR. Frequency of ocular metastases in patients dying of cancer in eye bank populations. Br J Ophthalmol. 1996;80:125–8.

Gubbiotti M, Pistilli B, Tudini M, et al. Retinal metastasis regression with eribulin in a heavily pretreated breast cancer patient. Future Oncol. 2015;11:17–22. https://doi.org/10.2217/fon.15.148.

Kanavati S, Ottensmeier C, Foria V, et al. Bilateral metastatic cutaneous melanoma to retina and vitreous after ipilimumab treated with pars plana vitrectomy and radiotherapy. Retin Cases Brief Rep. 2016;12(3):184–7. https://doi.org/10.1097/icb.0000000000000477.

Klufas MA, McCannel CA, McCannel TA. Simultaneous retinal and choroidal metastases in lung adenocarcinoma. JAMA Ophthalmol. 2016;134(5):e155368. https://doi.org/10.1001/jamaophthalmol.2015.5368.

Mack HG, Jakobiec FA. Isolated metastases to the retina or optic nerve. Int Ophthalmol Clin. 1997;37:251–60.

Manusow JS, Khoja L, Pesin N, et al. Retinal vasculitis and ocular vitreous metastasis following complete response to PD-1 inhibition in a patient with metastatic cutaneous melanoma. J Immunother Cancer. 2014;2(1):41. https://doi.org/10.1186/s40425-014-0041-1.

Nookala R, Batchu VV, Lee HM, et al. Difficult diagnosis of colon adenocarcinoma metastasis to retina: a case report and literature review. Int J Hematol Oncol Stem Cell Res. 2016;10:186–90.

Praidou A, Jacob S, Irion L, et al. Retinal and vitreous metastases from hepatocholangiocarcinoma. BMC Cancer. 2017;17(1):430. https://doi.org/10.1186/s12885-017-3429-8.

Rundle P, Rennie I. Photodynamic therapy for solitary retinal metastasis from breast carcinoma. Eye (Lond). 2006;20:1410–2.

Shaheen O, Ghibour A, Alsaid B. Esophageal cancer metastases to unexpected sites: a systematic review. Gastroenterol Res Pract. 2017;2017:1657310. https://doi.org/10.1155/2017/1657310.

Shields CL, Shields JA, Gross NE, et al. Survey of 520 eyes with uveal metastases. Ophthalmology. 1997;104:1265–76.

Shields CL, McMahon JF, Atalay HT, et al. Retinal metastasis from systemic cancer in 8 cases. JAMA Ophthalmol. 2014;132:1303–8.

Singh AD, Biscotti CV. Fine needle aspiration biopsy of ophthalmic tumors. Saudi J Ophthalmol. 2012;26:117–23.

Singh RP, Steinle NC, Bedi R, et al. Retinal infiltrates secondary to metastatic squamous cell carcinoma masquerading as infectious retinitis. Retin Cases Brief Rep. 2014;8:333–5.

Taubenslag KJ, Kim SJ, Attia A, et al. Retinal metastasis from unknown primary: diagnosis, management, and clinicopathologic correlation. Digit J Ophthalmol. 2015;21:1–10.

Uhler EM. Metastatic malignant melanoma of the retina. Am J Ophthalmol. 1940;23:158–62.

Vajzovic L, Mruthyunjaya P. Retinal metastatic tumors. In: Singh DA, Damato B, editors. Clinical ophthalmic oncology. 2nd ed. Heidelberg: Springer; 2014.

Whalen KE, Eagle RC, Jr, Vrabec TR. A case of metastatic urothelial carcinoma of the retina and vitreous. Retin Cases Brief Rep. 2016. https://doi.org/10.1097/icb.0000000000000474.

Yalcinbayir O, Gelisken O, Sen F et al. Retinal metastasis from squamous cell carcinoma of the lung: a case presentation. Retin Cases Brief Rep. 2017. https://doi.org/10.1097/icb.0000000000000553.

Peripheral Exudative Haemorrhagic Chorioretinopathy

13

Peter Heydon and Mandeep S. Sagoo

13.1 Introduction

Peripheral exudative haemorrhagic chorioretinopathy (PEHCR) is a commonly bilateral process characterised by exudative and/or haemorrhagic degeneration of the peripheral retina in the elderly population. It frequently regresses spontaneously to subretinal fibrosis and/or retinal pigment epithelial atrophy. PEHCR has various synonyms, including eccentric disciform degeneration, extramacular disciform degeneration (Bardenstein et al. 1992), haemorrhagic detachment of the retinal pigment epithelium (Silva and Brockhurst 1976), haemorrhagic peripheral pigment epithelial disease (Delaney Jr. et al. 1988) and peripheral choroidal neovascularisation (Vine and Johnson 1996). Its importance in the field of ocular oncology lies in that it is a pseudotumour that can mimic a range of tumours including naevus and melanoma.

13.2 Etiopathogenesis

The pathogenesis of PEHCR is unclear. Similarities between the clinical features of PEHCR and those of exudative age-related macula degeneration underlie the argument that choroidal neovascularisation is the cause for PEHCR. Histopathology studies of PEHCR are confined to one case which failed to demonstrate definitive peripheral neovascularisation (Mantel et al. 2009). Support for a neovascular theory is derived from histopathology on senile eyes, including a high incidence of neovascularisation of Bruch's membrane in the elderly (Sarks 1973). New vessel formation between Bruch's membrane and the retinal pigment epithelium at the ora serrata is common in those over the age of 60 (Friedman and Kuwabara 1963). Peripheral choroidal neovascularisation with associated peripheral subretinal haemorrhages and chorioretinal atrophy has been demonstrated histologically in two patients (Bec et al. 1980).

PEHCR also shares similarities with polypoidal choroidal vasculopathy (PCV), such as frequent bilaterality, haemorrhagic pigment epithelial detachment, lipid exudation and indocyanine green (ICG) angiography abnormalities. Delayed filling of the choriocapillaris; denser choroidal veins; polyp-like telangiectasia, often at the edge of a pigment epithelial detachment; and abnormal choroidal vascular networks have been demonstrated on a wide-field ICG angiography study (Mantel et al. 2012). The ethnic distribution of PEHCR is dissimilar to PCV, however, with PEHCR only being rarely reported in Asians (Kim et al. 2010). PCV also occurs in a younger age group, and a higher incidence of PCV amongst PEHCR patients has not been demonstrated as yet. It is possible that there may be distinct subgroups of PEHCR patients with polyps or without polyps (Goldman et al. 2013).

13.3 Clinical Features

PEHCR is a disease of the elderly with a mean age of between 70 to 80 years old in case series (Mantel et al. 2009; Annesley Jr. 1980; Shields et al. 2009). There is a female preponderance, perhaps accounted for by increased life expectancy. It predominantly affects the Caucasian population, although PEHCR lesions have been documented in a small series of Asian patients (Kim et al. 2010). An association with anticoagulant therapy and systemic hypertension has been noted (Mantel et al. 2009; Annesley Jr. 1980). Bilaterality is common, with an incidence of between 18 and 31%. Bilaterality is more likely to be associated with multifocal lesions in each eye individually (Annesley Jr. 1980;

P. Heydon
Medical Retina Service, Moorfields Eye Hospital, London, UK

M. S. Sagoo (✉)
Ocular Oncology Service, Moorfields Eye Hospital, London, UK

Retinoblastoma Service, Royal London Hospital, London, UK

UCL Institute of Ophthalmology, London, UK

D. Rojanaporn (ed.), *Ocular Oncology*, https://doi.org/10.1007/978-981-13-2336-2_13

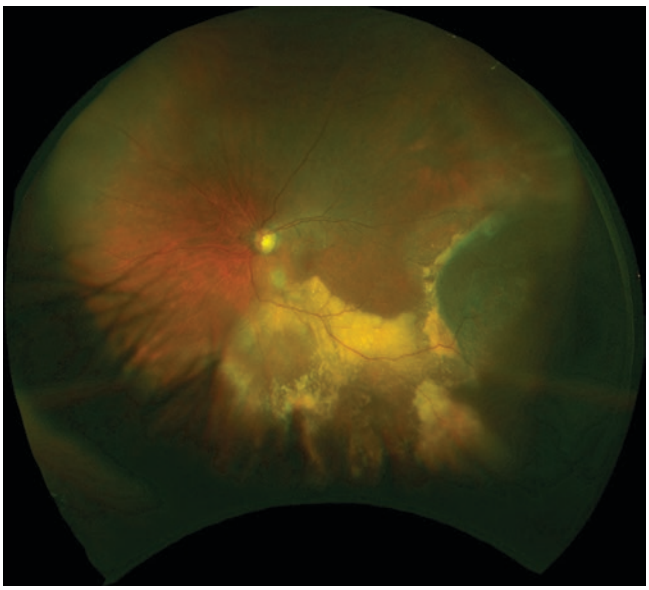

Fig. 13.1 Wide-angle colour fundus photograph of the left eye showing temporal choroidal mass with surrounding subretinal fluid and hard exudation, into the inferior retina and macula

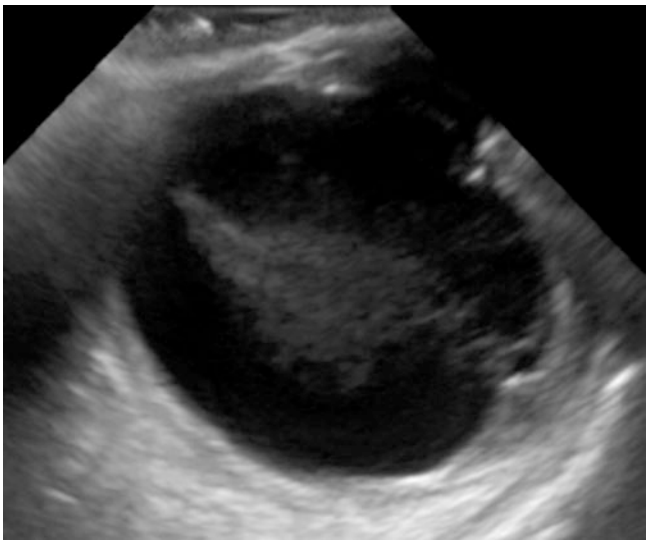

Fig. 13.2 Ultrasound B-scan of an eye with PEHCR. Elevated area is a shallow subretinal haemorrhage extending to the equator. Note associated vitreous haemorrhage (Courtesy of Dr. Marie Restori, Ultrasound Department, Moorfields Eye Hospital, London)

Mantel et al. 2009; Shields et al. 2009; Vine and Johnson 1996). Initial referral to ophthalmologists is often made on the basis of exclusion of malignancy (Shields et al. 2014; Shields et al. 2009; Shields et al. 2005).

Peripheral pigment epithelial detachment, haemorrhagic and lipid exudation are the hallmarks of PEHCR (Fig. 13.1). Haemorrhage is a slightly more common manifestation than lipid exudation. Lesions are most often found in the temporal quadrants, more so the inferior temporal quadrant, at the equatorial zone or further peripherally (Annesley Jr. 1980; Bardenstein et al. 1992; Mantel et al. 2009; Shields et al. 2009; Vine and Johnson 1996). Atrophic retinal pigment epithelial changes are often seen surrounding PEHCR lesions. Coexistent age-related macula degeneration is seen in a high number of PEHCR patients, in part due to a higher average age of such a cohort. Patients are commonly asymptomatic given the peripheral retinal location of lesions, although vision-threatening complications such as vitreous haemorrhage, macular oedema and submacular extension of haemorrhage have been documented (Cebeci et al. 2016; Mantel et al. 2012; Mantel et al. 2009; Pinarci et al. 2013; Vine and Johnson 1996).

13.4 Investigations

13.4.1 Ultrawide-Field Imaging

Serial imaging is particularly useful in PEHCR as the natural history is that of regression of lesions, unlike tumours of the choroid and retina (Fig. 13.1).

13.4.2 B-Scan Ultrasound

Features include a dome-shaped elevated lesion with intermediate or solid acoustic quality where haemorrhage predominates or hollow acoustic quality in serous exudation (Fig. 13.2). A lack of intrinsic vascular pulsations and a clot retraction cleft separating the subretinal or sub-RPE haemorrhage from the underlying choroid are important features to distinguish PEHCR from choroidal melanoma. However, colour flow mapping can sometimes mimic the blood flow in a melanoma if PEHCR has an actively bleeding vessel. In a large study of 133 patients, the mean diameter of PEHCR was 10 mm with a mean height of 3 mm (Shields et al. 2009).

13.4.3 Fluorescein Angiography

Fluorescein angiography (FFA) often demonstrates blockage of choroidal hyperfluorescence due to subretinal or sub-RPE haemorrhage or RPE hyperplasia. Irregular late leakage can sometimes be seen, but direct evidence of choroidal neovascularisation is only rarely visible (Bardenstein et al. 1992; Shields et al. 2009; Annesley Jr. 1980; Mantel et al. 2009). Hence FFA is not routinely performed in cases where the diagnosis is obvious from other imaging such as B-scan ultrasound.

13.4.4 Indocyanine Green Angiography

Polyp-like choroidal telangiectasia and abnormal choroidal vascular networks have been identified on ICG angiography,

raising the possibility of a similar pathogenesis to polypoidal choroidal vasculopathy. Lesions are often found at the edge of pigment epithelial detachments.

13.5 Differential Diagnosis

PEHCR can often simulate choroidal melanoma. In a large case series, it represented the second most common pseudomelanoma, after choroidal naevus, in those referred with a presumed diagnosis of uveal melanoma (Shields et al. 2005). Important differentiating features in PEHCR include the presence of retinal exudation, surrounding peripheral RPE atrophy and retraction clot cleft on ultrasonography hypofluorescence on fluorescein angiography, a lack of sentinel vessels on anterior segment exam and a lack of extension beyond the ora serrata on transpupillary transillumination. PEHCR also typically regress spontaneously to RPE atrophy, hyperplasia and fibrosis, unlike choroidal melanoma (Shields et al. 2009).

Differential diagnoses which can also cause a mixed haemorrhagic exudative peripheral chorioretinal lesion include retinal capillary haemangioma, retinal telangiectasia, retinal arterial macro-aneurysm and polypoidal choroidal vasculopathy. Primarily exudative conditions include choroidal metastases, choroidal detachments, uveal effusion syndrome, choroidal haemangioma, inflammatory subretinal granulomas or subretinal exudates associated with retinal vascular disorders (Tsui et al. 2009).

13.6 Treatment

PEHCR lesions often present in asymptomatic patients and will spontaneously regress to fibrosis. Treatment is indicated where there is a threat to macula from increasing subretinal haemorrhage or exudation, macula oedema or intractable vitreous haemorrhage.

There are no clear guidelines as to the optimal treatment of PEHCR. Successful treatment of lesions with intravitreal anti-vascular endothelial growth factor (anti-VEGF) agents has been reported (Alforja et al. 2011; Barkmeier et al. 2011; Goldman et al. 2013; Gonzales et al. 2010; Kim et al. 2010; Pinarci et al. 2013; Rishi et al. 2012; Seibel et al. 2016; Takayama et al. 2012; Takkar et al. 2017). Retreatment is often necessary and may suggest intermittent activity of lesions (Seibel et al. 2016). Photocoagulation may be required either alone or in combination with anti-VEGF therapy (Kim et al. 2010; Rishi et al. 2012; Takkar et al. 2017; Vine and Johnson 1996). Cryotherapy has similarly been used, although progressive submacular haemorrhage was reported despite therapy in one case report (Annesley Jr. 1980; Kim et al. 2010). Photodynamic therapy was unable to regress PEHCR in one report (Mashayekhi et al. 2013). Vitrectomy may be required in cases of vitreous haemorrhage with poor vision or where there is a diagnostic uncertainty, but caution is needed as the differential diagnosis includes cancerous tumours (Mirshahi et al. 2009). Consideration should be given towards discontinuation of anticoagulant therapy, particularly in cases of vitreous haemorrhage (Annesley Jr. 1980; Seibel et al. 2016).

13.7 Conclusion

PEHCR is a neovascular lesion that can mimic choroidal melanoma. Clinical features and ancillary studies, particularly ultrasound scans, help to distinguish this from more serious causes. Its importance to the retina specialist and ocular oncologist lies mainly in its role as an important pseudotumour.

References

Alforja MS, Sabater N, Giralt J, et al. Intravitreal bevacizumab injection for peripheral exudative hemorrhagic chorioretinopathy. Jpn J Ophthalmol. 2011;55:425–7.

Annesley WH Jr. Peripheral exudative hemorrhagic chorioretinopathy. Trans Am Ophthalmol Soc. 1980;78:321–64.

Bardenstein DS, Char DH, Irvine AR, et al. Extramacular disciform lesions simulating uveal tumors. Ophthalmology. 1992;99:944–51.

Barkmeier AJ, Kadikoy H, Holz ER, et al. Regression of serous macular detachment due to peripheral exudative hemorrhagic chorioretinopathy following intravitreal bevacizumab. Eur J Ophthalmol. 2011;21:506–8.

Bec PSP, Arnle JL, Aubry JP. La neo-vascularisation sous retinienne peripherique-une notion meconnue. Bull Soc Ophthalmol Fr. 1980;80:381–3.

Cebeci Z, Dere Y, Bayraktar S, et al. Clinical features and course of patients with peripheral exudative hemorrhagic chorioretinopathy. Turk J Ophthalmol. 2016;46:215–20.

Delaney WV Jr, Torrisi PF, et al. Hemorrhagic peripheral pigment epithelial disease. Arch Ophthalmol. 1988;106:646–50.

Friedman E, Kuwabara T. Senile choroidal vascular patterns and drusen. Arch Ophthalmol. 1963;69:220–30.

Goldman DR, Freund KB, McCannel CA, et al. Peripheral polypoidal choroidal vasculopathy as a cause of peripheral exudative hemorrhagic chorioretinopathy: a report of 10 eyes. Retina. 2013;33:48–55.

Gonzales JA, Kapoor KG, Gibran SK. Peripheral exudative hemorrhagic chorioretinopathy: a clinical, angiographic, and histologic study. Am J Ophthalmol. 2010;149:1013–4.

Kim YT, Kang SW, Lee JH, et al. Peripheral exudative hemorrhagic chorioretinopathy in Korean patients. Jpn J Ophthalmol. 2010;54:227–31.

Mantel I, Uffer S, Zografos L. Peripheral exudative hemorrhagic chorioretinopathy: a clinical, angiographic, and histologic study. Am J Ophthalmol. 2009;148:932–8.

Mantel I, Schalenbourg A, Zografos L. Peripheral exudative hemorrhagic chorioretinopathy: polypoidal choroidal vasculopathy and hemodynamic modifications. Am J Ophthalmol. 2012;153:910–22.

Mashayekhi A, Shields CL, Shields JA. Peripheral exudative hemorrhagic chorioretinopathy: a variant of polypoidal choroidal vasculopathy? J Ophthalmic Vis Res. 2013;8:264–7.

Mirshahi A, Hohn F, Baatz H, et al. Peripheral exudative haemorrhagic chorioretinopathy: clinical and angiographic findings. Klin Monatsbl Augenheilkd. 2009;226:659–63.

Pinarci EY, Kilic I, Bayar SA, et al. Clinical characteristics of peripheral exudative hemorrhagic chorioretinopathy and its response to bevacizumab therapy. Eye (Lond). 2013;27:111–2.

Rishi P, Das A, Sarate P, et al. Management of peripheral polypoidal choroidal vasculopathy with intravitreal bevacizumab and indocyanine green angiography-guided laser photocoagulation. Indian J Ophthalmol. 2012;60:60–3.

Sarks SH. New vessel formation beneath the retinal pigment epithelium in senile eyes. Br J Ophthalmol. 1973;57:951–65.

Seibel I, Hager A, Duncker T, et al. Anti-VEGF therapy in symptomatic peripheral exudative hemorrhagic chorioretinopathy (PEHCR) involving the macula. Graefes Arch Clin Exp Ophthalmol. 2016;254:653–9.

Shields JA, Mashayekhi A, Ra S, et al. Pseudomelanomas of the posterior uveal tract: the 2006 Taylor R. smith lecture. Retina. 2005;25:767–71.

Shields CL, Salazar PF, Mashayekhi A, et al. Peripheral exudative hemorrhagic chorioretinopathy simulating choroidal melanoma in 173 eyes. Ophthalmology. 2009;116:529–35.

Shields CL, Manalac J, Das C, et al. Choroidal melanoma: clinical features, classification, and top 10 pseudomelanomas. Curr Opin Ophthalmol. 2014;25:177–85.

Silva VB, Brockhurst RJ. Hemorrhagic detachment of the peripheral retinal pigment epithelium. Arch Ophthalmol. 1976;94:1295–300.

Takayama K, Enoki T, Kojima T, et al. Treatment of peripheral exudative hemorrhagic chorioretinopathy by intravitreal injections of ranibizumab. Clin Ophthalmol. 2012;6:865–9.

Takkar B, Roy S, Sodhi PK, et al. Peripheral choroidal neovascular membrane in a case of peripheral exudative hemorrhagic chorioretinopathy managed with combination therapy. Int Ophthalmol. 2017;37:429–31.

Tsui I, Jain A, Shah S, et al. Ultra widefield imaging of peripheral exudative hemorrhagic chorioretinopathy. Semin Ophthalmol. 2009;24:25–8.

Vine AK, Johnson MW. Peripheral choroidal neovascularization. Eur J Ophthalmol. 1996;6:44–9.

Optic Disc Melanocytoma

14

Minoru Furuta

14.1 Introduction

Optic disc melanocytoma is a unique variant of melanocytic nevus, first named by Zimmerman and Garron in 1962 (Zimmerman and Garron 1962), which sometimes contiguously involve adjacent choroid and retina. Optic disc melanocytoma is believed to congenital and non-hereditary lesion that does not show racial predilection such as uveal melanoma. Historically melanocytoma was confused with uveal melanoma both clinically and histopathologically. The diagnosis of melanocytoma is usually given by ophthalmoscopic findings because of characteristic pigment mass on the optic disc. Ancillary examinations include ultrasonography, fluorescein and indocyanine green angiography, fundus autofluorescence, optical coherent tomography (OCT), and OCT angiography. Histopathologically melanocytoma is deeply pigmented benign tumor composed with round to oval nevus cells primarily arising on the optic disc. It is generally considered as stationary lesion but can grow slowly and progressively affect visual field and visual acuity. In rare instances, it can get spontaneous necrosis or transform into melanoma that often cause severe visual loss.

14.2 Etiology and Pathogenesis

In a largest review of 115 patients with optic disc melanocytoma by Shields (Shields et al. 2004), the mean age at diagnosis was 50-year-old ranging 1–91. Unlike uveal melanoma, optic disc melanocytoma appears to have an equal distribution in all races. Slight sex predilection was noted that 62% of patients were females. The rare association with neurofibromatosis, meningioma, and ocular melanocytosis is suggested.

M. Furuta (✉)
Department of Ophthalmology, Fukushima Medical University, Fukushima, Japan

Histopathologically intensely pigmented melanocytoma locates on the optic disc that sometimes extends underneath the lamina cribrosa. The uniform size of tumor cell has cytoplasmic pigmentation, the low nuclear cytoplasmic ratio. Breached preparation shows the cells to be oval to round with abundant cytoplasm similar to uveal melanocytes in ocular melanocytosis (Zimmerman 1960, 1965). The pathogenesis of optic disc melanocytoma is unknown but thought to be a congenital lesion. Because the melanin pigment is presumed to increase by age, young children might have amelanotic lesion causing rare to diagnose with (Shields et al. 2002).

14.3 Clinical Features

14.3.1 Overview

In a review of 115 patients (Shields et al. 2004), the lesion was unilateral in 99%, pigmented in 100%, and related visual symptoms in 24%, and relative afferent pupillary defect was present in 9% of patients. The mean size of tumor was 2 mm in diameter and 1 mm in thickness. The tumor can extend over the margin of optic disc to adjacent choroid in 54% and sensory retina in 30%. If choroidal component is prominent, the differential diagnosis with choroidal melanoma extending to the optic disc becomes difficult. Most melanocytomas do not affect visual acuity; however, visual loss would occur in 26% due to retinal exudation, spontaneous tumor necrosis, central retinal vein occlusion, or malignant transformation (Archdale and Magnus 1993; García-Arumí et al. 1994). Related visual loss occurred in 18% of patients by 10 years, and minor tumor enlargement occurred in 11% of patients by 5 years and in 32% of patients by 10 years by Kaplan-Meier estimates. Malignant transformation was documented in 2%. If severe visual loss due to tumor necrosis or tumor growth was noted, most eyes have been enucleated because of suspicious of melanoma. However, there are few cases refused enucleation in patients with such vision loss; their

D. Rojanaporn (ed.), *Ocular Oncology*, https://doi.org/10.1007/978-981-13-2336-2_14

vision was recovered suggesting of transient ischemic change or inflammation (García-Arumí et al. 1994; Wiznia and Price 1974). Visual field defect is the most common complications of optic disc melanocytoma occurring approximately 90% of patients. Enlarged blind spot was seen in 15 patients out of 20 melanocytoma patients, in whom mostly associated with concomitant nerve fiber layer defect (Osher et al. 1979; Usui et al. 1990). The nerve fiber layer defect appears to be related to the amount of tumor extension of the optic disc or compression of axons in the optic disc. Figures 14.1, 14.2, and 14.3 show size variation of optic disc melanocytoma.

14.3.2 Visual Acuity and Visual Field

The extent of visual impairment varies by cases; tumor-associated mild visual loss can occur in about 26% (Shields et al. 2004) due to subfoveal exudation or neuroretinitis from spontaneous tumor necrosis. Severe visual loss can rarely occur secondary to central retinal vein occlusion, spontaneous tumor necrosis, or malignant transformation (Archdale and Magnus 1993; García-Arumí et al. 1994). However, most of their vision would be kept in the long run. Most melanocytomas show visual field defects according to a variety of mechanisms. Osher and associates (Osher et al. 1979) found that the blind spot enlargement appeared to be related to the amount of tumor extension on the disc margin, and the arcuate defects appeared to be related to compression of axons in the optic disc. They reported 90% of patients have visual field defect out of 20 patients with Goldmann perimeter. In the same series, the type of defect included minimal enlargement of the blind spot in three patients (15%) and greatly enlarged blind spot in 15 patients (75%), of whom

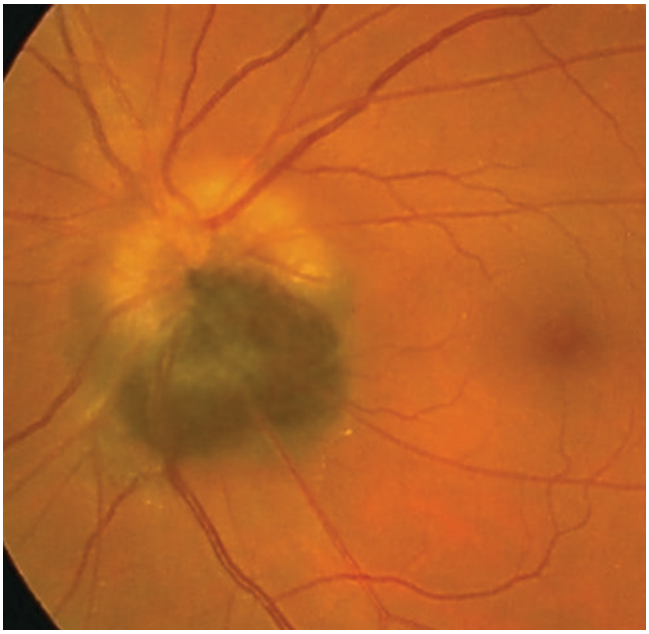

Fig. 14.2 A 39-year-old female with medium-sized optic disc melanocytoma in the left eye. The tumor is locating inferior portion of the optic disc with superior optic disc edema. She complained foggy vision, and her visual acuity was reduced to 0.6

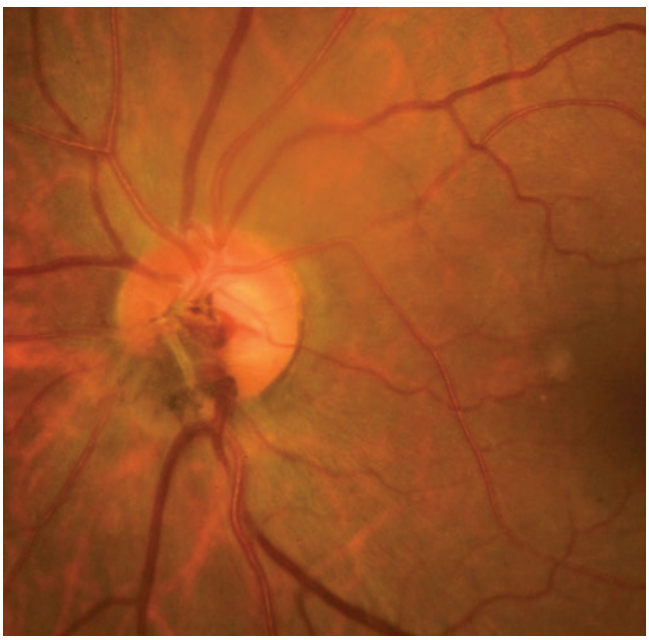

Fig. 14.1 A 64-year-old female with asymptomatic small-sized optic disc melanocytoma in the left eye. The tumor is locating inferonasal quadrant of the optic disc. Her visual acuity was 1.0

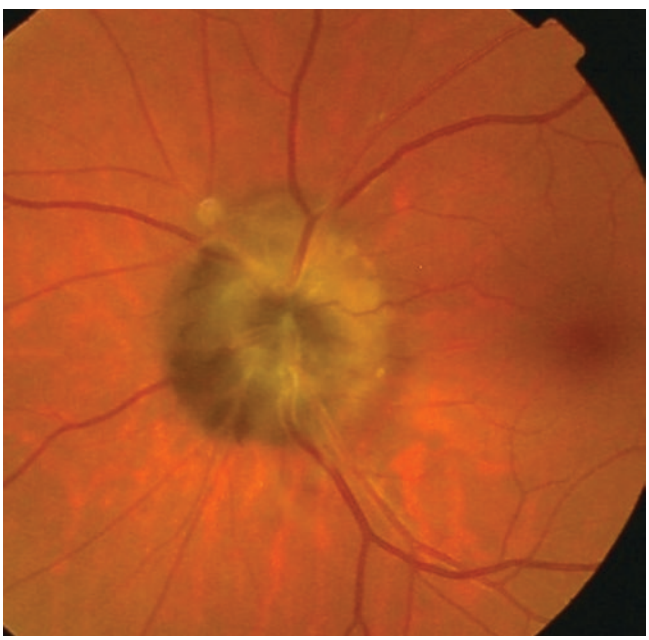

Fig. 14.3 A 49-year-old female with asymptomatic large-sized optic disc melanocytoma in the left eye. The tumor occupies 360° of the optic disc. Her visual acuity was 1.0

ten patients had concomitant nerve fiber bundle defects including nasal step, relative nerve fiber bundle defect, and an absolute arcuate defect. Usui and associates (Usui et al. 1990) found that seven out of ten patients (70%) show visual field defects. Six out of seven (86%) patients with visual field defects corresponded with the location of the tumor and retinal nerve fiber bundle defect. Recent imaging of spectral domain OCT depicts melanocytoma corresponding retinal nerve fiber bundle defect (Chaudhary et al. 2006; Punjabi et al. 2011). Figure 14.4 shows a case with papilledema treated with oral corticosteroids.

14.3.3 OCT

Shields and associates (Shields et al. 2008) described OCT imaging of optic disc melanocytoma in 15 cases and revealed that the tumor displayed a gradual sloping transition from normal retina into the mass, hyper-reflectivity at its anterior tumor surface, and dense posterior shadowing with an optically empty appearance in all 15 cases (100%). And they observed that thicker tumors displayed thinner anterior hyper-reflective borders and denser shadowing. Other findings of OCT included vitreous seeds in two cases (13%) and

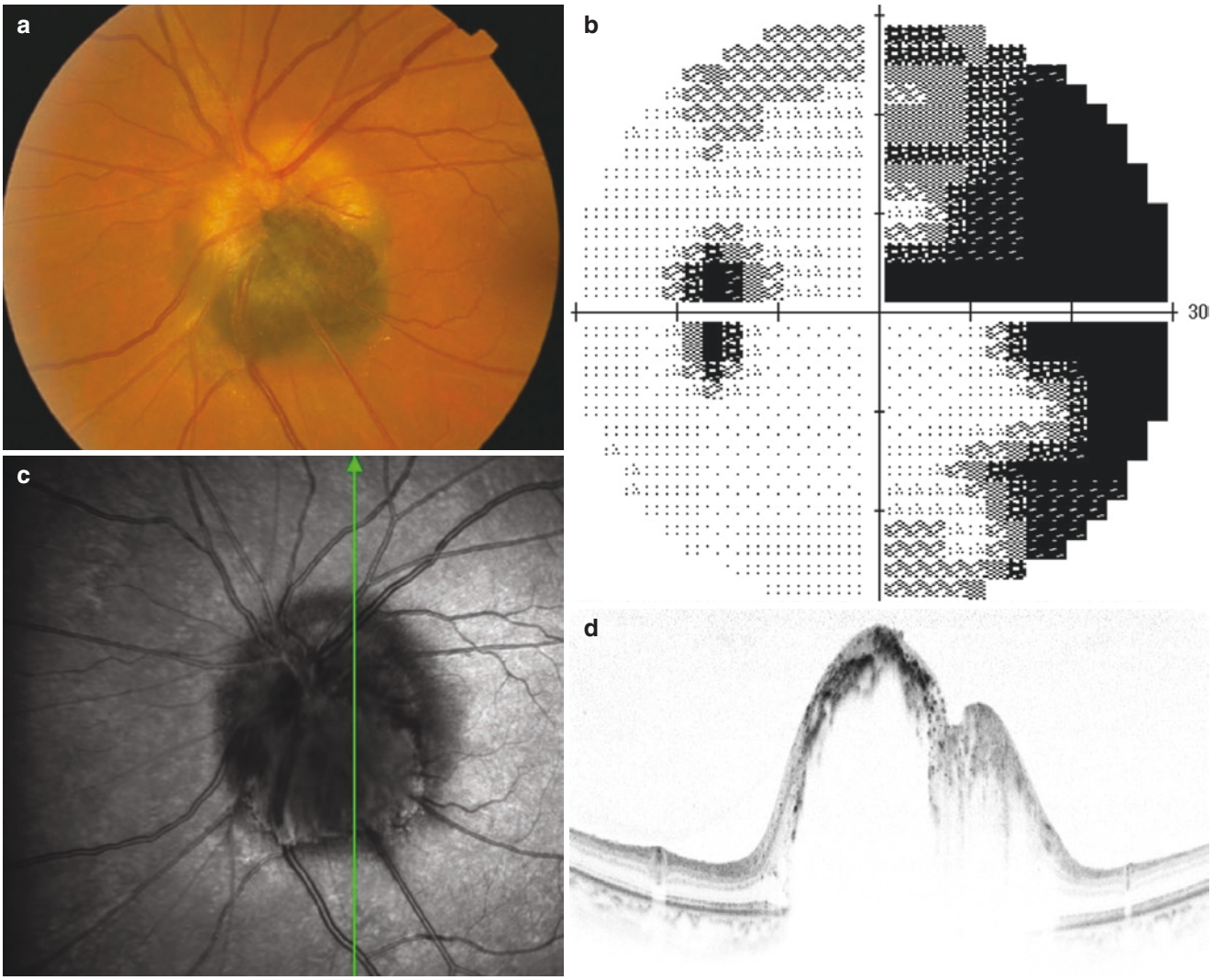

Fig. 14.4 Same patient with Fig. 14.2; before (**a**–**d**) and after (**e**–**h**) low-dose oral corticosteroid. (**a**) 39-year-old female with inferior optic nerve melanocytoma with papilledema in the left eye. (**b**) Humphrey 30–2 visual field testing shows superior arcuate scotoma and inferior nasal step with blind spot enlargement, corresponding to nerve fiber layer defect and optic disc edema. (**c**) Infrared SLO image shows hyporeflectance of the tumor. (**d**) OCT shows papilledema, optically empty mass and overlying nerve fiber layer with hyper-reflective dots surrounding the vessels representing pigmented clumps of melanin-phagocytizing macrophages known as melanophages. (**e**) 2 months after administrating oral steroids, papilledema was resolved, and margin of tumor became clear. (**f**) Humphrey 30–2 visual field testing shows slight improvement in the lower nasal scotoma compared with B. Visual acuity was also improved from 0.6 to 1.0. (**g**) Infrared SLO image shows hyper-reflectance of the tumor. Tumor margin is clearly defined. (**h**) OCT shows resolving papilledema and thinning of overlying nerve fiber layer with dense hyper-reflective dots

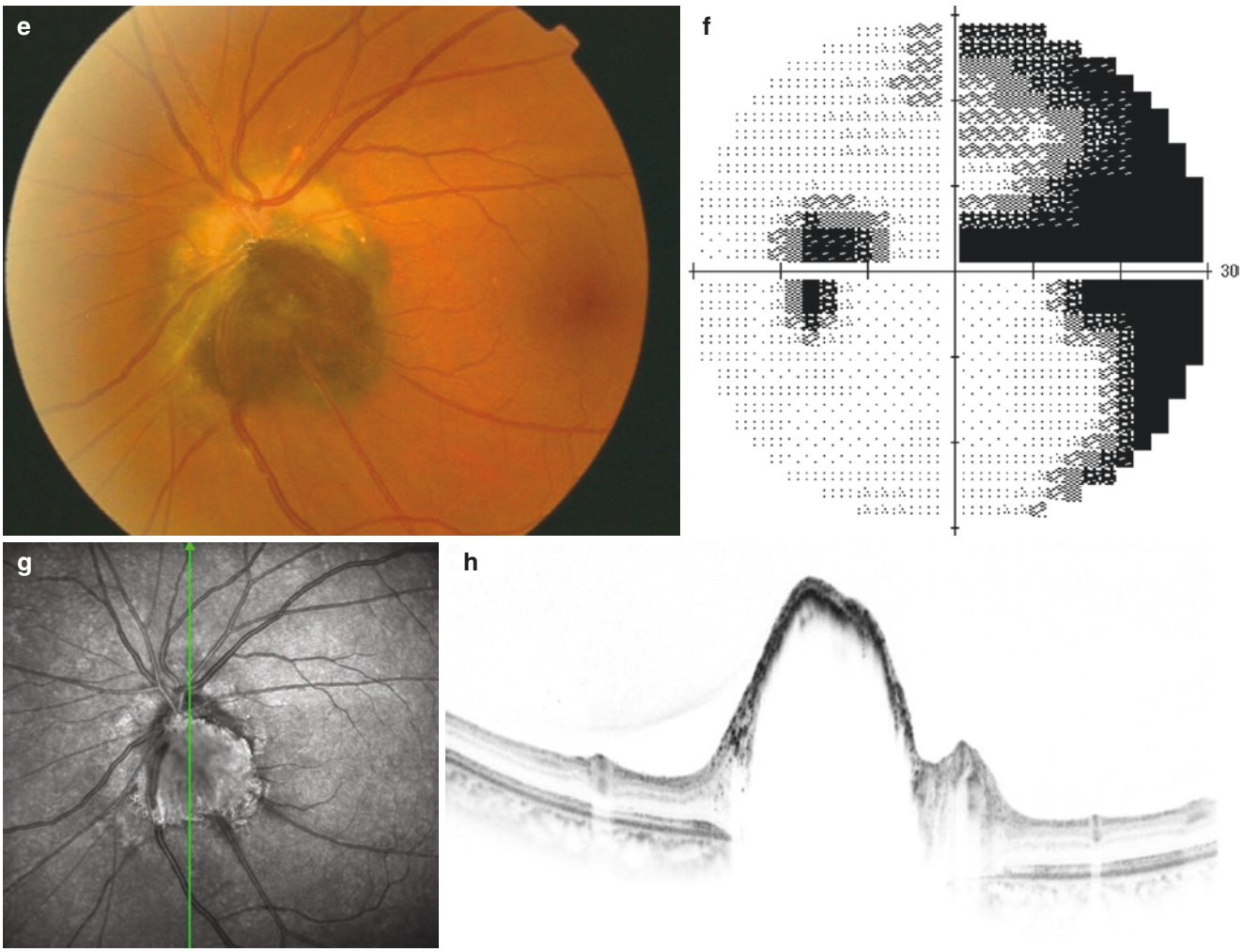

Fig. 14.4 (continued)

adjacent retinal edema in one case (7%). Finger and associates (Finger et al. 2010) studied correlation between combined OCT and scanning laser ophthalmoscope (SLO) images in 20 eyes and histopathology in 1 eye with melanocytoma. And they demonstrated the disruption of the internal limiting membrane, disorganization of the retina overlying the lesion, and visualization of the tumor's subretinal surface. Okubo and associates (Okubo et al. 2013) found hyper-reflective dots surrounding the central retinal veins and arteries on the optic disc. The mechanism of hyper-reflective dots was suggested of possible melanophages and/or tumor cells or proteins and/or lipid deposits. Using swept-source OCT, Filloy and associates (Filloy et al. 2017) described these hyper-reflective dots represent pigmented clumps of melanin-phagocytizing macrophages known as melanophages. Figure 14.5 shows OCTs of relatively large tumors.

14.3.4 Fundus Autofluorescence

Fundus autofluorescence is noninvasive imaging modality including shortwave autofluorescence (SWAF; excitation at 488 nm and emission >510 nm) and infrared autofluorescence (IRAF; excitation at 785 nm and emission: 805–840 nm). SWAF is highly correlated to the lipofuscin content at the RPE level and visualize state of metabolism of the RPE, while IRAF visualizes selectively the melanin granules in RPE cells, which are normally localized in the apical portion of RPE cells (Kellner et al. 2010). Salvanos and associates (Salvanos et al. 2015) reported the usefulness of making differential diagnosis with optic disc melanocytoma from peripapillary choroidal nevus and choroidal melanoma. Melanocytoma shows totally hypoautofluorescent SWAF with sharply demarcated and feathery edges with no hyperautofluorescent spots associated with orange pigment nor

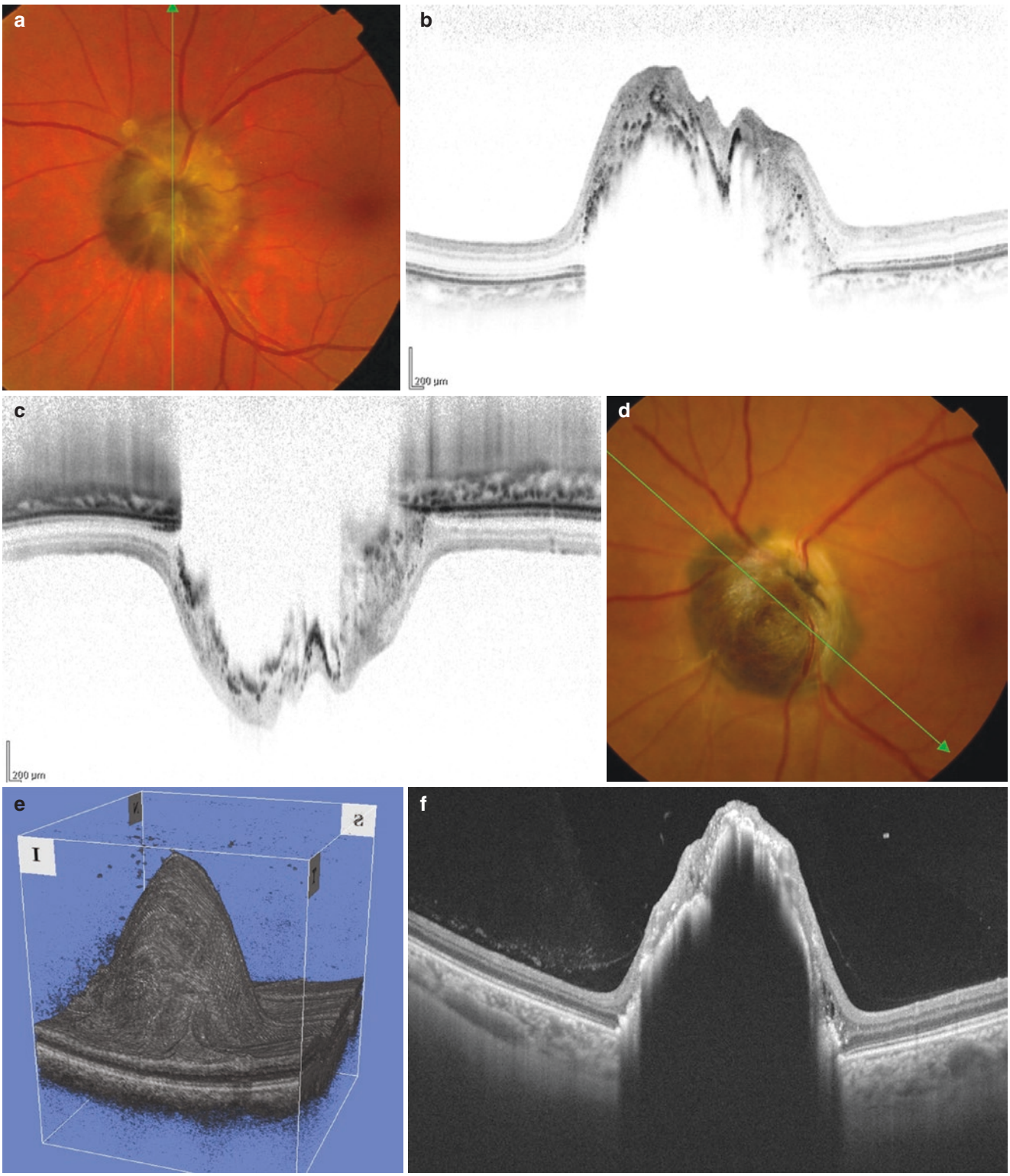

Fig. 14.5 OCT of the optic disc melanocytomas. (**a**) Same patient with Fig. 14.3. (**b**) SD-OCT shows dense posterior shadowing optically empty appearance with overlying thick retinal tissue in which supero-temporal whitish part of the tumor has thicker tissue. In overlying tissue, there are central retinal vessels and hyper-reflective dots that are considered of melanophages and/or tumor cells or proteins and/or lipid deposits by some reports. (**c**) EDI-OCT. Same comments with above. (**d**) A 42-year-old female with left optic disc melanocytoma affecting of 2–12 o'clock hour of disc margin in the left eye. Deeply pigmented tumor is appearing on the surface. (**e**) A 3D reconstructed image of swept-source OCT shows numerous vitreous seeds. (**f**) Swept-source OCT is also unable to depict internal structure of the deeply pigmented tumor. Overlying retinal tissue on the tumor is severely disorganized and contains hyper-reflective dots. At the tumor margin at 4 and 10 o'clock hour in color fundus photograph D, subretinal growth is suspected. However, OCT does not show horizontal subretinal growth; OCT is necessary to accurate evaluation of tumor extent

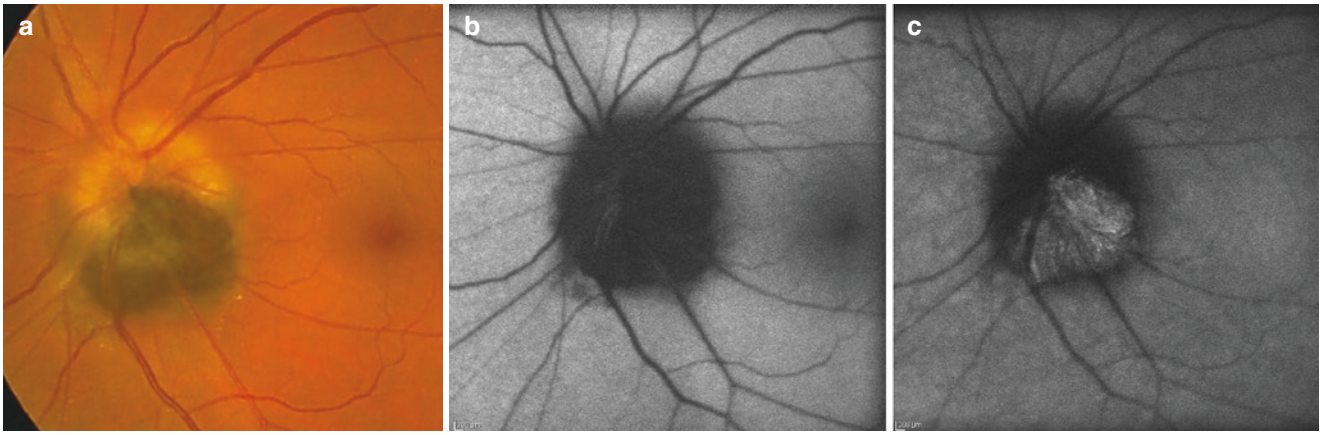

Fig. 14.6 Shortwave and infrared autofluorescence of optic disc melanocytoma. (**a**) Same patient as Figs. 14.2 and 14.4. (**b**) Shortwave autofluorescence imaging shows hypoautofluorescence. (**c**) Infrared autofluorescence imaging shows hyperfluorescence

subretinal fluid. On IRAF images, Zhang and associates (Zhang et al. 2016) reported that optic disc melanocytoma showed outstanding hyperautofluorescence with well-defined outline corresponding to the area of pigmented masses in eight of all cases. Figure 14.6 shows a case with typical autofluorescence.

14.3.5 Fluorescein Angiography (FA), Indocyanine Green Angiography (IA), and OCT Angiography (OCT-A)

FA of optic disc melanocytoma itself demonstrates hypofluorescence throughout the angiogram in most deeply pigmented cases. In cases with optic disc edema, there is dye leakage at the part of edematous optic disc. IA of most melanocytoma also demonstrates hypofluorescence throughout the angiogram. Although OCT-A depict abundant capillaries on the tumor surface, they do not appear on FA and IA, because massive melanin or hyper-reflective granules around the vessel appearing on the OCT presumably block fluorescence of the capillaries. OCT-A is a non-invasive 3D imaging modality recently available. The benefit of OCT-A is to visualize the circulation and vessels clearly without leakage by the retinal layer in both B- and C-scan of OCT. OCT-A of optic disc plexus and corresponding OCT B-scan shows the fine superficial vasculature, and OCT-A of radial peripapillary capillaries plexus and corresponding OCT B-scan shows the presence of dilated abnormal vessels in the deeper layers in the case with dye leakage in FA (Carnevali et al. 2017). Figure 14.7 shows that OCT-A visualize more clearly of vessels on the pigmented tumor compared with FA and IA.

14.4 Management

Optic disc melanocytoma is benign nature of tumor with possible slow growth and rare transformation into melanoma. Currently there is no established treatment for melanocytoma itself; observation is only choice of management. However, when acute or subacute visual impairment secondary to tumor necrosis, central retinal vein and artery occlusion, or choroidal neovascularization is documented, there are few reported treatment modalities. There are some reports treated with photodynamic therapy and intravitreal bevacizumab for optic disc melanocytoma with choroidal neovascularization (Urrets-Zavalia et al. 2015; Al-Halafi 2013; Kamisasanuk et al. 2012). Tumor necrosis can lead to misdiagnosis of progressive tumor growth which is suggesting of transformation into melanoma. In some eyes with tumor necrosis resulting from transient ischemic necrosis or inflammation in the tumor, visual acuity is recovered by observation according to patients' requests in the older reports (García-Arumí et al. 1994; Wiznia and Price 1974). Optic disc melanoma and suspicious conditions are usually managed with enucleation, because of lower visual function and higher recurrent rate by plaque radiotherapy incomparable with juxtapapillary choroidal melanoma (Shields et al. 1990; Shukla et al. 2012; Meyer et al. 1999; Sagoo et al. 2014).

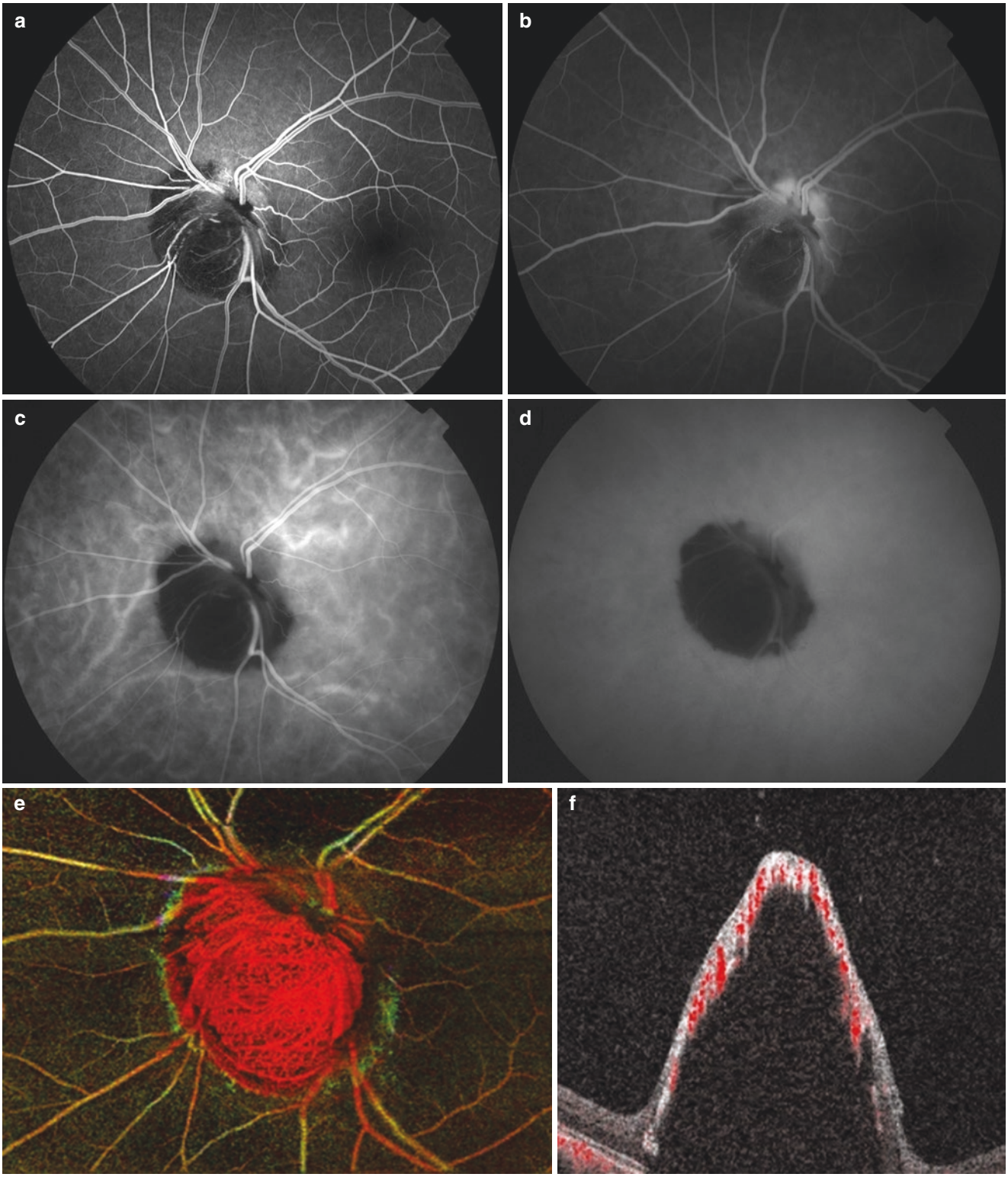

Fig. 14.7 Fluorescein and indocyanine green angiography (FA and IA), OCT angiography (OCT-A). Same patient with Fig. 14.5d–f. (**a**) FA early phase shows hypofluorescent tumor and hyperfluorescent optic disc tissue with fine few vessels on the tumor. (**b**) FA late phase shows dye leakage from optic disc tissue. (**c**) IA early phase shows hypofluorescent tumor. (**d**) IA late phase shows hypofluorescent tumor. (**e**) OCT-A depict abundant capillaries at the surface of the tumor. (**f**) B-scan image of OCT-A shows that blood flow is detected in the retinal tissue on the tumor

References

Al-Halafi AM. Successful treatment of melanocytoma associated choroidal neovascular membrane with intravitreal bevacizumab. Saudi J Ophthalmol. 2013;27:117–9.

Archdale TW, Magnus DE. Melanocytoma of the optic disc. J Am Optom Assoc. 1993;64(2):98–103.

Carnevali A, Querques L, Zucchiatti I, et al. Optical coherence tomography angiography features in melanocytoma of the optic nerve. Ophthal Surg Laser Imag Retina. 2017;48:364–6.

Chaudhary R, Arora R, Mehta DK, et al. Optical coherence tomography study of optic disc melanocytoma. Ophthal Surg Laser Imag Retina. 2006;37:58–61.

Filloy A, Arias L, Ascaso FJ, et al. Swept source optical coherence tomography imaging of optic disc melanocytoma. Clin Exp Ophthalmol. 2017;45:313–4.

Finger PT, Natesh S, Milman T. Optical coherence tomography: pathology correlation of optic disc melanocytoma. Ophthalmology. 2010;117:114–9.

García-Arumí J, Salvador F, Corcostegui B, et al. Neuroretinitis associated with melanocytoma of the optic disk. Retina. 1994;14:173–6.

Kamisasanuk T, Uchino E, Sakamoto T. Choroidal neovascularization of optic disk melanocytoma treated with bevacizumab. Eur J Ophthalmol. 2012;22:503–5.

Kellner U, Kellner S, Weinitz S. Fundus autofluorescence (488 NM) and near-infrared autofluorescence (787 NM) visualize different retinal pigment epithelium alterations in patients with age-related macular degeneration. Retina. 2010;30:6–15.

Meyer D, Ge J, Blinder KJ, et al. Malignant transformation of an optic disk melanocytoma. Am J Ophthalmol. 1999;127:710–4.

Okubo A, Unoki K, Yoshikawa H, et al. Hyperreflective dots surrounding the central retinal artery and vein in optic disc melanocytoma revealed by spectral domain optical coherence tomography. Jpn J Ophthalmol. 2013;57:108–12.

Osher RH, Shields JA, Layman PR. Pupillary and visual field evaluation in patients with melanocytoma of the optic disc. Arch Ophthalmol. 1979;97:1096–9.

Punjabi OS, Lin CF, Chung HS, et al. Melanocytoma of the optic disc associated with visual field defects: clinical features and imaging characteristics. Ophthalmic Surg Lasers Imaging. 2011;42:e75–80. https://doi.org/10.3928/15428877-20110804-06.

Sagoo MS, Shields CL, Emrich J, et al. Plaque radiotherapy for juxtapapillary choroidal melanoma: treatment complications and visual outcomes in 650 consecutive cases. JAMA Ophthalmol. 2014;132:697–702.

Salvanos P, Utheim TP, Moe MC, et al. Autofluorescence imaging in the differential diagnosis of optic disc melanocytoma. Acta Ophthalmol. 2015;93:476–80.

Shields JA, Shields CL, Eagle RC, et al. Malignant melanoma associated with melanocytoma of the optic disc. Ophthalmology. 1990;97:225–30.

Shields JA, Shields CL, Piccone M, et al. Spontaneous appearance of an optic disk melanocytoma in an adult. Am J Ophthalmol. 2002;134:614–5.

Shields JA, Demirci H, Mashayekhi A, et al. Melanocytoma of optic disc in 115 cases: the 2004 Samuel Johnson Memorial Lecture, part 1. Ophthalmology. 2004;111:1739–46.

Shields CL, Perez B, Benavides R, et al. Optical coherence tomography of optic disk melanocytoma in 15 cases. Retina. 2008;28:441–6.

Shukla SY, Shields JA, Eagle RC, et al. Transformation of optic disc melanocytoma into melanoma over 33 years. Arch Ophthalmol. 2012;130:1344–7.

Urrets-Zavalia JA, Crim N, Esposito E, et al. Bevacizumab for the treatment of a complicated posterior melanocytoma. Clin Ophthalmol. 2015;9:455–9.

Usui T, Shirakashi M, Kurosawa A, et al. Visual disturbance in patients with melanocytoma of the optic disk. Ophthalmologica. 1990;201:92–8.

Wiznia RA, Price J. Recovery of vision in association with a melanocytoma of the optic disk. Am J Ophthalmol. 1974;78:236–8.

Zhang P, Hui YN, Xu WQ, et al. Infrared autofluorescence, short-wave autofluorescence and spectral-domain optical coherence tomography of optic disk melanocytomas. Int J Ophthalmol. 2016;9:713–6.

Zimmerman LE. Pigmented tumors of the optic nerve head; The 22nd Annueal de Schweinitz Lecture. Am J Ophthalmol. 1960;50:338.

Zimmerman LE. Melanocytes, melanocytic nevi, and melanocytomas. Investig Ophthalmol. 1965;4:11–41.

Zimmerman LE, Garron LK. Melanocytoma of the optic disc. Int Ophthalmol Clin. 1962;2:431–40.

Intraocular Medulloepithelioma

15

Shweta Rathi Gupta and Swathi Kaliki

15.1 Introduction

Intraocular medulloepithelioma is a rare embryonal neuroepithelial tumor that originates from the undifferentiated medullary epithelium over the ciliary body or inner layer of the optic cup (Zimmerman 1971; Fuchs 1908). It commonly arises from the nonpigmented ciliary epithelium of the pars plicata and rarely in the iris, retina, optic nerve, and the central nervous system (Verhoeff 1904; Takei et al. 2007; Morris and Garner 1975; Vadmal et al. 1996; Green et al. 1974; Chavez et al. 2004; Sundaram et al. 2003; Steinkuller and Font 1997).

Badal and Lagrange initially recognized medulloepithelioma in 1892 as "carcinoma primitif" which was later termed as "teratoneuroma" by Verhoeff in 1904. Fuchs labelled it as "diktyoma" due to the presence of network of medullary epithelial bands. Finally, Grinker coined the term "medulloepithelioma" in 1931 (Verhoeff 1904; Fuchs 1908; Grinker 1931).

15.2 Etiopathogenesis

Medulloepithelioma in children arises from undifferentiated ciliary epithelium (Zimmerman 1971). However, acquired medulloepithelioma in adults is believed to arise from completely differentiated ciliary epithelium through a stage of nonneoplastic pseudoadenomatous hyperplasia (Broughton and Zimmerman 1978) and does not have embryonic features on histopathology (Shields et al. 1996a, b). According to Fuchs, adult medulloepitheliomas occur as a result of neoplastic transformation of hyperplastic ciliary epithelium, usually in inflamed or traumatized eyes (Fuchs 1908).

S. R. Gupta · S. Kaliki (✉)
Ocular Oncology Service, The Operation Eyesight Universal Institute for Eye Cancer (SRG, SK), L V Prasad Eye Institute, Hyderabad, India

15.3 Clinical Presentation

Medulloepithelioma is the second most common primary intraocular neoplasm in children. It occurs in children at a median age of 2–5 years with 75–90% of tumors presenting in the first decade of life (Broughton and Zimmerman 1978; Shields et al. 1996a, b; Canning et al. 1988; Kaliki et al. 2013a, b) Fig. 15.1. However, delayed presentation in adults (age more than 20 years) has been mentioned in isolated case reports (Husain et al. 1998; Jumper et al. 1999; Litricin and Latkovic 1985; Floyd et al. 1982; Wolter and James 1958; Font and Rishi 2005; Pushker et al. 2008). Unilateral presentation is common in this tumor, but a bilateral case has also been reported in the literature (Lumbroso et al. 2001).

15.3.1 Symptoms

Clinical diagnosis of intraocular medulloepithelioma is a huge challenge due to its rarity. Poor vision (41%), pain (30%), and leukocoria (18%) were the major symptoms as described in clinicopathologic study of 56 cases (Broughton and Zimmerman 1978). Initial misdiagnosis as well as mismanagement of ciliary body medulloepithelioma as neovascular glaucoma, congenital glaucoma, and uveitis is common, which results in delayed diagnosis (Shields et al. 1996a, b). This delay in diagnosis also occurs secondary to difficulty in directly visualizing the ciliary body mass until its enlargement leads to secondary effects (Alkatan et al. 2011; Kaliki et al. 2013a, b; Kanavi et al. 2007). Thus, the interval between age at first presentation and age at diagnosis may extend up to 5 years (Alkatan et al. 2011).

15.3.2 Signs

The typical secondary effects produced by ciliary body medulloepithelioma that are clinically detected include sec-

D. Rojanaporn (ed.), *Ocular Oncology*, https://doi.org/10.1007/978-981-13-2336-2_15

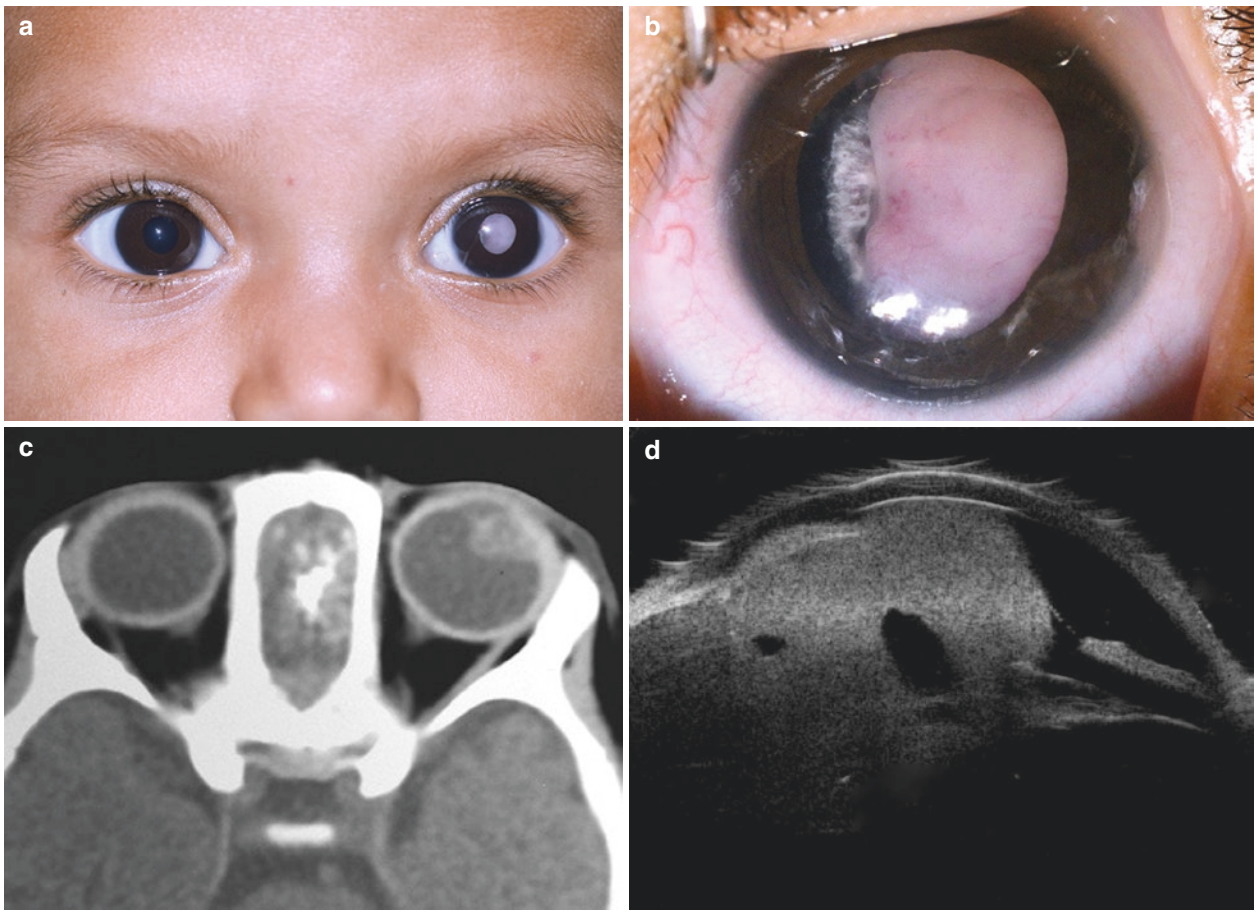

Fig. 15.1 Clinical presentation of ciliary body medulloepithelioma. A 3-year-girl presented with (**a**) leukocoria in the left eye. (**b**) Pinkish mass behind the iris with infiltration of the iris root (white arrow) causing lens resorption (yellow arrow). (**c**) Computed tomography of the orbit showed a heterogeneous hyperdense mass in the temporal aspect of ciliary body in the left eye. (**d**) Ultrasound biomicroscopy of the left eye showing solid mass involving the ciliary body with intralesional cystic spaces (white arrows)

ondary glaucoma (48–60%) and cataract with or without lens subluxation (26–50%), pupillary changes, and extraocular extension leading to proptosis (Broughton and Zimmerman 1978; Shields et al. 1996a, b; Canning et al. 1988; Kaliki et al. 2013a, b; Jumper et al. 1999; Husain et al. 1998).

A white, gray, yellow, or fleshy pink-colored nonpigmented cyst/mass in the ciliary body, iris, or anterior chamber is a classic clinical sign of medulloepithelioma in more than half of the cases (Broughton and Zimmerman 1978; Shields et al. 1996a, b). Although it arises from the nonpigment epithelium, pigmented medulloepitheliomas have also been reported (Shields et al. 2002; Gopal et al. 2004). The intratumoral cysts are detected in 60% cases (Shields et al. 1996a, b).

Secondary glaucoma either due to neovascularization, tumor infiltration, or angle closure is the second most common clinical sign. Another common clinical sign as well as the most common cause of decreased vision are lens changes including lens coloboma, subluxation, or cataract (Shields et al. 1996a, b). It is assumed that tumor growth at the ciliary body region interferes with the development of zonular complex due to mechanical effects. Therefore, a lens coloboma in the absence of uveal coloboma is a distinguishing feature and might be the earliest manifestation of mass in the ciliary body region (Gupta et al. 2001).

Iris neovascularization can be seen in about 86% of cases without an obvious cause; therefore it should be considered as another earliest indicator of medulloepithelioma (Singh et al. 2001). Masquerades such as uveitis can also be a manifestation of this tumor at the time of presentation (Alkatan et al. 2011).

Medulloepithelioma exhibits a unique tendency to produce a retrolental neoplastic cyclitic membrane in nearly half of the cases. This membrane occurs secondary to tumor extension, and it signifies the migration of neoplastic tissue from the mass over the anterior hyaloid (Shields et al. 1996a, b; Kaliki et al. 2013a, b).

15.3.3 Systemic Associations

Majority of these tumors are sporadic, but they can present as a manifestation of a tumor predisposition syndrome associated with DICER1-related pleuropulmonary blastoma. Systemic association of ciliary body medulloepithelioma and pleuropulmonary blastoma has been initially identified by Priest et al. Subsequently, Kaliki et al. described that <1% of patients with pleuropulmonary blastoma present with obvious ciliary body medulloepithelioma and 5% of patients with medulloepithelioma have a history of pleuropulmonary blastoma (Priest et al. 2011; Kaliki et al. 2013a, b).

Association of medulloepithelioma with central nervous system malformations such as schizencephaly, agenesis of the corpus callosum, and mass-like prominence of the quadrigeminal plate has also been described (Steinkuller and Font 1997). Rarely retinoblastoma and intracranial neoplasms such as pinealoblastoma can occur concurrently with medulloepithelioma (Mamalis et al. 1992; Minoda et al. 1993).

15.3.4 Differential Diagnosis

Differential diagnoses of medulloepithelioma include other intraocular tumors such as retinoblastoma and uveal melanoma as well as Coats' disease, persistent fetal vasculature, and Toxocara endophthalmitis (Steinkuller and Font 1997; Shields et al. 1989; Zhou et al. 2006). Medulloepithelioma can be easily distinguished from retinoblastoma by its location in the ciliary body and characteristic lack of calcification in the nonteratoid variant. On the other hand, retinoblastoma is commonly located in the posterior pole, has distinct clinical signs, and shows the presence of calcifications in 70% of patients. Similarly, it is very challenging to distinguish between a calcified anterior chamber retinoblastoma and a teratoid medulloepithelioma containing calcification. However, anterior chamber retinoblastoma is more common in older children and is frequently associated with diffuse infiltration of the iris and vitreous (Potter et al. 1996; Vajaranant et al. 2005). Although cystic variants of retinoblastomas have been described, classic retinoblastoma does not show intratumoral cysts, which is a characteristic feature of medulloepithelioma. Moreover, 95% of retinoblastomas occur in children younger than 5 years with mean age of presentation at 18 months, whereas 75–90% of medulloepitheliomas present in the first decade of life with mean age of presentation at 4 years (Broughton and Zimmerman 1978; Shields et al. 1996a, b; Canning et al. 1988; Kaliki et al. 2013a, b). Even though ciliary body melanomas closely resemble medulloepitheliomas on imaging and location, it is a rare tumor in pediatric age group (Barr et al. 1981) and is generally solid with isolated reports of cystic variants (Peyman and Mafee 1987).

Coats' disease is a unilateral retinal telangiectasia with the presence of subretinal exudates and does not show calcification or enhancement of the subretinal space on imaging. The presence of retrolental neoplastic cyclitic membrane in medulloepithelioma also assists in differentiating medulloepithelioma from retinoblastoma and Coats' disease (Sharma et al. 2011; Shields et al. 1996a, b). Toxocara endophthalmitis generally occurs in children older than 5 years, often having a history of contact with dogs and positive serology. Although less likely, metastatic disease, congenital iris epithelial/posttraumatic cysts, and xanthogranulomas should also be considered (Sansgiri et al. 2013).

15.4 Ancillary Investigations

Clinical examination plays a vital role in the diagnosis of medulloepithelioma. However, imaging modalities such as B-scan ultrasonography (USG B scan), ultrasound biomicroscopy (UBM), anterior segment optical coherence tomography (AS-OCT), computed tomography (CT scan), magnetic resonance imaging (MRI), and fundus fluorescein angiography (FFA) help in discerning the tumor from other ciliary body masses, in identifying tumor extension as well as distant spread, and in recognizing associated ocular complications (Sansgiri et al. 2013).

15.4.1 Ultrasonography, Ultrasound Biomicroscopy, and Anterior Segment Optical Coherence Tomography

On ultrasonography, the typical features of medulloepithelioma are highly echogenic heterogeneous mass arising from the ciliary body with multiple intratumoral cystic spaces and irregular internal reflectivity (Ayres et al. 2006; Zhou et al. 2006). It plays an important role in identifying cysts in large tumors. Sometimes there may be diffuse thickening of ciliary body or only enlarged globe with large axial length without an identifiable mass (Alkatan et al. 2011).

Retinal detachments and subretinal exudates can be seen clearly in USG. Teratoid type of medulloepithelioma may show hyperechoic foci or definite shadowing suggestive of intraocular calcifications (Sansgiri et al. 2013).

UBM and AS-OCT also help in visualization of the medium to highly reflective ciliary body mass with intratumoral cystic spaces (Gündüz et al. 2007). Sometimes, these cysts containing hyaluronic acid can dislodge from the tumor and float freely in the aqueous and vitreous (Broughton and

Zimmerman 1978; Spicer and Greeves 1915; Shields et al. 1996a, b).

15.4.2 Computed Tomography

CT scan of the orbit shows heterogeneous noncalcified tumor with solid and cystic elements along with intense enhancement of the solid component. Small tumors might lack the characteristic cystic components and appear as hyperdense enhancing masses. About one-third of teratoid medulloepitheliomas contain cartilage that can undergo dystrophic calcification and appear as a densely irregular calcified ciliary body mass. CT allows better visualization of calcification and the low-attenuation cartilaginous tissue in the teratoid variant (Shields et al. 1996a, b; Vajaranant et al. 2005).

15.4.3 MRI Imaging

Imaging findings play supportive role in diagnosis of a mass confined to the ciliary body area without retinal involvement, and understanding of such rare tumors is essential for precise diagnosis (Potter et al. 1996; Shields et al. 1996a, b). Imaging modalities are also beneficial in monitoring tumor recurrence and in ruling out associated intracranial CNS malformations or neoplasms (Steinkuller and Font 1997; Mamalis et al. 1992; Potter et al. 1996).

The solid component of the lesion characteristically appears as hyperintense to vitreous on T1-weighted images and hypointense on T2-weighted images, while cystic component appears isointense to hypointense to vitreous in both sequences. Additionally, there is moderate-intense contrast enhancement of solid components of the lesion on T1-W fat-saturated image after gadolinium administration (Vajaranant et al. 2005; Alkatan et al. 2011; Sansgiri et al. 2013).

15.4.4 Fluorescein Angiography

On fluorescein angiography, the retrolental neoplastic cyclitic membrane shows rapid filling of large, haphazard vessels emanating from the ciliary body across the hyaloid face. In contrast, total retinal detachment from retinoblastoma or Coats' disease, the vessels are regular, organized, and emanate from the closed central funnel of the detachment out toward the ciliary body region (Sharma et al. 2011; Shields et al. 1996a, b). This feature helps in differentiating medulloepithelioma from retinoblastoma and Coats' disease.

15.4.5 Histopathology

Histopathologic examination is still crucial for the definitive diagnosis of medulloepithelioma (Vajaranant et al. 2005). The tumor is characterized by nests, sheets, cords, and tubules composed of small, round blue cells surrounded by loose hyaluronic acid-rich mesenchymal tissue. These interlinking and interweaving neuroepithelial cells with a net-like appearance resemble the primitive medullary epithelium of the ciliary body or embryonic retina. Although not pathognomonic of medulloepithelioma, there can be scattered rosette formation (Homer–Wright, Flexner–Wintersteiner, and pseudorosettes) (Jumper et al. 1999; Husain et al. 1998; Steinkuller and Font 1997; Zhou et al. 2006; Sansgiri et al. 2013).

Histopathologically, medulloepitheliomas are classified into nonteratoid and teratoid types Figs. 15.2 and 15.3 based on the presence of heteroplastic tissue. Either group can be further classified as benign or malignant. On histopathologic examination, nonteratoid medulloepithelioma shows proliferation of primitive medullary epithelium, whereas teratoid medulloepithelioma contains heteroplastic elements, including hyaline cartilage (most common), rhabdomyoblasts or striated muscle, or brain-like tissue in addition to the proliferation of the neuroepithelial elements (Zimmerman 1971). Although calcification is the hallmark of retinoblastoma, mineralization is sometimes noted in heteroplastic tissues of teratoid medulloepitheliomas (Broughton and Zimmerman 1978).

As described in the four largest case series in literature, 50–63% were nonteratoid, and 38–50% were teratoid with malignant lesions (19–80%) being more common than benign tumors (0–31%) (Zimmerman 1971; Broughton and Zimmerman 1978; Shields et al. 1996a, b; Canning et al. 1988; Kaliki et al. 2013a, b).

Histopathologic criteria for malignancy proposed by Zimmerman et al. include (1) the presence of areas composed of poorly differentiated neuroblastic cells resembling those of retinoblastoma; (2) sarcomatous changes in the heterologous components resembling chondrosarcoma, rhabdomyosarcoma, or embryonal sarcoma; (3) nuclear pleomorphism, or markedly abnormal mitotic activity (the most subjective criterion); and (4) invasion of the uveal stroma, cornea, or sclera with or without extraocular extension (Broughton and Zimmerman 1978; Shields et al. 1996a, b; Canning et al. 1988).

These high-risk pathological features prompt additional metastatic workup including a bone scan, bone marrow aspirate and/or biopsy, and lumbar puncture for cerebrospinal fluid cytology (Sansgiri et al. 2013).

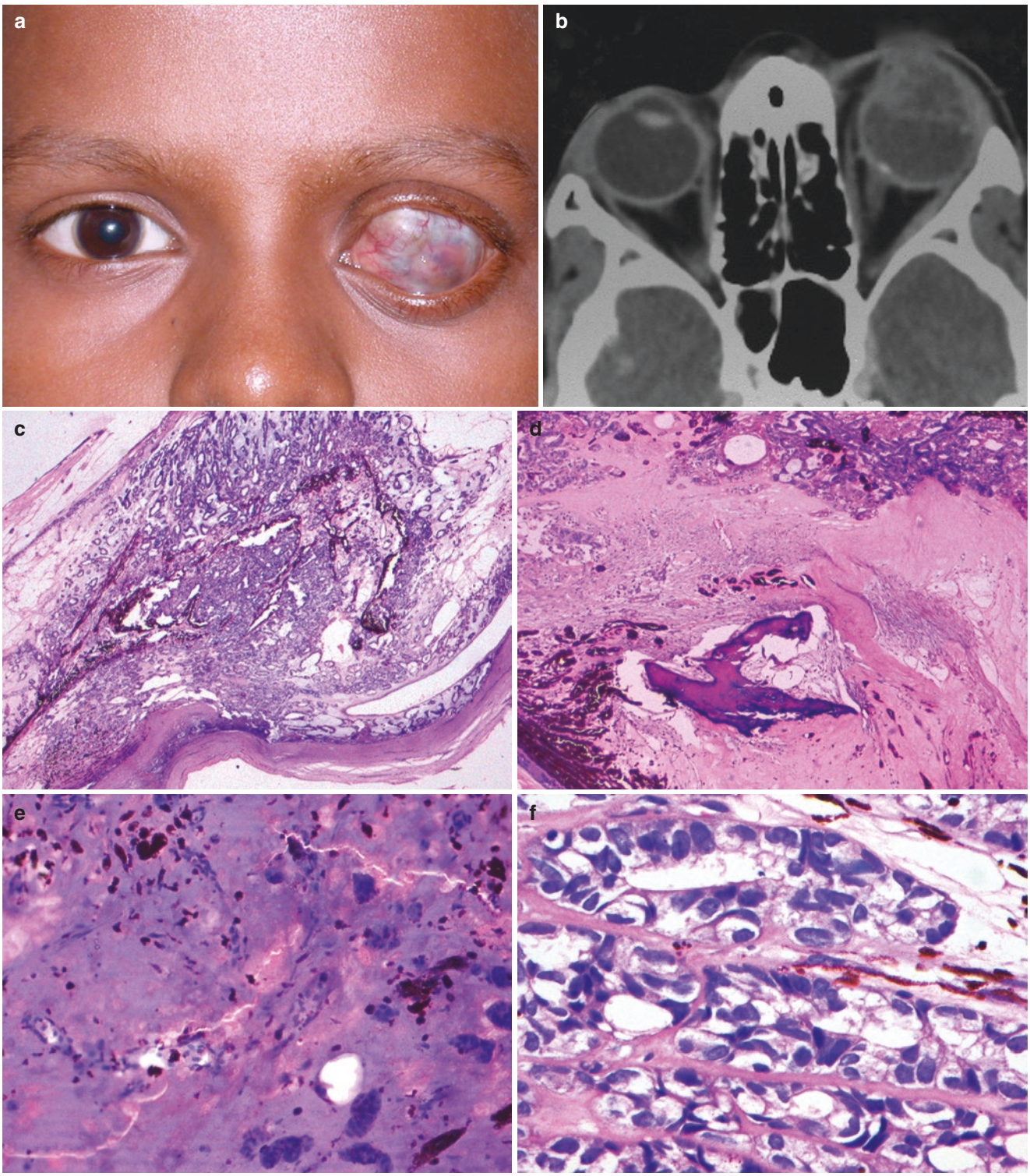

Fig. 15.2 Teratoid malignant ciliary body medulloepithelioma. A 13-year-old boy presented with (**a**) mass in the anterior chamber and ciliary staphyloma. (**b**) Computed tomography of the orbit showed enlarged anterior segment of the eye with a heterogeneous hyperdense mass involving the ciliary body and anterior chamber of the left eye. (**c**) Histopathology showed a highly cellular tumor with variegated appearance involving the ciliary body and filling the anterior chamber (hematoxylin and eosin stain, 2× magnification). (**d**) Abundant cytoplasm in the background with heterogeneous areas comprising of areas of the smooth muscle bundles, cartilage, bone, and glial tissue (hematoxylin and eosin stain, 4× magnification). (**e**) Tumor with cartilage background (hematoxylin and eosin stain, 10× magnification). (**f**) The individual cells are round with scant to moderate cytoplasm with vesicular nucleus and prominent nucleoli (hematoxylin and eosin stain, 40× magnification)

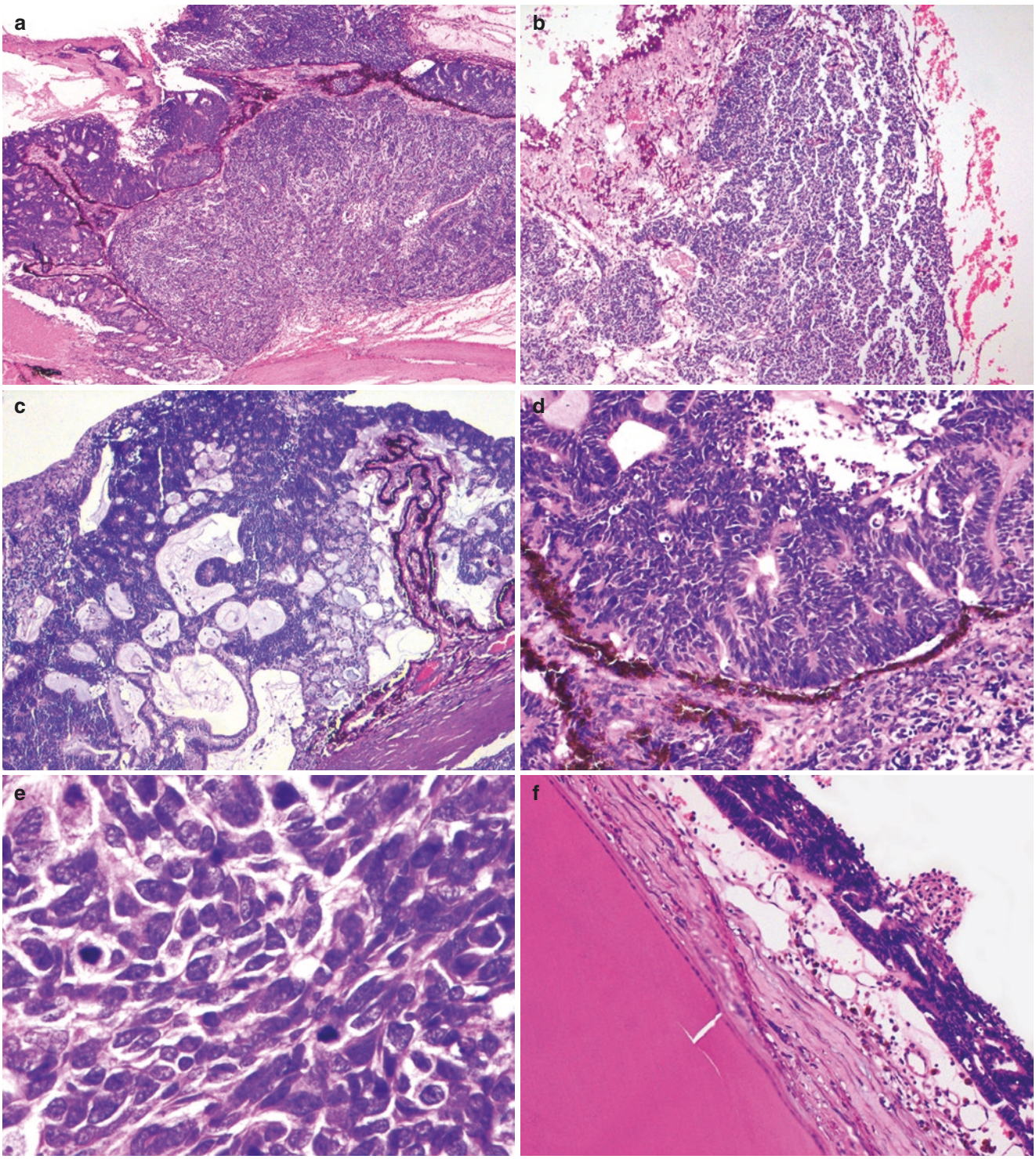

Fig. 15.3 Nonteratoid malignant ciliary body medulloepithelioma. (**a**) Cellular tumor involving the ciliary body, vitreous cavity, and anterior chamber (hematoxylin and eosin stain, 2× magnification). (**b**) Tumor involving the choroid (hematoxylin and eosin stain, 2× magnification). (**c**) Ciliary body tumor with neuroepithelial tissue arranged in tubules, sheets, glandular pattern, and cord-like arrangement (hematoxylin and eosin stain, 4× magnification). (**d**) Ciliary body tumor with medullary epithelium (hematoxylin and eosin stain, 10× magnification). (**e**) Oval basaloid tumor cells with high nucleus/cytoplasmic ratio with areas of mitosis (hematoxylin and eosin stain, 40× magnification). (**f**) Sheet of tumor tissue on the anterior surface of the lens (hematoxylin and eosin stain, 10× magnification)

15.5 Treatment

The treatment modalities for ciliary body medulloepithelioma include cryotherapy, local resection, plaque radiotherapy, enucleation, external beam radiotherapy, and systemic chemotherapy (Broughton and Zimmerman 1978; Shields et al. 1996a, b; Canning et al. 1988; Cassoux et al. 2010).

15.5.1 Cryotherapy

Cryotherapy can be used in smaller or minor local recurrent tumors (Broughton and Zimmerman 1978; Shields et al. 1996a, b).

15.5.2 Local Resection/Partial Lamellar Sclerouvectomy (PLSU)

Local resection can be considered for small well-circumscribed tumors (up to 4 clock hours) but is associated with tumor recurrence in 50–100% of cases. The reason for the recurrence is assumed to be the presence of thin membranes of tumor cells that are undetectable intraoperatively (Shields et al. 1996a, b; Shields et al. 2002; Ramasubramanian et al. 2012).

15.5.3 Plaque Radiotherapy

Plaque radiotherapy is the treatment option for smaller tumors either as a primary treatment or as adjuvant therapy after PLSU. Plaque radiotherapy (Ruthenium-106) with an apex dose of 2600–4000 cGy has shown tumor regression in various studies with no evidence of recurrence over a follow-up period of 12–26 months (Shields et al. 1996a, b; Davidorf et al. 2002; Kaliki et al. 2013a, b; Poon et al. 2015).

15.5.4 Enucleation

Enucleation is the preferred modality of treatment for large tumors and for smaller tumors that are unresponsive to conservative treatment. Most of the tumors are malignant based on histopathology and have poor visual potential, thus favoring enucleation. It has been shown that enucleation is effective in the absence of extrascleral extension with successful outcomes (Broughton and Zimmerman 1978; Shields et al. 1996a, b).

15.5.5 External Beam Radiotherapy (EBRT)

EBRT is planned to salvage eyes after surgical resection, as adjuvant therapy in the eyes with extrascleral or orbital extension (Canning et al. 1988) and extraocular dissemination because of the inadvertent intraocular surgery (Sansgiri et al. 2013).

15.5.6 Systemic Chemotherapy

The role of chemotherapy in treatment of medulloepithelioma is not well established. It is generally considered as adjuvant treatment after enucleation in tumors with extrascleral extension, in metastatic disease (Meel et al. 2010) as well as in cases of extraocular dissemination because of inadvertent intraocular surgery (Sansgiri et al. 2013).

15.6 Prognosis

Medulloepithelioma is slow-growing and locally invasive tumor (Shields et al. 1996a, b; Broughton and Zimmerman 1978).

The risk of metastatic disease and recurrence from ciliary body medulloepithelioma increases in the presence of extraocular tumor extension which can occur either through optic nerve/emissary vein invasion or in the setting of inadvertent intraocular surgery. Massive hematogenous spread to the lungs, mediastinum, and brain has been reported. Tumor-related death occurs mostly in cases with orbit involvement or intracranial extension or orbital recurrence (Broughton and Zimmerman 1978; Shields et al. 1996a, b; Canning et al. 1988; Kaliki et al. 2013a, b).

15.7 Conclusion

Medulloepithelioma is a rare childhood tumor. It should be considered in the differential diagnosis of an intraocular mass in a child, especially if it is near the ciliary body region.

References

Alkatan H, Al-Amry M, Al-Hussain H, et al. Medulloepithelioma of the ciliary body: the delay in diagnosis and frequent initial mismanagement. Can J Ophthalmol. 2011;46:431–8.

Ayres B, Brasil OM, Klejnberg C, et al. Ciliary body medulloepithelioma: clinical, ultrasound biomicroscopic and histopathologic correlation. Clin Exp Ophthalmol. 2006;34:695–8.

Barr CC, McLean IW, Zimmerman LE. Uveal melanoma in children and adolescents. Arch Ophthalmol. 1981;99:2133–6.
Broughton WL, Zimmerman LE. A clinicopathologic study of 56 cases of intraocular medulloepitheliomas. Am J Ophthalmol. 1978;85:407–18.
Canning CR, McCartney AC, Hungerford J. Medulloepithelioma (diktyoma). Br J Ophthalmol. 1988;72:764–7.
Cassoux N, Charlotte F, Sastre X, et al. Conservative surgical treatment of medulloepithelioma of the ciliary body [letter]. Arch Ophthalmol. 2010;128:380–1.
Chavez M, Mafee MF, Castillo B, et al. Medulloepithelioma of the optic nerve. J Pediatr Ophthalmol Strabismus. 2004;41:48–52.
Davidorf FH, Craig E, Birnbaum L, Wakely P Jr. Management of medulloepithelioma of the ciliary body with brachytherapy. Am J Ophthalmol. 2002;133:841–3.
Floyd BB, Minckler DS, Valentin L. Intraocular medulloepithelioma in a 79-year-old man. Ophthalmology. 1982;89:1088–94.
Font RL, Rishi K. Diffuse retinal involvement in malignant nonteratoid medulloepithelioma of ciliary body in an adult. Arch Ophthalmol. 2005;123:1136–8.
Fuchs E. Growths and tumors of the ciliary epithelium [in German]. Albrecht Von Graefes Arch Ophthalmol. 1908;68:534–87.
Gopal L, Babu K, Gupta S, et al. Pigmented malignant medulloepithelioma of the ciliary body. J Pediatr Ophthalmol Strabismus. 2004;41:364–6.
Green WR, Iliff WJ, Trotter RR. Malignant teratoid medulloepithelioma of the optic nerve. Arch Ophthalmol. 1974;91:451–4.
Grinker RR. Gliomas of the retina, including the results of studies with silver impregnations. Arch Ophthalmol. 1931;5:930–5.
Gündüz K, Hoşal BM, Zilelioğlu G, et al. The use of ultrasound biomicroscopy in the evaluation of anterior segment tumors and simulating conditions. Ophthalmologica. 2007;221:305–12.
Gupta NK, Simon JW, Walton DS, et al. Bilateral ectopia lentis as a presenting feature of medulloepithelioma. J AAPOS. 2001;5:255–7.
Husain SE, Husain N, Boniuk M, et al. Malignant nonteratoid medulloepithelioma of the ciliary body in an adult. Ophthalmology. 1998;105:596–9.
Jumper MJ, Char DH, Howes EL Jr, et al. Neglected malignant medulloepithelioma of the eye. Orbit. 1999;18:37–43.
Kaliki S, Eagle RC, Grossniklaus HE, et al. Inadvertent implantation of aqueous tube shunts in glaucomatous eyes with unrecognized intraocular neoplasms: a report of 5 cases. JAMA Ophthalmol. 2013a;131:925–8.
Kaliki S, Shields CL, Eagle RC Jr, et al. Ciliary body medulloepithelioma: analysis of 41 cases. Ophthalmology. 2013b;120:2552–9.
Kanavi MR, Soheilian M, Kamrava K, et al. Medulloepithelioma masquerading as chronic anterior granulomatous uveitis. Can J Ophthalmol. 2007;42:474–6.
Litricin O, Latkovic Z. Malignant teratoid medulloepithelioma in an adult. Ophthalmologica. 1985;191:17–21.
Lumbroso L, Disjardins L, Coue O, et al. Presumed bilateral medulloepithelioma. Arch Ophthalmol. 2001;119:449–50.
Mamalis N, Font RL, Anderson CW, et al. Concurrent benign teratoid medulloepithelioma and pineoblastoma. Ophthalmic Surg. 1992;23:403–8.
Meel R, Chawla B, Mohanti BK, et al. Ocular medulloepithelioma chemosensitivity. Ophthalmology. 2010;117:2440.
Minoda K, Hirose Y, Sugano I, et al. Occurrence of sequential intraocular tumors: malignant medulloepithelioma subsequent to retinoblastoma. Jpn J Ophthalmol. 1993;37:293–300.
Morris AT, Garner A. Medulloepithelioma involving the iris. Br J Ophthalmol. 1975;59:276–8.
Peyman GA, Mafee MF. Uveal melanoma and similar lesions: the role of magnetic resonance imaging and computed tomography. Radiol Clin N Am. 1987;25:471–86.
Poon DS, Reich E, Smith VM, et al. Ruthenium-106 plaque brachytherapy in the primary management of ocular medulloepithelioma. Ophthalmology. 2015;122:1949–51.
Potter PD, Shields CL, Shields JA, et al. The role of magnetic resonance imaging in children with intraocular tumors and simulating lesions. Ophthalmology. 1996;103:1774–83.
Priest JR, Williams GM, Manera R, et al. Ciliary body medulloepithelioma: four cases associated with pleuropulmonary blastomaea report from the International Pleuropulmonary Blastoma Registry. Br J Ophthalmol. 2011;95:1001–5.
Pushker N, Khuraijam N, Sen S, et al. Medulloepithelioma of the ciliary body associated with massive intravitreal hemorrhage in an adult [letter]. Can J Ophthalmol. 2008;43:253–4.
Ramasubramanian A, Shields CL, Kytasty C, et al. Resection of intraocular tumors (partial lamellar sclerouvectomy) in the pediatric age group. Ophthalmology. 2012;119:2507–13.
Sansgiri RK, Wilson M, McCarville M, et al. Imaging features of medulloepithelioma: report of four cases and review of the literature. Pediatr Radiol. 2013;43:1344–56.
Sharma P, Shields CL, Turaka K, et al. Ciliary body medulloepithelioma with neoplastic cyclitic membrane imaging with fluorescein angiography and ultrasound biomicroscopy. Graefes Arch Clin Exp Ophthalmol. 2011;249:1259–61.
Shields JA, Shields CL, Schwartz RL. Malignant teratoid medulloepithelioma of the ciliary body simulating persistent hyperplastic primary vitreous. Am J Ophthalmol. 1989;107:296–8.
Shields JA, Eagle RC Jr, Shields CL, et al. Fluorescein angiography and ultrasonography of malignant intraocular medulloepithelioma. J Pediatr Ophthalmol Strabismus. 1996a;33:193–6.
Shields JA, Eagle RC Jr, Shields CL, et al. Congenital neoplasms of the nonpigmented epithelium (medulloepithelioma). Ophthalmology. 1996b;103:1998–2006.
Shields JA, Eagle RC Jr, Shields CL, et al. Pigmented medulloepithelioma of the ciliary body. Arch Ophthalmol. 2002;120:207–10.
Singh A, Singh AD, Shields CL, et al. Iris neovascularization in children as a manifestation of underlying medulloepithelioma. J Pediatr Ophthalmol Strabismus. 2001;38:224–8.
Spicer WT, Greeves RA. Multiple cysts in the anterior chamber derived from a congenital cystic growth of the ciliary epithelium. Proc R Soc Med. 1915;8:9–26.
Steinkuller PG, Font RL. Congenital malignant teratoid neoplasm of the eye and orbit. Ophthalmology. 1997;104:38–42.
Sundaram C, Vydehi V, Jaganmohan Reddy J, et al. Medulloepithelioma: a case report. Neurol India. 2003;51:546–7. Br J Ophthalmol 59:276–8
Takei H, Florez L, Moroz K, et al. Medulloepithelioma: two unusual locations. Pathol Int. 2007;57:91–5.
Vadmal M, Kahn E, Finger P, et al. Nonteratoid medulloepithelioma of the retina with electron microscopic and immunohistochemical characterization. Pediatr Pathol Lab Med. 1996;16:663–72.
Vajaranant TS, Mafee MF, Kapur R, et al. Medulloepithelioma of the ciliary body and optic nerve: clinicopathologic, CT and MR imaging features. Neuroimaging Clin N Am. 2005;15:69–83.
Verhoeff FH. A rare tumor arising from the pars ciliaris retinae (teratoneuroma) of a nature hitherto unrecognized, and its relation to the so-called glioma-retinae. Trans Am Ophthalmol Soc. 1904;10:351–77.
Wolter JR, James BR. Adult type of medullo-epithelioma of the ciliary body. Am J Ophthalmol. 1958;46:19–26.
Zhou M, Xu G, Bojanowski CM, et al. Differential diagnosis of anterior chamber cysts with ultrasound biomicroscopy: Ciliary body medulloepithelioma. Acta Ophthalmol Scand. 2006;84:137–9.
Zimmerman LE. Verhoeff's "terato-neuroma". A critical reappraisal in light of new observations and current concepts of embryonic tumors. The Fourth Frederick H. Verhoeff Lecture. Am J Ophthalmol. 1971;72:1039–57.

Paraneoplastic-Related Retinopathy

16

Tharikarn Sujirakul and Stephen H. Tsang

16.1 Introduction

Paraneoplastic retinopathy is a spectrum of rare immune-mediated inflammatory diseases associated with advance stage of malignancy or metastasis tumor. Overall, paraneoplastic syndrome affecting nervous and visual system occurs in 0.01% of patients, but the true incidence of paraneoplastic retinopathy remains unknown (Darnell and Posner 2009). Common malignancies associated with paraneoplastic retinopathy include lung, breast, prostate, and gynecologic cancer and malignant melanoma.

Patients with paraneoplastic retinopathy usually presented with progressive painless visual loss, with the outer retina and photoreceptors being the major affected sites. It is not uncommon that the patients present without previous history of cancer, and the diagnosis of paraneoplastic retinopathy frequently leads to the discovery of underlying malignancy. Ocular symptoms may present years before the diagnosis of malignancy in some patients.

Selected clinical presentations such as cancer-associated retinopathy (CAR), melanoma-associated retinopathy (MAR), paraneoplastic vitelliform maculopathy (PVM), and bilateral diffuse uveal melanocytic proliferation (BDUMP) will be described here.

16.2 Etiopathogenesis

The pathophysiology of each paraneoplastic retinopathies is varying. Two major theories were described. First, the molecular mimicry between tumor antigen and retinal protein results in cross-reactivity between antibodies against the tumor antigen and normal retinal tissue. The immune reactions lead to dysfunction of normal retinal tissue with or without apparent structural abnormality. This mechanism is responsible for CAR, MAR, and PVM.

Second, the tumor produces functional protein similar to growth factor which released to circulation causing cellular proliferations in the distance tissue. This mechanism is believed to be responsible for BDUMP.

16.3 Clinical Features

16.3.1 Cancer-Associated Retinopathy (CAR)

First described in 1976 by Sawyer, it is characterized by rapid painless progressive bilateral visual loss over weeks to months (Sawyer et al. 1976). Rod system is predominantly affected in this disease setting; patients usually have nyctalopia, photopsia, and peripheral visual field loss as presenting symptoms. Later cone system will present with photosensitivity, decreased central vision, and impaired color vision.

CAR usually presents as a bilateral and symmetrical disease, but bilateral asymmetrical cases or unilateral cases have been reported (Chan 2003; Javaid et al. 2016; Roels et al. 2017). The average age of patients is 65 years, with women affected more frequently than men (2:1 ratio) (Adamus 2009). Approximately half of CAR patients have vision problem as presenting symptom before the diagnosis of malignancy can be made (Chan 2003).

Common malignancies associated with CAR include small-cell lung carcinoma and breast, colon, prostate, and gynecologic malignancies (Adamus 2009).

Other malignancies such as hematologic, non-small-cell lung cancer and thymus, thyroid, pancreatic, bladder, oral, and nasopharyngeal malignancies have been reported (Chan 2003; Toro et al. 2009; Javaid et al. 2016; Weixler et al. 2016; Nivean et al. 2016; Roels et al. 2017).

T. Sujirakul
Department of Ophthalmology, Faculty of Medicine,
Ramathibodi Hospital, Mahidol University, Bangkok, Thailand

S. H. Tsang (✉)
Columbia University Medical Center, New York, NY, USA
e-mail: sht2@cumc.columbia.edu

D. Rojanaporn (ed.), *Ocular Oncology*, https://doi.org/10.1007/978-981-13-2336-2_16

Fundus findings in CAR patients vary from normal in early disease or show attenuated retinal arterioles, optic disc pallor, alteration, or mottling of retinal pigment epithelium (RPE) (Fig. 16.1). But bony spicule or RPE hyperplasia which is a typical characteristic in inherited retinal dystrophy is rarely found (Heckenlively and Ferreyra 2008). Accompanying with subtle vitritis or cystoid macular edema is not uncommon (Chan 2003; Makiyama et al. 2013).

Fundus autofluorescence (AF) imaging varies from unremarkable in early disease, subtle abnormality, hyper-AF ring, or diffuse hyper-hypo-AF pattern throughout the fundus later (Lima et al. 2012; Makiyama et al. 2013). Spectral domain optical coherence tomography (SD-OCT) often shows outer retinal abnormalities such as thinning of photoreceptor layer and loss of ellipsoid line along with macular atrophy (Fig. 16.2) which is

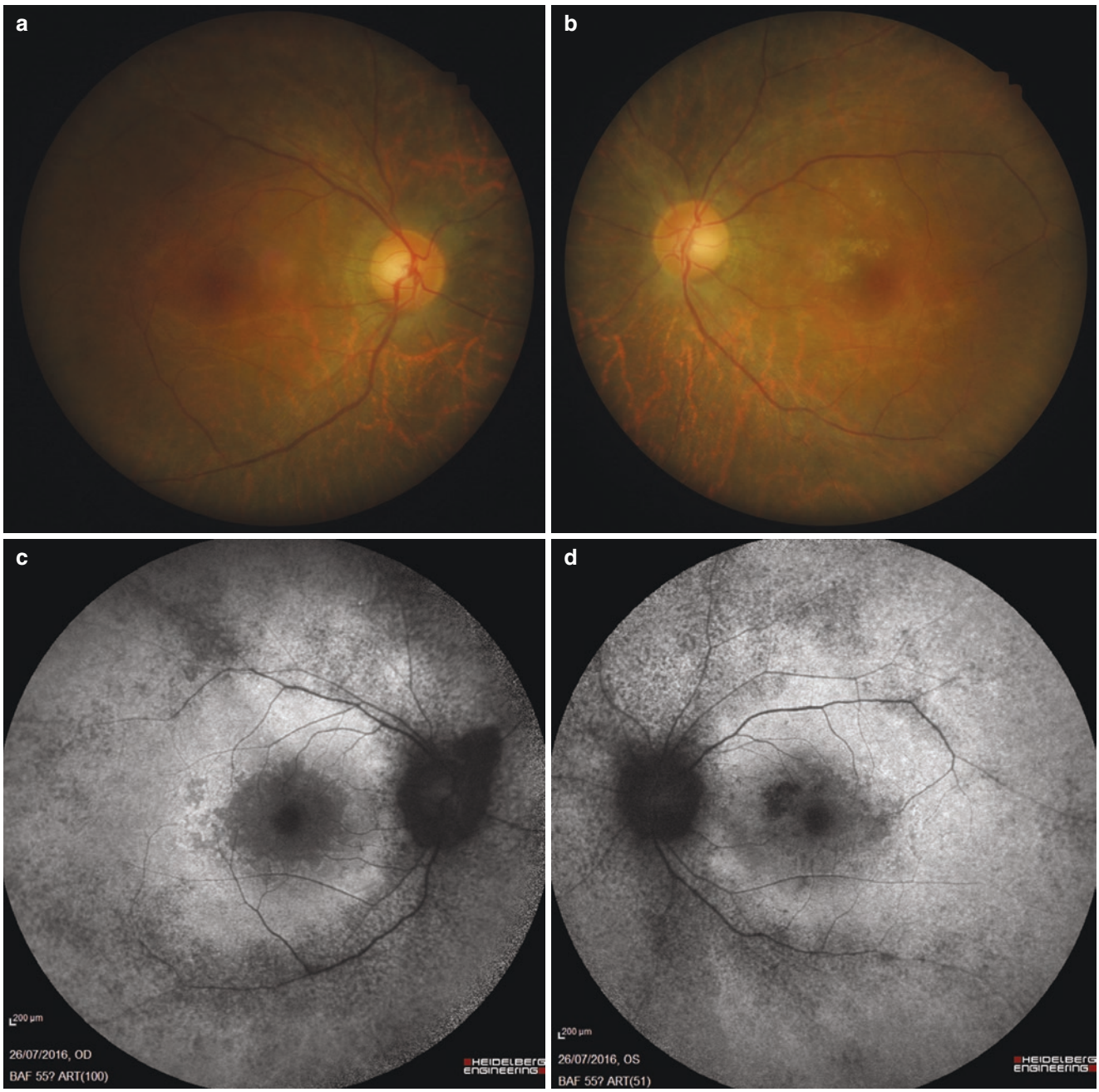

Fig. 16.1 A 43-year-old man with a history of nasopharyngeal carcinoma presented with decreased central vision to 20/30 in the right and 20/40 in the left and photopsia for 4 months. Color fundus photography at presentation showed retinal arterioles attenuation with RPE mottling throughout the retina without bony spicule in both eyes (**a**, **b**). Fundus autofluorescence (AF) imaging revealed area of hyper-hypo-AF progression from baseline (**c**, **d**) compared to 6 months later (**e**, **f**). Despite the AF progression, his vision remained stable with immunosuppressive therapy; no recurrent or metastasis of the cancer was identified

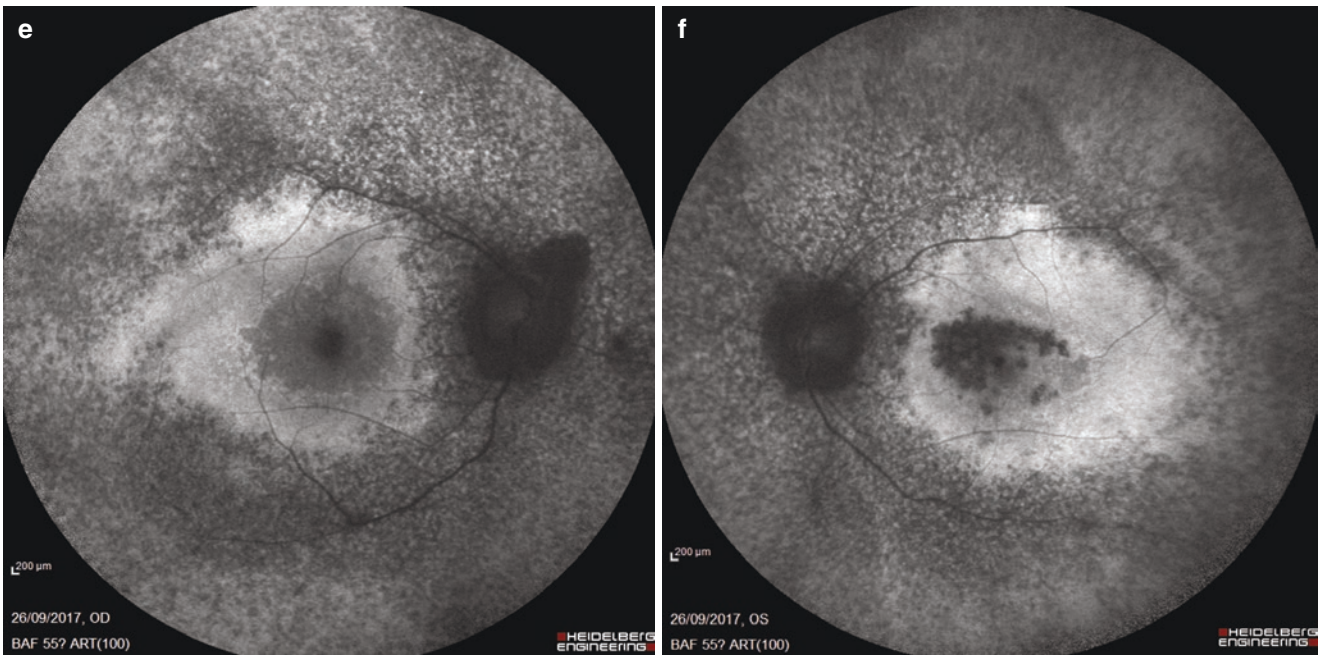

Fig. 16.1 (continued)

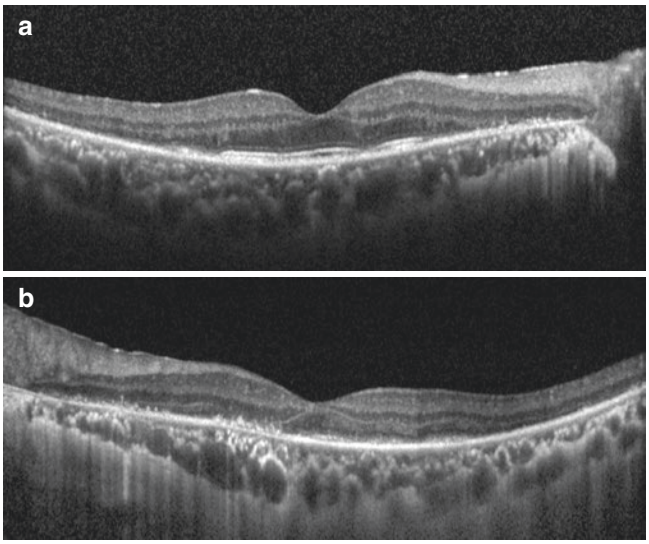

Fig. 16.2 SD-OCT of the same patient at presentation showed thinning of photoreceptor layer and loss of ellipsoid line. Ellipsoid disruption in macular area and macular atrophy is more pronounce in the left eye (**b**) compared to the right (**a**) and corresponded to visual acuity level and fundus autofluorescence findings

correlated to area of hyper-AF ring from AF imaging if presented.

Electroretinogram (ERG) provides an objective functional evaluation of both cone and rod systems and helps to differentiate photoreceptor dysfunction from inner retinal dysfunction. It is a valuable investigation for establishing the diagnosis of CAR especially when ophthalmic examinations are unremarkable. CAR patients always show severe rod and then cone dysfunction in ERG despite early disease or normal-looking fundus.

More severe cone dysfunction as compared to RP along with abnormal multifocal ERG or pattern ERG which reflected earlier macular involvement in CAR helps to differentiate the diagnosis from inherited rod-cone dystrophy (Braithwaite et al. 2014).

Many circulating anti-retinal antibodies have been reported to be associated with CAR. Approximately 65% of patients have detectable anti-retinal antibodies in their serum. Most frequent identified autoantibodies are anti-αenolase (46 kDA) 30%, anti-transducinα (40kDA) 17%, anti-carbonic anhydrase II (CAII) 14%, and anti-recoverin (23kDA) in 10% of patients (Adamus 2009).

Subgroup of CAR may exist according to different anti-retinal antibodies. Patients with anti-enolase antibody usually have history of malignancy by the time of presentation with symptoms related to isolated cone dysfunction. Patients usually have more indolent course and less severe disease compared to anti-recoverin antibody-related cases (Adamus et al. 1996; Weleber et al. 2005).

Unlike anti-enolase antibody-related disease, patients with anti-recoverin antibody often have ocular symptoms preceding the diagnosis of malignancy (Weleber et al. 2005). Patients usually have equally severe rod and cone dysfunction with rapidly deteriorating vision which often leads to blindness (Thirkill et al. 1993; Ohguro et al. 2004).

The major differential diagnoses of CAR include retinal dystrophy and autoimmune retinopathy. Patients with retinal

dystrophy typically have symptoms of rod dysfunction that slowly progress over the year without symptoms of cone or central vision problem until the later of disease unlike CAR. Autoimmune retinopathy is similar to anti-recoverin-related CAR in both clinical presentation and pathophysiology only without the association with malignancy (Heckenlively and Ferreyra 2008).

Patients with CAR often progress to severe visual loss; early treatment is necessary in order to preserve the vision. The goal for ocular treatment is to control the circulating autoantibodies since the treatment of tumor alone does not improve the course of ocular disease. Long-term immunosuppressive therapy is required. Multiple immunosuppressive agents such as corticosteroid and steroid-sparing immunomodulatory therapy such as azathioprine, cyclosporine, or mycophenolate mofetil have been used with variable outcome (Chan 2003; Shildkrot et al. 2011; Rahimy and Sarraf 2013; Grewal et al. 2014). Treatment with monoclonal antibodies against B-cell lymphocytes such as alemtuzumab and rituximab has shown some benefits in refractory cases (Espandar et al. 2007; Mahdi et al. 2010; Dy et al. 2013; Or et al. 2013). Periocular and intravitreal steroid injection has been used as an alternative treatment in order to minimize the side effects from systemic immunosuppressant (Ferreyra et al. 2009; Huynh et al. 2012). Other treatments including calcium channel blocker, plasmapheresis, and intravenous immunoglobulin (IVIg) have been tried (Guy and Aptsiauri 1999; Adamus et al. 2006).

16.3.2 Melanoma-Associated Retinopathy (MAR)

First reported by Berson and Lessel in 1988, patients typically have sudden onset of acquired night blindness along with shimmering light (Berson and Lessell 1988; Keltner et al. 2001). The symptoms usually associated with peripheral visual field constriction following with paracentral scotoma and central scotoma in later course of disease (Lu et al. 2009; Braithwaite et al. 2014). MAR patients usually present in their 50s and seem to affect men more than women (4.7:1 ratio) (Keltner et al. 2001).

Ophthalmic examination is usually normal in majority of cases; however retinal vessel attenuation, optic disc pallor, and presence of vitreous cell may be detected in some patients (Keltner et al. 2001; Lu et al. 2009). SD-OCT and AF findings are usually unremarkable (Keltner et al. 2001; Lu et al. 2009).

MAR is strongly associated with the metastasis of cutaneous malignant melanoma, although primary uveal or mucosal melanoma has been reported; once MAR is diagnosed, systemic workup for non-ocular metastasis is therefore indicated (Keltner et al. 2001; Rahimy and Sarraf 2013).

Since fundus findings are unremarkable in majority of MAR cases, ERG is a crucial investigation for making the diagnosis. Patients with MAR typically have electronegative ERG due to the loss of ON-bipolar cell function which resembles that of congenital stationary night blindness (Keltner et al. 2001; Lu et al. 2009; Braithwaite et al. 2014). Other differential diagnoses of electronegative ERG include central retinal artery occlusion, juvenile x-linked retinoschisis, vincristine toxicity, quinine toxicity, and ocular siderosis.

Antibodies against enolase, transducin, rhodopsin, arrestin, and transient receptor potential cation channel (TRMP1) have been reported in MAR patients (Potter et al. 2002; Hartmann et al. 2005; Adamus 2009; Bazhin et al. 2009; Duvoisin et al. 2017).

Treatments include decreasing tumor burden with surgical resection along with systemic immunosuppressive therapy such as corticosteroids and steroid-sparing agents. Other treatments such as plasma exchange, IVIg, interferon-β, and periocular or intraocular steroid injection have been used. The visual prognosis is still guarded despite all treatment modalities (Keltner et al. 2001; Rahimy and Sarraf 2013).

16.3.3 Paraneoplastic Vitelliform Maculopathy (PVM)

PVM is typically associated with cutaneous or choroidal melanoma but can be presented in the setting of lung, breast, and colon cancer (Sotodeh et al. 2005; Nieuwendijk and Hooymans 2007; Krema et al. 2010; Grunwald et al. 2011; Al-Dahmash et al. 2012; Kiratli et al. 2013; Williams et al. 2014; Gunduz et al. 2017; Nagiel et al. 2017).

Patients usually present with nyctalopia, blurring of vision, and metamorphopsia. Fundus findings show bilateral multifocal subretinal fluid with orange-yellow vitelliform lesions which sometimes gravitating to form vitelliform-fluid layer resemble those in acute exudative polymorphous vitelliform maculopathy and multifocal vitelliform Best's disease. Marked hyper-AF area is found corresponding to the vitelliform lesions seen in fundus findings (Fig. 16.3). SD-OCT shows multifocal area of subretinal fluid along with hyperreflective material beneath the interdigitation zone (Fig. 16.4).

ERG and electrooculogram (EOG) in PVM show variable results unlike in Best's disease that shows absent light rise in EOG consistently.

Anti-retinal and anti-RPE antibodies have been identified in PVM patients such as anti-26-kDa, anti-68-kDa RPE protein, anti-bestrophin-1, and anti-CAII which possibly resulted in accumulation of unprocessed cellular debris (Eksandh et al. 2008; Koreen et al. 2011; Aronow et al. 2012).

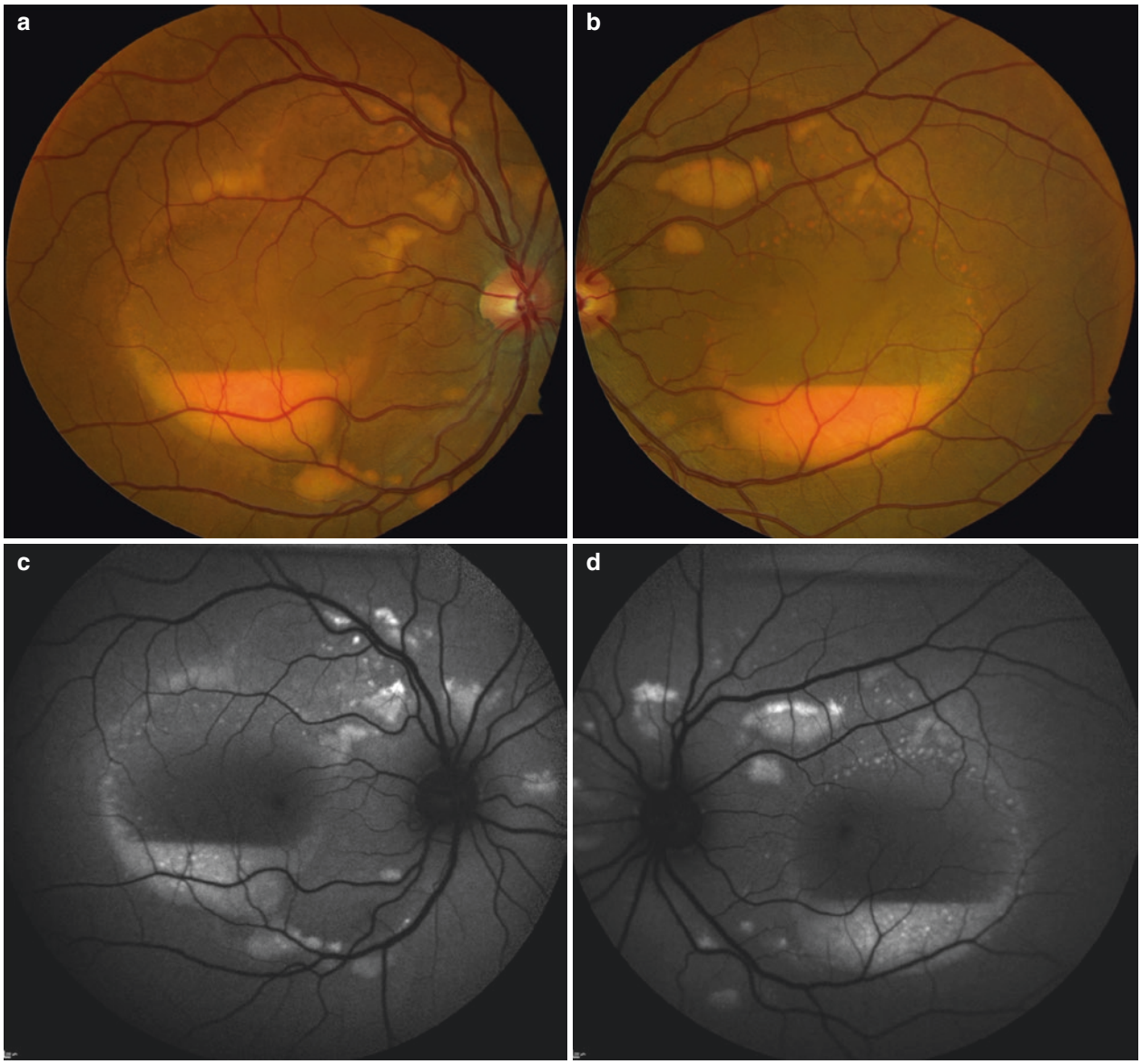

Fig. 16.3 A healthy, 34-year-old man presented with vision loss for 3 months in both eyes. Visual acuity was 20/25 in his right eye and 20/30 in his left eye. Funduscopy revealed multiple areas of yellowish lesions in the subretinal space with a gravitating pattern in the central lesion (**a**, **b**). Fundus autofluorescence (AF) imaging (**c**, **d**) revealed markedly hyper-AF lesions corresponding to vitelliform material in fundoscopy. Two months after presentation, he was found to have spinal, brain, and liver metastasis with malignant melanoma, but the primary site of the malignant melanoma could not be identified despite extensive workup

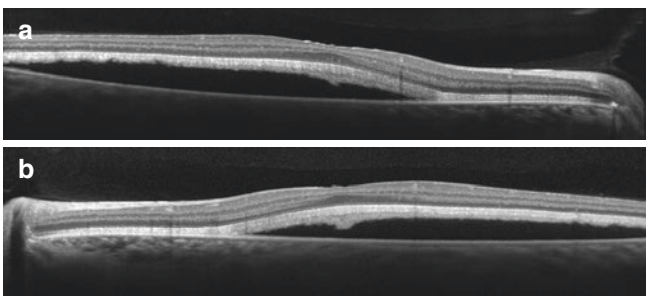

Fig. 16.4 SD-OCT across the fovea of the same patient shows the presence of subretinal fluid with hyperreflective materials deposited under the interdigitation zone (**a**, **b**)

PVM usually indicates metastasis disease; therefore, aggressive workup for systemic metastasis in the setting of PVM should be done despite long history of disease remission. The aim of treatments is to control the underlying metastasis disease including tumor resection, radiation, and chemotherapy. Ocular treatment such as intravitreal aflibercept injection has been tried recently showing some improvement of vision with reduction of subretinal fluid and vitelliform material (Gunduz et al. 2017). Despite all treatments, patients usually die from metastasis disease months to few years after the diagnosis of PVM was made (Rahimy and Sarraf 2013).

16.3.4 Bilateral Diffuse Uveal Melanocytic Proliferation (BDUMP)

First described in 1966 by Machemer and later classified by Gass (Machemer 1966; Gass et al. 1990), patients with BDUMP usually present with rapid onset of bilateral progressive visual loss. Ocular presentation often precedes the discovery of systemic malignancy months to years (Rahimy and Sarraf 2013). Frequent malignancies associated with BDUMP include urogenital in women and lung cancer in men, and other tumors such as pancreatic, breast, esophageal, and colon have been reported (O'Neal et al. 2003; Klemp et al. 2017).

Five cardinal signs of BDUMP were described by Gass (Gass et al. 1990):

(1) multiple subtle round or oval orange-red subretinal patches, (2) early hyperfluorescence in fluorescein angiogram corresponding to the patches, (3) slightly elevated pigmented and non-pigmented uveal melanocytic tumors with diffuse thickening of the choroid, (4) exudative retinal detachment, and (5) rapid cataract progression.

Fundus autofluorescence imaging is very helpful in order to highlight a typical BDUMP's "giraffe pattern" which is caused by polygonal or nummular RPE atrophy patches surrounded by RPE hypertrophy (Fig. 16.5).

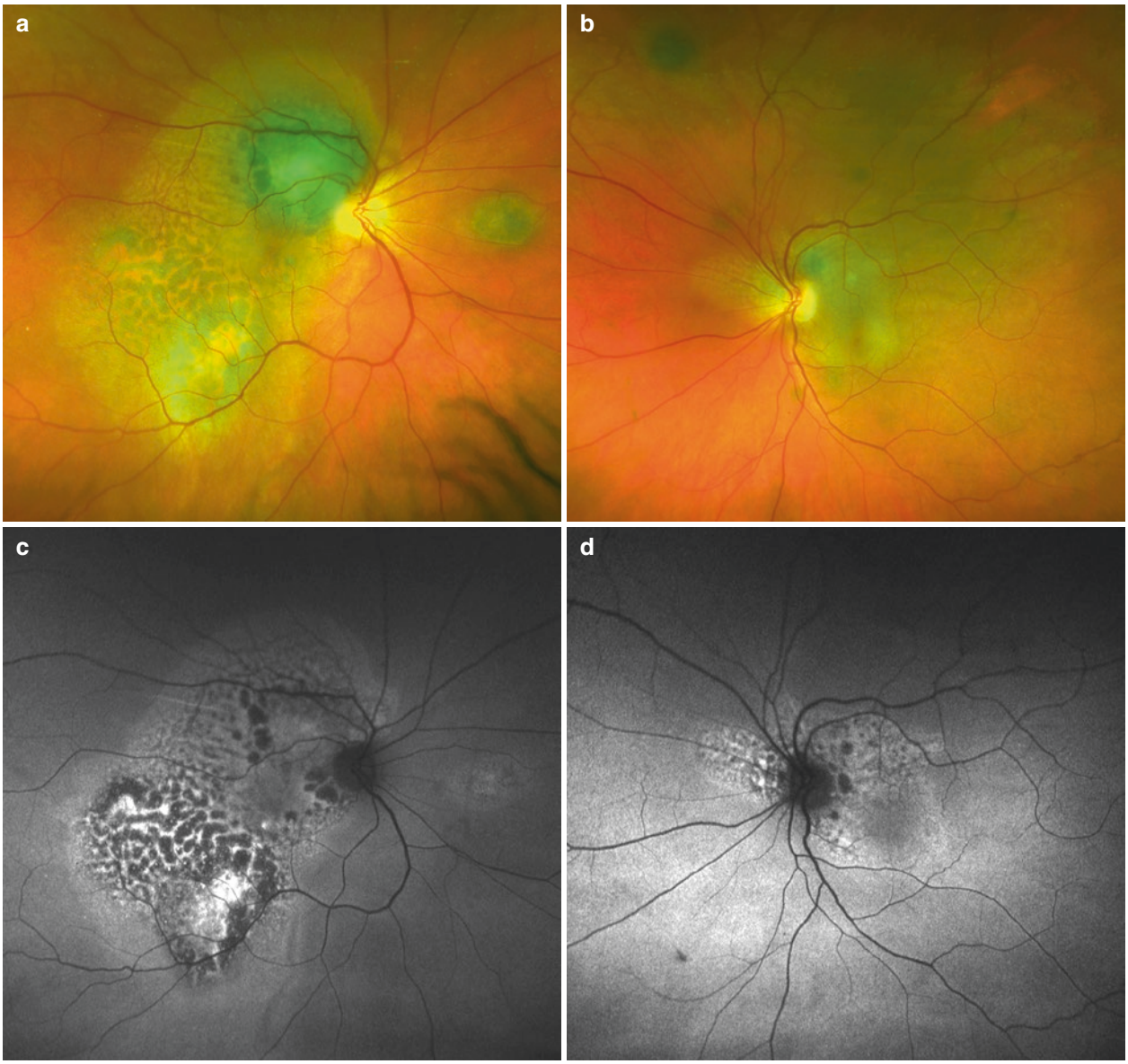

Fig. 16.5 A 59-year-old woman with a history of ovarian cancer presented with blurred vision for 1 month. Ultra-widefield color images (**a**, **b**) show exudative retinal detachment with multiple choroidal melanocytic lesions surrounded by subretinal orange lesions forming a "giraffe pattern." The pattern is more pronounced in fundus autofluorescence (AF) imaging (**c**, **d**). Hyper-AF area is corresponding to the subretinal orange lesions with hypo-AF area reflected RPE atrophy patches along with subretinal fluid tract (Photos courtesy of K. Bailey Freund, MD)

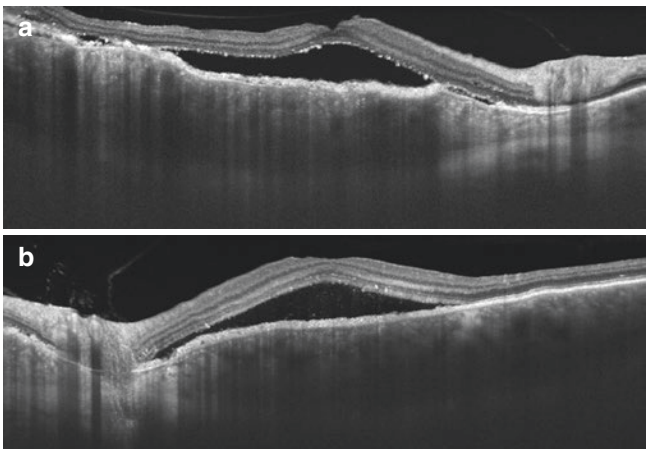

Fig. 16.6 Swept source OCT images (**a**, **b**) across the fovea demonstrate subretinal fluid with RPE thickening. RPE atrophy was noted in the scan corresponding to increased light transmission areas (arrow). Significantly increased in choroidal thickness is also shown here (Photos courtesy of K. Bailey Freund, MD)

SD-OCT overlying the lesions usually reveals subretinal fluid, RPD thickening, and increased choroidal thickness (Fig. 16.6).

Other associated findings such as iris mass and extraocular pigmented lesions have been reported in BDUMP patients (Joseph et al. 2014; Tada et al. 2015; Naysan et al. 2016).

Despite various ocular treatments with corticosteroid, radiation, and subretinal fluid drainage together with the treatment of underlying tumor, patients still suffer from visual deterioration. Newer studies have showed some promising results in patients treated with plasmapheresis (Jaben et al. 2011; Mets et al. 2011; Schelvergem et al. 2015).

16.4 Conclusion

Paraneoplastic retinopathies are a group of rare and devastating immune-mediated diseases which often lead to blindness. Making the diagnosis of paraneoplastic retinopathies can be very challenging given no characteristic fundus findings or clear diagnostic criteria.

One should be aware of the disease especially in patients presented with rapid progressive bilateral visual loss despite no previous history of malignancy. Electrophysiology testing is helpful to detect retinal dysfunction especially when ophthalmic examination is not contributing. Although the presence of circulatory anti-retinal antibodies shows some value aiding to the diagnosis, cautious interpretation is required because of the discrepancy between results when using different laboratory methods.

High suspicion of the disease in such clinical setting will lead to proper systemic investigation and early discovery of underlying tumor or metastasis. Prompt ocular treatment with immunosuppressive or immunomodulatory therapy together with the treatment of underlying malignancy might increase survival rate and preserve useful vision of the patients.

Acknowledgements The Jonas Children's Vision Care and Bernard & Shirlee Brown Glaucoma Laboratory are supported by the National Institutes of Health (P30EY019007, R01EY018213, R01EY024698, R01EY026682, R21AG050437), National Cancer Institute Core (5P30CA013696), Foundation Fighting Blindness (TA-NMT-0116-0692-COLU), the Research to Prevent Blindness (RPB) Physician-Scientist Award, and unrestricted funds from RPB, New York, NY, USA. S.H.T. is a member of the RD-CURE Consortium and is supported by Kobi and Nancy Karp, the Crowley Family Fund, the Rosenbaum Family Foundation, the Tistou and Charlotte Kerstan Foundation, the Schneeweiss Stem Cell Fund, New York State (C029572), and the Gebroe Family Foundation.

References

Adamus G. Autoantibody targets and their cancer relationship in the pathogenicity of paraneoplastic retinopathy. Autoimmun Rev. 2009;8:410–4.

Adamus G, Aptsiauri N, Guy J, et al. The occurrence of serum autoantibodies against enolase in cancer-associated retinopathy. Clin Immunol Immunopathol. 1996;78:120–9.

Adamus G, Webb S, Shiraga S, et al. Anti-recoverin antibodies induce an increase in intracellular calcium, leading to apoptosis in retinal cells. J Autoimmun. 2006;26:146–53.

Al-Dahmash SA, Shields CL, Bianciotto CG, et al. Acute exudative paraneoplastic polymorphous vitelliform maculopathy in five cases. Ophthalmic Surg Lasers Imaging. 2012;43:366–73.

Aronow ME, Adamus G, Abu-Asab M, et al. Paraneoplastic vitelliform retinopathy: clinicopathologic correlation and review of the literature. Surv Ophthalmol. 2012;57:558–64.

Bazhin AV, Dalke C, Willner N, et al. Cancer-retina antigens as potential paraneoplastic antigens in melanoma-associated retinopathy. Int J Cancer. 2009;124:140–9.

Berson EL, Lessell S. Paraneoplastic night blindness with malignant melanoma. Am J Ophthalmol. 1988;106:307–11.

Braithwaite T, Holder GE, Lee RW, et al. Diagnostic features of the autoimmune retinopathies. Autoimmun Rev. 2014;13:534–8.

Chan JW. Paraneoplastic retinopathies and optic neuropathies. Surv Ophthalmol. 2003;48:12–38.

Darnell RB, Posner JB. Autoimmune encephalopathy: the spectrum widens. Ann Neurol. 2009;66:1–2.

Duvoisin RM, Haley TL, Ren G, et al. Autoantibodies in melanoma-associated retinopathy recognize an epitope conserved between TRPM1 and TRPM3. Invest Ophthalmol Vis Sci. 2017;58:2732–8.

Dy I, Chintapatla R, Preeshagul I, et al. Treatment of cancer-associated retinopathy with rituximab. J Natl Compr Cancer Netw. 2013;11:1320–4.

Eksandh L, Adamus G, Mosgrove L, et al. Autoantibodies against bestrophin in a patient with vitelliform paraneoplastic retinopathy and a metastatic choroidal malignant melanoma. Arch Ophthalmol. 2008;126:432–5.

Espandar L, O'Brien S, Thirkill C, et al. Successful treatment of cancer-associated retinopathy with alemtuzumab. J Neuro-Oncol. 2007;83:295–302.

Ferreyra HA, Jayasundera T, Khan NW, et al. Management of autoimmune retinopathies with immunosuppression. Arch Ophthalmol. 2009;127:390–7.

Gass JD, Gieser RG, Wilkinson CP, et al. Bilateral diffuse uveal melanocytic proliferation in patients with occult carcinoma. Arch Ophthalmol. 1990;108:527–33.
Grewal DS, Fishman GA, Jampol LM. Autoimmune retinopathy and antiretinal antibodies: a review. Retina. 2014;34:827–45.
Grunwald L, Kligman BE, Shields CL. Acute exudative polymorphous paraneoplastic vitelliform maculopathy in a patient with carcinoma, not melanoma. Arch Ophthalmol. 2011;129:1104–6.
Gunduz K, Condu G, Shields CL. Acute exudative polymorphous paraneoplastic vitelliform maculopathy managed with intravitreal aflibercept. Ophthal Surg Laser Imag Retina. 2017;48:844–50.
Guy J, Aptsiauri N. Treatment of paraneoplastic visual loss with intravenous immunoglobulin: report of 3 cases. Arch Ophthalmol. 1999;117:471–7.
Hartmann TB, Bazhin AV, Schadendorf D, et al. SEREX identification of new tumor antigens linked to melanoma-associated retinopathy. Int J Cancer. 2005;114:88–93.
Heckenlively JR, Ferreyra HA. Autoimmune retinopathy: a review and summary. Semin Immunopathol. 2008;30:127–34.
Huynh N, Shildkrot Y, Lobo AM, et al. Intravitreal triamcinolone for cancer-associated retinopathy refractory to systemic therapy. J Ophthal Inflamm Infect. 2012;2:169–71.
Jaben EA, Pulido JS, Pittock S, et al. The potential role of plasma exchange as a treatment for bilateral diffuse uveal melanocytic proliferation: a report of two cases. J Clin Apher. 2011;26:356–61.
Javaid Z, Rehan SM, Al-Bermani A, et al. Unilateral cancer-associated retinopathy: a case report. Scott Med J. 2016;61:155–9.
Joseph A, Rahimy E, Sarraf D. Bilateral diffuse uveal melanocytic proliferation with multiple iris cysts. JAMA Ophthalmol. 2014;132:756–60.
Keltner JL, Thirkill CE, Yip PT. Clinical and immunologic characteristics of melanoma-associated retinopathy syndrome: eleven new cases and a review of 51 previously published cases. J Neuroophthalmol. 2001;21:173–87.
Kiratli H, Kadayifcilar S, Tarlan B. Paraneoplastic vitelliform retinopathy following ciliochoroidal melanoma. Ophthal Surg Laser Imag Retina. 2013;44:290–2.
Klemp K, Kiilgaard JF, Heegaard S, et al. Bilateral diffuse uveal melanocytic proliferation: case report and literature review. Acta Ophthalmol. 2017;95:439–45.
Koreen L, He SX, Johnson MW, et al. Anti-retinal pigment epithelium antibodies in acute exudative polymorphous vitelliform maculopathy: a new hypothesis about disease pathogenesis. Arch Ophthalmol. 2011;129:23–9.
Krema H, Simpson R, Altomare F, et al. Paraneoplastic vitelliform retinopathy in metastatic cutaneous melanoma. Retin Cases Brief Rep. 2010;4:246–50.
Lima LH, Greenberg JP, Greenstein VC, et al. Hyperautofluorescent ring in autoimmune retinopathy. Retina. 2012;32:1385–94.
Lu Y, Jia L, He S, et al. Melanoma-associated retinopathy: a paraneoplastic autoimmune complication. Arch Ophthalmol. 2009;127:1572–80.
Machemer R. On the pathogenesis of the flat malignant melanoma. Klin Monatsbl Augenheilkd. 1966;148(5):641–52.
Mahdi N, Faia LJ, Goodwin J, et al. A case of autoimmune retinopathy associated with thyroid carcinoma. Ocul Immunol Inflamm. 2010;18:322–3.
Makiyama Y, Kikuchi T, Otani A, et al. Clinical and immunological characterization of paraneoplastic retinopathy. Invest Ophthalmol Vis Sci. 2013;54:5424–31.
Mets RB, Golchet P, Adamus G, et al. Bilateral diffuse uveal melanocytic proliferation with a positive ophthalmoscopic and visual response to plasmapheresis. Arch Ophthalmol. 2011;129:1235–8.
Nagiel A, Rootman DB, McCannel TA. Paraneoplastic vitelliform maculopathy in the setting of choroidal melanoma: evolution over one year. Retin Cases Brief Rep. 2017;11(Suppl 1):S7–S10. https://doi.org/10.1097/ICB.0000000000000383.
Naysan J, Pang CE, Klein RW, Freund KB. Multimodal imaging of bilateral diffuse uveal melanocytic proliferation associated with an iris mass lesion. Int J Retina Vitreous. 2016;2:13. https://doi.org/10.1186/s40942-016-0038-7.
Nieuwendijk TJ, Hooymans JM. Paraneoplastic vitelliform retinopathy associated with metastatic choroidal melanoma. Eye (Lond). 2007;21:1436–7.
Nivean M, Muttuvelu DV, Afzelius P, et al. Paraneoplastic retinopathy associated with occult bladder cancer. Indian J Ophthalmol. 2016;64:248–50.
Ohguro H, Yokoi Y, Ohguro I, et al. Clinical and immunologic aspects of cancer-associated retinopathy. Am J Ophthalmol. 2004;137:1117–9.
O'Neal KD, Butnor KJ, Perkinson KR, et al. Bilateral diffuse uveal melanocytic proliferation associated with pancreatic carcinoma: a case report and literature review of this paraneoplastic syndrome. Surv Ophthalmol. 2003;48:613–25.
Or C, Collins DR, Merkur AB, et al. Intravenous rituximab for the treatment of cancer-associated retinopathy. Can J Ophthalmol. 2013;48(2):e35–8. https://doi.org/10.1016/j.jcjo.2012.11.010.
Potter MJ, Adamus G, Szabo SM, et al. Autoantibodies to transducin in a patient with melanoma-associated retinopathy. Am J Ophthalmol. 2002;134:128–30.
Rahimy E, Sarraf D. Paraneoplastic and non-paraneoplastic retinopathy and optic neuropathy: evaluation and management. Surv Ophthalmol. 2013;58:430–58.
Roels D, Ueno S, Talianu CD, et al. Unilateral cancer-associated retinopathy: diagnosis, serology and treatment. Doc Ophthalmol. 2017;135:233–40.
Sawyer RA, Selhorst JB, Zimmerman LE, et al. Blindness caused by photoreceptor degeneration as a remote effect of cancer. Am J Ophthalmol. 1976;81:606–13.
Schelvergem KV, Wirix M, Nijs I, et al. Bilateral diffuse uveal melanocytic proliferation with good clinical response to plasmapheresis and treatment of the primary tumor. Retin Cases Brief Rep. 2015;9:106–8.
Shildkrot Y, Sobrin L, Gragoudas ES. Cancer-associated retinopathy: update on pathogenesis and therapy. Semin Ophthalmol. 2011;26:321–8.
Sotodeh M, Paridaens D, Keunen J, et al. Paraneoplastic vitelliform retinopathy associated with cutaneous or uveal melanoma and metastases. Klin Monatsbl Augenheilkd. 2005;222:910–4.
Tada K, Higashi Y, Uchida Y, et al. Bilateral diffuse uveal melanocytic proliferation with mucocutaneous pigmentation. J Dermatol. 2015;42:1183–5.
Thirkill CE, Keltner JL, Tyler NK, et al. Antibody reactions with retina and cancer-associated antigens in 10 patients with cancer-associated retinopathy. Arch Ophthalmol. 1993;111:931–7.
Toro C, Rinaldo A, Silver CE, et al. Paraneoplastic syndromes in patients with nasopharyngeal cancer. Auris Nasus Larynx. 2009;36:513–20.
Weixler B, Oertli D, Nebiker CA. Cancer-associated retinopathy as the leading symptom in colon cancer. Clin Case Rep. 2016;4:171–6.
Weleber RG, Watzke RC, Shults WT, et al. Clinical and electrophysiologic characterization of paraneoplastic and autoimmune retinopathies associated with antienolase antibodies. Am J Ophthalmol. 2005;139:780–94.
Williams SL, McDonald HR, Jumper JM, et al. Paraneoplastic vitelliform retinopathy in a patient with treated choroidal melanoma. Retin Cases Brief Rep. 2014;8:269–72.

Sclerochoroidal Calcification

17

Tero T. Kivelä

17.1 Introduction

Sclerochoroidal calcification, deposition of calcium pyrophosphate within the sclera with secondary compression and atrophy of the choroid that can mimic a choroidal tumor, especially an osteoma, first appeared in case reports of patients with pseudohypoparathyroidism and hyperparathyroidism between 1979 and 1982 (Wong et al. 1979; Goldstein and Miller 1982). A patient with normal calcium and phosphorous metabolism was first published in 1989 by Lim and Goldberg (Lim and Goldberg 1989) after hearing a talk on another idiopathic case that Jerry Shields delivered at a meeting of the American Academy of Ophthalmology Fluorescein Angiography Club (Lim and Goldberg 1989; Shields and Shields 2002) in 1987; the same year, two cases misdiagnosed as osteomas were published (Wiesner et al. 1987). In 1989, seven patients with idiopathic sclerochoroidal calcification from the Wills Eye Hospital, Northwestern University, and University of Kentucky were reported in the annual meeting of the American Academy of Ophthalmology and published in 1991 by Sivalingam, Shields, Shields, McNamara, Jampol, Wood, and Daubert (Sivalingam et al. 1991), followed in 1992 by a report of 19 patients collected from seven hospitals (Schachat et al. 1992). The latter two papers established sclerochoroidal calcification as an entity: a benign, degenerative, usually bilateral lesion, located in the postequatorial, usually superotemporal fundus of patients who either are elderly or have a systemic abnormality of calcium, phosphorous, or magnesium metabolism. Sclerochoroidal calcification has later been shown to be a scleral lesion with secondary choroidal atrophy (Fung et al. 2013; Hasanreisoglu et al. 2015).

T. T. Kivelä (✉)
Department of Ophthalmology, University of Helsinki and Helsinki University Hospital, Helsinki, Finland

17.2 Etiopathogenesis

Because sclerochoroidal calcification is almost always asymptomatic and initially invisible ophthalmoscopically (Sivalingam et al. 1991; Schachat et al. 1992; Vezzoli et al. 2000; Honavar et al. 2001; Shields et al. 2004; Sugarman et al. 2017), it is not known at which age the calcifications first appear, but the earliest occurrences of the metastatic type have been at the age of 26 and 49 years in two patients with Gitelman syndrome (Vezzoli et al. 2000), 29 and 39 years in three patients with either hyperparathyroidism or pseudohypoparathyroidism (Wong et al. 1979; Suzuki et al. 1992; Kobune et al. 1993), 40 years in one of three patients with familial chondrocalcinosis (Boutboul et al. 2004), and 40–42 years in two patients with Bartter syndrome (Sun et al. 2005; Caminal-Mitjana et al. 2013; Caminal-Mitjana and Padrón-Pérez 2013). Only 3 patients reported to have the idiopathic type have been diagnosed equally early, at the age of 40, 41, and 43 years (McCabe et al. 1997; Zuercher and Zografos 2002; Caminal-Mitjana et al. 2013).

In metastatic calcification, calcium pyrophosphate dihydrate deposits in normal tissues because of either elevated serum levels or decreased excretion of calcium. Moreover, hypomagnesemia is postulated as a factor favoring the deposition. Hypomagnesemia inhibits pyrophosphate hydrolysis and reduces calcium pyrophosphate crystal solubility. The patients show deposition of calcium also often in the joints and sometime in the kidneys (Marchini et al. 1998; Bourcier et al. 1999; Gupta et al. 2005). An important underlying cause of *hyper*calcemia is primary hyperparathyreosis caused by a parathyroid adenoma. Secondary hyperparathyreosis, which most often results from renal failure, is characterized by insufficient conversion of vitamin D to its active form as well as by inadequate excretion of phosphate, leading to hyperplasia of the parathyroid glands, deposition of insoluble calcium phosphate in soft tissues, and *hypo*calcemia.

The histogenesis of idiopathic sclerochoroidal calcification is unresolved (Sivalingam et al. 1991; Schachat et al. 1992; Shields and Shields 2002). The typically bilateral involvement

D. Rojanaporn (ed.), *Ocular Oncology*, https://doi.org/10.1007/978-981-13-2336-2_17

hints to a systemic cause although the patients have no underlying derangement of calcium or phosphorous metabolism upon screening. Alternatively, chronic pulling by the oblique muscles might give rise to degenerative scleral changes that would predispose scleral collagen to dystrophic calcification (Sivalingam et al. 1991), a mechanism that is thought to explain scleral plaques, senile calcifications localized to the insertions of the horizontal rectus muscles (Wong and Kawasaki 2014). This theory finds support from the fact that the calcium deposits preferentially localize close to the insertion of the superior oblique muscle (Shields and Shields 2002).

17.3 Clinical Features

17.3.1 Incidence

Sclerochoroidal calcification is infrequent but more common than what might be judged from the medical literature. Between 2010 and 2017, over 65 patients appeared as small case series (Cooke et al. 2003; Schönherr and Graupner 2003; Boutboul et al. 2004; Lindstedt et al. 2007; Rao et al. 2012; Fung et al. 2013; Caminal-Mitjana et al. 2013) and as case reports in PubMed, and additionally a referral-based series of 118 patients spanning 30 years was described (Shields et al. 2015). However, only a fraction of sclerochoroidal calcifications diagnosed in retinal and ocular oncology services will ever be published. In our service, we diagnose approximately six cases per year, suggesting a minimum incidence on the order of three to six cases per million in our catchment area.

17.3.2 Age

The median age at presentation of all patients with sclerochoroidal calcification, calculated for 86 individuals reported from 1986 to 2017, is 70 years, 70 years for males and 72 years for females (Fig. 17.1). The median age of 26 patients with the metastatic type was 65 years with a range from 26 to 85 years as compared to a median age of 72 years and a range from 40 to 88 years for 60 patients with the idiopathic type; the diagnosis is made significantly earlier in the former group (Fig. 17.1). Of all patients, 13% were 50 years of age or younger and 34% were 75 years or older. These percentages were 31 and 14%, respectively, for the metastatic type as compared to 3 and 42%, respectively, for the idiopathic type. The mean age for all patients was 68 years, which corresponds with the mean age of 69 years reported in the referral-based series of 118 patients (Shields et al. 2015).

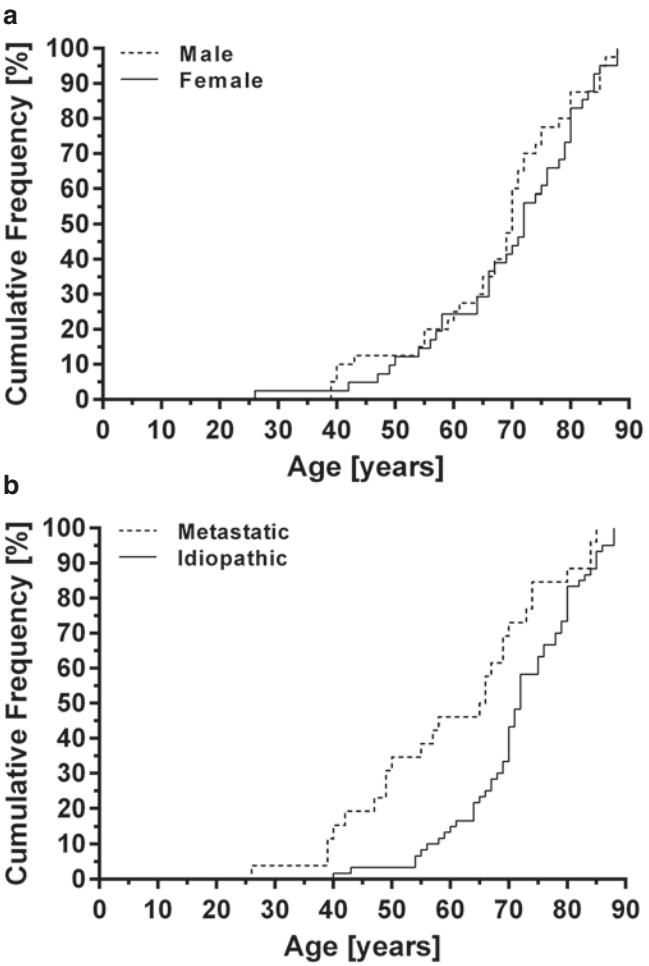

Fig. 17.1 Cumulative frequency of having a sclerochoroidal calcification diagnosed plotted according to (**a**) gender and (**b**) type of lesion for 86 patients reported from 1986 to 2017 in the literature. Metastatic lesions in patients with predisposing systemic disease are diagnosed significantly earlier than idiopathic lesions in patients with apparently normal calcium and phosphorous metabolism

17.3.3 Gender and Race

Sclerochoroidal calcification was equally common in males (49%) and females (51%) among 81 patients reported from 1989 to 2017, whereas females slightly predominated (60%) in the large referral-based series (Shields et al. 2015). Almost all patients have been white Caucasian. Additionally, six Hispanic (Caminal-Mitjana et al. 2013; Sierra-Rodríguez et al. 2014; Shields et al. 2015), three Asian (Suzuki et al. 1992; Kobune et al. 1993; Saatci et al. 1996; Hara et al. 2013), and one black patient (Schachat et al. 1992) have been reported; all but one of them had the metastatic type of sclerochoroidal calcification.

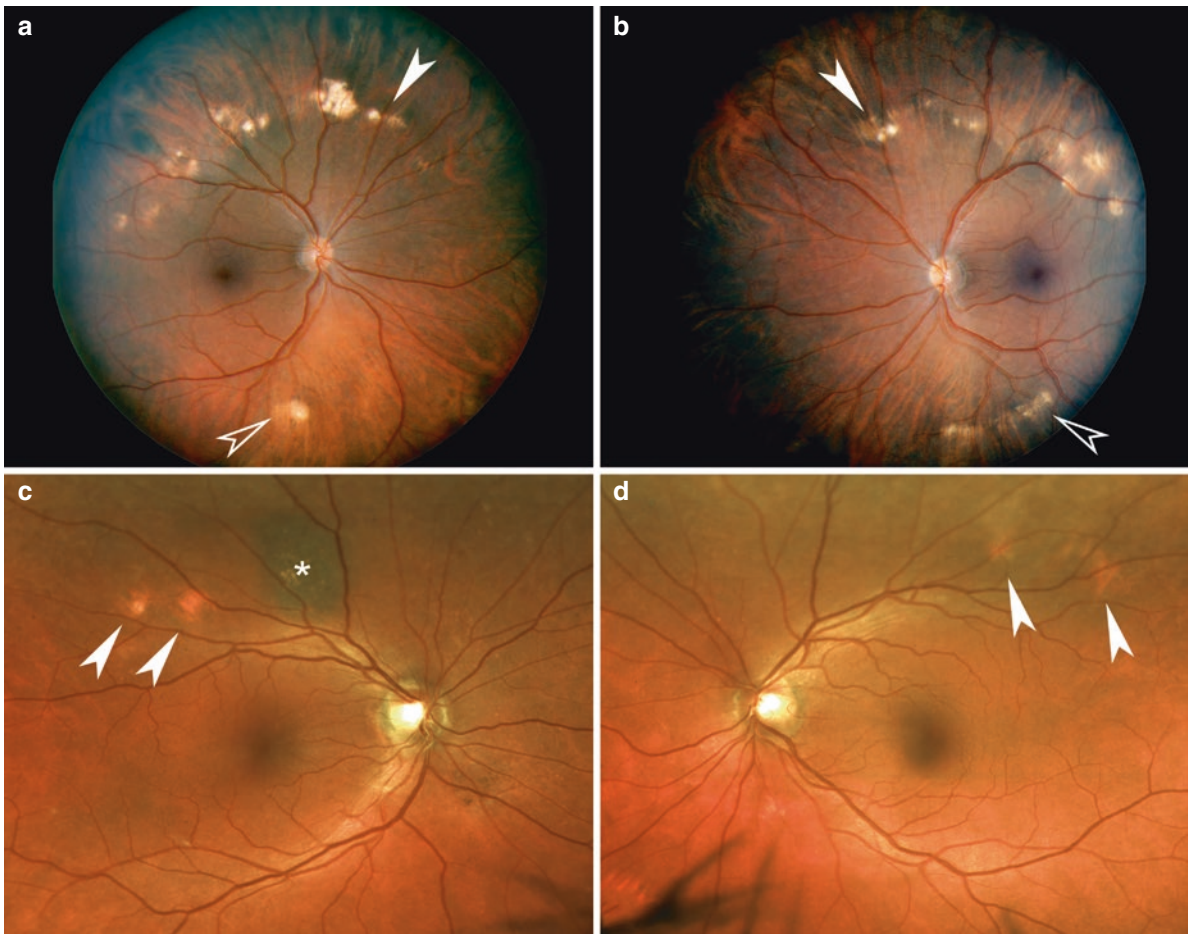

Fig. 17.2 Advanced and moderately advanced idiopathic sclerochoroidal calcification, note the typical midperipheral location. (**a**) The right eye and (**b**) the left eye of a 51-year-old male show an arc of multiple yellowish lesions that likely correspond to the thickest parts of a partially hidden superotemporal calcification, and additional lesions are visible superonasally (*arrowhead*) and inferotemporally (*open arrowhead*). (**c**) The right eye and (**d**) the left eye of a 70-year-old male show two peaks (*arrowheads*) of an underlying calcification that are still covered by variably attenuated choroid that is still thicker in the left eye. The right eye has a coincidental choroidal nevus (*asterisk*)

17.3.4 Location and Laterality.

Among 54 patients reported from 1989 to 2017, sclerochoroidal calcification typically occurred posterior to the equator of the eye peripheral to or along the vascular arcades (Figs. 17.2, 17.3, and 17.4), preferably in the superotemporal quadrant (Sivalingam et al. 1991; Schachat et al. 1992; Wong and Kawasaki 2014; Hasanreisoglu et al. 2015; Slean et al. 2017; Sugarman et al. 2017) followed equally frequently by the superonasal and inferotemporal ones, and was least common in the inferonasal quadrant (Bessette and Singh 2016). In five patients, all with the metastatic type, the calcification was large enough to eventually involve the macula (Zaman and Spalton 1995; Leys et al. 2000; Floegel et al. 2002; Boutboul et al. 2004; Hara et al. 2013).

The calcification typically was multifocal (Sivalingam et al. 1991; Schachat et al. 1992; Shields et al. 2015) but appeared to be limited to one quadrant (and then always the superotemporal one) (Figs. 17.2, 17.3, and 17.4) in two thirds (67%) of 51 patients reported from 1989 to 2017, whereas in one quarter (25%) it involved two quadrants (the second one was equally often the inferotemporal and superonasal one), and in a small number of patients, they involved either three (Fig. 17.2) (McCabe et al. 1997; Zaheen et al. 2000; Sun et al. 2005; Choi et al. 2009) or four quadrants (Caminal-Mitjana et al. 2013; Caminal-Mitjana and Padrón-Pérez 2013; Hara et al. 2013). However, in one referral-based series, superonasal involvement was more frequent than inferotemporal (Honavar et al. 2001), a difference that narrowed in a follow-up paper (Shields et al. 2015). With one

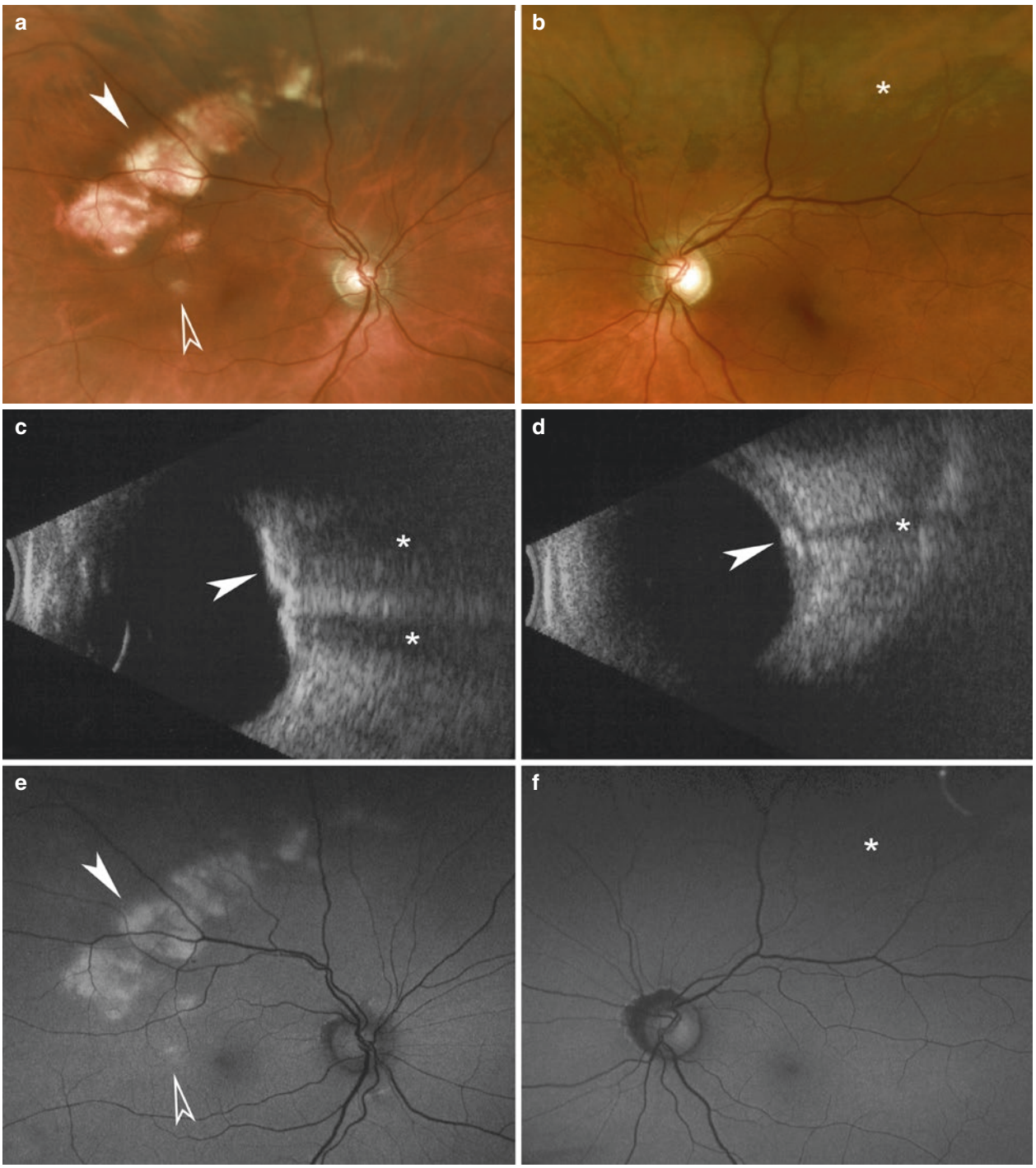

Fig. 17.3 An asymmetrically advanced idiopathic sclerochoroidal calcification, note the typical midperipheral, superotemporal location. (**a**) The right eye of a 64-year-old male shows an arc of advanced mountain-like lesions with only larger choroidal vessels remaining over them (*arrowhead*) and two adjacent perimacular peaks still covered with attenuated choroid. (**b**) The left eye harbors an early lesion completely hidden by a full-thickness choroid (*asterisk*). (**c**) The right eye shows a continuous calcified scleral plaque by ultrasonography, the thicker parts of which cast acoustic shadows (*asterisks*). (**d**) The hidden lesion is visualized by ultrasonography, and its thickest part also casts an acoustic shadow (*asterisk*). (**e**) The lesions of the right eye are moderately hyperautofluorescent (*arrowhead* and *open arrowhead*); note the partially preserved choroid and isoautofluorescent retinal pigment epithelium in the center of the mountain-like lesions that are thickest at their margins. (**f**) The fundus autofluorescence image of the left eye is normal, hiding the calcification (asterisk). For optical coherence tomography images, see Fig. 17.5

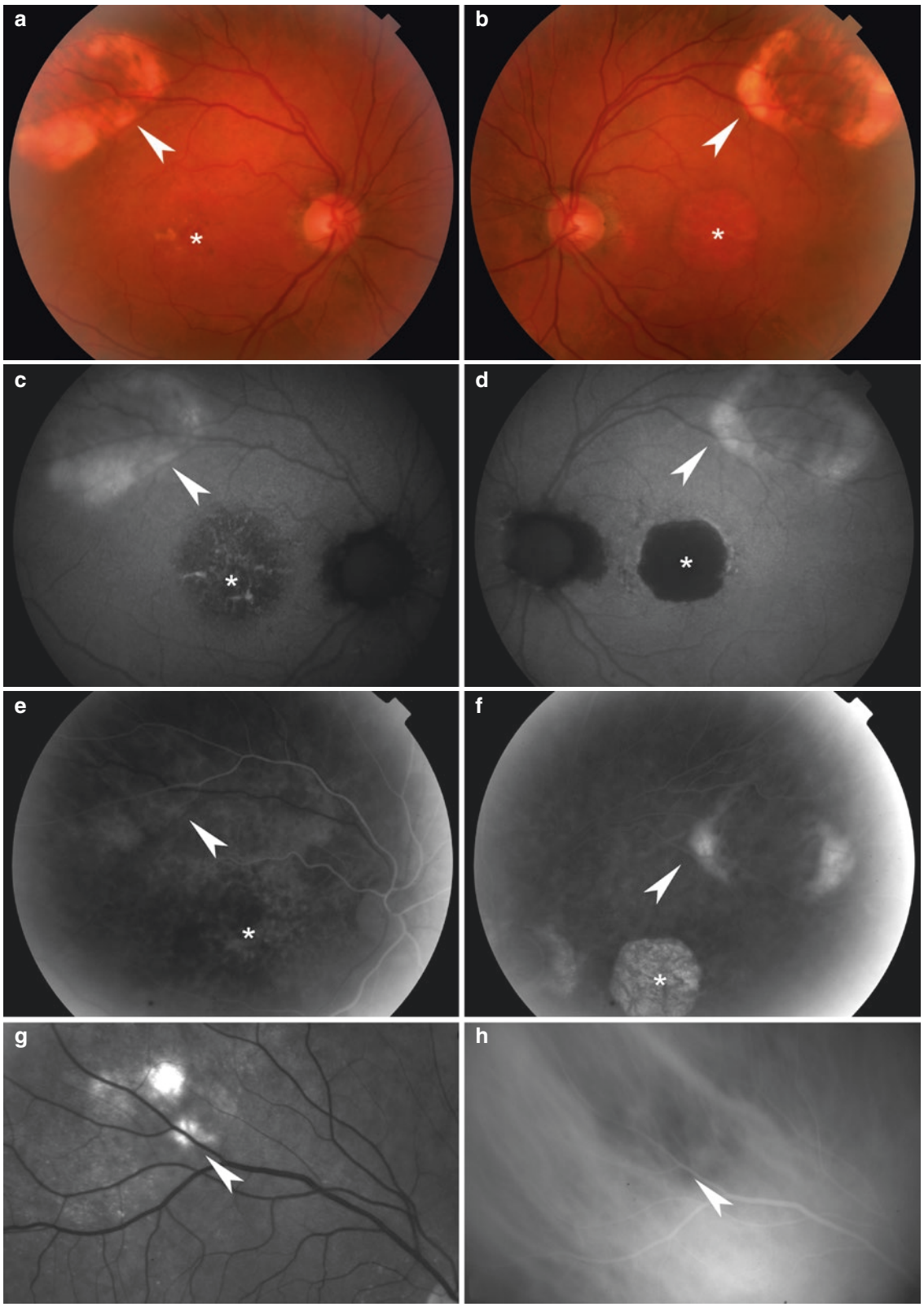

Fig. 17.4 Multimodal imaging of an advanced idiopathic sclerochoroidal calcification, note the typical superotemporal location. (**a**) The right eye and (**b**) the left eye of an 84-year-old female show symmetrical single large mountain-like lesions (*arrowhead*) that are thickest at the margins with some preserved choroid in their center. Both eyes have coincident dry senile macular degeneration (*asterisk* in all images). (**c**) The lesions in the right and (**d**) the left eye are moderately hyperautofluorescent at their margins (*arrowhead*); the dry macular degeneration shows hypoautofluorescence from loss of retinal pigment epithelium bilaterally and scattered hyperautofluorescence of metabolically stressed pigment epithelial cells in the right eye. (**e**) The lesions (*arrowhead*) are mostly isofluorescent in early frames of fluorescein angiography (right eye) and show (**f**) hyperfluorescence from staining in late frames (left eye); the dry macular degeneration is also hyperfluorescent because of a window defect and scleral staining. (**g**) The right eye of another patient with a moderately advanced superotemporal lesion (*arrowhead*) seen in a red-free photograph (**h**) remains hypofluorescent in late frames during indocyanine green angiography

exception (McCabe et al. 1997), all patients with calcifications in more than two quadrants had the metastatic type that was responsible for one third of the less widespread lesions.

The calcifications were bilateral in 86% (Figs. 17.2, 17.3, and 17.4) of 95 patients reported between 1989 and 2017, although they are not infrequently asymmetric so that the fundus of one eye can appear normal (Slean et al. 2017); its involvement was confirmed by ultrasonography in 3 patients (Fig. 17.3) (Vezzoli et al. 2000; Shields et al. 2004; Sugarman et al. 2017), and unilateral in 14% of patients, in contrast to the largest referral-based series in which as many as 48% of 118 patients were reported to have unilateral lesions (Shields et al. 2015).

17.3.5 Symptoms and Signs

Sclerochoroidal calcification is most often asymptomatic and detected during a routine eye examination (Sivalingam et al. 1991; Schachat et al. 1992; Bessette and Singh 2016; Shields et al. 2015) although patients can rarely present after they experience visual loss and metamorphopsia related to a choroidal neovascular membrane and subretinal bleeding (Zaheen et al. 2000; Dedes et al. 2008). A hyperopic shift in two patients and choroidal folds with Adie's tonic pupil (from presumed compression of parasympathetic nerve fibers in the suprachoroidal space) in one patient have been ascribed to sclerochoroidal calcification (Zhang et al. 2015; Brahma et al. 2017), and rarely visual field defects may develop from large lesions extending to the macular region, often from an associated systemic condition (Zaman and Spalton 1995; Zaheen et al. 2000).

Sclerochoroidal calcification varies from orange to yellow to white in color (Figs. 17.2, 17.3, and 17.4), likely reflecting the extent of choroidal and retinal pigment epithelium (RPE) attenuation over the whitish scleral degeneration (Sivalingam et al. 1991; Schachat et al. 1992; Honavar et al. 2001; Lindstedt et al. 2007; Hara et al. 2013; Shields et al. 2015). If the choroid is intact, the lesions may be ophthalmoscopically invisible (Shields and Shields 2002; Garuti et al. 2005; Hasanreisoglu et al. 2015) and might be serendipitously detected during an ultrasound or computed tomography examination for unrelated reasons. This is quite often the case in the fellow eye (Fig. 17.3). Variable choroidal atrophy often gives the impression of multiple lesions that can number up to 7 in one eye (Hasanreisoglu et al. 2015) although in the referral-based series of 118 patients they were unifocal in 71% (Shields et al. 2015). The patches may merge into geographic shapes (Shields and Shields 2002). The margins of the lesion can be either relatively sharp or diffuse but are typically irregular, giving it a geographic or amoeboid shape. Larger choroidal vessels may be visible over the calcification (Kaur and Anthony 2017). The RPE gradually degenerates, resulting in pigment dispersion and mottling (Honavar et al. 2001; Shields and Shields 2002; Bessette and Singh 2016). Serous retinal detachment, pigment epithelial detachment, lipid exudates, and intraretinal edema (Schachat et al. 1992; Cohen et al. 1998; Bessette and Singh 2016) from disruption of the RPE (Fig. 17.5), a choroidal neovascular membrane (CNV), or both are exceptional (Cohen et al. 1998; Bessette and Singh 2016).

Exceptionally, the lesions can extend anteriorly enough to be visible by biomicroscopy as small gray scleral patches (Shields and Shields 2002). A quarter of patients have a concurrent anterior senile scleral plaque adjacent to rectus muscle insertion (Honavar et al. 2001). However, scleral plaques are frequent in the general population as well; they were visible in 7 (3%) of 200 patients aged 70–79 years and in 16 (22%) of 71 patients 80 years or more, imaged with computed tomography for unrelated reasons (Moseley 2000).

17.3.6 Size

The size of sclerochoroidal calcification has rarely been reported. In the largest referral-based series, the largest lesion measured a median of 3.6 mm in diameter, with a range from 0.5 mm to 9.5 mm, followed by a median diameter of 2.1 and 1.7 mm for the second and third largest lesion, respectively (Shields et al. 2015), whereas the median thickness of the largest lesion was 1.8 mm, with a range from 1.0 to 3.8 mm. Single largest reported lesions have measured 10 mm in diameter (Schachat et al. 1992; Brahma et al. 2017) and 5–6 mm in thickness (Schachat et al. 1992; Floegel et al. 2002).

17.3.7 Systemic Associations

Most sclerochoroidal calcifications are idiopathic and unassociated with abnormalities in calcium, phosphorous, magnesium, and parathyroid hormone levels or kidney or skeletal disease (Sivalingam et al. 1991; Schachat et al. 1992; Lindstedt et al. 2007; Rao et al. 2012; Wong and Kawasaki 2014; Slean et al. 2017; Brahma et al. 2017). Some patients have a history of kidney stones, which appears to be coincidental (Lindstedt et al. 2007).

Hyperparathyroidism, either past (Schachat et al. 1992; Cohen et al. 1998; Yohannan et al. 2012) or present (Goldstein and Miller 1982; Suzuki et al. 1992; Kobune et al. 1993; Honavar et al. 2001; Lindstedt et al. 2007; Choi et al. 2009; Shields et al. 2015) from a parathyroid adenoma, and secondary hyperparathyroidism from renal failure (Floegel et al. 2002; Shields et al. 2004; Hara et al. 2013) are the most frequently reported systemic associations for metastatic sclerochoroidal calcification.

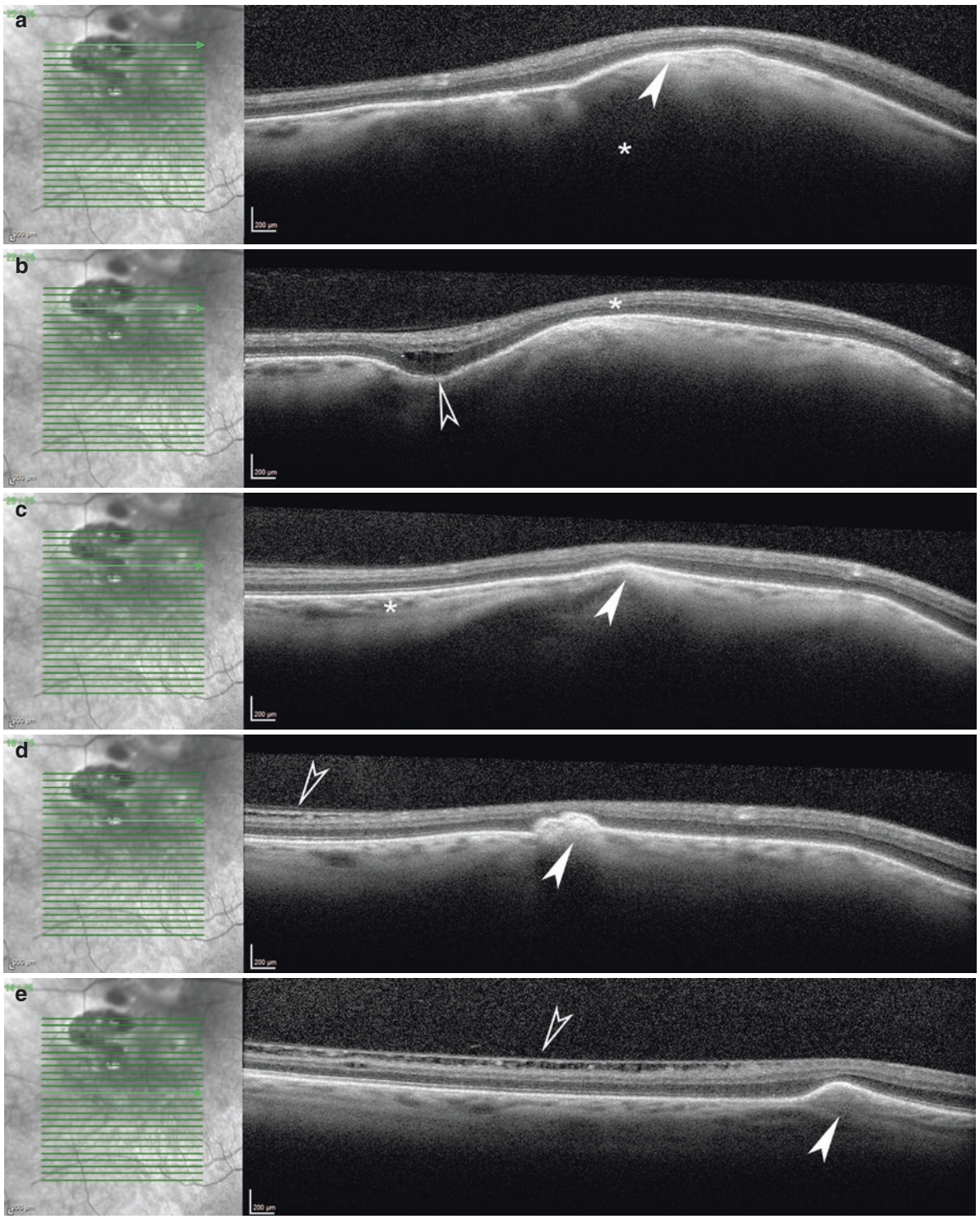

Fig. 17.5 An advanced idiopathic sclerochoroidal calcification in the right eye of a 64-year-old male; for clinical images, see Fig. 17.2. An optical tomography scan through the lesion shows different configurations. (**a**) Dome-shaped (type 2) configuration with preserved retinal pigment epithelium (RPE) but extreme attenuation of choroid and thinning of the retina at the top (*arrowhead*); note optical shadowing (*asterisk*). (**b**) Undulating (type 3) configuration; note the thinned retina (*asterisk*) and secondary focal retinoschisis (*open arrowhead*) in the valley between the two hills. (**c**) In three adjacent sections, note the relatively preserved choroid (*asterisk*) adjacent to a peak (*arrowhead*) that (**d**) breaks Bruch's membrane into the subretinal space, apparently leading to cystic retinal changes (*open arrowhead*) seen inferior to the peak; note another peak (*arrowhead*) that respects Bruch's membrane. A break might lead to a choroidal neovascular membrane that sometimes can be associated with sclerochoroidal calcification

Vitamin D deficiency is a common disorder that results either from inadequate sunlight exposure or dietary intake or from impaired absorption or conversion into active metabolites (Holick 2017). It can led to *hypo*calcemia, secondary hyperparathyroidism, and poor bone mineralization and can worsen osteomalacia and osteoporosis in adults (Goltzman 2018). Sclerochoroidal calcification was reported in 67 and 69-year-old patients with vitamin D deficiency (Sierra-Rodríguez et al. 2014; Ali and David 2017). One of them also showed calcifications in the cerebral fornix and choroid plexus (Ali and David 2017). Their calcium levels were normal. Given the high frequency of vitamin D deficiency and the fact that it is usually not associated with calcifications elsewhere, the causal relationship between these two conditions is uncertain.

In some patients, metastatic sclerochoroidal calcification also has been reported in association with rare hereditary syndromes:

Gitelman syndrome (OMIM 263800) is an autosomal recessive renal tubular salt-wasting disorder that from mutations in *SLC12A3* on chromosome 16q13, a gene that encodes a thiazide-sensitive sodium-chloride cotransporter in the distal convoluted tubule (Blanchard et al. 2017). It usually presents in adolescents and young adults and is characterized by normal serum calcium, phosphate, and parathyroid hormone levels, metabolic alkalosis, hypokalemia, hypomagnesemia, *hypo*calciuria, deposition of calcium pyrophosphate dihydrate, and normal calcium absorption. The prevalence in Caucasians is 1:40,000. Gitelman syndrome can be mimicked by autoimmune diseases, most often by Sjögren's syndrome (Blanchard et al. 2017).

Among five patients with Gitelman syndrome screened for sclerochoroidal calcification, a 50-year-old female with associated chondrocalcinosis had multiple, bilateral, minimally elevated superotemporal lesions, and another 26-year-old female without chondrocalcinosis had bilateral inferotemporal lesions that were only visible by ultrasonography (Vezzoli et al. 2000). Additionally, case reports of bilateral sclerochoroidal calcification in Gitelman syndrome in two 49- and 58-year-old females and a 59-year-old male, all with associated chondrocalcinosis, have appeared (Marchini et al. 1998; Bourcier et al. 1999; Gupta et al. 2005). None of these cases were genetically verified.

Conversely, in two series of 13 (Honavar et al. 2001) and 7 (Lindstedt et al. 2007) patients with sclerochoroidal calcification who underwent metabolic screening, 4 (31%) and none, respectively, had laboratory findings consistent with Gitelman syndrome, suggesting referral bias in the former study. Two additional patients showed isolated hypomagnesemia (Honavar et al. 2001). The former center later reported a smaller number, 6 (11%) of 53 patients to have *acquired* Gitelman syndrome from diuretic use (Shields et al. 2015), suggesting that the 49-, 70-, 73-, and 84-year-old patients in their earlier report did not have true Gitelman syndrome.

Bartter syndrome (OMIM 263800) is a related, genetically heterogeneous autosomal or X-linked recessive renal tubular salt-wasting disorder that results from mutations in *SLC12A1* on chromosome 15q21 that encodes a sodium-potassium-chloride cotransporter (Bartter syndrome type 1), in *KCNJ1* on chromosome 11q24 encoding a renal potassium channel (type 2), in *CLCNKB* on chromosome 1p36 encoding a renal chloride channel (type 3), in *BSND* on chromosome 1p32 encoding a subunit of renal chloride channels (type 4), or in *MAGED2* on chromosome Xp11, all of which affect the thick ascending loop of Henle. Depending on the mutated gene, the syndrome is antenatal and life-threatening (types 1, 2, and 5), neonatal and mild (type 4) or, in its classic form, presents later in life with variable phenotype (type 3). Bartter syndrome is characterized by normal serum calcium, phosphate, and parathyroid hormone levels, metabolic alkalosis, hypokalemia, occasional hypomagnesemia, *hyper*calciuria, deposition of calcium pyrophosphate dihydrate, and normal calcium absorption. Hypomagnesemia, when present, might contribute to the deposits. The prevalence of Bartter syndrome in Caucasians is 1:million. It can be mimicked by acquired conditions, including excessive use of laxatives.

Bilateral sclerochoroidal calcification involving three to four quadrants has been reported in two 42- and 65-year-old women with classic Bartter syndrome (Sun et al. 2005; Caminal-Mitjana and Padrón-Pérez 2013; Caminal-Mitjana et al. 2013). Conversely, in two series of 13 (Honavar et al. 2001) and 7 (Lindstedt et al. 2007) patients with sclerochoroidal calcification who underwent identical metabolic screening, one patient in the former series was reported to have isolated hypercalciuria (Honavar et al. 2001). This patient was later referred to as having a "suggested diagnosis of Bartter syndrome" (Shields and Shields 2002) and finally as "possible classic Bartter syndrome" (Sun et al. 2005).

Familial articular chondrocalcinosis (OMIM 118600), also known as calcium pyrophosphate deposition disease, is characterized by deposition of calcium pyrophosphate dihydrate in articular hyaline and fibrocartilage. Chondrocalcinosis occurs also in association with metabolic disorders, including hyperparathyroidism and hypomagnesemia, and sporadically, however, and is a common condition. It may be asymptomatic, associated with acute attacks of pseudogout or cause chronic arthritis. The familial form is inherited as an autosomal dominant trait and in most cases results from mutations in the homolog of mouse ank (*ANKH*) gene (Williams 2016). Sclerochoroidal calcification was reported at the age of 40–74 years in three family members affected

with familial chondrocalcinosis, although the genetic defect was not explored (Boutboul et al. 2004).

Pseudohypoparathyroidism, type IA (OMIM 103580), also known as Albright's hereditary osteodystrophy with multiple hormone resistance was reported to be the cause of sclerochoroidal calcification in 29- and 47-year-old patients (Wong et al. 1979; Lee et al. 2012). These patients are characterized by skeletal anomalies that include short stature, obesity, round facies, subcutaneous ossifications, and brachydactyly. Some patients also have mental retardation. The prevalence estimate is 1:100,000 in Caucasians.

17.4 Examination

17.4.1 Ultrasonography

Ophthalmoscopy and ultrasonography (Fig. 17.3) are both necessary and sufficient to diagnose sclerochoroidal calcification. Ultrasonography shows intensely reflective, typically multiple plaque-like or nodular scleral lesions that often bulge into the choroid and sometimes also elevate the retina (Lim and Goldberg 1989; Sivalingam et al. 1991; Schachat et al. 1992; Honavar et al. 2001; Floegel et al. 2002; Zhang et al. 2015; Slean et al. 2017; Brahma et al. 2017; Sugarman et al. 2017). They cause orbital shadowing and remain visible when the gain is lowered between 25 and 50 dB (Vezzoli et al. 2000; Gupta et al. 2005; Sun et al. 2005; Yohannan et al. 2012; Bessette and Singh 2016). Scanning often reveals larger and more widespread lesions than what can be appreciated with ophthalmoscopy and not infrequently finds lesions also in ophthalmoscopically normal appearing fellow eyes (Sivalingam et al. 1991; Vezzoli et al. 2000; Shields et al. 2004; Sugarman et al. 2017). In less advanced cases, ultrasonography is the only means of visualizing the calcifications in the office (Garuti et al. 2005).

17.4.2 Fluorescein and Indocyanine Green Angiography

Fluorescein angiography is not needed for diagnosis of sclerochoroidal calcification and is needed only if a CNV is suspected. The calcification usually shows early hypo- to isofluorescence (Honavar et al. 2001; Leys et al. 2000; Shields and Shields 2002; Rao et al. 2012; Wong and Kawasaki 2014) but sometimes hyperfluorescence (Schachat et al. 1992; Floegel et al. 2002; Pakrou and Craig 2006; Lindstedt et al. 2007) from a window defect, and late hyperfluorescence from staining is typical (Fig. 17.4) (Sivalingam et al. 1991; Schachat et al. 1992; Leys et al. 2000; Honavar et al. 2001; Floegel et al. 2002; Shields and Shields 2002; Schönherr and Graupner 2003; Kim et al. 2004; Pakrou and Craig 2006; Lindstedt et al. 2007; Rao et al. 2012; Wong and Kawasaki 2014; Brahma et al. 2017). Findings are similar on indocyanine green angiography (Honavar et al. 2001; Shields and Shields 2002; Brahma et al. 2017) although the lesion may remain hypofluorescent (Fig. 17.4), and a CNV, when present, is visualized with either method (Cohen et al. 1998; Leys et al. 2000; Zuercher and Zografos 2002; Shields and Shields 2002; Dedes et al. 2008; Bessette and Singh 2016).

17.4.3 Optical Coherence Tomography

Sclerochoroidal calcification is characteristically an elevated scleral lesion that can have a flat (type 1; ophthalmoscopically invisible, mean thickness 1.4 mm) (Hasanreisoglu et al. 2015; Sugarman et al. 2017), dome-shaped (type 2; mean thickness 1.5 mm) (Wong and Kawasaki 2014; Hasanreisoglu et al. 2015; Brahma et al. 2017), undulating (type 3; mean thickness 2.1 mm) (Fung et al. 2013; Wong and Kawasaki 2014; Hasanreisoglu et al. 2015; Slean et al. 2017), or table mountain-like (type 4; mean thickness 1.9 mm) (Hasanreisoglu et al. 2015; McNabb et al. 2016; Brahma et al. 2017; Sugarman et al. 2017) contour on optical coherence tomography (OCT) (Fig. 17.5) (Caminal-Mitjana et al. 2013; Hasanreisoglu et al. 2015; McNabb et al. 2016).

Best seen with enhanced-depth imaging OCT (EDI-OCT), the lesion has a hyperreflective surface and absorbs the signal with posterior shadowing (Miller and Eller 2009; Yohannan et al. 2012; McNabb et al. 2016; Sugarman et al. 2017). The choroid is variably attenuated, even by flat type 1 lesions and especially by type 3 lesions (Rao et al. 2012; Caminal-Mitjana et al. 2013; Hasanreisoglu et al. 2015; Bessette and Singh 2016; Slean et al. 2017; Sugarman et al. 2017), and its architecture may be distorted (Yohannan et al. 2012). The choriocapillaris is usually maintained, and the choroidal-scleral junction is continuous over the calcification (Slean et al. 2017; Sugarman et al. 2017; Kaur and Anthony 2017).

The RPE overlying the choroidal lesions appears normal in flat, type 1 lesions, and no subretinal fluid is present (Sun et al. 2005; Yohannan et al. 2012; Hasanreisoglu et al. 2015; McNabb et al. 2016), with rare exceptions (Schachat et al. 1992; Fung et al. 2013). The retinal layers may be elevated, and the retinal thickness may be mildly reduced (Fig. 17.5) (Hasanreisoglu et al. 2015). In type 2–4 lesions, the calcification often has spikes (Fung et al. 2013; Bessette and Singh 2016) that elevate the choriocapillaris complex and RPE with concomitant atrophy with or without focal reactive proliferation of the RPE (Caminal-Mitjana et al. 2013; McNabb et al. 2016) and minor abnormalities of the outer retina, including focal retinoschisis (Fig. 17.5). In some cases, the RPE and Bruch's membrane may become disrupted which may give

rise to intraretinal edema (Fig. 17.5) and, potentially, be a harbinger of a CNV. Type 4 lesions often are most elevated at their margins (McNabb et al. 2016; Brahma et al. 2017; Kaur and Anthony 2017) which gives the lesion a circular or semicircular appearance ophthalmoscopically (Fig. 17.4) as is seen in many published images (Sivalingam et al. 1991; Shields and Shields 2002; Pakrou and Craig 2006; Choi et al. 2009).

17.4.4 Fundus Autofluorescence Imaging

Sclerochoroidal calcification may show areas with hypoautofluorescence (Fung et al. 2013; Caminal-Mitjana et al. 2013), isoautofluorescence (Caminal-Mitjana et al. 2013; Kaur and Anthony 2017), and, most often, hyperautofluorescence (Figs. 17.3 and 17.4) (Shields and Shields 2002; Cooke et al. 2003; Fung et al. 2013; Caminal-Mitjana et al. 2013; Slean et al. 2017), sometimes in a patchy pattern (Caminal-Mitjana et al. 2013) depending on the state of the overlying choroid and RPE. Adjacent to focal elevations, the RPE shows relative hyperautofluorescence, interpreted by some as evidence of lipofuscin accumulation due to compromised choriocapillary circulation (Caminal-Mitjana et al. 2013). Alternatively, unmasking of hyperautofluorescence of scleral origin is postulated (Fung et al. 2013). Hypoautofluorescent patches at the tip of the elevation from focal atrophy of the RPE may occur (Caminal-Mitjana et al. 2013).

17.4.5 Computed Tomography and Magnetic Resonance Imaging

Computed tomography is unnecessary for making the diagnosis (Honavar et al. 2001). It is discouraged because it provides no additional information compared with ultrasonography while exposing the patient to ionizing radiation. However, sometimes sclerochoroidal calcification is an incidental finding when the eye or the orbit is imaged for other reasons (Kobune et al. 1993; Garuti et al. 2005; Hara et al. 2013). Sclerochoroidal calcification appears as hyperdense scleral plaques or nodules located behind the equator, usually bilaterally and often both temporally and nasally (Lim and Goldberg 1989; Sivalingam et al. 1991; Suzuki et al. 1992; Kobune et al. 1993; Zaman and Spalton 1995; McCabe et al. 1997; Bourcier et al. 1999; Leys et al. 2000; Zaheen et al. 2000; Honavar et al. 2001; Shields and Shields 2002; Pakrou and Craig 2006; Floegel et al. 2002; Lee et al. 2012; Hara et al. 2013; Zhang et al. 2015; Ali and David 2017). The calcifications may not be visible on a routine radiograph (Zaheen et al. 2000). Magnetic resonance imaging has not been reported.

17.5 Differential Diagnosis

Sclerochoroidal calcification must be differentiated from other scleral and choroidal lesions that are calcified and mimic it in ultrasonography. The most common of these is a choroidal osteoma (Aylward et al. 1998; Honavar et al. 2001; Shields et al. 2005) that typically affects children and young adults at a median age of 25 years (range, 0–67) and is located in the peripapillary or macular area. Metaplastic bone in a phthisical eye may be difficult to distinguish from sclerochoroidal calcification (Munteanu et al. 2013) because the fundus typically is not visible, but the former is the more likely diagnosis in this setting. Rare lesions to be differentiated from osteomas include a calcified choroidal hemangioma (Munteanu et al. 2013), a calcified choroidal melanoma (Gianniou et al. 2017), a scleral ossification (Patrinely et al. 1982), and a calcified posterior scleral choristoma in organoid nevus syndrome (Traboulsi et al. 1999).

Other common referral diagnoses such as amelanotic nevus or melanoma, lymphoma, metastasis, and scleral or choroidal granuloma (Sivalingam et al. 1991; Schachat et al. 1992; Honavar et al. 2001; Shields and Shields 2002; Shields et al. 2014; Shields et al. 2015; Sugarman et al. 2017) can be excluded simply by performing ultrasonography that demonstrates a choroidal localization, except for scleral granuloma, and absence of calcification.

17.6 Histopathology

Sclerochoroidal calcification is not managed surgically, and thus histopathological reports are scarce. In two case reports of three patients, one of whom died of complications of pseudohypoparathyroidism and one who had a kidney transplant, the deposit in the metastatic type extended from the immediate vicinity of the outer scleral surface to the inner scleral surface and the deposits bulged forward, causing secondary choroidal atrophy (Wong et al. 1979). The patient with the idiopathic type showed monoclinic and triclinic calcium pyrophosphate crystals that merged in places with a diffuse inner scleral calcification (Daicker 1996).

17.7 Management

There is no need to treat a sclerochoroidal calcification (Shields and Shields 2002) unless it is associated with a CNV, which is rarely present.

17.7.1 Observation

Patients with sclerochoroidal calcification can routinely be observed, and the lesions typically remain quiescent and stationary with minimal risk to vision (Sivalingam et al. 1991; Schachat et al. 1992). Patients who develop a break in Bruch's membrane may need to be watched for development of a CNV. If a CNV is detected, one can either continue the observation (Honavar et al. 2001; Zuercher and Zografos 2002) or treat it, depending on its location.

Patients should be screened for a possible underlying systemic condition (Schachat et al. 1992), especially if they are younger than 50 years of age (Fig. 17.1). If calcium, phosphorous, magnesium, parathyroid hormone, and 25-hydroxyvitamin D levels are all normal, and no systemic findings or symptoms are present, the idiopathic type of sclerochoroidal calcification is likely.

17.7.2 Magnesium Supplementation

If the patient has hypomagnesemia, magnesium supplementation is recommended because of potential hazard to general health; whether the supplementation has any effect on progression of sclerochoroidal calcification is unknown.

17.7.3 Anti-vascular Endothelial Growth Factor Agents

Intravitreal injections of 1.25 mg bevacizumab has been used in an effort to achieve regression of a CNV associated with sclerochoroidal calcification (Bessette and Singh 2016).

17.7.4 Laser Therapy

Because patches of sclerochoroidal calcification are almost always located away from the macula, direct argon laser photocoagulation can be used to eradicate an associated CNV (Cohen et al. 1998; Leys et al. 2000; Bessette and Singh 2016). Photodynamic therapy (PDT) with verteporfin was tried in one eye, but the CNV recurred (Bessette and Singh 2016).

17.8 Prognosis

Sclerochoroidal calcification typically remains asymptomatic (Sivalingam et al. 1991; Schachat et al. 1992; Honavar et al. 2001). In 6 patients who were observed for 7–24 years, the lesions slowly enlarged sometimes approaching the foveal region (Munier et al. 1991; Boutboul et al. 2004; Slean et al. 2017), however, and new lesions appeared (Slean et al. 2017). It is likely that both gradual deposition of calcium salts and attenuation of the choroid over the lesion contribute to the apparent growth.

Visual prognosis is good even when an associated CNV develops, because it will likely be extramacular (Honavar et al. 2001; Shields and Shields 2002; Bessette and Singh 2016). Life prognosis is determined by the underlying systemic disease, if any.

References

Ali ZC, David VP. Sclerochoroidal calcification associated with hypovitaminosis D. Can J Ophthalmol. 2017;52:e121–2.

Aylward GW, Chang TS, Pautler SE, et al. A long-term follow-up of choroidal osteoma. Arch Ophthalmol. 1998;116:1337–41.

Bessette AP, Singh AD. Multimodal imaging of choroidal neovascularization associated with sclerochoroidal calcification. Ocul Oncol Pathol. 2016;2:234–8.

Blanchard A, Bockenhauer D, Bolignano D, et al. Gitelman syndrome: consensus and guidance from a Kidney Disease: Improving Global Outcomes (KDIGO) Controversies Conference. Kidney Int. 2017;91:24–33.

Bourcier T, Blain P, Massin P, et al. Sclerochoroidal calcification associated with Gitelman syndrome. Am J Ophthalmol. 1999;128:767–8.

Boutboul S, Bourcier T, Heligon JP, et al. Familial pseudotumoral sclerochoroidal calcification associated with chondrocalcinosis. Br J Ophthalmol. 2004;88:1094–5.

Brahma VL, Shah SP, Chaudhry NA, et al. Bilateral idiopathic sclerochoroidal calcifications. Open Ophthalmol J. 2017;11:76–9.

Caminal-Mitjana JM, Padrón-Pérez N. Calcifications sclérochoroïdiennes. J Fr Ophtalmol. 2013;36:292.

Caminal-Mitjana JM, Padron-Perez N, Arias-Barquet L, et al. Correlation between spectral-domain optical coherence tomography and autofluorescence findings in sclerochoroidal calcification. Can J Ophthalmol. 2013;48:331–4.

Choi JY, Bianciotto C, Shields JA, et al. Sclerochoroidal calcification in a patient with chronic hypercalcemia from undiagnosed parathyroid adenoma. Retin Cases Brief Rep. 2009;3:431–3.

Cohen SY, Guyot-Sionnest M, Puech M. Choroidal neovascularization as a late complication of hyperparathyroidism. Am J Ophthalmol. 1998;126:320–2.

Cooke CA, McAvoy C, Best R. Idiopathic sclerochoroidal calcification. Br J Ophthalmol. 2003;87:245–6.

Daicker B. Tophus-like, conglomerated, crystalline calcification of the sclera. Ophthalmologica. 1996;210:223–8.

Dedes W, Schmid MK, Becht C. Sklerochoroidale Kalzifikationen mit visusbedrohender choroidaler Neovaskularisation. Klin Monatsbl Augenheilkd. 2008;225:473–5.

Floegel I, Klein A, Langmann G. Metastatic sclerochoroidal calcification involving the fovea. Retina. 2002;22:503–5.

Fung AT, Arias JD, Shields CL, et al. Sclerochoroidal calcification is primarily a scleral condition based on enhanced depth imaging optical coherence tomography. JAMA Ophthalmol. 2013;131:960–3.

Garuti S, Klais CM, Fisher YL, et al. Unusual clinical manifestation of sclerochoroidal calcifications. Retina. 2005;25:517–9.

Gianniou C, Zografos L, Hrbacek J, et al. Kalzifiziertes nicht pigmentiertes Aderhautmelanom: Fallbericht einer seltenen Entität. Klin Monatsbl Augenheilkd. 2017;234:608–10.
Goldstein BG, Miller J. Metastatic calcification of the choroid in a patient with primary hyperparathyroidism. Retina. 1982;2:76–9.
Goltzman D. Functions of vitamin D in bone. Histochem Cell Biol. 2018;149(4):305–12.
Gupta R, Hu V, Reynolds T, et al. Sclerochoroidal calcification associated with Gitelman syndrome and calcium pyrophosphate dihydrate deposition. J Clin Pathol. 2005;58:1334–5.
Hara K, Tanito M, Kodama T, et al. A case of chorioretinal atrophy due to sclerochoroidal calcification. Acta Ophthalmol. 2013;91:e167–8.
Hasanreisoglu M, Saktanasate J, Shields PW, et al. Classification of sclerochoroidal calcification based on enhanced depth imaging optical coherence tomography "mountain-like" features. Retina. 2015;35:1407–14.
Holick MF. The vitamin D deficiency pandemic: approaches for diagnosis, treatment and prevention. Rev Endocr Metab Disord. 2017;18:153–65.
Honavar SG, Shields CL, Demirci H, et al. Sclerochoroidal calcification: clinical manifestations and systemic associations. Arch Ophthalmol. 2001;119:833–40.
Kaur G, Anthony SA. Multimodal imaging of suspicious choroidal neoplasms in a primary eye-care clinic. Clin Exp Optom. 2017;100:549–62.
Kim M, Pian D, Ferrucci S. Idiopathic sclerochoroidal calcification. Optometry. 2004;75:487–95.
Kobune M, Neda H, Mogi Y, et al. Ectopic choroidal calcification of the eyes of a patient with parathyroid adenoma. Intern Med. 1993;32:57–9.
Lee H, Kumar P, Deane J. Sclerochoroidal calcification associated with Albright's hereditary osteodystrophy. BMJ Case Rep. 2012;2012 https://doi.org/10.1136/bcr-1103-2012-6022.
Leys A, Stalmans P, Blanckaert J. Sclerochoroidal calcification with choroidal neovascularization. Arch Ophthalmol. 2000;118:854–7.
Lim JI, Goldberg MF. Idiopathic sclerochoroidal calcification. Arch Ophthalmol. 1989;107:1122–3.
Lindstedt EW, van den Born LI, Veckeneer M, et al. Sclerochoroidal calcification: idiopathic or associated with systemic disease? Retin Cases Brief Rep. 2007;1:141–4.
Marchini G, Tosi R, Parolini B, et al. Choroidal calcification in Bartter syndrome. Am J Ophthalmol. 1998;126:727–9.
McCabe CM, Mieler WF, Postel EA. Idiopathic sclerochoroidal calcification in a 41-year-old woman. Arch Ophthalmol. 1997;115:1082–3.
McNabb RP, Grewal DS, Mehta R, et al. Wide field of view swept-source optical coherence tomography for peripheral retinal disease. Br J Ophthalmol. 2016;100:1377–82.
Miller KV, Eller AW. Sclerochoroidal calcifications: wide-field imaging. Semin Ophthalmol. 2009;24:5–8.
Moseley I. Spots before the eyes: a prevalence and clinicoradiological study of senile scleral plaques. Clin Radiol. 2000;55:198–206.
Munier F, Zografos L, Schnyder P. Idiopathic sclerochoroidal calcification: new observations. Eur J Ophthalmol. 1991;1:167–72.
Munteanu M, Munteanu G, Giuri S, et al. Ossification of the choroid: three clinical cases and literature review of the pathogenesis of intraocular ossification. Romanian J Morphol Embryol. 2013;54:871–7.
Pakrou N, Craig JE. Idiopathic sclerochoroidal calcification in a 79-year-old woman. Clin Exp Ophthalmol. 2006;34:76–8.
Patrinely JR, Green WR, Connor JM. Bilateral posterior scleral ossification. Am J Ophthalmol. 1982;94:351–6.
Rao RC, Choudhry N, Gragoudas ES. Enhanced depth imaging spectral-domain optical coherence tomography findings in sclerochoroidal calcification. Retina. 2012;32:1226–7.
Saatci AO, Kaynak S, Kazanci L, et al. Calcification at the posterior pole in scleritis. A case report. Int Ophthalmol. 1996;20:285–7.
Schachat AP, Robertson DM, Mieler WF, et al. Sclerochoroidal calcification. Arch Ophthalmol. 1992;110:196–9.
Schönherr U, Graupner M. Sklerochoroidale Kalzifikation -ein seltenes Krankheitsbild - Bericht über zwei Patienten, Differenzialdiagnose und Literaturübersicht. Klin Monatsbl Augenheilkd. 2003;220:39–43.
Shields JA, Shields CL. CME review: sclerochoroidal calcification: the 2001 Harold Gifford Lecture. Retina. 2002;22:251–61.
Shields JA, Karatza EC, Shields CL, et al. Drusenlike deposits and sclerochoroidal calcification in a patient with glomerulonephritis. Retina. 2004;24:304–6.
Shields CL, Sun H, Demirci H, et al. Factors predictive of tumor growth, tumor decalcification, choroidal neovascularization, and visual outcome in 74 eyes with choroidal osteoma. Arch Ophthalmol. 2005;123:1658–66.
Shields CL, Pellegrini M, Ferenczy SR, et al. Enhanced depth imaging optical coherence tomography of intraocular tumors: from placid to seasick to rock and rolling topography - the 2013 Francesco Orzalesi Lecture. Retina. 2014;34:1495–512.
Shields CL, Hasanreisoglu M, Saktanasate J, et al. Sclerochoroidal calcification: clinical features, outcomes, and relationship with hypercalcemia and parathyroid adenoma in 179 eyes. Retina. 2015;35:547–54.
Sierra-Rodríguez MA, Bailez Fidalgo C, Sáenz-Francés F, et al. Calcificaciones esclerocoroideas asociadas a hipovitaminosis D. Arch Soc Esp Oftalmol. 2014;89:290–2.
Sivalingam A, Shields CL, Shields JA, et al. Idiopathic sclerochoroidal calcification. Ophthalmology. 1991;98:720–4.
Slean GR, Kalevar A, Chen J, et al. Enlargement of sclerochoroidal calcifications: multimodal imaging update. Retin Cases Brief Rep. 2017;12(Suppl 1):S122–4. https://doi.org/10.1097/ICB.0000000000000644.
Sugarman JA, Douglass AM, Say EA, et al. Stones, bones, groans, thrones, and psychiatric overtones: systemic associations of sclerochoroidal calcification. Oman J Ophthalmol. 2017;10:47–9.
Sun H, Demirci H, Shields CL, et al. Sclerochoroidal calcification in a patient with classic Bartter's syndrome. Am J Ophthalmol. 2005;139:365–6.
Suzuki J, Takeda M, Sekine N, et al. Bilateral metastatic sclerochoroidal calcification in a patient with hyperparathyroidism. Ophthalmologica. 1992;205:10–4.
Traboulsi EI, Zin A, Massicotte SJ, et al. Posterior scleral choristoma in the organoid nevus syndrome (linear nevus sebaceus of Jadassohn). Ophthalmology. 1999;106:2126–30.
Vezzoli G, Soldati L, Jansen A, et al. Choroidal calcifications in patients with Gitelman's syndrome. Am J Kidney Dis. 2000;36:855–8.
Wiesner PD, Nofsinger K, Jackson WE. Choroidal osteoma: two case reports in elderly patients. Ann Ophthalmol. 1987;19:19–23.
Williams CJ. The role of ANKH in pathologic mineralization of cartilage. Curr Opin Rheumatol. 2016;28:145–51.
Wong CM, Kawasaki BS. Idiopathic sclerochoroidal calcification. Optom Vis Sci. 2014;91:e32–7.
Wong S, Zakov ZN, Albert DM. Scleral and choroidal calcifications in a patient with pseudohypoparathyroidism. Br J Ophthalmol. 1979;63:177–80.
Yohannan J, Channa R, Dibernardo CW, et al. Sclerochoroidal calcifications imaged using enhanced depth imaging optical coherence tomography. Ocul Immunol Inflamm. 2012;20:190–2.
Zaheen M, Sellar W, Mucci B. Idiopathic sclerochoroidal calcification. Eye (Lond). 2000;14(Pt 4):681–4.
Zaman AG, Spalton DJ. Visual loss in metastatic sclerochoroidal calcification. Eye (Lond). 1995;9(Pt 5):655–7.
Zhang J, Davis AS, Spitze A, et al. Bilateral Adie's tonic pupil and hyperopic shift in idiopathic sclerochoroidal calcification. Neuroophthalmology. 2015;39:96–9.
Zuercher D, Zografos L. Sklerochoroidale Kalzifikationen mit subretinaler neovaskulärer Membran bei einem Patienten mit hoher Myopie. Ophthalmologe. 2002;99:785–8.

Correction to: Ocular Oncology

Duangnate Rojanaporn

Correction to:
Duangnate Rojanaporn (ed.), *Ocular Oncology*,
https://doi.org/10.1007/978-981-13-2336-2

In the original publication, the series title and the names of series editors on the cover and in the front matter pages had been inadvertently omitted. The series title "Retina Atlas" and the names of series editors (Sandeep Saxena, Richard F. Spaide, Eric H. Souied and Timothy Y.Y. Lai) have been included on the cover and the series title page in the front matter in the updated version.

The updated online version of this book can be found at
https://doi.org/10.1007/978-981-13-2336-2

D. Rojanaporn (ed.), *Ocular Oncology*, Retina Atlas, https://doi.org/10.1007/978-981-13-2336-2_18